

Optimisation of GMAW via the alternating shielding gas technique

PhD Thesis

Misael P. E. e Silva

James Weir Welding Laboratory
Mechanical & Aerospace Engineering
University of Strathclyde, Glasgow

April 2019

This thesis is the result of the author's original research. It has been composed by the author and has not been previously submitted for examination, which has led to the award of a degree.

The copyright of this thesis belongs to the author under the terms of the United Kingdom Copyright Acts as qualified by University of Strathclyde Regulation 3.50. Due acknowledgement must always be made of the use of any material contained in, or derived from, this thesis.

Misael P. E. e Silva

May 2019

This PhD was fully granted by the Brazilian National Council for Scientific and Technological Development (CNPq - Conselho Nacional de Desenvolvimento Científico e Tecnológico) through the scholarship 201249/2014-6.



Abstract

The use of the alternating shielding gas technique in arc welding systems has been previously studied due to advantages such as greater penetration of the weld joint, refined microstructure of the fusion zone, reduced heat input, and increased travel speeds of the welding torch. Yet, relatively little work has been carried out utilising this novel method. For instance, shielding gases employed during the arc welding procedures have been limited to Ar, CO₂ and He, since the reactive behaviour of N₂ within the arc plasma causes porosity development within the fusion zone.

The present thesis extended the scientific knowledge regarding the alternating shielding gas technique via a systematic analysis utilising the gas metal arc welding process. It explored reductions in the shielding gas flow rate via variations in the frequency of alternation between the protective gases, investigated additions of N₂ as a protective gas to weld DH36 grade steel plates, and examined ways to optimise the welding parameters.

Measurements of the distortion of the workpiece, temperature of the weld, heat-affected zone (HAZ) and weld shape demonstrated the impact of the alternating shielding gas technique in reducing the heat input to the weldment. Microstructural characterisation coupled with analyses of the mechanical properties of the joint exhibited improved strength due to the

faster welding procedures and greater formation of acicular ferrite. Additionally, mathematical modelling coupled with the genetic algorithm heuristic assisted with enhancing the efficiency of welds under the supply of N₂ as a protective gas.

The study carried out was able to diminish the shielding gas consumption even further by employing the alternating shielding gas technique. It also offered new insights in terms of shielding gas options, where the replacement of CO₂ for N₂ lowered the welding fume progression, eliminated the porosity development within welds, and generated a more uniform weld shape.

Keywords: Gas metal arc welding, alternating shielding gas, shielding gas flow rate, nitrogen, genetic algorithm, response surface methodology, desirability function.

À minha Família

Para à qual a distância apenas fortalece nossos laços

Amo vocês!

Acknowledgements

I would like to thank everyone that, somehow, was involved in this important chapter in my life. Without any of your support, help, advice, experience, and friendship I don't think I would have done this far.

My sincere thanks to Doctor Alex Galloway and Doctor Athanasios Toumpis. Thank you for the opportunity to work with you, learn from you and contribute with you. Thank you for the tough meetings, the constructive criticism and the patience towards me as a professional. I would not have achieved this stage in my life without your guidance.

I would like to acknowledge the financial support provided by the Conselho Nacional de Desenvolvimento Científico e Tecnológico (CNPq) through the scholarship 201249/2014-6.

Thanks to all technicians and staff that helped me throughout this process. In special, thank you James Kelly for the moments you made yourself available when you were busy. I acquired significant knowledge from our discussions and I sure will apply those during my entire career. My thanks also to Drew Irvine and his team of technicians. I would not have finished this work without you guys.

To all my friends that were around, I would not be able to accomplish this thesis work without the nice chats, good laughs, lunch breaks, and random drinks. You made these last four years one of the best in my life. You were my family in Europe, with your presence adding a positive spirit to this entire doctorate.

Obrigado a você Jeziel for the times you heard me when you didn't have to, for the talks that made me feel I could finish this, and for the advices of a very experienced researcher. I'm thankful that you were part of this important stage in my life. This journey would not be complete without you.

To you Binho (a.k.a Savvas) one word: **Καλημέρα**. You might have not noticed, but you made challenges lighter, work easier, doubts clearer and life happier. Without you around my journey wouldn't have colours, being just an experience. **Ευχαριστώ!**

Obrigado família. Obrigado Papai pela sabedoria e pragmatismo, Mamãe pelo amor incondicional, Mirian pela saudade sem fim, Joãozinho por ser meu espelho e Mari pelo carinho gratuito. Vocês foram, são e serão minha motivação para encarar cada dia, cada semana, mês e ano nesse mundo. Essa tese é para vocês, assim como meu amor.

*“Don’t worry about being successful but work toward being
significant and the success will naturally follow”*

Oprah Winfrey

Contents

Abstract	iii
Acknowledgements	vi
1 Introduction	1
1.1 Background	1
1.2 Research purpose.....	3
1.3 Thesis structure.....	4
1.4 Bibliography	6
2 Literature review.....	12
2.1 The protective gases.....	12
2.1.1 Chemical activity.....	12
2.1.2 Transport coefficients and thermodynamic properties.....	14
2.1.3 Arc properties	16
2.1.4 Metal vapour	21
2.2 The alternating shielding gas method	23
2.2.1 Background.....	23
2.2.2 Benefits of employing the alternating shielding gas method.....	24
2.2.3 Understanding the alternating shielding gas mechanism	25
2.3 Distortion	29
2.3.1 Distortion development	29
2.3.2 Deformation directions: thin-plates.....	31
2.4 Microstructural and mechanical properties	34

2.4.1 Ferrite and its properties	34
2.5 Mathematical modelling and searching methods	37
2.5.1 The genetic algorithm heuristic	37
2.5.2 The response surface methodology	40
2.5.3 The desirability function	42
2.5.4 Applications in the welding process	45
2.6 Bibliography	46
3 Methodology	64
3.1 Gas metal arc welding	64
3.2 The welding rig	65
3.3 The alternating shielding gas technique	68
3.4 Portable arc and shielding gas monitoring systems	69
3.5 Materials	71
3.6 Metallographic preparation	72
3.7 Microscopy analysis	74
3.8 Grain size measurements	75
3.9 Weld geometry	77
3.10 Mechanical testing	78
3.10.1 Hardness measurements	78
3.10.2 Mechanical property testing	78
3.11 Radiographic assessment	80
3.12 Bibliography	81
4 Preliminary analysis of the shielding gas flow rate reduction in the GMAW process	84
4.1 Introduction	84
4.2 Experimental setup	86
4.3 Results and discussion	87
4.3.1 Distortion of the parent material	87

4.3.2	Temperature measurements.....	91
4.3.3	Weld characteristics.....	93
4.3.4	Microstructural characterisation.....	95
4.3.5	Radiography of the joints.....	100
4.3.6	Mechanical property evaluation.....	101
4.4	Conclusions.....	106
4.5	Bibliography.....	107
5	Exploring the benefits of the alternating shielding gas technique...112	
5.1	Introduction.....	112
5.2	Experimental setup	114
5.3	Results and discussion.....	116
5.3.1	Distortion of the parent material.....	116
5.3.2	Temperature measurements.....	118
5.3.3	Weld characteristics.....	120
5.3.4	Microstructural characterisation.....	125
5.3.5	Mechanical properties evaluation.....	131
5.4	Conclusions.....	133
5.5	Bibliography.....	135
6	Exploring the use of N₂ in the alternating shielding gas technique 143	
6.1	Introduction.....	143
6.2	Experimental setup	145
6.2.1	Determining suitable parameters for defect free welds	145
6.2.2	Welding process.....	149
6.3	Results and discussion.....	151
6.3.1	Distortion of the parent material.....	151
6.3.2	Temperature measurements.....	154
6.3.3	Weld characteristics.....	155
6.3.4	Microstructural characterisation.....	161

6.3.5 Mechanical property evaluation.....	166
6.4 Conclusions.....	177
6.5 Bibliography.....	179
7 Heuristic and mathematical optimisation of the GMAW process...	189
7.1 Introduction.....	189
7.2 Methodology.....	192
7.2.1 Experimental setup.....	192
7.2.2 Optimisation process.....	192
7.3 The genetic algorithm phase.....	195
7.3.1 Systematic initialisation: orthogonal arrays.....	195
7.3.2 Fitness stage.....	197
7.3.3 Crossover and mutation stages.....	198
7.4 The response surface methodology phase.....	201
7.5 The desirability function phase.....	203
7.6 Results and discussion.....	205
7.6.1 Welding process optimisation.....	205
7.6.2 Experimental validation.....	213
7.7 Conclusions.....	225
7.8 Bibliography.....	226
8 Thesis conclusion.....	236
8.1 Final remarks.....	236
8.2 Future contributions.....	239
Appendix A - LabVIEW: visual programming.....	241
Appendix B - Coding in Java and R.....	249
Appendix C - All-weld tensile test plots.....	293

Chapter 1

Introduction

1.1 Background

Introduced in the 1920s [1.1-1.3], the gas metal arc welding (GMAW) process was originally created to join aluminium and other non-ferrous metals, being later on expanded to join a broader range of metallic materials. Through this technique, a shielding gas is supplied to protect the molten pool from atmospheric gases such as O_2 and N_2 that might cause porosity development [1.4-1.7]. This protective gas ionises due to the intense electric current [1.4, 1.8], forming an arc plasma that melts an electrode fed through a welding torch, joining the parts together.

The unique thermodynamic and transport properties of each gas influence arc characteristics such as the temperature gradient and electric fields, impacting the weld shape and microstructure of the joint for instance [1.4, 1.5, 1.8, 1.9]. Moreover, when joining metals like high strength low alloy steels, $ArCO_2$ mixtures and pure He are preferred compared to gases such as N_2 due to the reactive behaviour above certain temperatures of the latter, resulting in blowholes within the joint [1.6, 1.10-1.16].

The shielding gas flow rate (SGFR) also influences the weld integrity [1.3, 1.4, 1.17-1.21]. SGFRs above or below certain thresholds can be

deleterious to the final joint and harmful effects include irregular coverage of the weld pool, porosity development and excessive spatter formation [1.17, 1.22, 1.23]. However, the complexity involved in establishing an optimum SGFR results in choices for the flow rates based on preference or experience. Advancements in the GMAW have shown the importance of a dynamic fluidity within the molten pool during the welding process since it influences the weld geometry, penetration of the joint and porosity reduction, impacting the weld quality [1.1, 1.2, 1.5, 1.19].

The alternating shielding gas method has been proposed to improve this dynamic behaviour and, consequently, the properties of the joint. Differing from the premixed gas supply, in this technique the discrete supply of shielding gases takes advantage of their different properties, creating three autonomous phenomena [1.2, 1.3, 1.19]: 1) arc pressure variation, 2) varying weld pool fluidity, 3) peaks in the arc pressure. Literature [1.2, 1.3, 1.18, 1.19, 1.24, 1.25] demonstrated that by alternating the protective gases, benefits like greater penetration of the weld, reduced heat transfer to the workpiece and higher travel speeds were achieved, increasing productivity and reducing costs.

Greater productivity and lower costs in the welding process have also been attempted by employing mathematical models and search methods such as the response surface methodology, the desirability function and the genetic algorithm [1.26-1.37]. The response surface methodology is a multi-response optimisation to mathematically and statistically relate control variables and responses, while the desirability function optimises the many conflicting responses combining them into a compound function. The genetic algorithm approach is a technique that heuristically searches for an ideal solution using a basic Darwinian evolution principle through genetic selection. Employed during

experiments in this study, the aforementioned approaches were capable of finding optimum parameters for the joining process by correlating input and output variables through a reduced amount of experiments using N₂.

1.2 Research purpose

Previous studies [1.1, 1.3, 1.18, 1.19, 1.24, 1.38-1.42] have investigated gases like Ar, CO₂ and He as well as different frequencies between the respective protective gases using the alternating shielding gas method. Yet, the available literature [1.1-1.3, 1.17-1.19, 1.38, 1.43] related to the alternating shielding gas technique has been limited in terms of its performance under reduced SGFRs or increased travel speeds of the welding torch. Additionally, N₂ as a protective gas has not been considered to weld low alloy steels due to its reactive behaviour, since it results in the formation of porosity within the fusion zone [1.6, 1.10-1.16].

Exploring the above-mentioned limitations is the challenge of this thesis. In this study the use of the alternating shielding gas method in the GMAW process is investigated and extended both experimentally and computationally. The main objectives in this work will be:

- Extend the literature studies carried out regarding gas wastage reductions, defining further minimum limits to the SGFR in a draft-free environment without compromising the weld integrity.
- Investigate the effect of employing the alternating shielding gas method under low SGFRs, evaluating the impact of this novel technique in features such as distortion of the workpiece and weld shape.

- Implement methods to improve mechanical properties of the joint, namely strength and hardness using an alternating shielding gas composition of N₂ mixtures and He.
- Expand the shielding gas alternatives and study different protective options utilising the discrete gas supply technique.
- Ameliorate the joining process timing with faster welding speeds through the alternating shielding gas method.
- Implement microstructural improvements of the joint as well as porosity reductions when employing N₂ mixtures alternated with He by increasing the travel speed of the welding torch.
- Develop mathematical models and search methods to optimise the distortion mitigation, temperature reduction and grain refinement when N₂ mixtures are supplied alternately.

1.3 Thesis structure

This thesis is subdivided in chapters; background details and experimental methods are described in chapters 2 and 3, whilst the remaining chapters investigate factors such as reductions in the SGFR, different shielding gas mixtures and faster GMAW procedures under the alternating shielding gas technique.

Chapter 2 encompasses a general review of the types of shielding gases employed in the GMAW process and the alternating shielding gas approach. The various modelling methods employed in this work are also considered, namely the application of the genetic algorithm, response surface methodology

and desirability function. Chapter 3 presents the experimental setup, quantification systems and the theory of procedures employed throughout this study.

Preliminary analysis regarding reductions in the SGFR under a premixed gas supply with varied nozzle diameters are initially discussed in chapter 4. The various experimental conditions were carried out in order to clarify the SGFR reduction vs. nozzle constriction outcomes, namely distortion, welding geometry and joint temperature fields.

Chapter 5 continues exploring the reduction in the SGFR by introducing the alternating shielding gas method with four different SGFR combinations under two frequencies. Features such as the workpiece distortion, the temperature of the joint, and the microstructural and mechanical properties of the weld were analysed.

In chapter 6, Ar5N₂ mixture alternated with He is introduced as the shielding gas to extend the benefits of utilising the alternating shielding gas technique. Increases in both the travel speed of the welding torch and the wire-feed speed were analysed in terms of joint quality by reducing the heat transfer while promoting faster procedures.

Chapter 7 optimises the use of N₂ with the alternating shielding gas method via mathematical models and searching methods. By employing the genetic algorithm, response surface methodology, and desirability function, input variables (wire-feed speed, voltage and travel speed) are correlated to outputs namely the distortion of the weldment, the temperature of the joint and the grain size of the fusion zones.

The final chapter concludes the main findings obtained from this thesis, summarises the many outcomes from the proposed work and presents new challenges arisen from this research project.

1.4 Bibliography

- [1.1] S. W. Campbell, A. M. Galloway, N. A. McPherson, and A. Gillies, “Evaluation of gas metal arc welding with alternating shielding gases for use on AA6082T6,” *Proc. Inst. Mech. Eng. Part B J. Eng. Manuf.*, vol. 226, no. 6, pp. 992–1000, 2012.
- [1.2] Y. H. Chang, “Improve GMAW and GTAW with alternating shield gases,” *Weld. J.*, vol. 85, no. 2, pp. 41–43, 2006.
- [1.3] S. W. Campbell, A. M. Galloway, and N. A. McPherson, “Techno-economic evaluation on the effects of alternating shielding gases for advanced joining processes,” *Proc. Inst. Mech. Eng. Part B J. Eng. Manuf.*, vol. 225, no. 10, pp. 1863–1872, 2011.
- [1.4] B. Mvola and P. Kah, “Effects of shielding gas control: welded joint properties in GMAW process optimization,” *Int. J. Adv. Manuf. Technol.*, vol. 88, no. 9–12, pp. 2369–2387, 2017.
- [1.5] L. L. Wang, F. G. Lu, H. P. Wang, A. B. Murphy, and X. H. Tang, “Effects of shielding gas composition on arc profile and molten pool dynamics in gas metal arc welding of steels,” *J. Phys. D. Appl. Phys.*, vol. 47, no. 46, p. 465202 (14pp), 2014.
- [1.6] P. Kah and J. Martikainen, “Influence of shielding gases in the welding of metals,” *Int. J. Adv. Manuf. Technol.*, vol. 64, no. 9–12, pp. 1411–1421, 2013.
- [1.7] S. Kodama et al., “Nitrogen absorption phenomenon of GTA welding

- with nitrogen-mixed shielding gases: effect of plasma characteristics on nitrogen content in GTA welded metal,” *Weld. Int.*, vol. 29, no. 4, pp. 262–269, 2015.
- [1.8] C. S. Wu, L. Wang, W. J. Ren, and X. Y. Zhang, “Plasma arc welding: Process, sensing, control and modeling,” *J. Manuf. Process.*, vol. 16, no. 1, pp. 74–85, 2014.
- [1.9] M. Tanaka, S. Tashiro, T. Satoh, A. B. Murphy, and J. J. Lowke, “Influence of shielding gas composition on arc properties in TIG welding,” *Sci. Technol. Weld. Join.*, vol. 13, no. 3, pp. 225–231, 2008.
- [1.10] H. Sekiguchi, I. Masumoto, H. Konishi, and I. Suzuki, “Use of Nitrogen in Welding Atmosphere (Report 1),” *J. Japan Weld. Soc.*, vol. 34, no. 2, pp. 128–136, 1965.
- [1.11] T. Kobayashi, T. Kuwana, and R. Kiguchi, “Effect of Alloying Elements on Nitrogen Content of Steel Weld Metals (Report 2),” *J. Japan Weld. Soc.*, vol. 41, no. 4, pp. 415–424, 1972.
- [1.12] T. Kobayashi, T. Kuwana, and R. Kiguchi, “Effect of Alloying Elements on Nitrogen Content of Steel Weld Metals (Report 1),” *J. Japan Weld. Soc.*, vol. 41, no. 3, pp. 308–321, 1972.
- [1.13] T. Wegrzyn, “An attempt at the classification of steel weld metals and arc-welding methods on the basis of nitrogen concentration in the weld metal,” *Weld. Int.*, vol. 13, no. 3, pp. 173–179, 1999.
- [1.14] J. Littleton, J. Lammas, and M. F. Jordan, “Nitrogen Porosity in Gas Shielded Arc Welding of Copper,” *Weld. J.*, vol. 12, pp. 561–565, 1974.
- [1.15] K. V. S. Kumar, S. Gejendhiran, and M. Prasath, “Comparative Investigation of Mechanical Properties in GMAW/GTAW for Various Shielding Gas Compositions,” *Mater. Manuf. Process.*, vol. 29, no. 8, pp.

996–1003, 2014.

- [1.16] D. L. Olson, R. D. Dixon, and A. L. Liby, *Welding: Theory and Practice*. 1990.
- [1.17] S. W. Campbell, A. M. Galloway, and N. A. McPherson, “Techno-economic evaluation of reducing shielding gas consumption in GMAW whilst maintaining weld quality,” *Int. J. Adv. Manuf. Technol.*, vol. 63, no. 6–9, pp. 975–985, 2012.
- [1.18] N. V. Shinde and M. T. Telsang, “Effect of Alternate Supply of Shielding Gases of Tungsten Inert Gas Welding on Mechanical Properties of Austenitic Stainless Steel,” *J. Inst. Eng. Ser. C*, vol. 97, no. 3, pp. 299–307, 2016.
- [1.19] B. Y. Kang, Y. K. D. V Prasad, M. J. Kang, H. J. Kim, and I. S. Kim, “Characteristics of alternate supply of shielding gases in aluminum GMA welding,” *J. Mater. Process. Technol.*, vol. 209, no. 10, pp. 4716–4721, 2009.
- [1.20] R. G. Tazetdinov, O. M. Novikov, A. S. Persidskii, B. A. Khasyanov, E. N. Ivanov, and L. T. Plaksina, “Arc welding in shielding gases with alternate pulsed supply of dissimilar gases,” *Weld. Int.*, vol. 7116, no. May 2015, pp. 1–4, 2012.
- [1.21] American Welding Society, “Choosing Shielding Gases for Gas Metal Arc Welding,” in *Welding Handbook*, vol. 2, no. May, 2008, pp. 32–35.
- [1.22] V. Beyer, S. W. Campbell, G. M. Ramsey, A. M. Galloway, A. J. Moore, and N. A. McPherson, “Systematic study of effect of cross-drafts and nozzle diameter on shield gas coverage in MIG welding,” *Sci. Technol. Weld. Join.*, vol. 18, no. 8, pp. 652–660, 2013.
- [1.23] G. D. Uttrachi, “GMAW shielding gas flow control systems,” *Weld. J.*,

- vol. 86, no. 4, pp. 22–23, 2007.
- [1.24] S. W. Campbell, A. M. Galloway, and N. A. McPherson, “Arc pressure and fluid flow during alternating shielding gases. Part 2: arc force determination,” *Sci. Technol. Weld. Join.*, vol. 18, no. 7, pp. 597–602, 2013.
- [1.25] A. Traidia and F. Roger, “A computational investigation of different helium supplying methods for the improvement of GTA welding,” *J. Mater. Process. Technol.*, vol. 211, no. 9, pp. 1553–1562, 2011.
- [1.26] D. Kim and S. Rhee, “Optimization of Arc Welding Process Parameters Using a Genetic Algorithm,” *Weld. J.*, vol. 80, no. 7, p. 184s–189s, 2001.
- [1.27] D. Kim, M. Kang, and S. Rhee, “Determination of Optimal Welding Conditions with a Controlled Random Search Procedure,” *Weld. J.*, no. August, pp. 125–130, 2005.
- [1.28] S. Mishra and T. DebRoy, “Tailoring gas tungsten arc weld geometry using a genetic algorithm and a neural network trained with convective heat flow calculations,” *Mater. Sci. Eng. A*, vol. 454–455, pp. 477–486, 2007.
- [1.29] P. Sathiya, P. M. Ajith, and R. Soundararajan, “Genetic algorithm based optimization of the process parameters for gas metal arc welding of AISI 904 L stainless steel,” *J. Mech. Sci. Technol.*, vol. 27, no. 8, pp. 2457–2465, 2013.
- [1.30] D. S. Correia, C. V. Gonçalves, S. S. C. Junior, and V. A. Ferraresi, “GMAW welding optimization using genetic algorithms,” *J. Brazilian Soc. Mech. Sci. Eng.*, vol. 26, no. 1, pp. 28–32, 2004.
- [1.31] A. Kumar and T. DebRoy, “Tailoring complex weld geometry through reliable heat-transfer and fluid-flow calculations and a genetic algorithm,”

- Metall. Mater. Trans. A, vol. 36A, no. October, pp. 2725–2735, 2005.
- [1.32] J. P. Jia, H. Zhang, and H. Huang, “Optimization of Welding Process Parameters for Rotating Arc Welding Sensor Based on Genetic Algorithm,” *Mater. Sci. Forum*, vol. 575–578, pp. 769–773, 2008.
- [1.33] D. T. Thao, I. S. Kim, H. H. Na, S. M. Jung, and J. Y. Shim, “Development of mathematical model with a genetic algorithm for automatic GMA welding process,” *Int. J. Adv. Manuf. Technol.*, pp. 837–847, 2014.
- [1.34] S. Bag and A. De, “Development of efficient numerical heat transfer model coupled with genetic algorithm based optimisation for prediction of process variables in GTA spot welding,” *Sci. Technol. Weld. Join.*, vol. 14, no. 4, pp. 333–345, 2009.
- [1.35] D. S. Correia, C. V. Gonçalves, S. S. Da Cunha, and V. A. Ferraresi, “Comparison between genetic algorithms and response surface methodology in GMAW welding optimization,” *J. Mater. Process. Technol.*, vol. 160, no. 1, pp. 70–76, 2005.
- [1.36] A. S. Shahi and S. Pandey, “Welding current prediction in GMAW and UGMAW processes using response surface methodology,” *Sci. Technol. Weld. Join.*, vol. 11, no. 3, pp. 341–346, 2006.
- [1.37] D. Kim and S. Rhee, “Optimization of a gas metal arc welding process using the desirability function and the genetic algorithm,” *J. Eng. Manuf.*, vol. 218, pp. 35–41, 2004.
- [1.38] I. Bitharas, S. W. Campbell, A. M. Galloway, N. A. Mcpherson, and A. J. Moore, “Visualisation of alternating shielding gas flow in GTAW,” *Mater. Des.*, vol. 91, pp. 424–431, 2016.
- [1.39] I. S. Kim, J. S. Son, and H. J. K. B. A. Chin, “A study on variation of

- shielding gas in GTA welding using finite element method,” *Manuf. Eng.*, vol. 17, no. 1, pp. 249–252, 2006.
- [1.40] B. Y. Kang, Y. K. D. V Prasad, M. J. Kang, H. J. Kim, and I. S. Kim, “The effect of alternate supply of shielding gases in austenite stainless steel GTA welding,” *J. Mater. Process. Technol.*, vol. 209, no. 10, pp. 4722–4727, 2009.
- [1.41] N. S. Barabokhin et al., “Technological special features of welding 1460 high-strength aluminium alloy,” *Weld. Int.*, vol. 14, no. 6, pp. 468–470, 2000.
- [1.42] S. W. Campbell, A. M. Galloway, and G. M. Ramsey, “A potential solution to GMAW gas flow optimisation.”
- [1.43] F. H. Ley, S. W. Campbell, A. M. Galloway, and N. A. McPherson, “Effect of shielding gas parameters on weld metal thermal properties in gas metal arc welding,” *Int. J. Adv. Manuf. Technol.*, vol. 80, no. 5–8, pp. 1213–1221, 2015.

*“Someone is sitting in the shade today because
someone planted a tree a long time ago”*

Warren Buffett

Chapter 2

Literature review

2.1 The protective gases

Shielding gases are added during the arc welding process to protect the molten pool from direct contact to atmospheric gases namely oxygen (O_2) and nitrogen (N_2), which may result in undesirable features such as porosity within the joint [2.1-2.5]. The ionisation of the shielding gas creates an arc plasma state during the gas metal arc welding (GMAW) that works as a path to current flow and consequent energy transfer. The arc plasma is influenced by the specific thermophysical properties of the type of gas and impacts features like penetration, travel speed of the welding torch, weld shape and metal vapour development [2.6-2.9].

2.1.1 Chemical activity

A number of protective gases are available for use in the GMAW process, each with its particular properties (see Table 2.1). The reactivity of a shielding gas defines how easily it will react within the arc-weld system, where the gas is either active (oxidising or reducing) or inert [2.3].

Active gases are split into oxidising and reducing. Oxidising gases form oxides and have O_2 as part of its composition. Reducing gases reduce the

formation of oxides in the liquid metal by bonding to O₂. Inert gases do not react chemically within the weld pool. Existing inert gases include argon (Ar), helium (He), krypton (Kr), neon (Ne), radon (Rn) and xenon (Xe). Yet, considering the price and rarity, Ar and He are preferred as shielding gases in the welding industry. At room temperature N₂ is inert. However, it becomes reactive within the arc plasma system due to the high temperatures experienced [2.10-2.12].

Table 2.1 Shielding gas properties [2.3, 2.10, 2.13].

Gas type	Composition in air (vol%)	Density [kg/m ³] ^a	Specific gravity to air ^a	Atomic or molecular weight	Ionisation energy [eV] ^b	Reactivity during welding
Ar	0.934	1.784	1.380	39.948	15.76	Inert
CO ₂	0.033 ^c	1.977	1.529	44.011	13.78	Oxidising
He	5.2 x 10 ⁻⁶ ^c	0.178	0.138	4.002	24.56	Inert
H ₂	0.5 x 10 ⁻⁶ ^c	0.090	0.070	2.016	13.60	Reducing
N ₂	78.084	1.251	0.968	28.013	14.53	Reactive
O ₂	20.946	1.429	1.105	31.998	13.62	Oxidising

a Specified at 0 °C and 0.101 MPa (1.013 bar)

b 1 eV = 1.6 x 10⁻⁶ J

c Not extracted from the atmosphere

2.1.2 Transport coefficients and thermodynamic properties

The transport and thermodynamic properties of the shielding gas influence directly the arc plasma behaviour, namely its temperature gradients, and electric and magnetic fields [2.8, 2.14, 2.15]. For instance, increasing the density and enthalpy of the arc plasma induces constriction in the current flow, greater current density and arc constriction, whilst higher electrical conductivity affects the temperature and velocity distributions in the arc [2.16, 2.17].

Despite the possibility of estimating many of these properties experimentally, methods of calculation still provide the most reliable data [2.15, 2.18-2.20]. However, uncertainties in the values of the molecular potentials add large variations to the calculated data of the transport coefficients. Additionally, to simplify calculations most computational modelling of atmospheric plasmas consider the ionised gas within a local thermodynamic equilibrium [2.15, 2.18-2.20]. Some gas properties and coefficients are presented in Fig. 2.1 for Ar, He, H₂ and N₂ [2.14]. The properties of carbon dioxide (CO₂) are similar to those of the Ar shielding gas and can be found elsewhere [2.16, 2.21, 2.22].

The specific heat capacity and thermal conductivity show the dissociation and ionisation peaks [2.23]. As molecular gases, H₂ and N₂ first dissociate at temperatures of around 3500 and 7000 K, respectively. The extra peaks represent the temperature of ionisation and occur at around 15000 K for Ar, H₂ and N₂ and 22000 K for He [2.23].

Viscosity increases with the square root of the atomic mass and decreases with the collision integral [2.23]. Due to its low mass, H₂ exhibits low

viscosity at all temperatures. Ar, He and N₂ have similar viscosities up to 10000 K, after which the viscosity of He is greater. Murphy et al. [2.14] showed that increasing the viscosity reduced the axial flow velocity near the arc axis, affecting the arc pressure and shear stress at the anode, which influences the final weld shape [2.24].

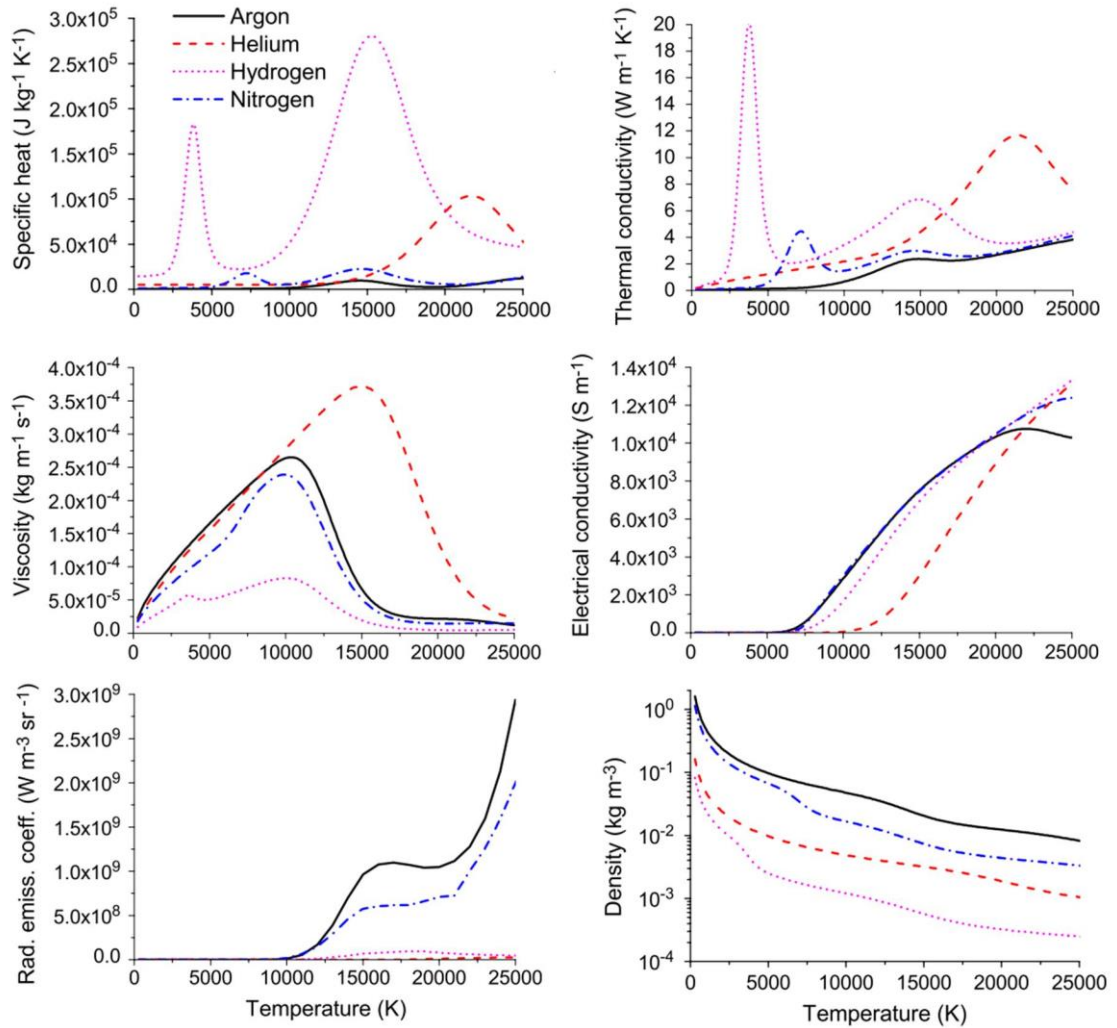


Fig. 2.1 Variations of the specific heat, thermal conductivity, electrical conductivity, viscosity, density and net radiative emission coefficient with temperature for Ar, He, H₂ and N₂ at 1 atm (adapted from [2.14]).

The electrical conductivity is proportional to the electron density and occurs after the gas ionisation. Measurements show that Ar, N₂ and H₂ have similar electrical conductivities, which are greater than that of He [2.14, 2.22, 2.23]. Hence, the latter requires higher temperatures for ionisation to occur. The radiative emission coefficient of H₂ and He is lower compared to Ar and N₂ due to their reduced number of electrons: one and two, respectively.

The density is mainly determined by the atomic or molecular weight of the gas. It decreases upon dissociation, ionisation and under high temperatures due to changes in the kinetic energy. For instance, the greater density of Ar (see Fig. 2.1) lowers its plasma axial velocity compared to He, affecting the weld shape properties [2.25, 2.26].

2.1.3 Arc properties

2.1.3.1 Pure shielding gas supply

The shielding gas type influences important properties of the arc, including its voltage, temperature and flow fields. Computational studies [2.14, 2.22, 2.23] in gas tungsten arc welding (GTAW) assessed the arc properties of Ar, He, H₂, N₂ and CO₂ (see Fig. 2.2). Findings showed that Ar has the lowest arc voltage (10.8 V), arc temperature (17000 K), anode temperature (600 K) and flow velocity (217 m/s). Apart from He and CO₂ (to some extent), all the other gases exhibited the typical bell shape found in most GTAW arcs. The highest arc heat flux to the water-cooled copper was found in the H₂ case (2500 K) [2.14, 2.23]. This was correlated to the clustered current density at smaller radii and greater thermal conductivity near the water cooled copper central regions [2.15]. N₂, CO₂ and He displayed similar arc properties, with differences in the maximum flow velocity and arc shape.

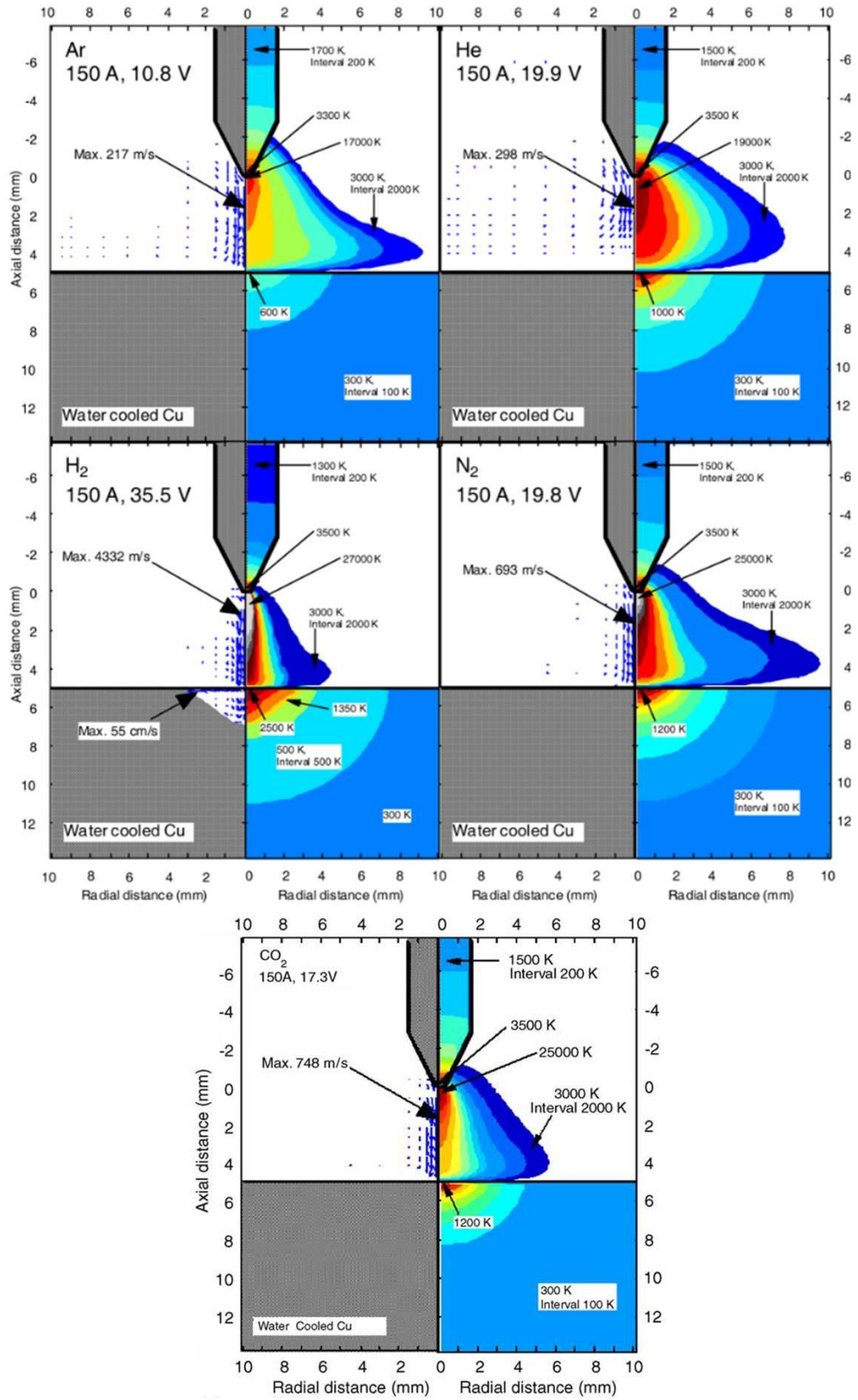


Fig. 2.2 Velocity fields and temperatures for Ar, He, H₂, N₂ and CO₂ arcs. Current: 150 A; arc length: 5 mm (adapted from [2.14, 2.23]).

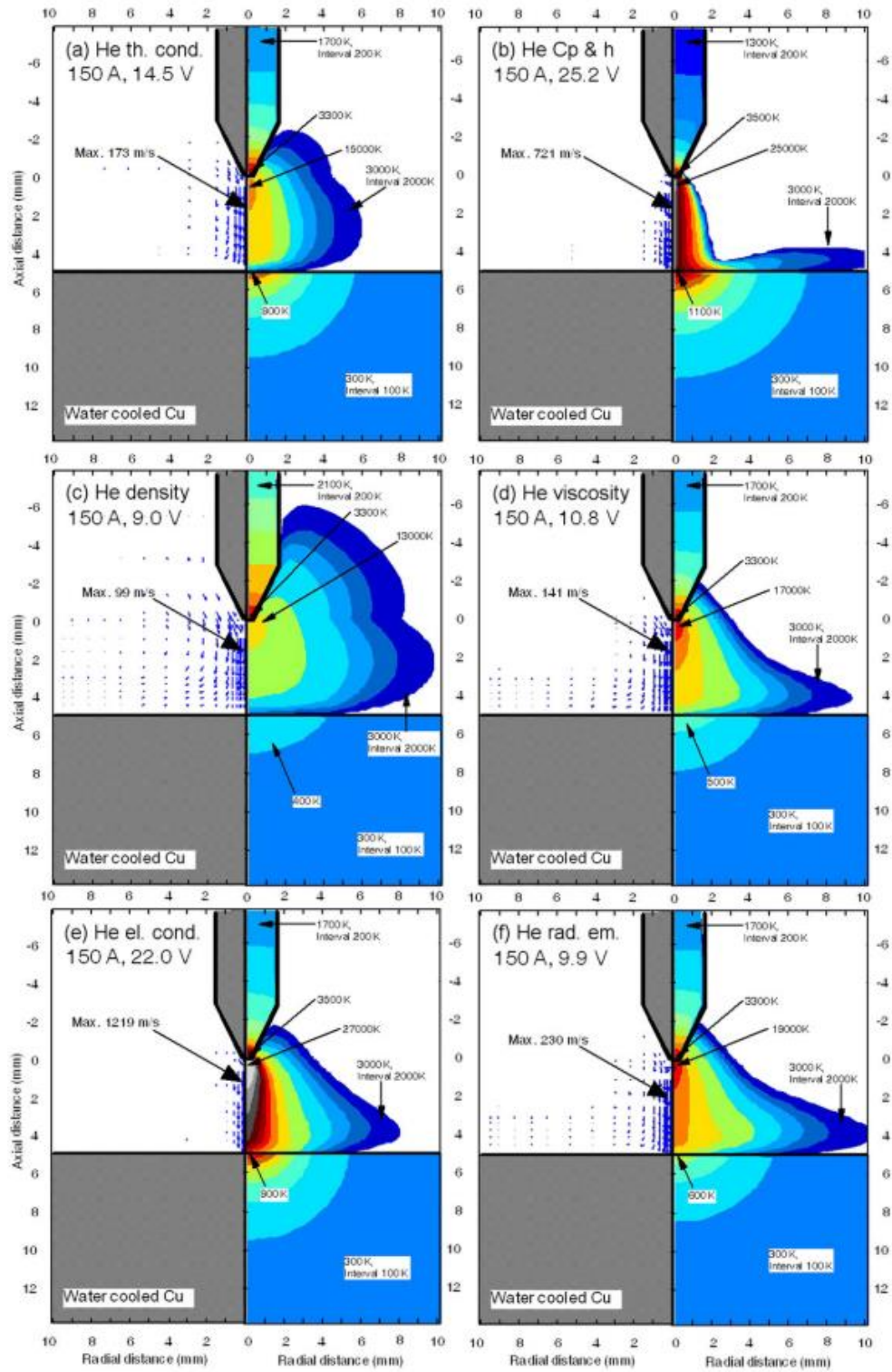


Fig. 2.3 Imaginary gases (150 A; 1 atm): velocity and temperature profiles. Ar with (a) thermal conductivity, (b) specific enthalpy and heat, (c) mass density, (d) viscosity, (e) electrical conductivity, and (f) net radiative emission coefficient modified to that of He [2.14].

Being aware and understanding the many arc plasma properties in advance based on the selected shielding gas adds great advantages to the welding process. For instance, Ar is expected to induce lower heat input to the workpiece than He due to the lower arc voltage of the former [2.8, 2.10, 2.27]. Conversely, increased weld penetration and travel speeds of the welding torch are achieved by employing He as a protective gas compared to Ar due to the greater ionisation potential and consequent arc plasma constriction of the former [2.26, 2.28, 2.29].

Considering that almost all the thermophysical properties of the shielding gases differ considerably from one another, the isolation of a particular property controlling a certain effect in the arc plasma during experimental work becomes difficult [2.14]. To overcome this, Murphy et al. [2.14] simulated imaginary gases by replacing one specific thermophysical property of a gas (Ar) by that of another gas (He). This helped to understand how each gas property considered systematically affected the arc behaviour (see Fig. 2.3).

The study [2.14] found greater arc constriction by replacing the specific heat and enthalpy of Ar by that of He. Conversely, no significant changes were found in the arc shape by changing the electrical conductivity and net radiative emission properties. Increasing the thermal conductivity to that of He promoted evident arc constriction, while the viscosity significantly reduced the axial flow velocity near the arc axis.

2.1.3.2 Mixed shielding gas supply

As a commonly employed shielding gas, Ar is relatively cheap and inert [2.10, 2.30]. Yet, its low heat flux to the workpiece limits the penetration of the weld pool due to a moderate and expanded arc compared to that of He [2.15, 2.26]. This is a critical problem when welding high thermal conductivity metals like aluminium since it limits the weld depth [2.23, 2.31]. Hence, Ar is either replaced or mixed with shielding gases such as CO₂ or N₂.

The higher specific heat of ArCO₂ mixtures is found to cause increased maximum temperature of the arc, jet velocity and its constriction to some extent compared to the pure Ar case, enhancing the current density [2.18, 2.32]. This is related to improvements in the thermal and electrical conductivities and heat capacity. Furthermore, studies [2.16, 2.33, 2.34] concluded that additions of CO₂ to Ar increased the heat transfer to the molten pool, impacting the final weld shape with increased weld width and penetration.

Computational analysis by Murphy et al. [2.15] investigated the use of protective ArN₂ mixtures (see Fig. 2.4). Findings showed that small amounts of N₂ added to Ar increased significantly the thermal conductivity, specific heat and maximum arc temperature. Conversely, changes in both the viscosity and electrical conductivity were negligible. In contrast to the pure Ar case (see Fig. 2.2) there was some constriction of the ArN₂ arc attributed to the thermal pinch effect, causing greater concentration of the heat flux near the anode. Such constriction effect was found in the pure N₂ arc plasma, which exhibited higher magnetic pinch pressure compared to the Ar arc plasma [2.35, 2.36].

The described properties of He and N₂ will be explored in chapters 5, 6 and 7, since they are expected to induce greater penetration of the molten pool while reducing the heat input. Adding N₂ and He as protective gases will also permit faster welding procedures, which were performed utilising the alternating shielding gas method (discussed in section 2.2).

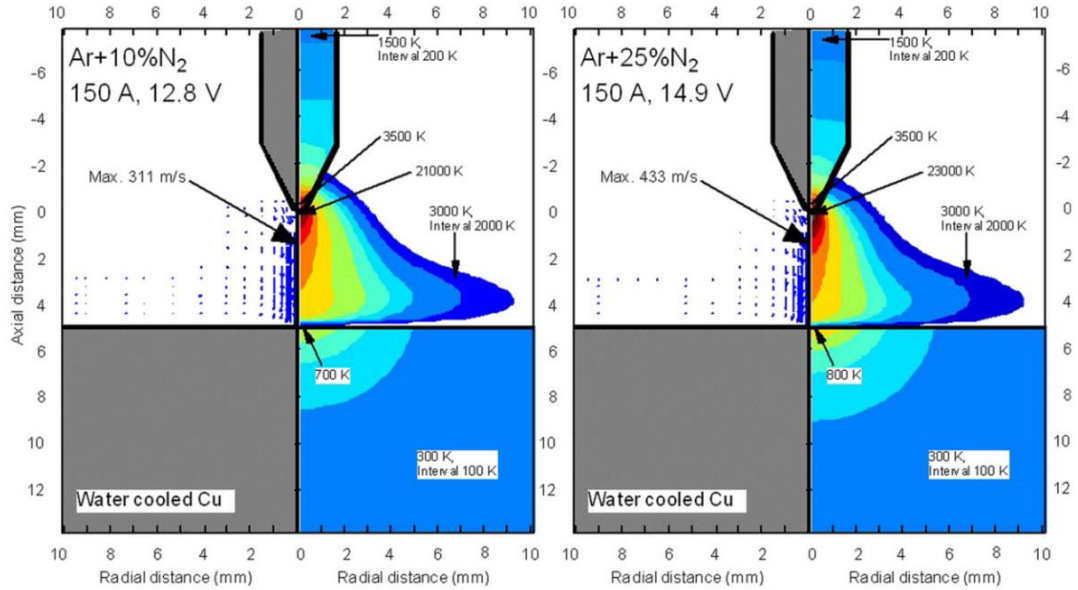


Fig. 2.4 Velocity fields and temperature for Ar10N₂ and Ar25N₂ mixtures. Current: 150 A; arc length: 5 mm (adapted from [2.15]).

2.1.4 Metal vapour

Metal vapour is vaporised matter formed during the welding process, which emanates from both the melted workpiece and the molten wire tip in the GMAW process [2.37, 2.38]. The presence of metal vapour within the arc plasma is known to modify its thermodynamic and transport properties [2.38-2.43]. For instance, it is estimated to enhance the radiative emission coefficient, with lower temperature and higher constriction of the arc [2.9, 2.11, 2.37, 2.42, 2.44-2.46]. As a consequence, lower heat input to the system and greater

penetration of the weld are expected [2.28, 2.47, 2.48]. Additionally, the existence of metal vapour modifies the size and shape of the weld pool and produces welding fume, which is a health concern [2.9, 2.44].

Tashiro et al. [2.37], using computational simulations, added metal vapour (5 to 30%) to the He arc-plasma system, which caused reduced arc voltage (see Fig. 2.5). The plasma temperature fell by 6000 K on the fringe of the arc column and by 400 K in the surroundings of the water cooled copper due to the concentration of vaporised metal near low temperature regions just above the weld pool surface [2.44]. There was clear constriction of the arc and lower jet velocity (see Fig. 2.5 (B)) compared to the case of pure He (see Fig. 2.5 (A)).

The addition of 5% of iron vapour to the simulated model [2.37] was enough to significantly improve the electrical conductivity of the arc. At temperatures below 15000 K the arc plasma electrical conductivity in the presence of metal vapour was found to be 10x higher than that of pure He, but did not differ in temperatures above 15000 K. Conversely, the radiation heat loss increased almost proportionally to the amount of metal vapour developed in the arc region [2.37, 2.44].

In this thesis the development of metal vapour within the He arc plasma [2.11, 2.44, 2.45] was explored, assisted by the choice of such gas during the alternating shielding gas technique (discussed in section 2.2). By alternating Ar5N₂ and He, lower arc temperature of the latter caused by the metal vapour formation [2.9, 2.11, 2.37, 2.42, 2.44-2.46] is expected to hinder the dissociation of N₂ and its consequent absorption by the molten pool [2.11, 2.45], helping to eliminate the porosity formation [2.5, 2.10, 2.49-2.52].

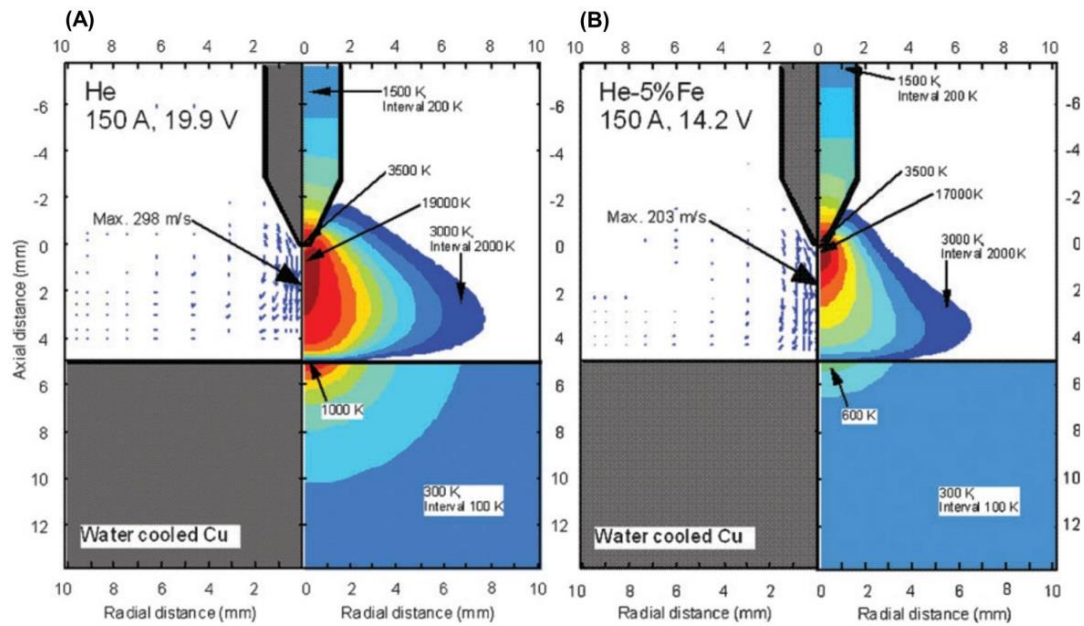


Fig. 2.5 Fluid flow velocity and temperature distribution of the arc plasma (2D model). (A) Pure He. (B) He - 5%Fe (adapted from [2.37]).

2.2 The alternating shielding gas method

2.2.1 Background

First introduced in 1967 [2.53-2.55], the alternating shielding gas technique comprises the supply of two different shielding gases or gas mixtures in an alternately manner. This method provides better control of the arc features and characteristics of the final joint due to the transitory thermophysical behaviour of the arc plasma.

Cunningham [2.53] was the first author to propose the alternating shielding gas method, describing an apparatus that varied the shielding gas composition, such as Ar and CO₂, and caused pulsations in the current through a welding or cutting arc. Since the arc was not maintained continuously, the average weld current would then be reduced, the weld pool temperature diminished, and overheating prevented.

Studies involving the alternating shielding gas method with shielding gases such as pure Ar and He [2.6, 2.25, 2.28, 2.55-2.59] and Ar₂₀CO₂ and pure He [2.30, 2.60] have been carried out using both GMAW and GTAW processes. Materials such as aluminium alloys [2.7, 2.28, 2.58, 2.59, 2.61] and stainless and carbon steels [2.6, 2.30, 2.54, 2.57, 2.61-2.63] were also utilised, exhibiting improvements to the overall welding process.

2.2.2 Benefits of employing the alternating shielding gas method

Many authors [2.2, 2.6, 2.7, 2.28, 2.30, 2.54, 2.55, 2.58] reported benefits by employing the alternating shielding gas technique during the arc welding process in contrast to the constant gas supply method (hereafter called premixed method).

In terms of productivity and cost, decreased edge preparation due to the improved penetration from the He arc [2.30, 2.54, 2.63] and higher momentum transfer towards the molten pool from peaks in the arc pressure [2.28, 2.55] were achieved. Utilising He in the alternating shielding gas method permitted increased travel speeds of the welding torch due to the higher thermal conductivity and arc energy, allowing for better fusion of the joint [2.28, 2.30, 2.57]. Furthermore, the requirement for post-welding straightening (distortion control) was minimised due to the lower heat input to the workpiece from the reduced contact between the He arc and the molten pool, and the higher travel speeds [2.7, 2.28, 2.30, 2.57, 2.64].

Faster welds, edge preparation reduction and lower deformation of the weldment add cost savings to the welding procedure. For instance, a cost

analysis carried out by Stuart et al. [2.30] demonstrated that the travel speed has a major impact on the welding cost. The study [2.30] showed that the travel speed increase contributed to 17% savings in comparison to the total costs of each gas configuration.

The alternating shielding gas method was able to improve the mechanical and microstructural properties of the joint [2.28, 2.30, 2.59, 2.63]. A more homogeneous and refined microstructure was found due to the lower heat input and consequent accelerated cooling, promoting greater strength and hardness of the joints [2.28, 2.30, 2.59, 2.63].

Another advantage of employing the alternating shielding gas method is the porosity reduction in the fusion zone. Porosity is known to reduce the joint strength [2.65-2.67]. The dynamic action from the alternating shielding gas method usage assisted the buoyancy effect with the removal of bubbles in the molten pool, further reducing the porosity development within the weld [2.28, 2.30, 2.58, 2.67].

Despite its many advantages, it is important to highlight a few drawbacks from the alternating shielding gas technique. For instance, it would require extra hoses and adjustments in the nozzle, which can be difficult depending on the location of the manufacturing process. Additionally, He could impose difficulties in terms of cost, since it is not a cheap shielding gas compared to Ar and N₂.

2.2.3 Understanding the alternating shielding gas mechanism

The alternation of two different shielding gases results in a dynamic welding pool behaviour. This dynamic action is explained by three discrete

phenomena [2.7, 2.30, 2.58], which are the ionisation characteristics of different gases, causing variations in the arc pressure, the dissimilar weld pool temperature of different gases and consequent variations in the weld pool fluidity, and the variations in the pressure impulse by changes in the shielding gas supplied, resulting in arc pressure peaks.

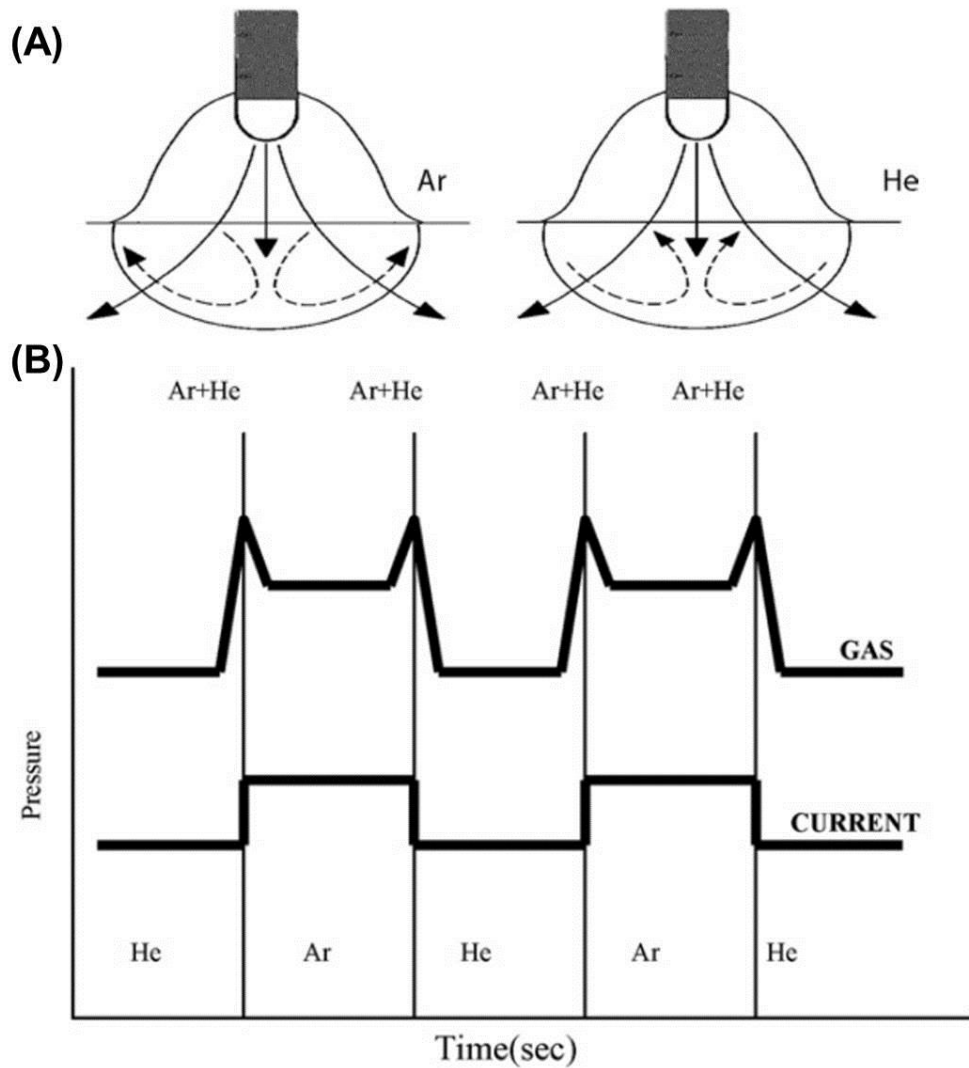


Fig. 2.6 Alternating shielding gas method. (A) Weld pool behaviour. (B) Arc pressure variations (adapted from [2.57, 2.58]).

For instance, the lower molten pool temperature caused by the Ar arc plasma, and consequent low fluidity, alternated with He, which behaves in an opposite manner, generates a dynamic flow within the molten pool. Additionally, the higher Ar welding current in contrast to that of He induces a higher arc pressure, changing the weld pool dynamics (Fig. 2.6 (B)), i.e. a downwards movement in the central region of the weld pool is expected from Ar, while He would create an upwards disturbance (Fig. 2.6 (A)) [2.25, 2.58, 2.68, 2.69].

A dynamic pressure around 24 times greater than that of He was found to be produced by Ar [2.24, 2.63]. The pressure in the arc column is defined by both the static and dynamic pressures, where the former is determined by the intensity of the arc current [2.24, 2.25, 2.63]. In the work published by Tazetdinov et al. [2.63], the arc current was found to be approximately constant during the alternating cycle. Conversely, there was notable change in the dynamic pressure; directly related to the density of the gas.

Both the arc drag forces and the Marangoni stress are significant in shaping the weld pool [2.15, 2.62]. The drag forces increase according to the velocity parallel to the molten pool surface and the viscosity. The Marangoni stress changes with surface tension variations ($d\gamma$) on the weld pool, ruled by the gradient of temperature (dT). For most pure metals and those containing surface-active elements such as O and S below a threshold level, the surface tension coefficient $d\gamma/dT$ is negative. However, beyond the threshold, $d\gamma/dT$ turns to a positive value. For $d\gamma/dT < 0$, there is radial outwards and axial upwards circulation of the molten pool, resulting in a shallower weld shape. Conversely, for $d\gamma/dT > 0$, there is the development of a radially inwards and axially downwards flow, increasing the weld penetration.

A more detailed understanding of the weld pool behaviour of Ar and He was provided by Traidia and Roger [2.62]. Using computational fluid dynamics analysis, temperature fields as well as the fluid flow within the molten pool were described for both the premixed and alternate cases and a more complex fluid flow was presented compared to Kang et al. [2.57].

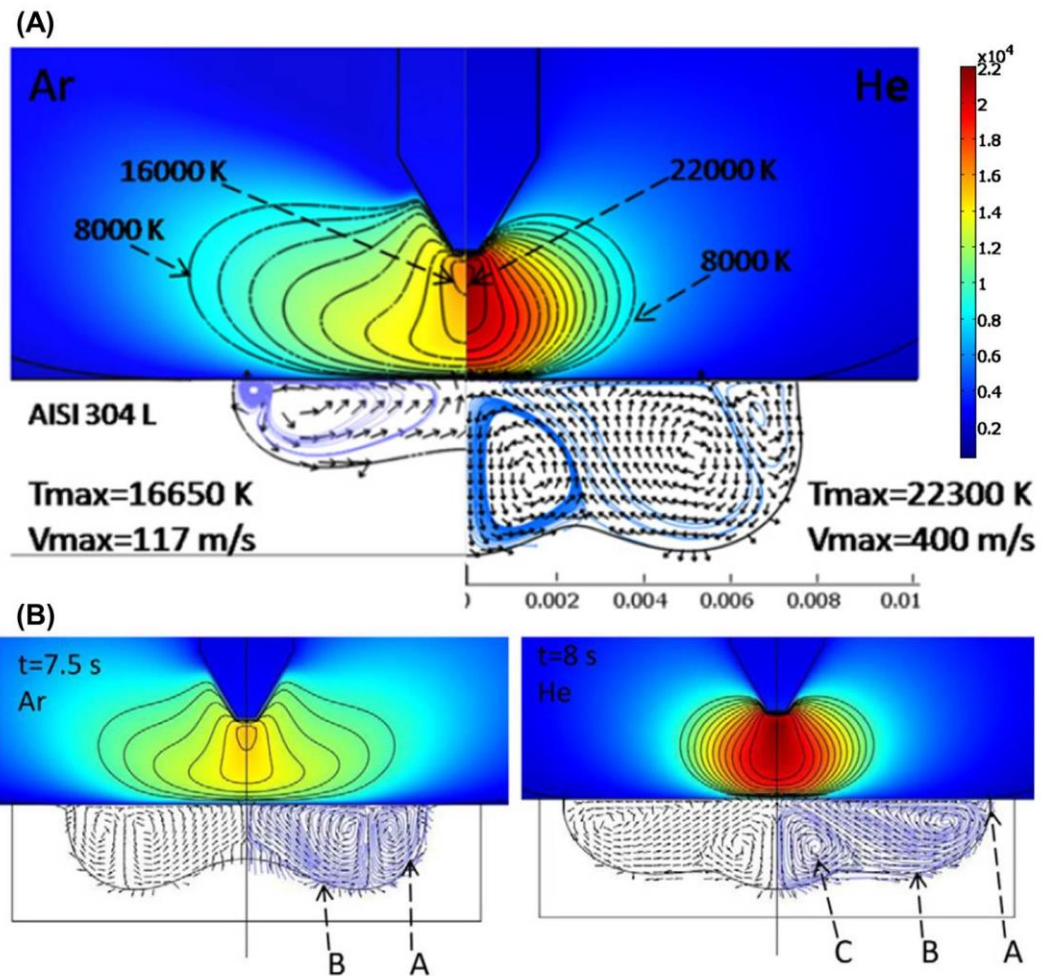


Fig. 2.7 Streamlines, weld pool flow and temperature measurements. (A) Comparison between pure Ar (left) and pure He (right) arcs at the final time of 8 s. (B) Alternate Ar (left - 7.5 s) and He (right - 8 s) (adapted from [2.62]).

The alternation of Ar and He in the Traidia and Roger's study [62] (see Fig. 2.7 (B)) generated a dynamic weld pool where inwards (letter A) and

outwards (letter B) Marangoni shear stress vortices were coupled with an electromagnetically induced vortex (letter C). The latter increased the penetration of the weld pool and emerged due to the presence of He, which exhibited electromagnetic forces 14 times greater than pure Ar. The heat flux density to the workpiece was improved by the higher thermal conductivity and arc constriction of He (see Fig. 2.7 (A)) [2.28, 2.30, 2.57]. Additionally, similar dimensions of the weld pool to that of pure He were found, suggesting that the use of the alternating shielding gas method could diminish manufacturing costs [2.7, 2.28, 2.30, 2.57, 2.64].

2.3 Distortion

Distortion is caused by the non-steady expansion-contraction response during the arc welding process attributed to the heat induced into the metal structure [2.70-2.73]. It is an undesirable outcome of great concern in many industries and manufacturing areas, namely ship-building, which has been moving towards thinner, high strength steels [2.64, 2.74].

2.3.1 Distortion development

As an important outcome to be controlled and reduced in the welding process, the distortion of all welded structures was measured and assessed throughout this thesis. The schematic diagram of a welding procedure is presented in Fig. 2.8, which includes an analysis of the weld and the workpiece, temperature variations along several cross-sections and thermal-stress components parallel to the weld [2.75]. Metal is deposited by the welding torch,

which is located at the origin O and progresses at a speed v along the x axis of the workpiece.

The cross-section A-A situated ahead of the origin is still to be affected by the heat source and changes in the temperature and thermal stresses are negligible. Section B-B crosses the welding arc and consequently exhibits a very steep temperature distribution. The expansion of the molten pool just underneath the welding torch due to high temperatures is restrained by the cooler surroundings, explaining the compressive stress closer to the arc region. Hence, to balance these compression stresses, tensile stresses develop in regions away from the arc.

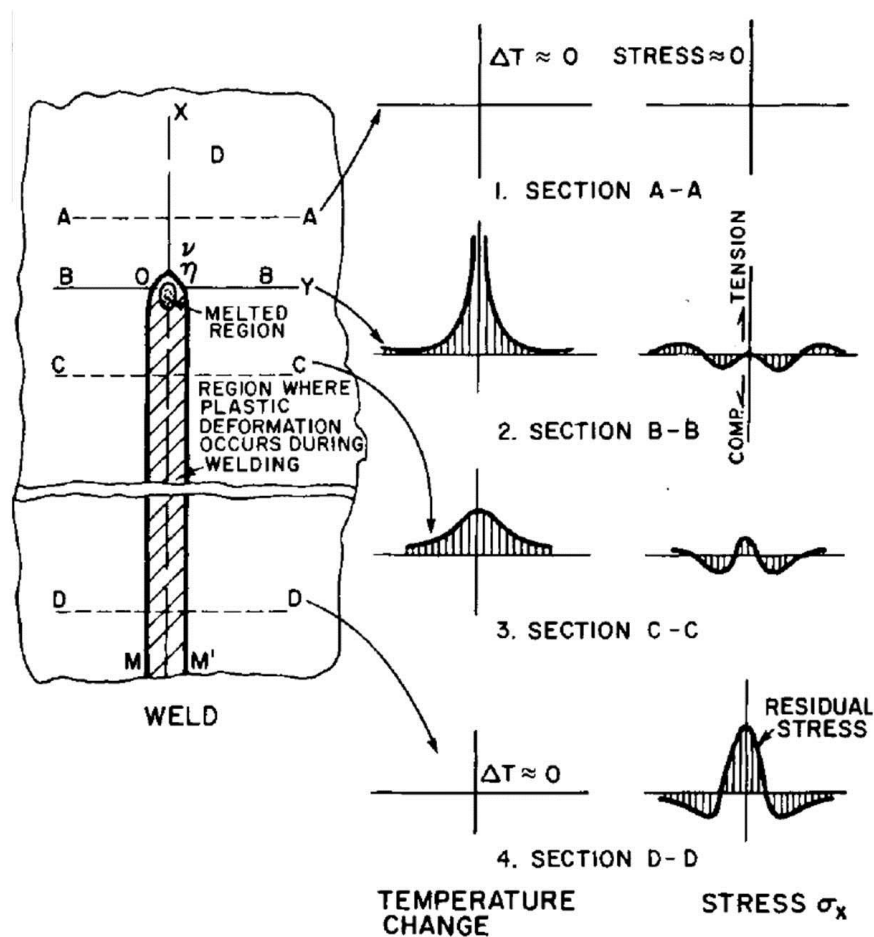


Fig. 2.8 Schematic representation of a weld and its temperature and stress variations during the joining process (adapted from [2.75]).

In section C-C the weld is cooler compared to the B-B section, giving space to shrinkage initiation of both the weld and base metal and the development of tensile stresses. Subsequently, thermal equilibrium is expected with the final cooling stage occurring by convection. Additionally, an almost uniform thermal contraction of the material is found at this point.

Without thermal gradients and at room temperature, the workpiece exhibits peak tensile stress surrounding the weld area and compressive stresses further away (section D-D). If the thermal gradients from the process lead to thermal stresses that surpassed the yield stress of the material, permanent deformation will occur.

2.3.2 Deformation directions: thin-plates

Many factors influence the final distortion of the workpiece, namely the material type, the positioning of restraints, the sequence of welding, the residual stresses and the heat input [2.28, 2.72, 2.73, 2.76, 2.77]. The Ishikawa diagram in Fig. 2.9 details other important factors that affect deformations in the workpiece [2.78].

Most of the distortion of the workpiece takes place during the cooling phase [2.54, 2.74, 2.79]. However, the plate deformation develops in many directions during the entire procedure, i.e. from the first contact between the electrode and the workpiece until the complete cooling of the entire welded structure [2.73]. Fig. 2.10 exemplifies such movements separately for better clarity.

Shrinkage in the transverse direction of the weld culminates in transverse in-plane contraction (see Fig. 2.10 (A)), which is influenced by the

average width of the joint. The usual weld shape, where the top surface of the fusion zone narrows towards its base, causes uneven stress development and consequent transverse angular contraction (see Fig. 2.10 (B)). Thus, welding procedures and edge preparations that lower differences between the top and root widths of the fusion zone are important to minimise the transverse angular contraction effect.

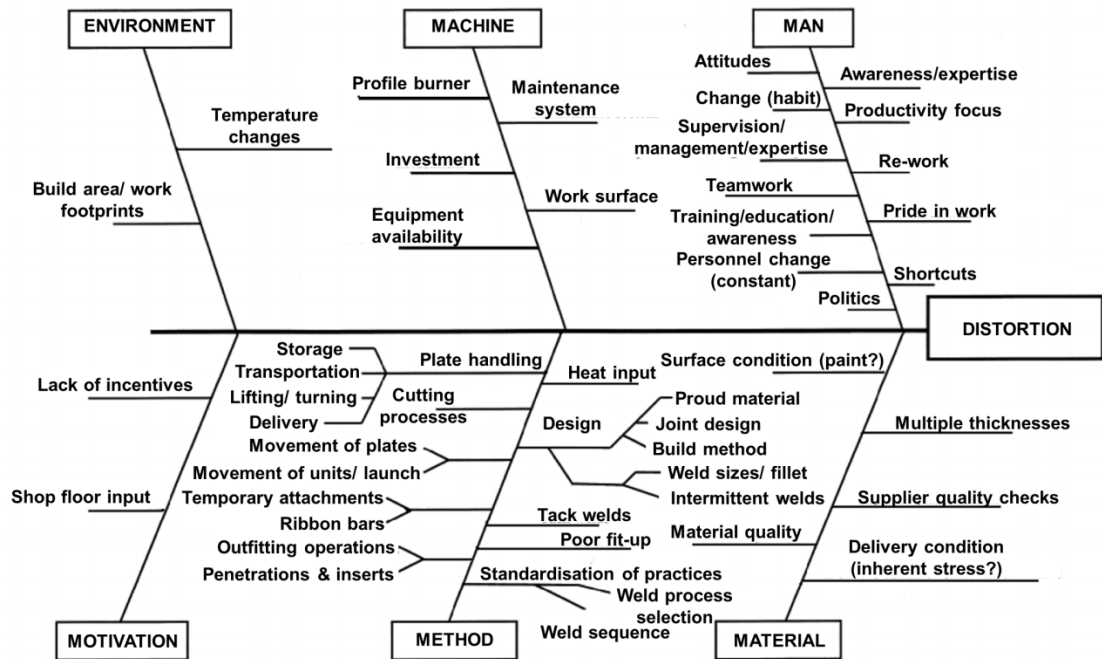


Fig. 2.9 Ishikawa diagram of factors influencing the workpiece distortion (adapted from [2.78]).

The longitudinal in-plane contraction emerges from cooling contraction in the central region of the weld, surrounded by cooler regions that are still expanding longitudinally (see Fig. 2.10 (C)). Additionally, the extremes of the weld are affected by a small field of transverse in-plane bending.

The V-shape of the fusion zone generates the sagging curvature (see Fig. 2.10 (D)) in the workpiece due to contraction forces usually developed closer to the upper area of the welded structure. Closer to the edges, the small transverse or “anticlastic” curvature tends to be compensated by the distortion modes in Fig. 2.10 ((B), (C)). Finally, contraction forces nearer the root of the weld (longitudinal bending) lead to a hogging longitudinal deformation (see Fig. 2.10 (E)).

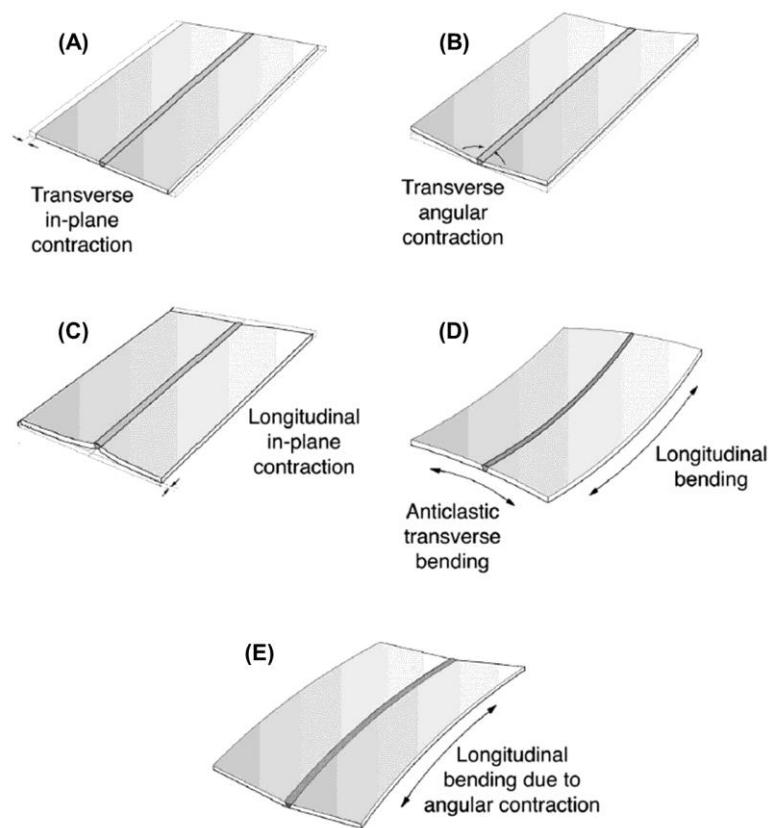


Fig. 2.10 Conventional deformation modes in thin-plates during welding. (A) Transverse in-plane contraction. (B) Transverse angular contraction. (C) Longitudinal in-plane contraction. (D) Longitudinal and anticlastic transverse bending. (E) Longitudinal bending and angular contraction combined (adapted from [2.73]).

2.4 Microstructural and mechanical properties

The microstructural characteristics of the weld and heat affected zone (HAZ) impact directly the mechanical properties of the weldment [2.61, 2.80-2.83]. For instance, refinement in the grain size is known to improve the strength and hardness of the joint, since the increased quantity of boundaries hinder crack propagation and deformation when stress is applied to the weld [2.28, 2.30, 2.82, 2.83].

A scheme to identify morphologies in steel was first employed in 1958 [2.84]. Bainite and martensite are examples of the many microstructural constituents found in various ferrous alloys, including the weld metal [2.80, 2.85-2.88]. In this thesis, however, the weld and HAZ microstructures were almost exclusively composed by acicular ferrite, allotriomorphic ferrite, and Widmanstätten ferrite, stimulated by the low carbon content in the joined materials [2.89, 2.90]. Hence, despite appreciating the importance of each microstructural phase, only the listed ferrite-type constituents will be contemplated in this section.

2.4.1 Ferrite and its properties

Ferrite (α -iron) is a solid solution of iron, stable at room temperature and composed by a body-centered cubic crystal structure, which limits the solubility of elements like C and N [2.86, 2.88, 2.90, 2.91]. The solid solution can be either interstitial or substitutional. While in the former elements with small atomic diameter (C, N) occupy interstitial sites, in the latter elements with bigger atomic diameter (Si, Cr, Mn, Ni) replace iron atoms [2.85, 2.88]. This behavior influences the mechanical properties of the joint. For instance,

the increase of N and C in the solid solution promotes welds with higher strength and hardness [2.5, 2.10, 2.88, 2.92].

Typical ferrite microphases are exemplified in Fig. 2.11. Allotriomorphic ferrite is located mainly on prior austenite grain boundaries, while idiomorphic ferrite (with its random orientation) nucleates within austenite grains, where non-metallic inclusions are present (see Fig. 2.11) [2.87, 2.89, 2.93, 2.94]. Widmanstätten ferrite occurs at a relatively low undercooling [2.84, 2.89]. The primary ferrite plates grow from the grain boundaries of austenite and may also grow from inclusions, whereas the secondary ferrite plates develop from the allotriomorphic ferrite at the prior austenite grain boundaries and intragranular idiomorphic ferrite [2.84, 2.87, 2.93, 2.95].

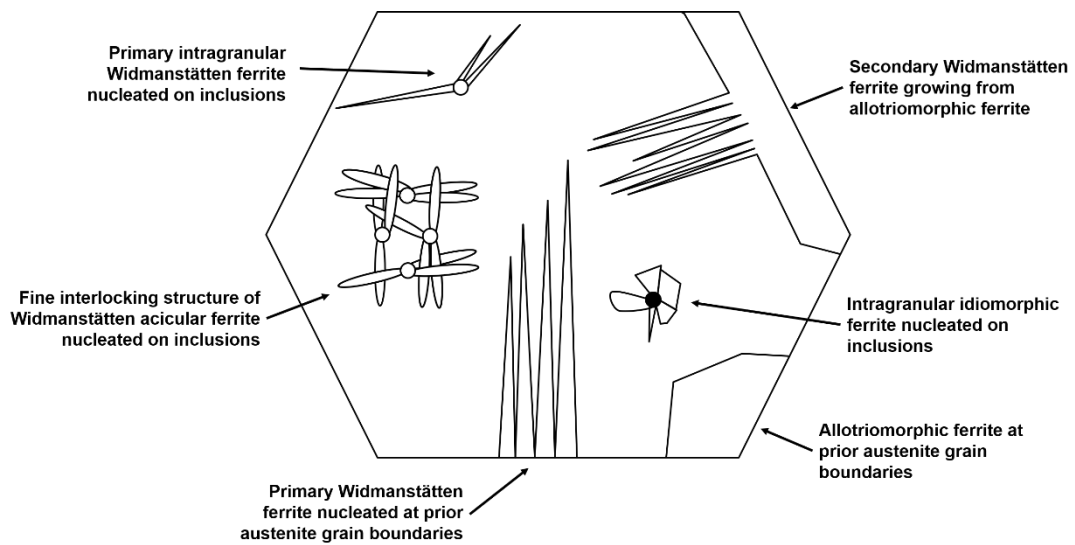


Fig. 2.11 Schematic of some ferrite constituents: primary allotriomorphic, idiomorphic and Widmanstätten ferrite and second Widmanstätten ferrite.

Despite being an anathema in steel structures, the presence of non-metallic inclusions can be positive to the development of chaotic structures,

enhancing toughness and hindering crack propagation [2.85, 2.89, 2.96-2.98]. Known as acicular ferrite (see Fig. 2.11), this random and fine interlocking constituent is composed by individual Widmanstätten ferrite plates nucleating from non-metallic inclusions [2.85, 2.86, 2.97].

Compared to allotriomorphic and Widmanstätten ferrite microphases, the development of acicular ferrite is preferable. The grain size of the former constituents is coarser and detrimental to mechanical properties of the joint such as toughness and strength, since they work as preferential routes for the propagation of cracks [2.99, 2.100].

Conversely, increasing the volume of acicular ferrite has demonstrated notable improvements in strength and fracture resistance [2.86, 2.101-2.103]. Generally associated with welding [2.104-2.106], the fine interlocking characteristics of this microphase hinders the propagation of cracks due to the high angled density of grain boundaries per unit length [2.97, 2.101, 2.107-2.110]. For instance, in pressure vessel, automotive and pipeline industries, steels with high content of acicular ferrite, namely medium and low carbon have been developed [2.110-2.112] due to the better mechanical properties and resistance [2.110, 2.111, 2.113, 2.114]. Yield strength as well as absorbed impact energy, which correlates to the fracture toughness have been reported to be in the range of 480-750 MPa and 140-190 J, respectively [2.102, 2.109, 2.112, 2.115].

This positive impact of the acicular ferrite presence in the weld microstructure will be discussed in further chapters. It will be shown that the presence of N_2 compared to CO_2 as well as modifying the gas supply from premixed to alternated stimulate the formation of acicular ferrite. For instance, the addition of N_2 as a shielding gas during the alternating shielding gas

welding process promoted the development of a finer microstructure composed mainly by acicular ferrite. Consequently, improvements in the mechanical properties of the joint were found, with better strength and hardness of the weld.

2.5 Mathematical modelling and searching methods

The determination of optimal welding conditions is of great significance during the joining process [2.116, 2.117]. Yet, to achieve such can be difficult and very complex, requiring considerable time and cost from trial-and-error methods. Hence, mathematical modelling and searching methods present an alternative to accelerate the process towards high quality joints. In this section, the genetic algorithm heuristic, the response surface methodology and the desirability function are described as well as their functionalities.

2.5.1 The genetic algorithm heuristic

Genetic algorithms utilise computer procedures to heuristically search for good solutions to a particular problem based on the natural process of human evolution. First presented in the beginning of the 1960s [2.118-2.120], genetic algorithms analyse individuals (chromosomes/strings) of a randomly generated population within a defined search space. Each individual is usually composed by binary numbers selected in a casual manner.

To mimic evolution, genetic algorithms count on its main genetic operators: initial population, fitness, selection, crossover, mutation, new population (see Fig. 2.12). It is important to notice that the number of individuals, crossover and mutation rates, and chromosome length impact

directly the genetic algorithm method, seeing that they determine the algorithm's efficiency [2.120, 2.121].

The initial population is usually randomly generated and coded as a binary string. Once such is decoded, the next step is to define how desirable each individual is to the new generation. This is carried out by assigning a fitness value to each individual, where the higher the fitness value the higher the chances of a certain string being selected for the next generation.

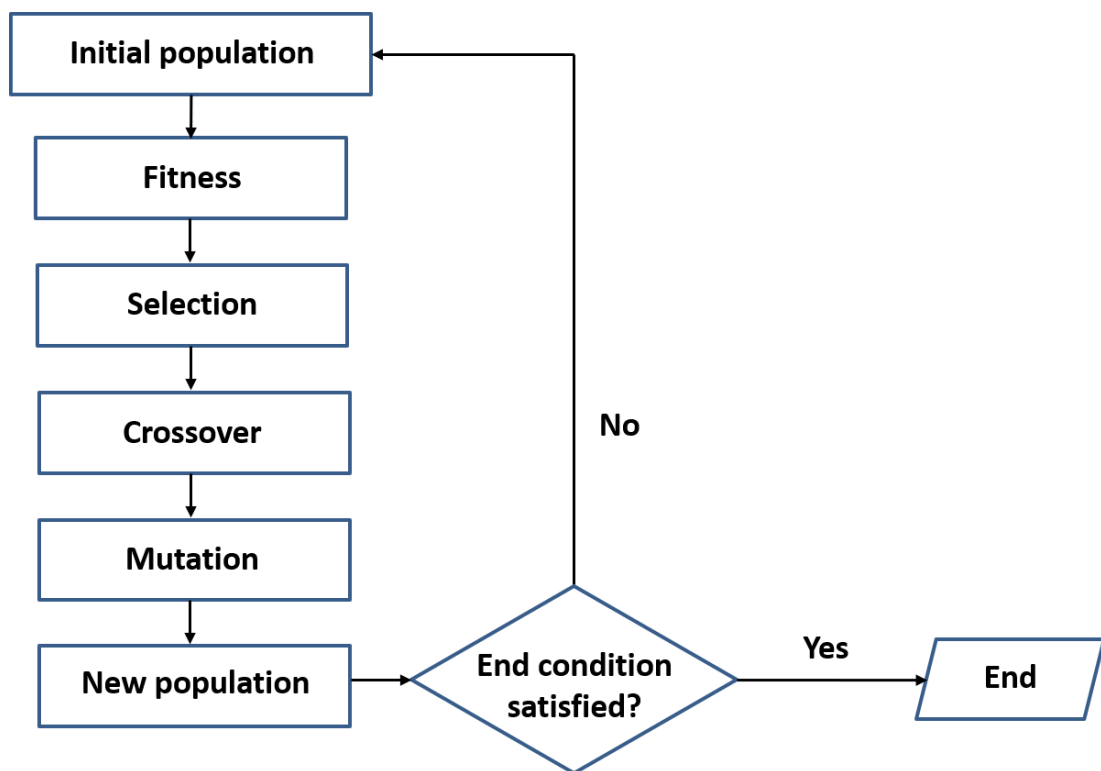


Fig. 2.12 Simplified flowchart of the genetic algorithm method.

Subsequently, the selection operator is performed based on the values of fitness. Three frequent techniques are the rank selection, the steady-state selection and the roulette wheel, the latter being the most commonly utilised method [2.122]. Employed in this study, in the roulette wheel selection a

circular shape is created (see Fig. 2.13), where each slice represents a string. The slice size is proportional to the individual's fitness and can be calculated using equation 2.1 [2.118].

$$p_k = \frac{f_k}{\sum_{j=1}^n f_j} \quad 2.1$$

Once the sum of the fitness of all n individuals is determined, the division of the string (k) fitness (f_k) by the total fitness of the population determines its slice proportion in the wheel (p_k) (see Fig. 2.13). Next, the roulette procedure takes place by a random number being generated within the wheel's interval. This random number is then allocated within the wheel, pointing to the individual to be stored in a mating pool before the crossover procedure.

During crossover, two strings (parents) are randomly taken from the mating pool. Locations (crossover sites) in each string are unsystematically designated as exchanging portions, which are interchanged to form two offspring individuals. It is highlighted here that not all strings will participate of this process since it is restricted by the crossover rate.

Finally, the mutation genetic operator randomly chooses and modifies bits of a string within a certain interval. This is to maintain the variety of the population, explore information not available in the initial stage and avoid missing the optimal solution, i.e. reaching a local maximum or minimum, although this is not always possible. The loss of good individuals is prevented by a low mutation rate.

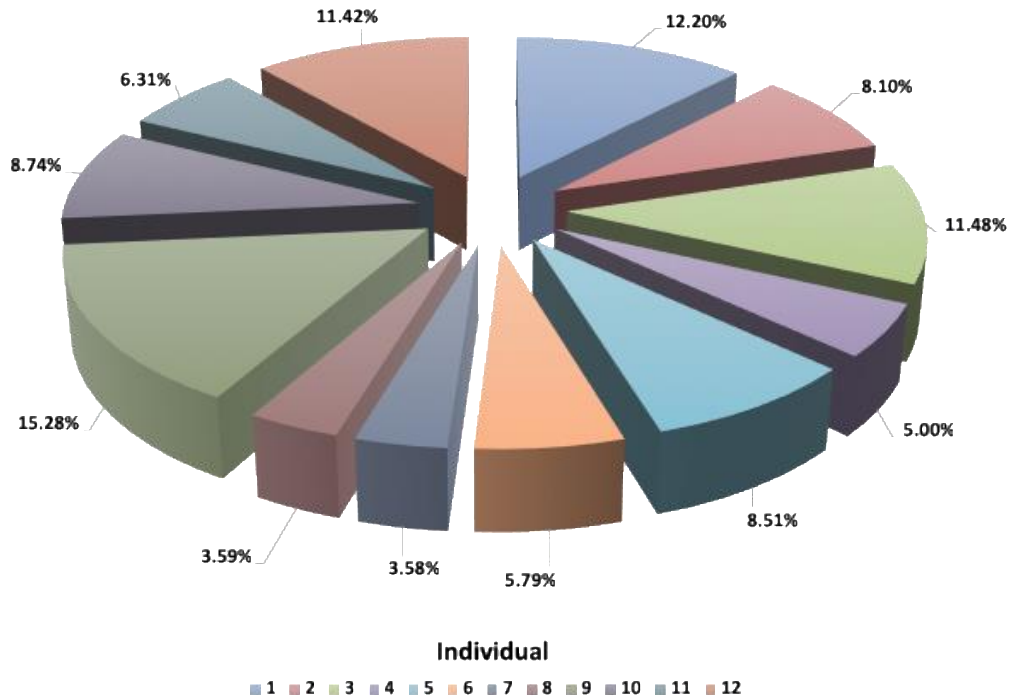


Fig. 2.13 Schematic example of proportions (%) assigned to individuals during fitness.

The advantages of using genetic algorithms include: 1) the convergence prevention to a unique answer by considering a set of feasible solutions, 2) the fitness value of each individual does not require differentiation or to be continuous, i.e. it is not affected by external welding factors such as burn-through [2.116, 2.123], 3) different from conventional optimisation methods, genetic algorithms operate with many search data [2.118].

2.5.2 The response surface methodology

Introduced in the early 1950s [2.124], the response surface methodology is a multi-response optimisation that utilises mathematical and statistical methods to relate control variables (inputs) and responses (outputs). The multi-response optimisation aims to improve the quality level of control

variables via a search that results in the best responses [2.125], where the response surface methodology allows for local approximations to the actual relationship between input and output variables, permitting predictions and reductions of experimental work.

The low-degree polynomial model in equation 2.2 is usually applied, where y , $\mathbf{x} = (x_1, x_2, \dots, x_n)'$, $f(\mathbf{x})$ and ϵ are the response of interest, input variables, vector function and experimental error, respectively. The vector function comprises elements of powers and cross-products of power of x_1, x_2, \dots, x_n up to a defined degree ≥ 1 . Equation 2.3 represents a second-degree model commonly employed in the response surface methodology, with $j < i$.

The response surface methodology provides work improvements in industrial environments, since it helps to justify changes in the responses based on the values chosen for the inputs [2.118]. However, to achieve such, data from experimental designs are required, with the central composite design being the most popular in the response surface methodology framework.

$$y = f'(\mathbf{x})\beta + \epsilon \tag{2.2}$$

$$y = \beta_0 + \sum_{i=1}^n \beta_i x_i + \sum_{i=1}^n \beta_{ii} x_i^2 + \sum_{j=1}^n \sum_{i=1}^n \beta_{ji} x_i x_j + \epsilon \tag{2.3}$$

A two-factor central composite design (see Fig. 2.14) is composed by n_o centre points and a factorial portion with n_f points, extracted from the 2^n experiments carried out. It also includes $2k$ axial points distanced α from the

origin [2.126]. Such composition determines the process space that the mathematical model will be working with.

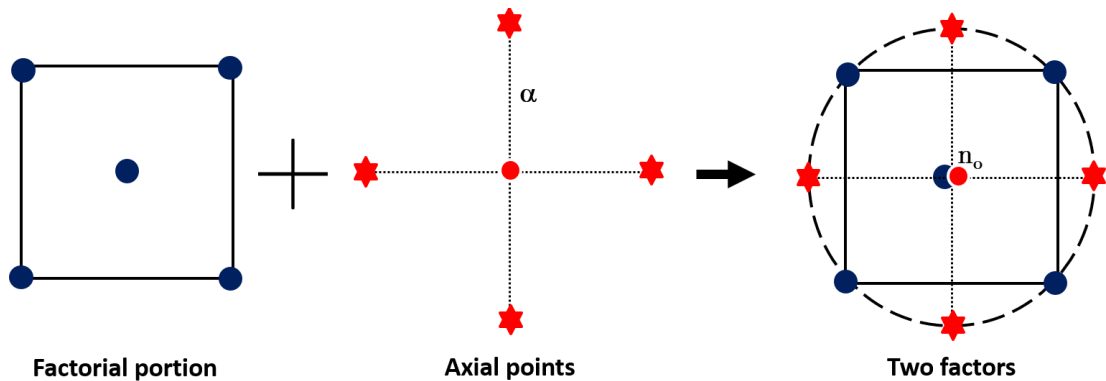


Fig. 2.14 Basic schematic of a two-factor central composite design generation.

As from Fig. 2.14 the factorial portion estimates linear and two-factor relation effects, while the axial points estimate curvature effects [2.118]. The central composite design's efficiency is a result of a low number of runs required to supply information regarding the effects of the chosen experimental variables together with the general experimental error. Furthermore, central composite designs are quite flexible, allowing its many types to be selected according to the regions of interest and feasibility.

2.5.3 The desirability function

Apart from correlating input and output variables, it is important to address and optimise the many conflicting responses concurrently and concertedly. Usually, a simultaneous optimisation of the multiple responses is required since their separate analysis may cause incompatibility in the system of interest. One common strategy to overcome this situation in the response

surface methodology framework is to combine the many output variables into a compound function.

This can be accomplished by many approaches, where the most popular one is the desirability function. Introduced in the 1960s [2.125], the desirability function develops a composite function (D) by aggregating single desirability functions (d) created from the estimated response models (y). Many less and more sophisticated desirability function approaches were discussed by Costa et al. [2.127], which showed that the former can compete with the different methods developed to perform well under unfavourable conditions.

Less sophisticated desirability functions, such as the proposed by Derringer and Suich [2.128], are flexible in terms of priorities and weights assigned by the user to the responses and simple to comprehend and utilise. As a modified version of the first desirability function introduced by Harrington [2.129], in the desirability function by Derringer and Suich [2.128] individual desirability functions are developed based on the response type. Equations 2.4, 2.5 and 2.6 represent the target-is-best (TIB), larger-is-best (LIB) and smaller-is-best (SIB) cases, respectively [2.125, 2.127]. While TIB is a two-sided type of function, both the LIB and SIB cases represent a one-sided type. The value of the desirability function ranges between 0 and 1 and the closer to 1 the most favourable the combination of responses. For $s = t = 1$ there is linearity of the desirability function towards the target, while for $s, t > 1$ and $s, t < 1$ the function will be concave and convex towards the target, respectively [2.130].

TIB type

$$d = \begin{cases} \left(\frac{y-L}{T-L}\right)^s, & L \leq y \leq T \\ \left(\frac{y-U}{T-U}\right)^t, & T < y \leq U \\ 0, & \text{otherwise} \end{cases} \quad 2.4$$

LIB type

$$d = \begin{cases} 1, & y \geq T \\ \left(\frac{y-L}{T-L}\right)^s, & L < y < T \\ 0, & y \leq L \end{cases} \quad 2.5$$

SIB type

$$d = \begin{cases} 1, & y \leq T \\ \left(\frac{y-U}{T-U}\right)^s, & T < y < U \\ 0, & y \geq U \end{cases} \quad 2.6$$

In the TIB type the response of interest is expected to reach a defined target value (T), i.e. $y = T$ is desirable since d will be equal to 1. If the aim is to maximise the response (LIB case), $y > L$ is expected, where L represents the lower limit. If minimising the response is the priority (SIB case), then y is expected to be smaller than the upper limit U .

$$D = (d_1 \cdot d_2 \cdot \dots \cdot d_m)^{\frac{1}{m}} \quad 2.7$$

Following the generation of individual desirability functions, the composite function D using the geometric mean is generated (see equation 2.7) for the m responses in the multi-response optimisation problem [2.125]. The

closer to 1 the better the composite function, whereas the closer to 0 the less desirable the composite function.

2.5.4 Applications in the welding process

Many studies aiming to systematically improve the weld bead geometry have been carried out using the genetic algorithm approach [2.123, 2.131-2.135]. For instance, Correia et al. [2.135] demonstrated that the difference between the most important response (penetration depth) and its target when using the genetic algorithm was lower than 4%. Yet, the study also concluded that a good setting of parameters in the search space was required, otherwise there would be a risk of the genetic algorithm heuristic not covering the entire space of interest.

Mechanical properties of the weld have also been optimised by Prasad et al. [2.136] through the genetic algorithm. The algorithm helped with minimising the grain size of the weld and maximising both its tensile strength and hardness. It was found that the soft computing results and the measured values from the experiments were in good agreement, with differences lower than 4%.

Correia et al. [2.118] compared the genetic algorithm and response surface methodology, aiming for the best values of three control variables (voltage, wire-feed speed and travel speed of the welding torch) based on four responses (deposition efficiency, bead width, penetration and reinforcement). The study concluded that both models were able to find optimum conditions, requiring a relatively low amount of experiments.

Kim and Rhee [2.133] made use of both the genetic algorithm and desirability function to find welding process parameters that minimise the variance of the output variable (penetration), whilst producing the desired target value. The study showed that superior results were found by utilising the genetic algorithm and desirability function when compared to optimisation algorithms previously employed.

The genetic algorithm, response surface methodology and desirability function were employed in chapter 7 to optimise the usage of Ar₅N₂ alternated with He. By correlating input and output parameters, the search method and mathematical models developed were able to reduce the heat input to the weldment as well as lowering the distortion of the workpiece.

2.6 Bibliography

- [2.1] V. Beyer, S. W. Campbell, G. M. Ramsey, A. M. Galloway, A. J. Moore, and N. A. McPherson, “Systematic study of effect of cross-drafts and nozzle diameter on shield gas coverage in MIG welding,” *Sci. Technol. Weld. Join.*, vol. 18, no. 8, pp. 652–660, 2013.
- [2.2] S. W. Campbell, A. M. Galloway, and N. A. McPherson, “Techno-economic evaluation of reducing shielding gas consumption in GMAW whilst maintaining weld quality,” *Int. J. Adv. Manuf. Technol.*, vol. 63, no. 6–9, pp. 975–985, 2012.
- [2.3] B. Mvola and P. Kah, “Effects of shielding gas control: welded joint properties in GMAW process optimization,” *Int. J. Adv. Manuf. Technol.*, vol. 88, no. 9–12, pp. 2369–2387, 2017.
- [2.4] H. S. Ham, D. S. Oh, and S. M. Cho, “Measurement of arc pressure and

- shield gas pressure effect on surface of molten pool in TIG welding,” *Sci. Technol. Weld. Join.*, vol. 17, no. 7, pp. 594–600, 2012.
- [2.5] T. Wegrzyn, “An attempt at the classification of steel weld metals and arc-welding methods on the basis of nitrogen concentration in the weld metal,” *Weld. Int.*, vol. 13, no. 3, pp. 173–179, 1999.
- [2.6] N. V. Shinde and M. T. Telsang, “Effect of Alternate Supply of Shielding Gases of Tungsten Inert Gas Welding on Mechanical Properties of Austenitic Stainless Steel,” *J. Inst. Eng. Ser. C*, vol. 97, no. 3, pp. 299–307, 2016.
- [2.7] Y. H. Chang, “Improve GMAW and GTAW with alternating shield gases,” *Weld. J.*, vol. 85, no. 2, pp. 41–43, 2006.
- [2.8] American Welding Society, “Choosing Shielding Gases for Gas Metal Arc Welding,” in *Welding Handbook*, vol. 2, no. May, 2008, pp. 32–35.
- [2.9] Anthony B Murphy, “The effects of metal vapour in arc welding,” *J. Phys. D. Appl. Phys.*, vol. 43, no. 16, p. 165204, 2010.
- [2.10] P. Kah and J. Martikainen, “Influence of shielding gases in the welding of metals,” *Int. J. Adv. Manuf. Technol.*, vol. 64, no. 9–12, pp. 1411–1421, 2013.
- [2.11] S. Kodama et al., “Nitrogen absorption phenomenon of GTA welding with nitrogen-mixed shielding gases: effect of plasma characteristics on nitrogen content in GTA welded metal,” *Weld. Int.*, vol. 29, no. 4, pp. 262–269, 2015.
- [2.12] K. V. S. Kumar, S. Gejendhiran, and M. Prasath, “Comparative Investigation of Mechanical Properties in GMAW/GTAW for Various Shielding Gas Compositions,” *Mater. Manuf. Process.*, vol. 29, no. 8, pp. 996–1003, 2014.

- [2.13] British Standard Institution, “BS EN ISO 14175:2008. Welding consumables — Gases and gas mixtures for fusion welding and allied processes.” BSI, London, 2008.
- [2.14] A. B. Murphy, M. Tanaka, K. Yamamoto, S. Tashiro, T. Sato, and J. J. Lowke, “Modelling of thermal plasmas for arc welding: the role of the shielding gas properties and of metal vapour,” *J. Phys. D. Appl. Phys.*, vol. 42, no. 19, p. 194006 (20pp), 2009.
- [2.15] A. B. Murphy, M. Tanaka, S. Tashiro, T. Sato, and J. J. Lowke, “A computational investigation of the effectiveness of different shielding gas mixtures for arc welding,” *J. Phys. D. Appl. Phys.*, vol. 42, p. 115205, 2009.
- [2.16] L. L. Wang, F. G. Lu, H. P. Wang, A. B. Murphy, and X. H. Tang, “Effects of shielding gas composition on arc profile and molten pool dynamics in gas metal arc welding of steels,” *J. Phys. D. Appl. Phys.*, vol. 47, no. 46, p. 465202 (14pp), 2014.
- [2.17] J. Mostaghimi-Tehrani and E. Pfender, “Effects of metallic vapor on the properties of an argon arc plasma,” *Plasma Chem. Plasma Process.*, vol. 4, no. 2, pp. 129–139, 1984.
- [2.18] M. Schnick, G. Wilhelm, M. Lohse, U. Füssel, and A. B. Murphy, “Three-dimensional modelling of arc behaviour and gas shield quality in tandem gas-metal arc welding using anti-phase pulse synchronization,” *J. Phys. D. Appl. Phys.*, vol. 44, no. 18, 2011.
- [2.19] A. B. Murphy and C. J. Arundell, “Transport Coefficients of Argon , Nitrogen , Oxygen , Argon-Nitrogen , and Argon-Oxygen Plasmas,” vol. 14, no. 4, 1994.
- [2.20] L. Sansonnens, J. Haidar, and J. J. Lowke, “Prediction of properties of

- free burning arcs including effects of ambipolar diffusion,” *J. Phys. D. Appl. Phys.*, vol. 33, no. 2, pp. 148–157, 2000.
- [2.21] M. Tanaka, S. Tashiro, M. Ushio, T. Mita, A. B. Murphy, and J. J. Lowke, “CO₂-shielded arc as a high-intensity heat source,” *Vacuum*, vol. 80, no. 11–12, pp. 1195–1198, 2006.
- [2.22] S. Tashiro, M. Tanaka, M. Ushio, A. B. Murphy, and J. J. Lowke, “Prediction of energy source properties of free-burning arcs,” *Vacuum*, vol. 80, no. 11–12, pp. 1190–1194, 2006.
- [2.23] M. Tanaka, S. Tashiro, T. Satoh, A. B. Murphy, and J. J. Lowke, “Influence of shielding gas composition on arc properties in TIG welding,” *Sci. Technol. Weld. Join.*, vol. 13, no. 3, pp. 225–231, 2008.
- [2.24] S. W. Campbell, A. M. Galloway, and N. A. McPherson, “Arc pressure and weld metal fluid flow while using alternating shielding gases. Part 1: arc pressure measurement,” *Sci. Technol. Weld. Join.*, vol. 18, no. 7, pp. 591–596, 2013.
- [2.25] S. W. Campbell, A. M. Galloway, and N. A. McPherson, “Arc pressure and fluid flow during alternating shielding gases. Part 2: arc force determination,” *Sci. Technol. Weld. Join.*, vol. 18, no. 7, pp. 597–602, 2013.
- [2.26] P. G. Jönsson, T. W. Eagar, and J. Szekely, “Heat and Metal Arc Metal Transfer Welding Using in Gas Argon and Helium,” *Metall. Mater. Trans. B*, vol. 26, no. 2, pp. 383–395, 1995.
- [2.27] J. S. Rudas, J. S. Restrepo, and L. M. Gómez, “Prediction of Metal Transfer Modes in the GMAW Process,” in *2015 IEEE 2nd Colombian Conference on Automatic Control (CCAC)*, 2015, pp. 1–6.
- [2.28] S. W. Campbell, A. M. Galloway, N. A. McPherson, and A. Gillies,

- “Evaluation of gas metal arc welding with alternating shielding gases for use on AA6082T6,” *Proc. Inst. Mech. Eng. Part B J. Eng. Manuf.*, vol. 226, no. 6, pp. 992–1000, 2012.
- [2.29] J. J. Lowke, M. Tanaka, and M. Ushio, “Mechanisms giving increased weld depth due to a flux,” *J. Phys. D. Appl. Phys.*, vol. 38, no. 18, pp. 3438–3445, 2005.
- [2.30] S. W. Campbell, A. M. Galloway, and N. A. McPherson, “Techno-economic evaluation on the effects of alternating shielding gases for advanced joining processes,” *Proc. Inst. Mech. Eng. Part B J. Eng. Manuf.*, vol. 225, no. 10, pp. 1863–1872, 2011.
- [2.31] S. W. Campbell, “Shielding Gas Parameter Optimisation in Arc Welding Processes,” University of Strathclyde, 2015.
- [2.32] Y. Ogino, Y. Hirata, and A. B. Murphy, “Numerical simulation of GMAW process using Ar and an Ar-CO₂ gas mixture,” *Weld. World*, vol. 60, no. 2, pp. 345–353, 2016.
- [2.33] M. Ebrahimnia, M. Goodarzi, M. Nouri, and M. Sheikhi, “Study of the effect of shielding gas composition on the mechanical weld properties of steel ST 37-2 in gas metal arc welding,” *Mater. Des.*, vol. 30, no. 9, pp. 3891–3895, 2009.
- [2.34] J. Lozano, P. Moreda, C. L. Llorente, and P. D. Bilmes, “Fusion characteristics of austenitic stainless steel gmaw welds,” *Lat. Am. Appl. Res.*, vol. 33, no. 1, pp. 27–31, 2003.
- [2.35] S. Lu, W. Dong, D. Li, and Y. Li, “Numerical study and comparisons of gas tungsten arc properties between argon and nitrogen,” *Comput. Mater. Sci.*, vol. 45, no. 2, pp. 327–335, 2009.
- [2.36] B. Zorc, “Automatic TIG welding of austenitic stainless steels in

- nitrogen and nitrogen-based gas mixtures,” *Rev. Metal.*, vol. 47, no. 1, pp. 29–37, 2011.
- [2.37] S. Tashiro et al., “Plasma properties of helium gas tungsten arc with metal vapour,” *Sci. Technol. Weld. Join.*, vol. 12, no. 3, pp. 202–207, 2007.
- [2.38] A. B. Murphy, “Influence of metal vapour on arc temperatures in gas–metal arc welding: convection versus radiation,” *J. Phys. D. Appl. Phys.*, vol. 46, no. 22, p. 224004 (10pp), 2013.
- [2.39] J. Haidar, “The dynamic effects of metal vapour in gas metal arc welding,” *J. Phys. D. Appl. Phys.*, vol. 43, no. 16, p. 165204 (11pp), 2010.
- [2.40] T. Iwao et al., “Modelling of metal vapour in pulsed TIG including influence of self-absorption,” *J. Phys. D. Appl. Phys.*, vol. 43, p. 434010 (10pp), 2010.
- [2.41] G. Wilhelm, R. Kozakov, G. Gött, H. Schöpp, and D. Uhrlandt, “Behaviour of the iron vapour core in the arc of a controlled short-arc GMAW process with different shielding gases,” *J. Phys. D. Appl. Phys.*, vol. 45, no. 8, p. 085202 (11pp), 2012.
- [2.42] M. Schnick et al., “Numerical Investigations of the Influence of Metal Vapour in GMA Welding,” *Weld. World*, vol. 55, no. 11–12, pp. 114–120, 2011.
- [2.43] H. Yu, J. Song, G. Zhang, J. Pu, H. Chen, and S. Chen, “The Effects of Arc Length on Welding Arc Characteristics in Al-Mg Alloy Pulsed Gas Tungsten Arc Welding,” in *Robotic Welding, Intelligence and Automation: Advances in Intelligent Systems and Computing.*, vol. 363, Shanghai, China: Springer, 2015, pp. 321–335.

- [2.44] K. Yamamoto et al., “Metal vapour behaviour in thermal plasma of gas tungsten arcs during welding,” *Sci. Technol. Weld. Join.*, vol. 13, no. 6, pp. 566–572, 2008.
- [2.45] S. Kodama, K. Sugiura, S. Nakanishi, Y. Tsujimur, M. Tanaka, and A. B. Murphy, “Effect of plasma heat source characteristics on nitrogen absorption in gas tungsten arc weld metal,” *Weld. World*, vol. 57, no. 6, pp. 925–932, 2013.
- [2.46] L. L. Wang, H. P. Wang, F. G. Lu, A. B. Murphy, and B. E. Carlson, “Numerical analysis of Al vapour effects in gas metal arc welding of Al alloys,” *Sci. Technol. Weld. Join.*, vol. 19, no. 5, pp. 361–368, 2014.
- [2.47] D. S. Howse and W. Lucas, “Investigation into arc constriction by active fluxes for tungsten inert gas welding,” *Sci. Technol. Weld. Join.*, vol. 5, no. 3, pp. 189–193, 2000.
- [2.48] M. H. Cho, Y. C. Lim, and D. F. Farson, “Simulation of weld pool dynamics in the stationary pulsed gas metal arc welding process and final weld shape,” *Weld. J.*, vol. 85, no. 12, p. 271s–283s, 2006.
- [2.49] H. Sekiguchi, I. Masumoto, H. Konishi, and I. Suzuki, “Use of Nitrogen in Welding Atmosphere (Report 1),” *J. Japan Weld. Soc.*, vol. 34, no. 2, pp. 128–136, 1965.
- [2.50] T. Kobayashi, T. Kuwana, and R. Kiguchi, “Effect of Alloying Elements on Nitrogen Content of Steel Weld Metals (Report 2),” *J. Japan Weld. Soc.*, vol. 41, no. 4, pp. 415–424, 1972.
- [2.51] T. Kobayashi, T. Kuwana, and R. Kiguchi, “Effect of Alloying Elements on Nitrogen Content of Steel Weld Metals (Report 1),” *J. Japan Weld. Soc.*, vol. 41, no. 3, pp. 308–321, 1972.
- [2.52] J. Littleton, J. Lammas, and M. F. Jordan, “Nitrogen Porosity in Gas

- Shielded Arc Welding of Copper,” *Weld. J.*, vol. 12, pp. 561–565, 1974.
- [2.53] J. W. Cunningham, “Pulsed welding and cutting by variation of composition of shielding gas,” 3, 1969.
- [2.54] F. H. Ley, S. W. Campbell, A. M. Galloway, and N. A. McPherson, “Effect of shielding gas parameters on weld metal thermal properties in gas metal arc welding,” *Int. J. Adv. Manuf. Technol.*, vol. 80, no. 5–8, pp. 1213–1221, 2015.
- [2.55] I. Bitharas, S. W. Campbell, A. M. Galloway, N. A. Mcpherson, and A. J. Moore, “Visualisation of alternating shielding gas flow in GTAW,” *Mater. Des.*, vol. 91, pp. 424–431, 2016.
- [2.56] I. S. Kim, J. S. Son, and H. J. K. B. A. Chin, “A study on variation of shielding gas in GTA welding using finite element method,” *Manuf. Eng.*, vol. 17, no. 1, pp. 249–252, 2006.
- [2.57] B. Y. Kang, Y. K. D. V Prasad, M. J. Kang, H. J. Kim, and I. S. Kim, “The effect of alternate supply of shielding gases in austenite stainless steel GTA welding,” *J. Mater. Process. Technol.*, vol. 209, no. 10, pp. 4722–4727, 2009.
- [2.58] B. Y. Kang, Y. K. D. V Prasad, M. J. Kang, H. J. Kim, and I. S. Kim, “Characteristics of alternate supply of shielding gases in aluminum GMA welding,” *J. Mater. Process. Technol.*, vol. 209, no. 10, pp. 4716–4721, 2009.
- [2.59] N. S. Barabokhin et al., “Technological special features of welding 1460 high-strength aluminium alloy,” *Weld. Int.*, vol. 14, no. 6, pp. 468–470, 2000.
- [2.60] S. W. Campbell, A. M. Galloway, G. M. Ramsey, and N. A. McPherson, “A potential solution to GMAW gas flow optimisation,” in *ASM*

- Proceedings of the International Conference: Trends in Welding Research, 2012.
- [2.61] O. M. Novikov, A. S. Persidskii, E. P. Rad'ko, A. V. Baranovskii, and B. A. Khasyanov, "Effect of changes in the composition of the gas shielding medium on the properties of arc welded joints in aluminium alloys," *Weld. Int.*, vol. 27, no. 3, pp. 222–225, 2013.
- [2.62] A. Traidia and F. Roger, "A computational investigation of different helium supplying methods for the improvement of GTA welding," *J. Mater. Process. Technol.*, vol. 211, no. 9, pp. 1553–1562, 2011.
- [2.63] R. G. Tazetdinov, O. M. Novikov, A. S. Persidskii, B. A. Khasyanov, E. N. Ivanov, and L. T. Plaksina, "Arc welding in shielding gases with alternate pulsed supply of dissimilar gases," *Weld. Int.*, vol. 7116, no. May 2015, pp. 1–4, 2012.
- [2.64] T. Gray, D. Camilleri, and N. McPherson, "Fabrication of stiffened thin-plate structures and the problem of welding distortion," in *Control of Welding Distortion in Thin-Plate Fabrication*, 2014, pp. 14–38.
- [2.65] J. F. Rudy and E. J. Rupert, "Effects of porosity on mechanical properties of aluminum welds," *Weld J*, vol. 49, no. 7, p. 322, 1970.
- [2.66] D. Hartman, V. Rajan, C. Jiang, A. N. A. Elliott, C. Karas, and A. Joaquin, "Gas Metal Arc Welding of Coated Advanced High Strength Steel (AHSS) - Developments for Improved Weld Quality," *SAE Tech. Pap. Ser.*, vol. 1, no. 724, 2010.
- [2.67] S. W. Campbell, F. H. Ley, A. M. Galloway, and N. A. McPherson, "Artificial neural network optimisation of shielding gas flow rate in gas metal arc welding subjected to cross drafts when using alternating shielding gases," *Proc. Inst. Mech. Eng. Part B J. Eng. Manuf.*, vol. 229,

- no. 1, pp. 122–129, 2015.
- [2.68] Y. Adonyi, R. W. Richardson, and W. A. Baeslack, “Investigation of Arc Force Effects in Subsurface GTA Welding,” *Weld. J.*, vol. 71, no. 9, pp. S321–S330, 1992.
- [2.69] K. Hiraoka, A. Okada, and M. Inagaki, “Effect of Helium Gas on Arc Characteristic in Gas Tungsten Arc Welding,” *J. Japan Weld. Soc.*, vol. 3, no. 2, pp. 5–10, 1985.
- [2.70] T. Gray, D. Camilleri, and N. McPherson, “Finite-element thermo-mechanical techniques for welding distortion prediction,” in *Control of Welding Distortion in Thin-Plate Fabrication*, 2014, pp. 177–198.
- [2.71] L. D. Cozzolino, H. E. Coules, P. A. Colegrove, and S. Wen, “Investigation of post-weld rolling methods to reduce residual stress and distortion,” *J. Mater. Process. Technol.*, vol. 247, no. August 2016, pp. 243–256, 2017.
- [2.72] T. Gray, D. Camilleri, and N. McPherson, “Computational simulation of welding distortion: an overview,” in *Control of Welding Distortion in Thin-Plate Fabrication*, 2014, pp. 77–101.
- [2.73] T. Gray, D. Camilleri, and N. McPherson, “Understanding welding distortion: thermal fields thermo-mechanical effects,” in *Control of Welding Distortion in Thin-Plate Fabrication*, Woodhead Publishing Limited, 2014, pp. 53–76.
- [2.74] D. Camilleri, T. Comlekci, and T. G. F. Gray, “Computational prediction of out-of-plane welding distortion and experimental investigation,” *J. Strain Anal. Eng. Des.*, vol. 40, no. 2, pp. 161–176, 2005.
- [2.75] K. Masubuchi, “Models of Stresses and Deformation Due to Welding—

- A Review,” *J. Miner. Met. Mater. Soc.*, vol. 33, no. 12, pp. 19–23, 1981.
- [2.76] C. Heinze, C. Schwenk, and M. Rethmeier, “The effect of tack welding on numerically calculated welding-induced distortion,” *J. Mater. Process. Technol.*, vol. 212, no. 1, pp. 308–314, 2012.
- [2.77] Y. H. P. Manurung et al., “Welding distortion analysis of multipass joint combination with different sequences using 3D FEM and experiment,” *Int. J. Press. Vessel. Pip.*, vol. 111–112, pp. 89–98, 2013.
- [2.78] N. McPherson, A. Galloway, and W. McGhee, “Thin plate buckling mitigation and reduction challenges for naval ships,” *J. Mar. Eng. Technol.*, vol. 12, no. 2, pp. 3–10, 2013.
- [2.79] T. Gray, D. Camilleri, and N. McPherson, “Simulating welding distortion in butt welding of thin plates,” in *Control of Welding Distortion in Thin-Plate Fabrication*, 2014, pp. 199–232.
- [2.80] S. Ragu Nathan, V. Balasubramanian, S. Malarvizhi, and a. G. Rao, “Effect of welding processes on mechanical and microstructural characteristics of high strength low alloy naval grade steel joints,” *Def. Technol.*, vol. 11, no. 3, pp. 308–317, 2015.
- [2.81] J. C. Lippold and D. J. Kotecki, *Welding metallurgy and weldability of stainless steels*. Wiley-Interscience, 2005.
- [2.82] P. K. Ghosh, S. R. Gupta, and H. S. Randhawa, “Characteristics of a Pulsed-Current, Vertical-Up Gas Metal Arc Weld in Steel,” *Metall. Mater. Trans. A*, vol. 31, no. 9, pp. 2247–2259, 2000.
- [2.83] Y. Zheng et al., “An experimental study of nitrogen gas influence on the 443 ferritic stainless steel joints by double-shielded welding,” *Int. J. Adv. Manuf. Technol.*, vol. 87, no. 9–12, pp. 3315–3323, 2016.
- [2.84] G. Thewlis, “Classification and quantification of microstructures in

- steels,” *Mater. Sci. Technol.*, vol. 20, no. 2, pp. 143–160, 2004.
- [2.85] W. L. Costin, O. Lavigne, and A. Kotousov, “A study on the relationship between microstructure and mechanical properties of acicular ferrite and upper bainite,” *Mater. Sci. Eng. A*, vol. 663, pp. 193–203, 2016.
- [2.86] A. F. Gourgues, H. M. Flower, and T. C. Lindley, “Electron backscattering diffraction study of acicular ferrite, bainite, and martensite steel microstructures,” *Mater. Sci. Technol.*, vol. 16, no. 1, pp. 26–40, 2000.
- [2.87] R. Ghomashchi, W. Costin, and R. Kurji, “Evolution of weld metal microstructure in shielded metal arc welding of X70 HSLA steel with cellulosic electrodes: A case study,” *Mater. Charact.*, vol. 107, pp. 317–326, 2015.
- [2.88] J. R. Davis, “Structure / Property Relationships in Irons and Steels,” *Met. Handb. Desk, Second Ed.*, pp. 153–173, 1998.
- [2.89] H. Bhadeshia and R. Honeycombe, *Steels: Microstructure and Properties*, 4th ed. Elsevier Ltd., 2017.
- [2.90] W. D. C. Jr. and D. G. Rethwisch, *Materials Science and Engineering: An Introduction*, 8th ed. John Wiley & Sons, Inc, 2009.
- [2.91] T. Wegrzyn, “The Classification of Metal Weld Deposits in Terms of the Amount of Nitrogen,” in *Proceedings of the Tenth (2000) International Offshore and Polar Engineering Conference*, 2000, vol. IV, pp. 130–134.
- [2.92] D. D. Nage, V. S. Raja, and R. Raman, “Effect of nitrogen addition on the microstructure and mechanical behavior of 317L and 904L austenitic stainless steel welds,” *J. Mater. Sci.*, vol. 41, no. 7, pp. 2097–2112, 2006.

- [2.93] G. Thewlis, J. A. Whiteman, and D. J. Senogles, “Dynamics of austenite to ferrite phase transformation in ferrous weld metals,” *Mater. Sci. Technol.*, vol. 13, no. 3, pp. 257–274, 1997.
- [2.94] T. Koseki, “A Review on Inclusion-Assisted Microstructure Control in C-Mn and Low-Alloy Steel Welds,” *Weld. World*, vol. 49, no. 5–6, pp. 22–28, 2005.
- [2.95] G. Thewlis, “Weldability of X100 linepipe,” *Sci. Technol. Weld. Join.* ISSN, vol. 5, no. 6, pp. 365–377, 2000.
- [2.96] H. Bhadeshia and R. Honeycombe, “Acicular Ferrite,” in *Steels: Microstructure and Properties*, 4th ed., Elsevier Ltd, 2017, pp. 203–216.
- [2.97] I. Madariaga, I. Gutiérrez, C. García-De Andrés, and C. Capdevila, “Acicular ferrite formation in a medium carbon steel with a two stage continuous cooling,” *Scr. Mater.*, vol. 41, no. 3, pp. 229–235, 1999.
- [2.98] R. A. Ricks, P. R. Howell, and G. S. Barritte, “The nature of acicular ferrite in HSLA steel weld metals,” *J. Mater. Sci.*, vol. 17, no. 3, pp. 732–740, 1982.
- [2.99] Q. L. Jiang, Y. J. Li, J. Wang, and L. Zhang, “Effects of inclusions on formation of acicular ferrite and propagation of crack in high strength low alloy steel weld metal,” *Mater. Sci. Technol.*, vol. 27, no. 10, pp. 1565–1569, 2011.
- [2.100] J. S. Byun, J. H. Shim, Y. W. Cho, and D. N. Lee, “Non-metallic inclusion and intragranular nucleation of ferrite in Ti-killed C-Mn steel,” *Acta Mater.*, vol. 51, no. 6, pp. 1593–1606, 2003.
- [2.101] R. A. Farrar and P. L. Harrison, “Acicular ferrite in carbon-manganese weld metals: An overview,” *J. Mater. Sci.*, vol. 22, no. 11, pp. 3812–3820, 1987.

- [2.102] J. R. Yang, C. Y. Huang, C. F. Huang, and J. N. Aoh, "Influence of acicular ferrite and bainite microstructures on toughness for an ultra-low-carbon alloy steel weld metal," *J. Mater. Sci. Lett.*, vol. 12, no. 16, pp. 1290–1293, 1993.
- [2.103] D. V. Edmonds and R. C. Cochrane, "Structure-property relationships in bainitic steels," *Metall. Trans. A*, vol. 21, no. 6, pp. 1527–1540, 1990.
- [2.104] S. Ohkita, H. Homma, S. Tsushima, and N. Mori, "The effect of oxide inclusions on microstructure of Ti-B-containing weld metal," *Aust. Weld. J.*, vol. 29, no. 3, pp. 29–36, 1984.
- [2.105] D. J. Abson, R. E. Dolby, and P. H. M. Hart, "No Title," in *Proc. Int. Conf. Trends in Steel and Consumables for Welding*, 1978, pp. 75–101.
- [2.106] J. G. Garland and P. R. Kirkwood, "No Title," *Met. Constr.*, vol. 7, no. 5, pp. 275–83, 1975.
- [2.107] J. Du, M. Strangwood, and C. L. Davis, "Effect of TiN Particles and Grain Size on the Charpy Impact Transition Temperature in Steels," *J. Mater. Sci. Technol.*, vol. 28, no. 10, pp. 878–888, 2012.
- [2.108] H. K. D. H. Bhadeshia, "Bainite in Steels: transformations, microstructure and properties." IOM Communications, London, 2001.
- [2.109] M. Díaz-Fuentes, A. Iza-Mendia, and I. Gutiérrez, "Analysis of different acicular ferrite microstructures in low-carbon steels by electron backscattered diffraction. Study of their toughness behavior," *Metall. Mater. Trans. A Phys. Metall. Mater. Sci.*, vol. 34 A, no. 11, pp. 2505–2516, 2003.
- [2.110] W. Wang, W. Yan, L. Zhu, P. Hu, Y. Shan, and K. Yang, "Relation among rolling parameters, microstructures and mechanical properties in an acicular ferrite pipeline steel," *Mater. Des.*, vol. 30, no. 9, pp. 3436–

3443, 2009.

- [2.111] W. Wang, Y. Shan, and K. Yang, "Study of high strength pipeline steels with different microstructures," *Mater. Sci. Eng. A*, vol. 502, no. 1–2, pp. 38–44, 2009.
- [2.112] L. Shi et al., "Improved toughness and ductility in ferrite/acicular ferrite dual-phase steel through intercritical heat treatment," *Mater. Sci. Eng. A*, vol. 590, pp. 7–15, 2014.
- [2.113] M. C. Zhao, B. Tang, Y. Y. Shan, and K. Yang, "Role of microstructure on sulfide stress cracking of oil and gas pipeline steels," *Metall. Mater. Trans. A Phys. Metall. Mater. Sci.*, vol. 34 A, no. 5, pp. 1089–1096, 2003.
- [2.114] Y. Zhong, F. Xiao, J. Zhang, Y. Shan, W. Wang, and K. Yang, "In situ TEM study of the effect of M/A films at grain boundaries on crack propagation in an ultra-fine acicular ferrite pipeline steel," *Acta Mater.*, vol. 54, no. 2, pp. 435–443, 2006.
- [2.115] M. C. Zhao, K. Yang, and Y. Y. Shan, "Comparison on strength and toughness behaviors of microalloyed pipeline steels with acicular ferrite and ultrafine ferrite," *Mater. Lett.*, vol. 57, no. 9–10, pp. 1496–1500, 2003.
- [2.116] D. Kim, M. Kang, and S. Rhee, "Determination of Optimal Welding Conditions with a Controlled Random Search Procedure," *Weld. J.*, no. August, pp. 125–130, 2005.
- [2.117] M. Abid and M. Siddique, "Numerical simulation to study the effect of tack welds and root gap on welding deformations and residual stresses of a pipe-flange joint," *Int. J. Press. Vessel. Pip.*, vol. 82, no. 11, pp. 860–871, 2005.

- [2.118] D. S. Correia, C. V. Gonçalves, S. S. Da Cunha, and V. A. Ferraresi, “Comparison between genetic algorithms and response surface methodology in GMAW welding optimization,” *J. Mater. Process. Technol.*, vol. 160, no. 1, pp. 70–76, 2005.
- [2.119] J.H.Holland, *Adaptation in Natural and Artificial System*. University of Michigan Press, Ann Arbor, MI, 1975.
- [2.120] D. E. Goldberg, *Genetic Algorithms in Search, Optimization and Machine Learning*. Boston: Addison-Wesley Longman, 1989.
- [2.121] P. Sathiya, P. M. Ajith, and R. Soundararajan, “Genetic algorithm based optimization of the process parameters for gas metal arc welding of AISI 904 L stainless steel,” *J. Mech. Sci. Technol.*, vol. 27, no. 8, pp. 2457–2465, 2013.
- [2.122] R. Malhotra, N. Singh, and Y. Singh, “Genetic Algorithms: Concepts, Design for Optimization of Process Controllers,” *Comput. Inf. Sci.*, vol. 4, no. 2, pp. 39–54, 2011.
- [2.123] D. Kim and S. Rhee, “Optimization of Arc Welding Process Parameters Using a Genetic Algorithm,” *Weld. J.*, vol. 80, no. 7, p. 184s–189s, 2001.
- [2.124] A. I. Khuri and S. Mukhopadhyay, “Response surface methodology,” *Wiley Interdiscip. Rev. Comput. Stat.*, vol. 2, no. 2, pp. 128–149, 2010.
- [2.125] B. A. Öztürk, G. W. Weber, and G. Köksal, “Desirability Functions in Multiresponse Optimization,” in *Communications in Computer and Information Science*, vol. 499, 2015, pp. 129–146.
- [2.126] P. Angelopoulos, H. Evangelaras, and C. Koukouvinos, “Small , balanced , efficient and near rotatable central composite designs,” *J. Stat. Plan. Inference*, vol. 139, no. 6, pp. 2010–2013, 2008.
- [2.127] N. R. Costa, J. Lourenço, and Z. L. Pereira, “Desirability function

- approach: A review and performance evaluation in adverse conditions,”
Chemom. Intell. Lab. Syst., vol. 107, no. 2, pp. 234–244, 2011.
- [2.128] G. Derringer and R. Suich, “Simultaneous Optimization of Several Response Variables,” J. Qual. Technol., vol. 12, no. 4, pp. 214–219, 1980.
- [2.129] E. C. Harrington, “The desirability functions,” Ind. Qual. Control, vol. 21, pp. 494–498, 1965.
- [2.130] J. F. Kros and C. M. Mastrangelo, “Comparing multi-response design methods with mixed responses,” Qual. Reliab. Eng. Int., vol. 20, no. 5, pp. 527–539, 2004.
- [2.131] J. P. Jia, H. Zhang, and H. Huang, “Optimization of Welding Process Parameters for Rotating Arc Welding Sensor Based on Genetic Algorithm,” Mater. Sci. Forum, vol. 575–578, pp. 769–773, 2008.
- [2.132] D. T. Thao and I. S. Kim, “An Evaluation Approach for Prediction of Process Parameters with Genetic Algorithm,” Mater. Sci. Forum, vol. 580–582, pp. 375–378, 2008.
- [2.133] D. Kim and S. Rhee, “Optimization of a gas metal arc welding process using the desirability function and the genetic algorithm,” J. Eng. Manuf., vol. 218, pp. 35–41, 2004.
- [2.134] D. T. Thao, I. S. Kim, H. H. Na, S. M. Jung, and J. Y. Shim, “Development of mathematical model with a genetic algorithm for automatic GMA welding process,” Int. J. Adv. Manuf. Technol., pp. 837–847, 2014.
- [2.135] D. S. Correia, C. V. Gonçalves, S. S. C. Junior, and V. A. Ferraresi, “GMAW welding optimization using genetic algorithms,” J. Brazilian Soc. Mech. Sci. Eng., vol. 26, no. 1, pp. 28–32, 2004.
- [2.136] K. S. Prasad, C. S. Rao, and D. N. Rao, “Optimization of fusion zone

grain size, hardness, and ultimate tensile strength of pulsed current micro plasma arc welded Inconel 625 sheets using genetic algorithm,” *Acta Metall. Sin. (English Lett.*, vol. 25, no. 3, pp. 179–189, 2012.

Chapter 3

Methodology

3.1 Gas metal arc welding

In gas metal arc welding (GMAW), the arc plasma is generated by the direct contact between a consumable electrode and the surface of a workpiece, the former being constantly supplied by a wire feed unit [3.1, 3.2]. The energy originated from the arc is sufficient to melt both the electrode and workpiece, which fuse together and then solidify. In addition, the molten pool is protected from atmospheric gases by the shielding gas supplied through the welding torch [3.3, 3.4].

In this research, the GMAW technique was performed using a 3-phase Miller XMT 304 Series DC inverter arc welder with a 60% duty cycle rating of 300 A at 32 VDC. A Miller 20 Series 24V wire feeder was connected to the inverter. The semi-automated welding torch was an Abicor Binzel ABIMIG 350 TM attached to the welding rig. The torch was upright in relation to the plate, with a 90° angle between the nozzle and the workpiece. The nozzle diameter was equal to 16 mm in all experiments, apart from those in chapter 4 where the nozzle diameter was varied between 13 and 16 mm to evaluate its impact on the weld properties.

In chapter 4, where reductions in the shielding gas flow rate and variations in the nozzle diameter are studied, a pre-calibrated Regula EWR welding monitor was used to record and monitor the shielding gas flow rate (SGFR), whilst in all the other experiments the SGFR was adjusted according to a set of flowmeters. Additionally, the SGFR was measured at the exit of the nozzle before initialising the welding process, using a flowmeter to ensure precision.

3.2 The welding rig

The welding rig is presented in Fig. 3.1. During the welding process, the workpiece moved below the welding torch, which was stationary throughout each procedure. While the welding torch was semi-automated, the workpiece travel speed was controlled by a computer using visual programming in the LabVIEW software (see Appendix A).

A one-pass butt weld was carried out using 4 mm thick plates for all welds. All welds had a square-edge butt preparation with a ceramic backing strip on the underside of the weldment. Each workpiece was composed of two plates, tack welded before the welding procedure. Plates used in chapters 4, 5 and 6 were 500x200x4 mm (see Fig. 3.1), whereas those utilised in chapter 7 were 250x200x4 mm (see Fig. 3.2). All workpieces were positioned on four corner supports, calibrated to have the same height, so that plates could distort freely during the cooling process after welding.

Stepper motors controlled the movement of an optical distance sensor attached to the rig, measuring the distortion of the workpiece (see Fig. 3.3). The optical distance sensor type was a M5L/100. The sensor provided a stand-

off distance of 220 mm, a linearity of 0.3 and a resolution of 0.03 mm, being able to measure displacements ± 50 mm. The difference between the workpiece distortion before and after welding was used to compare the welded structures. In addition, a 45-minute period was allowed for plates to cool down after the joining process before recording the respective deformation.

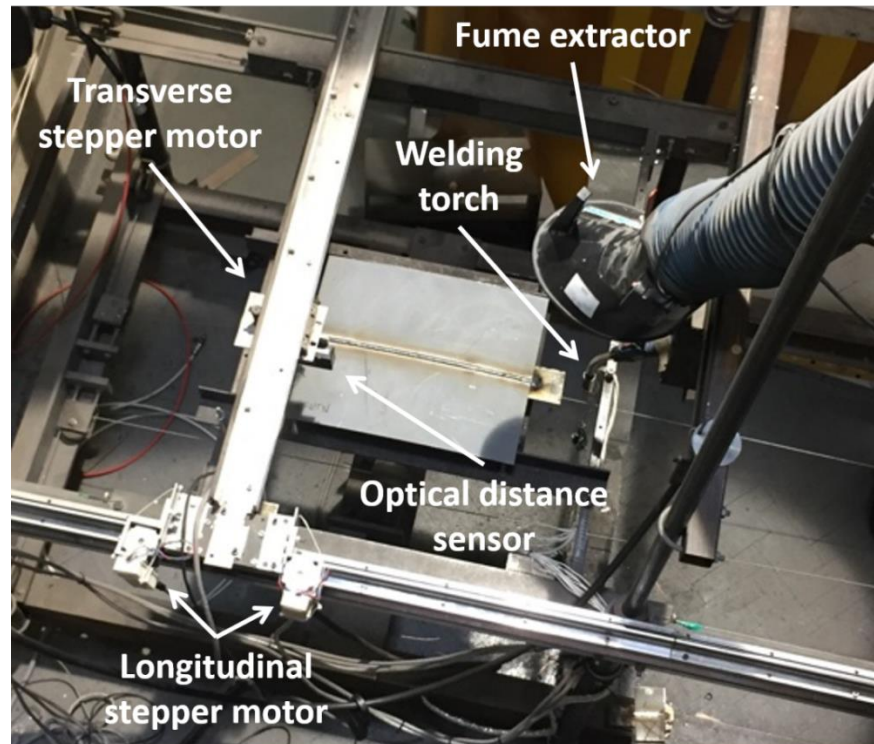


Fig. 3.1 Welding rig with the workpiece after welding.

The temperature of the joints was measured for each weld via pre-calibrated K-type thermocouples, from which signals were interpreted using the LabVIEW software. The thermocouples were positioned underneath the workpiece's mid-section and spaced at 10 mm intervals. The temperature range of this thermocouple type was -180 to 1350 °C, conforming with a minimum of class two tolerance error, i.e. ± 2.5 °C (-40 to 333 °C) and ± 0.0075 T (333 to

1200 °C) [3.5]. The thermocouples were inserted 10 and 20 mm away from the plate root gap before welding, with both sides of the plate being quantified to guarantee completeness.

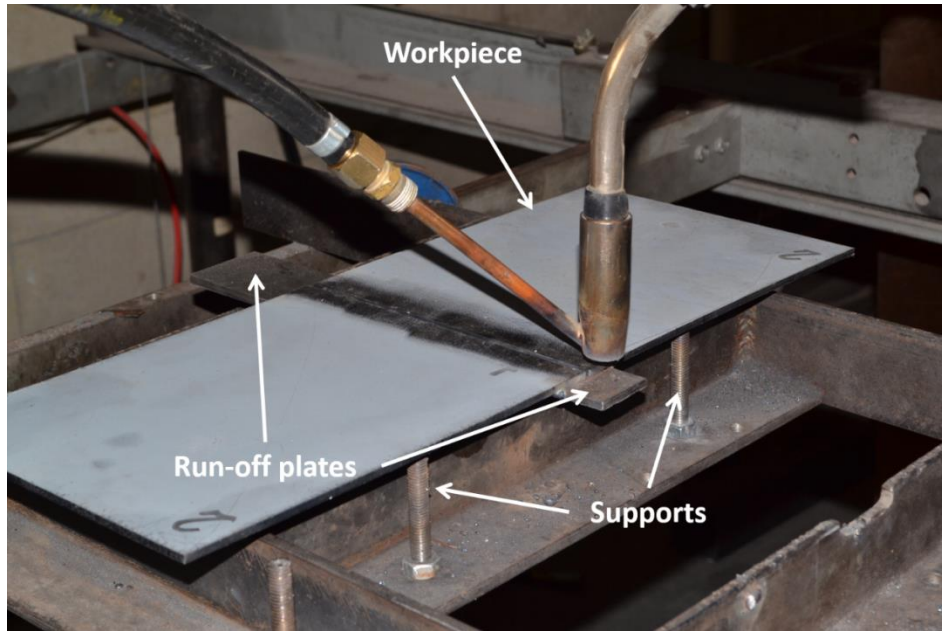


Fig. 3.2 Workpiece setup before the alternating shielding gas welding procedure.

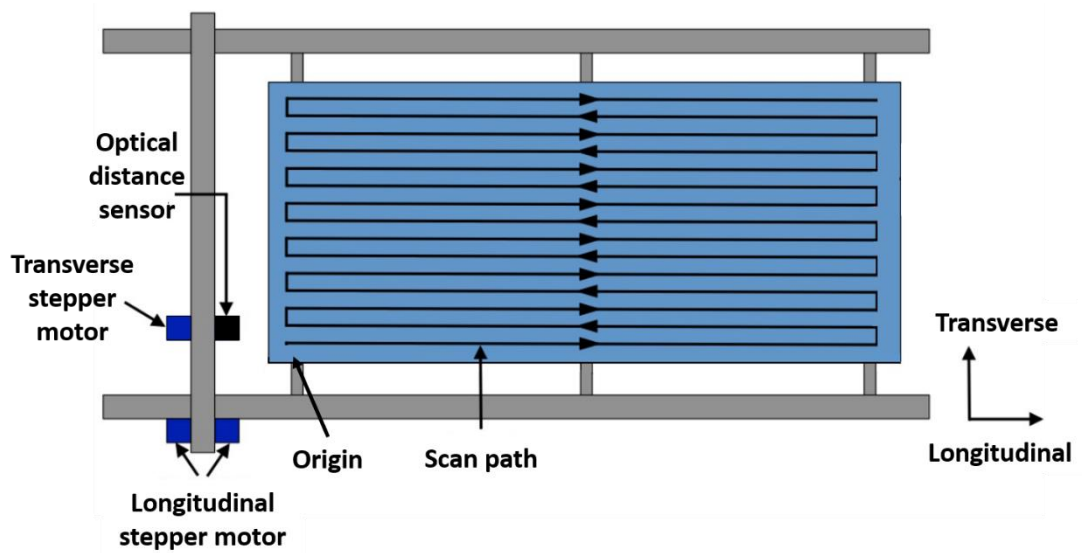


Fig. 3.3 Schematic of the distortion measurement procedure (adapted from [3.6])

3.3 The alternating shielding gas technique

The frequency of each SGFR during the alternating shielding gas process was regulated by an electronic gas control unit (see Fig. 3.4), assisted by an oscilloscope for validation. The system worked via two, eight-pin, triple five (555) timing circuits, which directed a control signal to the solenoid valve on each gas supply line, adjusting the gas supply [3.6]. The on/off functionality of the control unit permitted maintaining the final gas consumption (initially set for each gas) as the predetermined value, despite the chosen frequency. However, some uncertainty it is appreciated in terms of gas mixing at the nozzle exit. The welding torch utilised during the alternating shielding gas experiments is presented in Fig. 3.5.



Fig. 3.4 Electronic gas control unit used to alternate the shielding gases [3.6].



Fig. 3.5 Nozzle utilised for the alternating shielding gas technique.

3.4 Portable arc and shielding gas monitoring systems

Values for voltage and current during experiments were documented by an AMV3500 portable arc monitoring system (see Fig. 3.6), which works with a sample frequency of 5 kHz, and an accuracy of 0.012 V and 0.12 A. The system is composed of 6 data channels, being able to record and analyse up to 5000 samples per second per channel [3.7]. In chapter 4 the SGFR was calibrated, monitored and recorded by a Regula EWR welding monitor, which

also displayed the welding current and gas pressure during experiments (see Fig. 3.7).

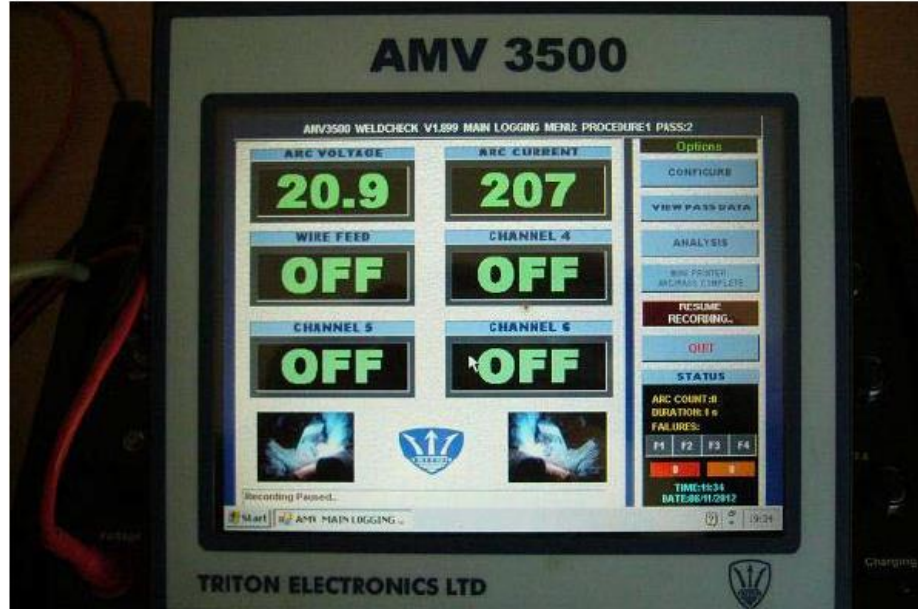


Fig. 3.6 AMV 3500 portable arc monitoring system (adapted from [3.7]).

The heat input was calculated according to equation 3.1 by utilising data collected from the AMBV3500, where Q is the heat input, V is the arc voltage, I is the welding current and v is the torch speed. The thermal efficiency factor (n) was considered to be equal to 1 since GMAW was the only welding process used throughout this thesis. It is appreciated, however, that the thermal efficiency factor impacts directly the heat input and vary according to the welding process.

$$Q = \frac{(V \cdot I)}{v} \cdot n \quad 3.1$$

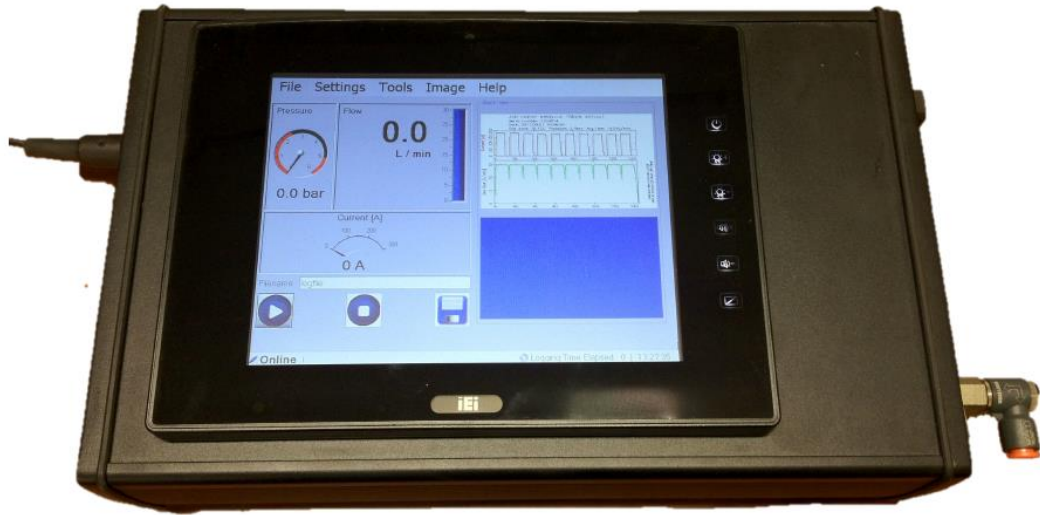


Fig. 3.7 Regula EWR welding monitor (adapted from [3.6]).

3.5 Materials

Various weld filler types have been documented in the technical literature [3.8]. For this study, a 1.2 mm diameter flux-cored filler wire SF-1A was employed to weld steel grade DH36 plates [3.9]. The chemical compositions of both materials as well as their mechanical properties are presented in Table 3.1 and Table 3.2.

Table 3.1 Chemical composition of DH36 steel [3.10] and SF-1A filler wire [3.11].

	C	Mn	Si	P	S	Al (min)	Nb	V	Ti
DH36 (*%max)	0.18*	0.9- 1.6	0.5*	0.035*	0.035*	0.015	0.02- 0.05	0.05- 0.1	0.02
SF-1A	0.04	0.41	1	0.01	0.008	-	-	-	-

Particles (0.6 - 1 mm) were shot blasted via a steel grit on the surface of each DH36 grade steel plate, subsequently coated with an Interplate 937 primer. Typically employed in the shipbuilding industry, the primer was composed of ZnO in a silicate binder (17 μm film thickness) [3.6].

Table 3.2 Mechanical properties of DH36 steel [3.10] and SF-1A filler wire [3.11].

	Yield strength [MPa]	Tensile strength [MPa]	Elongation [%]
DH36	> 355	490-620	>21
SF-1A	530	590	28

3.6 Metallographic preparation

From each weld, four specimens were sectioned, hot mounted, ground and polished, followed by etching. A water jet was utilised to cut specimens from the weldment for microstructural characterisation. This avoided changes in the microstructure through heating, chemical attack or mechanical damage since a coolant was employed during the sectioning procedure. The dimensions of each specimen were 27x4x10 mm.

To reduce any possible damage to the specimens and ease handling, specimens were further hot-mounted. Struers Multifast thermosetting phenolic resin was employed on a Struers ProntoPress-10 mounting press together with the weld specimen, resulting in a uniform, well protected specimen shape.

The next step was to grind off extra material from the damaged surface of the hot-mounted specimen so proper analysis could be carried out in the

microscope. Silicon carbide (SiC) abrasive papers were progressively applied to the specimen's surface in the respective order: 120, 220, 500, 800, 1200, and 2400 (see Fig. 3.8). These numbers indicate the amount of SiC grains per square inch. Additionally, water was used as a coolant to reduce the heat to the specimen.

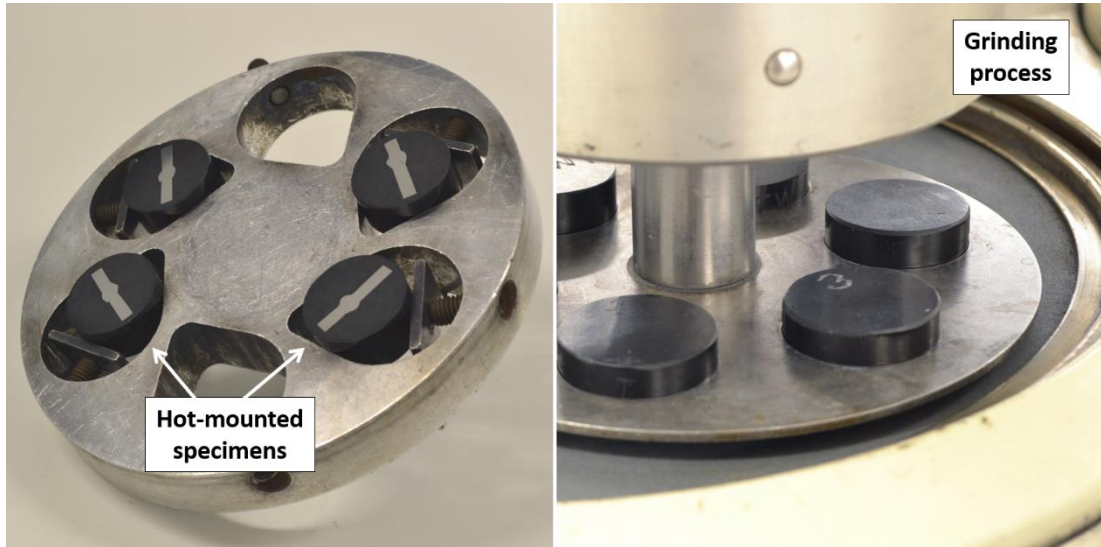


Fig. 3.8 Grinding process after hot mounting the specimens.

Subsequently, the weld surface was polished using three different polishing pads with a soft cloth surface. This permitted abrasive particles suspended in lubricant to roll/slide across the cloth and specimen. A first DP-MOL pad with a diamond suspension of 6 μm was initially used followed by a second with a 3 μm suspension. A DP-lubricant composed of alcohol based with high cooling and low smearing was added during the process in both cases. Afterwards, an OP-CHEM pad was employed utilising a 0.05 μm colloidal silica polishing suspension.

The result of a polished surface is a mirror finish, which appears as a plain white field on the microscope. In order to expose grain boundaries, highlight different phases, and identify inclusions it is necessary to corrode the specimen's microstructure, which is achieved by applying etchants (chemical solutions) to the specimen's surface. In this study, the etching agent Nital solution (2 ml nitric acid/ 98 ml ethanol) was employed to reveal the austenite grain boundaries and other phases in the steel microstructure.

3.7 Microscopy analysis

A light optical Olympus GX51 inverted microscope [3.12] was employed to first assess the specimen's microstructure. The system was composed of a UIS2 infinity-corrected optical system and depolariser lens, which combined a set of polariser and analyser plates to remove spot flares and perform high quality images. The instrument comprised a differential interference contrast (DIC), utilising a simple switching slider type single prism system. The U-DICR (for all imaging applications), U-DICRH (for high resolution) and U-DICRHC (for high contrast) prisms permitted high quality resolution and contrast images based on a trade-off system (see Fig. 3.9).

A scanning electron Hitachi S-3700N variable pressure microscope [3.13] allowed for a more detailed assessment of the steel's microstructure. It utilises an electron beam accelerated at 0.3 to 30 kV, designed mainly for observation and evaluation of specimens prepared for scanning electron microscopy. The instrument's chamber permitted specimens of up to Ø300 mm and magnifications of up to x300000. Additionally, it features a pre-centred

cartridge type tungsten hairpin filament and a low vacuum observation method between 6 and 270 Pa, enabling the observation of non-conductive specimens.

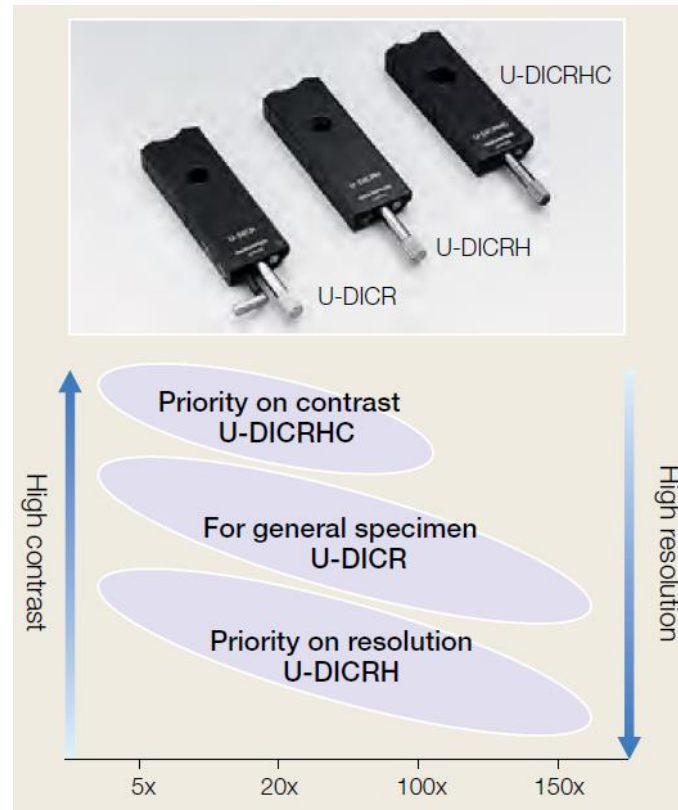


Fig. 3.9 Resolution and contrast trade-off system for DIC prisms.

3.8 Grain size measurements

Assisted by scanning electron microscopy images, the Abrams three-circle procedure, a circular intercept procedure type, was performed to measure the mean grain size of all welds (see Fig. 3.10) [3.14]. The three concentric and equally spaced circumferences were applied to a minimum of five randomly selected and widely spaced (≥ 1 mm) weld areas, counting the number of intersections between the grain boundary and each circumference.

Once the number of intersections N_i was counted per weld area for a specific weld, it was utilised to calculate the lineal intercept \bar{l} (see equation 3.2), where L is the length's sum of each of the three employed circumferences and M is the magnification. With all the lineal intercept values of the respective weld determined, the mean lineal intercept l is calculated and used in equation 3.3 to define the ASTM grain size number G and, consequently, the mean grain size g of the selected fusion zone (see equation 3.4). Furthermore, statistical analyses were carried out to define the precision of the data collected, with a 95% normal confidence.

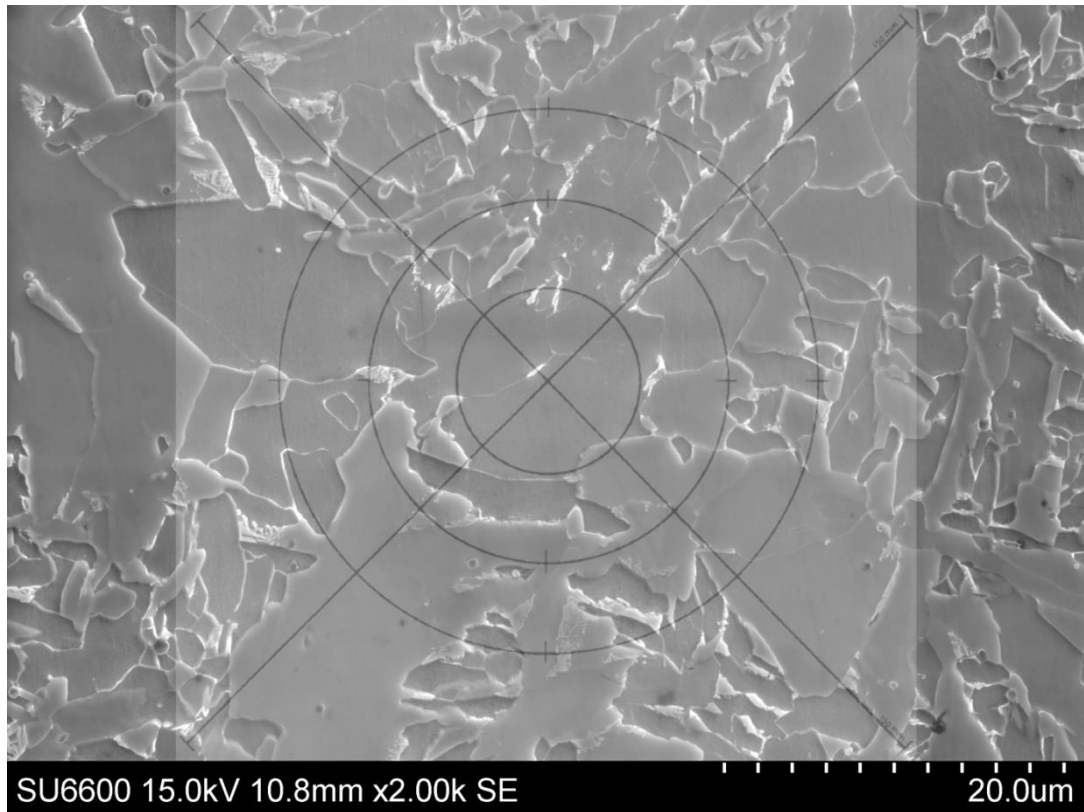


Fig. 3.10 Weld microstructure of a 4.5WT case exemplifying the grain size measurement method.

$$\bar{l} = \frac{(L/M)}{N_i} \quad 3.2$$

$$G = (-6.643856 \log_{10} l) - 3.288 \quad 3.3$$

$$g = \frac{10^6}{15.5(2^{G-1})} \quad 3.4$$

3.9 Weld geometry

Data of the cap width, root width and heat affected zone (HAZ) area were collected using the ImageJ software (see Fig. 3.11). Aiming for precision, a minimum of two specimens per weld was measured and the respective mean value, reported.

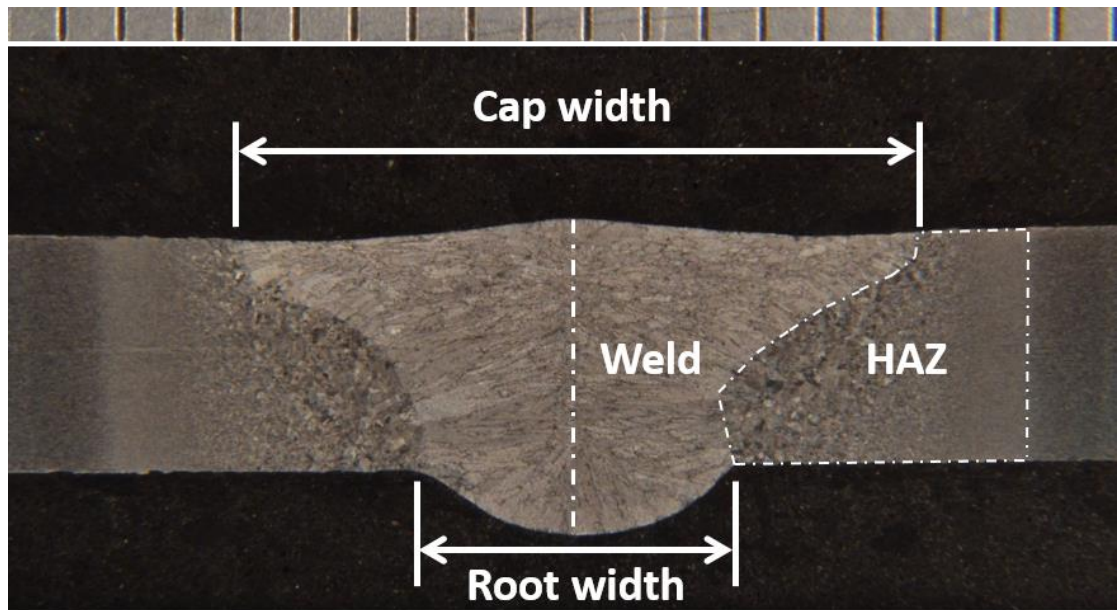


Fig. 3.11 Features of the weld geometry measured in this study.

3.10 Mechanical testing

3.10.1 Hardness measurements

Micro-hardness measurements were taken from two specimens across each weld joint along the mid-thickness region employing a Mitutoyo MVK-G1 tester with a 200 g load. A distance of 1 mm was left between each indentation to ensure local work hardening would not impact the determined hardness. A minimum of 10 indentations were taken from each region.

3.10.2 Mechanical property testing

Transverse tensile testing was executed to assess the full cross section of the weld bead, HAZ and parent material. Longitudinal all-weld tensile tests were required to understand the impact of the many welding parameters on the mechanical properties of the weld. Bend tests were performed to further evaluate the presence of defects within the weld. The sectioning process was automated in a water jet cutting system to ensure that samples were taken from similar sections of the weld and increase consistency in replicability.

Transverse tensile tests (see Fig. 3.12) were carried out based on BS EN ISO 4136:2012 [3.15] using an Instron 8802 servo-hydraulic tensile testing system with a strain rate of 0.5 mm/min up to 1.25 mm extension and 5 mm/min thereafter.

Longitudinal all-weld tensile (see Fig. 3.13) and bend (see Fig. 3.14) tests were performed based on BS EN ISO 6892-1:2016 [3.16] and BS EN ISO 5173:2010 [3.17], respectively, with an Instron 5969 servo-hydraulic tensile testing system. The all-weld tests were performed using a strain rate of 0.5 mm/min up to 1.25 mm extension and 1 mm/min thereafter, whilst bend tests

used a 7 mm/min strain rate. All the stress-strain curves for the all weld tensile tests are provided in Appendix C. The transverse tensile stress-strain curves are not included since there was failure within the parent material for all the respective cases. A minimum of three longitudinal and transverse tensile as well as three root and three face bend specimens were tested. The radii on the bend test specimen's edge were machined on the side of the respective test being carried out, i.e. face or root bend test.

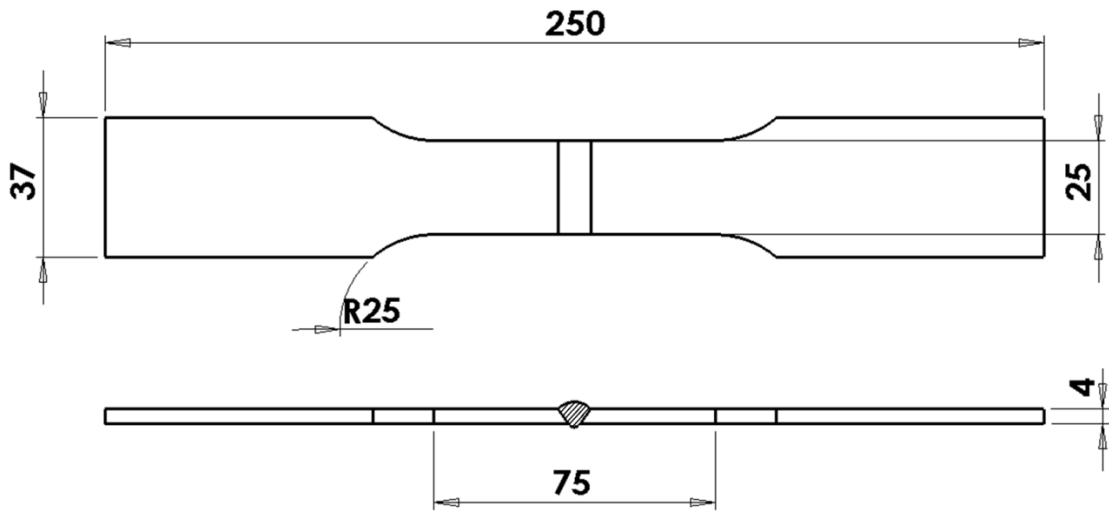


Fig. 3.12 Schematic of a transverse tensile test specimen [mm].

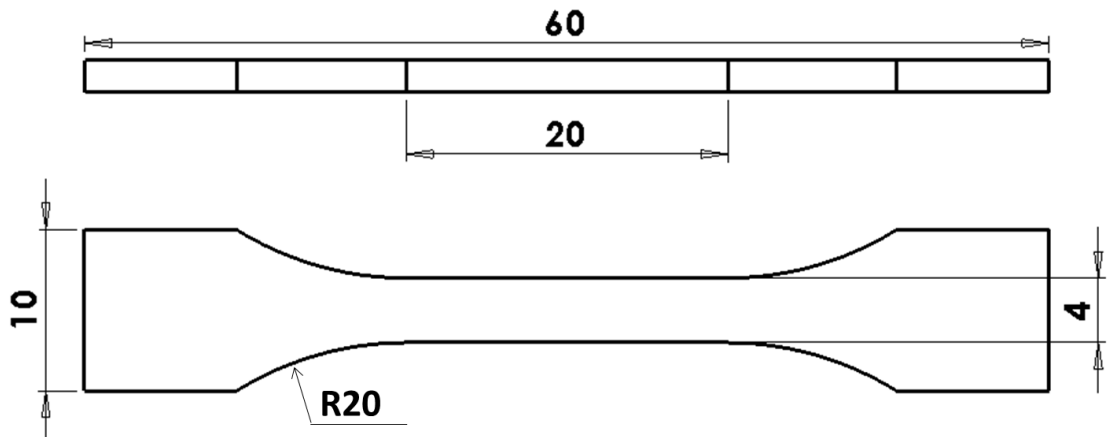


Fig. 3.13 Schematic of a longitudinal all-weld tensile test specimen [mm].

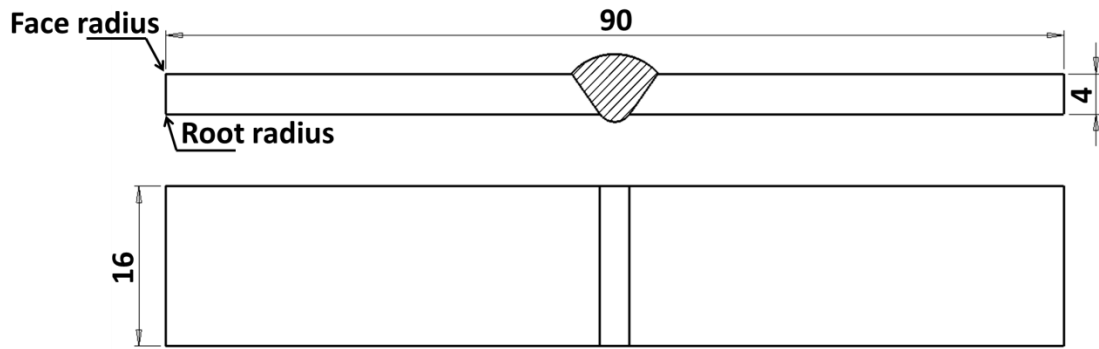


Fig. 3.14 Schematic of a bend test specimen [mm].

3.11 Radiographic assessment

To assess the presence of porosity and any other imperfections within the joints in chapters 4 and 6, radiographs were taken using Smart Andrex 200 X-ray equipment [3.18] after welding all plates (see Fig. 3.15). Analyses were carried out utilising a Yenway SZMN stereomicroscope based on BS EN ISO 10675-1 standard [3.19] and an interpretation guide [3.20].

A Structurix AGFA D7 type radiographic film surrounded by lead screens (0.125 mm thick) was employed since its fine grain film allowed for data at high speed. The focal point size was 1.3 x 1.3 mm, having a power source of 145 kV and 4.5 mA for 50 seconds duration. Additionally, the distance between the object and the source was 800 mm.

The described equipment and methods were employed throughout this thesis to produce joints and assess its many features. Additionally, variables utilised during the welding procedures are provided accordingly in the respective experimental setup section of each experimental chapter.

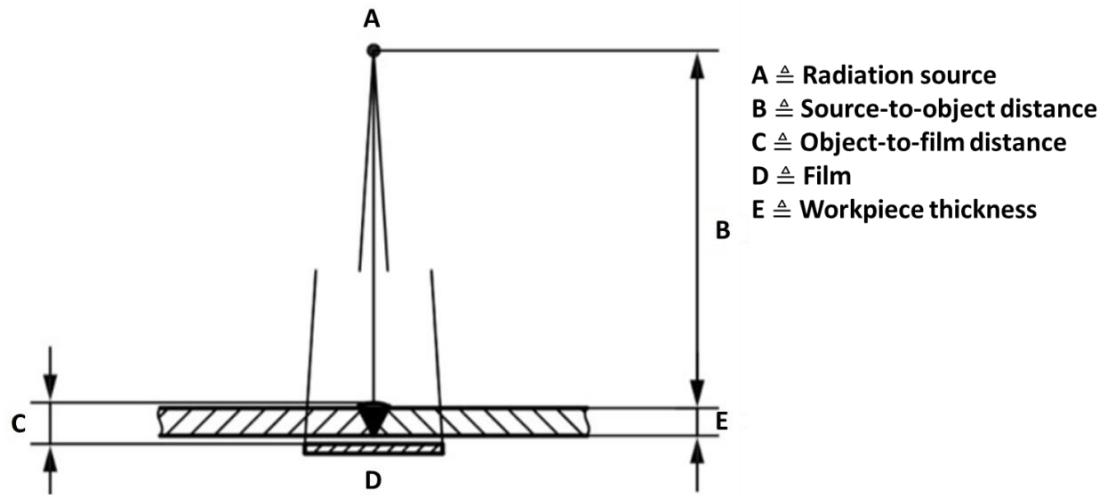


Fig. 3.15 Schematic diagram of the radiographic assessment [3.6].

3.12 Bibliography

- [3.1] A. Moarrefzadeh, “Numerical simulation analysis for Thermal Optimization of Heat Affected Zone (HAZ) in GMAW Process,” WSEAS Trans. Appl. Theor. Mech., vol. 6, no. 2, pp. 59–68, 2011.
- [3.2] S. Zielińska et al., “Investigations of GMAW plasma by optical emission spectroscopy,” Plasma Sources Sci. Technol., vol. 16, no. 4, pp. 832–838, 2007.
- [3.3] C. H. Kim, H. B. Chae, J. H. Kim, and S. Rhee, “The effect of shielding gas composition in CO₂ laser-gas metal arc hybrid welding,” Proc. Inst. Mech. Eng. Part B-Journal Eng. Manuf., vol. 222, no. 11, pp. 1315–1324, 2008.
- [3.4] G. M. Ramsey, A. M. Galloway, S. W. Campbell, N. A. McPherson, and T. J. Scanlon, “A computational fluid dynamic analysis of the effect of side draughts and nozzle diameter on shielding gas coverage during gas metal arc welding,” J. Mater. Process. Technol., vol. 212, no. 8, pp. 1694–1699, 2012.

- [3.5] British Standard Institution, “BS EN 60584-1:2013. Thermocouples - Part 1 : EMF specifications and tolerances,” London: BSI, 2013.
- [3.6] S. W. Campbell, “Shielding Gas Parameter Optimisation in Arc Welding Processes,” University of Strathclyde, 2015.
- [3.7] K. Chawla, “AMV3500 Weldcheck v1.87 Software Manual,” no. January. Triton Electronics Ltd., pp. 1–56, 2010.
- [3.8] American Bureau of Shipping, “Rules for Materials and Welding - Part 2.” 2010.
- [3.9] I. Bitharas, N. A. McPherson, W. McGhie, D. Roy, and A. J. Moore, “Visualisation and optimisation of shielding gas coverage during gas metal arc welding,” *J. Mater. Process. Technol.*, vol. 255, no. December, pp. 451–462, 2018.
- [3.10] Lloyd’s Register Group, “Rules for the Manufacture, Testing and Certification of Materials,” 2011.
- [3.11] Norsk Sveiseteknikk AS, “NST - Product Catalogue.” p. 98, 2012.
- [3.12] “Olympus GX51 inverted microscope specifications.” Olympus, 2013.
- [3.13] “Manual for Model S-3700N Scanning Electron Microscope.” Hitachi High-Technologies Corporation, 2006.
- [3.14] ASTM international, “ASTM E112-13: Standard test methods for determining average grain size,” ASTM International. pp. 1–28, 2013.
- [3.15] British Standard Institution, “BS EN ISO 4136:2012. Destructive tests on welds in metallic materials - Transverse tensile test.” BSI, London, 2012.
- [3.16] British Standard Institution, “BS EN ISO 6892-1:2016. Metallic materials — Tensile testing. Part 1: Method of test at ambient temperature.” BSI, London, 2016.

- [3.17] British Standard Institution, “BS EN ISO 5173:2010 +A1:2011. Destructive tests on welds in metallic materials - Bend tests.” BSI, London, 2011.
- [3.18] British Standard Institution, “BS EN ISO 17636-1:2013. Non-destructive testing of welds — Radiographic testing — Part 1: X- and gamma-ray techniques with film.” BSI, London, 2013.
- [3.19] British Standard Institution, “BS EN ISO 10675-1. Non-destructive testing of welds - Acceptance levels for radiographic testing - Part 1: Steel, nickel, titanium and their alloys.” BSI, London, 2015.
- [3.20] Carestream, “Radiographic Interpretation Guide.” Carestream Inc., New York, 2014.

Chapter 4

Preliminary analysis of the shielding gas flow rate reduction in the GMAW process

4.1 Introduction

There is an ongoing drive to diminishing the shielding gas consumption while guaranteeing high-integrity, porosity-free welds [4.1-4.5]. Benefits include, but are not limited to, the decrease on CO₂ emissions, the reduction of the energy required for gas production and delivery, and the decline on shielding gas wastage, increasing productivity and permitting cost and time savings.

Campbell et al. [4.1] demonstrated that the shielding gas flow rate (SGFR) of ArCO₂ can be reduced to 6 L/min while maintaining the quality of the weld, with savings of around 50% compared to the 15 L/min SGFR base case. Bitharas et al. [4.5] established the 5 L/min SGFR as the most economical option compared to a 10 L/min SGFR by visualising the protective gas flow using the alternating shielding gas technique. Ley et al. [4.6], based on thermal analysis, investigated the effect of various SGFRs on the post-weld thermal properties, suggesting that a 5 L/min SGFR was able to reduce the distortion of the welded structure, which was also proposed by Bitharas et al. [4.4]. Although these studies [4.1, 4.4-4.6] were able to achieve high integrity

welds under low SGFRs, there have been no distortion or temperature measurements providing consistent data to support claims regarding the deformation behaviour of the workpiece.

Chapter 2 showed that the weldment distortion is directly related to the thermal contraction behaviour of the weld throughout the cooling stage [4.6-4.10]. The contraction intensity is affected by the SGFR and influences the quality and integrity of structures after the welding process [4.1, 4.10, 4.11]. As discussed in chapter 2, some of the factors that affect the distortion level are the heat transferred to the parent material as well as the temperature distribution, weld shape, tack welding, residual stresses due to operations prior to assembly and, in many cases, gravity [4.8, 4.11-4.15]. Therefore, it is important to control the aforementioned factors so no rework of the welded structure is required, which can generate significant residual stress fields in the weldment and increase the time and cost of the welding process [4.11, 4.16, 4.17].

Another relevant factor that influences the final weld properties is the nozzle diameter [4.2, 4.18, 4.19]. Ramsey et al. [4.2], through computational and experimental work, found that constrictions in the nozzle permitted better protection of the molten pool and reductions in the shielding gas consumption. This was due to the higher velocity of the protective gas exiting the nozzle, which was also reported by Ham et al. [4.18] using gas tungsten arc welding (GTAW). Numerical simulations by Konishi et al. [4.19] in GTAW showed that the constriction of the nozzle enhanced the temperature and velocity of the arc plasma due to the higher thermal pinch effect, with consequent increase in the heat input. Despite demonstrating the effects of decreasing the nozzle diameter on the weld, these studies [4.2, 4.18, 4.19] were limited in terms of

distortion measurements, microstructural characterisation of the weld and its mechanical properties. Additionally, no correlation between variations in the SGFR and nozzle diameter was exhibited, which could assist with reductions in the shielding gas wastage.

In the present chapter, extensive testing programmes were carried out to examine the effects of reducing the SGFR used during the GMAW process on factors such as distortion and temperature of the joint. Upon the combination of different nozzle diameters and SGFRs, the post weld microstructure and mechanical properties of DH36 grade steel plates were assessed. The findings from this evaluation were directly correlated to the final attributes of the weld such as distortion, temperature and weld shape, and contribute towards the reduction of the gas usage during the GMAW process.

4.2 Experimental setup

Beyer et al. [4.20] suggested that a move to a Ø14 mm nozzle would allow for a reduction in the flow rate to 9 L/min, stated elsewhere [4.1] to generate low levels of impurity and high integrity welds. Campbell et al. [4.1] were not able to further reduce the SGFR since it was limited by the gas saving device to 6 L/min.

Based on literature findings [4.1, 4.20], the benchmark for the study carried out in this chapter was Ar20CO₂ shielding gas with a flow rate of 9 L/min and a Ø16 mm nozzle (Ø16_9L/min). Two different SGFRs were evaluated in a draft-free environment: 5 and 9 L/min and nozzle diameters equal to 16 and 13 mm, employed with a stand-off distance of 10 mm. The lowest SGFR was defined based on previous work [4.4] suggesting that 5 L/min

produced good quality welds. Table 4.1 presents the mean welding parameters used for this set of experiments, with a 4 mm root gap, 5 mm/s travel speed of the welding torch, and 7.5 m/min wire-feed speed.

Table 4.1 Mean experimental welding parameters.

Shielding Gas	SGFR [L/min]	Nozzle diameter [mm]	Voltage [V]	Current [A]	Heat Input (J/mm)
Ar20CO ₂	9	16	22.8	238	1085
Ar20CO ₂	9	13	22.7	236	1071
Ar20CO ₂	5	16	22.8	240	1094
Ar20CO ₂	5	13	22.7	238	1080

Thermal efficiency factor = 1

4.3 Results and discussion

4.3.1 Distortion of the parent material

To clarify the distortion behaviour, saddle-like shape [4.8, 4.21] plots and severity maps of the workpiece were generated (see Fig. 4.1 (A - H)). The analysis of all four combinations provided similar distortions between all presented welds, being more pronounced on the midside of each structure (darker regions). Measurements were then taken in both longitudinal and transverse directions (dashed lines) to compare the cross-sectional distortion of all the studied cases.

Findings demonstrated that using a SGFR of 5 L/min resulted in modest, but consistent reduction in both transverse (see Fig. 4.2) and longitudinal (see Fig. 4.3) distortions compared to the benchmark (\varnothing 16 mm

nozzle - 9 L/min SGFR). The 5 L/min SGFR provided reductions in the distortion for both nozzles, with the $\text{\O}16$ mm case presenting the highest reductions: 0.86 and 1.23 mm in the transverse and longitudinal directions, respectively.

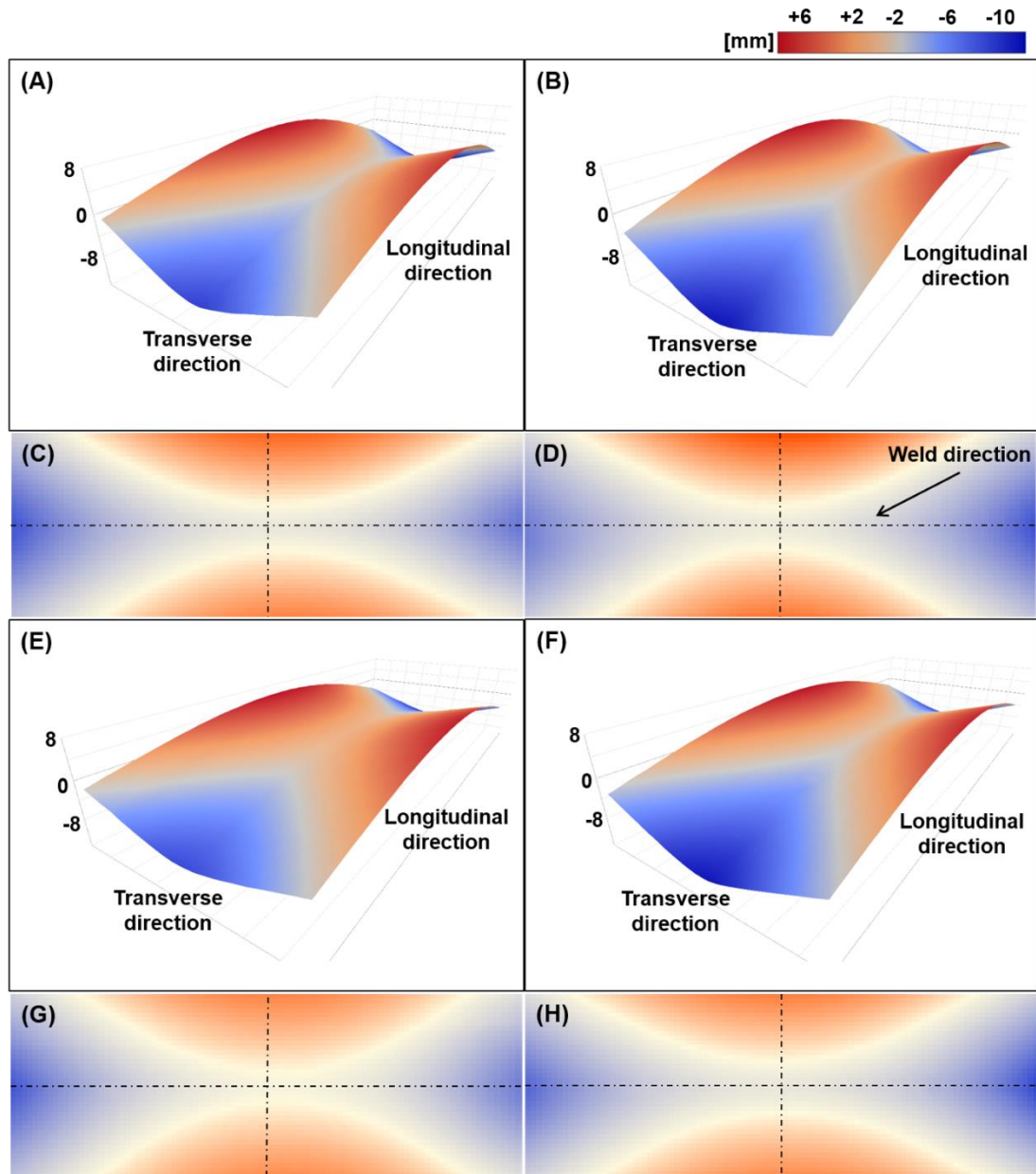


Fig. 4.1 Typical 3D plots and severity maps (top view) of the distortion of the welded plates. (A) and (C) $\text{\O}16$ mm - 9 L/min. (B) and (D) $\text{\O}13$ mm - 9 L/min. (E) and (G) $\text{\O}16$ mm - 5 L/min. (F) and (H) $\text{\O}13$ mm - 5 L/min.

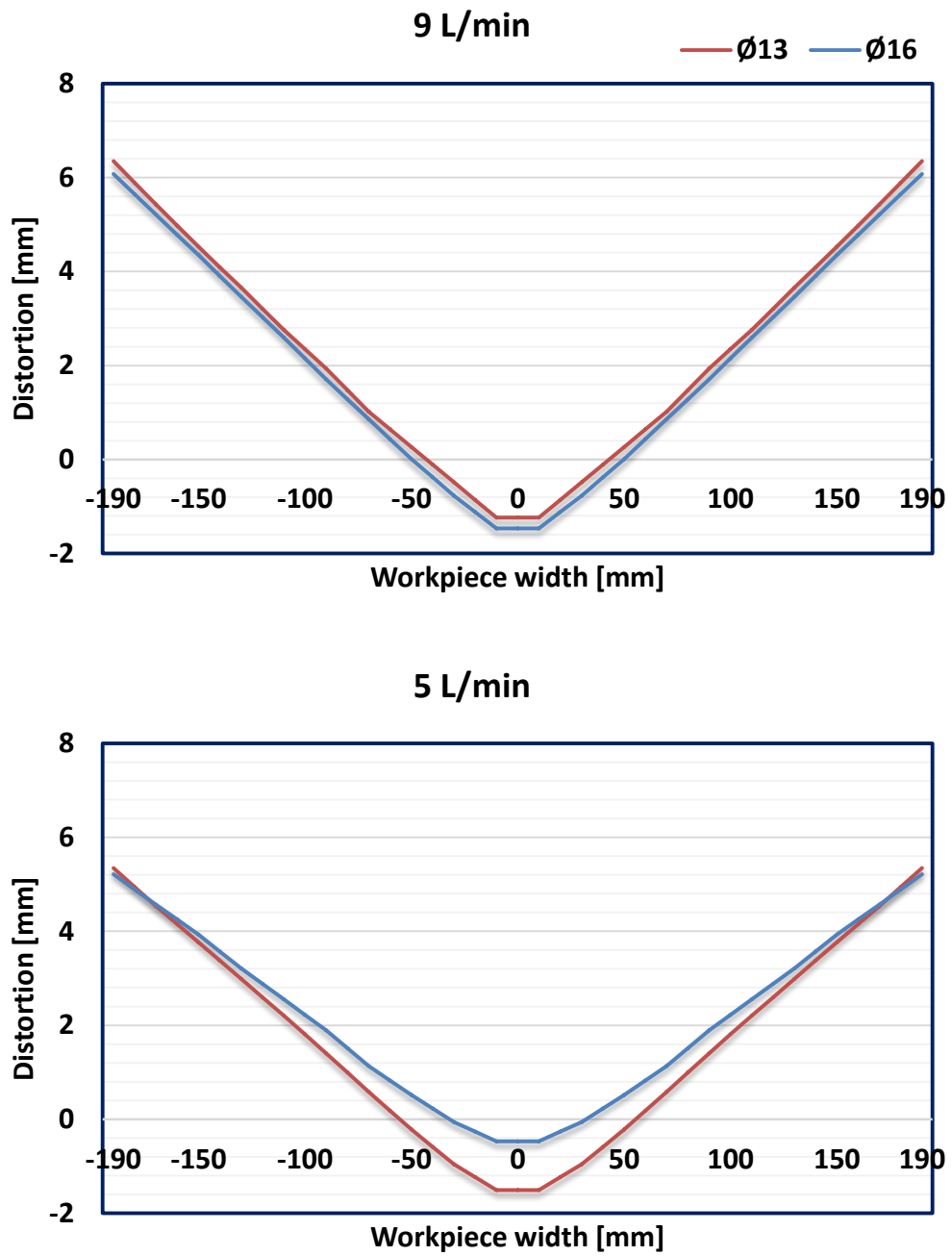


Fig. 4.2 Mean distortion of weldment's cross-sections in the transverse direction.

These findings were suggested by Bitharas et al. [4.4], who showed that lowering the SGFR would reduce the convective heat transfer due to a lower

momentum of the fluid towards the workpiece. Ley et al. [4.6] was of the same point of view, demonstrating that the higher SGFR increased the thermal expansion coefficient of the joint and consequently its volumetric expansion-contraction. Thus, higher residual stress within the structure was generated, affecting the overall distortion of the workpiece.

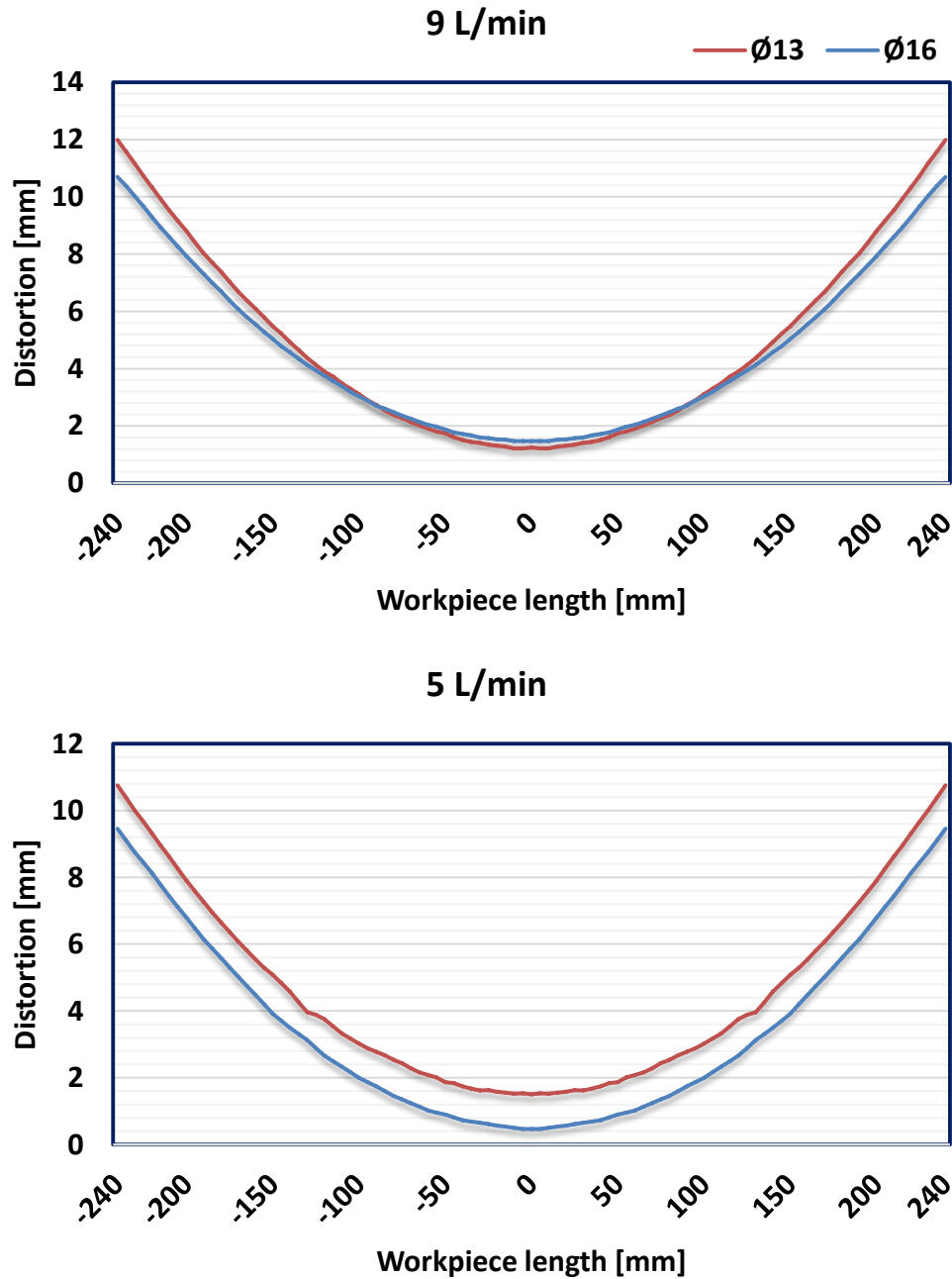


Fig. 4.3 Mean distortion of weldment's cross-sections in the longitudinal direction.

Similarly, numerical simulations in GTAW by Kyohei et al. [4.19] showed that, under a smaller nozzle diameter, the plasma constriction caused increased thermal conduction and thermal flux. This is in line with findings of the present study, where, compared to the benchmark, the 9 L/min - Ø13 mm nozzle case induced the maximum distortion on the extremes of the joined plates in both directions.

4.3.2 Temperature measurements

Temperature and distortion data were found to be proportional to one another. Either a flow rate of 9 L/min or a Ø13 mm nozzle presented a trend of increased temperature of the weld. This is in line with the numerical model by Kyohei et al. [4.19], who explained that the nozzle constriction promotes a narrower arc plasma, with the arc energy concentrated on the central part of the arc. Hence, the restricted heat source enhances the heat input on the workpiece, resulting in increased thermal flux and temperature of the joint.

The variance between temperatures (see Fig. 4.4 and 4.5), however, was minor compared to the benchmark, with differences below 10°C for data collected 10 mm away from the root gap and 25°C, 20 mm away.

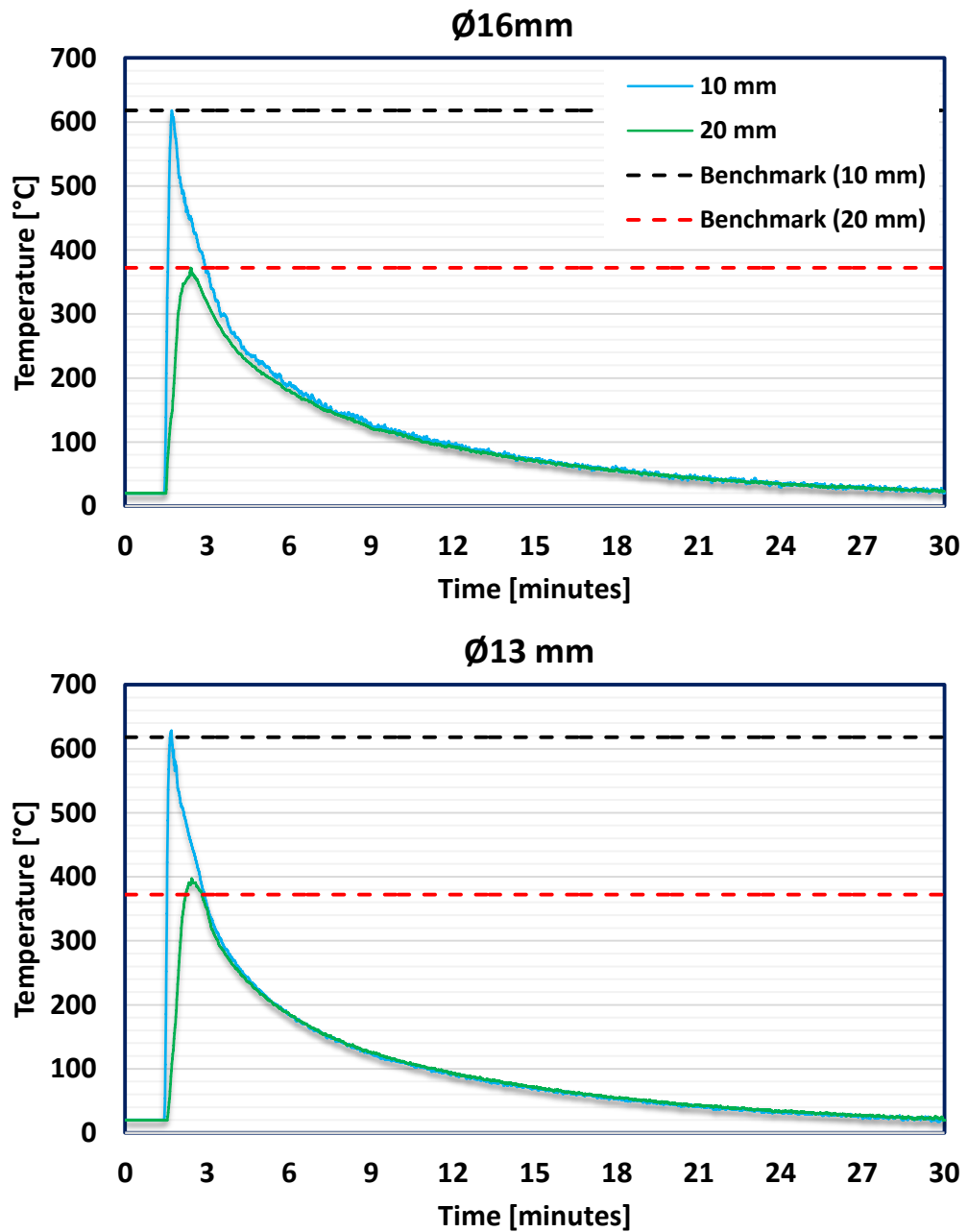


Fig. 4.4 Mean thermal transients in positions 10 and 20 mm under 9 L/min.

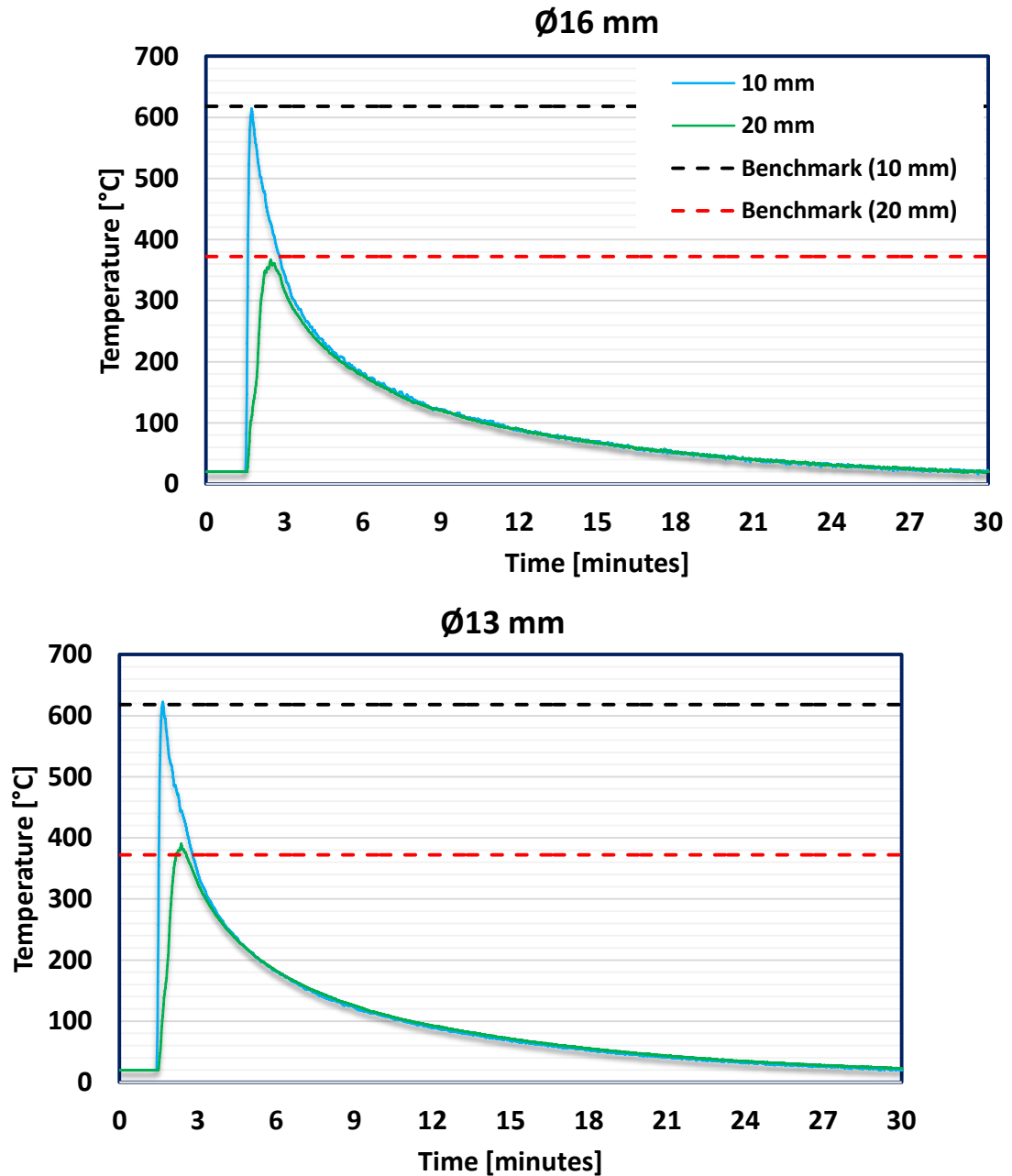


Fig. 4.5 Mean thermal transients in positions 10 and 20 mm under 5 L/min.

4.3.3 Weld characteristics

The weld shape was assessed to check for dissimilarities between the cap and root widths of the fusion zone as well as heat input, which can influence the weldment distortion [4.11, 4.14, 4.22, 4.23]. The shape of each weld was

measured to better clarify how modifications of either the nozzle diameter or the SGFR would affect the final joint. Three variables were considered: the cap and root widths of the weld and the heat affected zone (HAZ) area (see Fig. 4.6 (A), (B)).

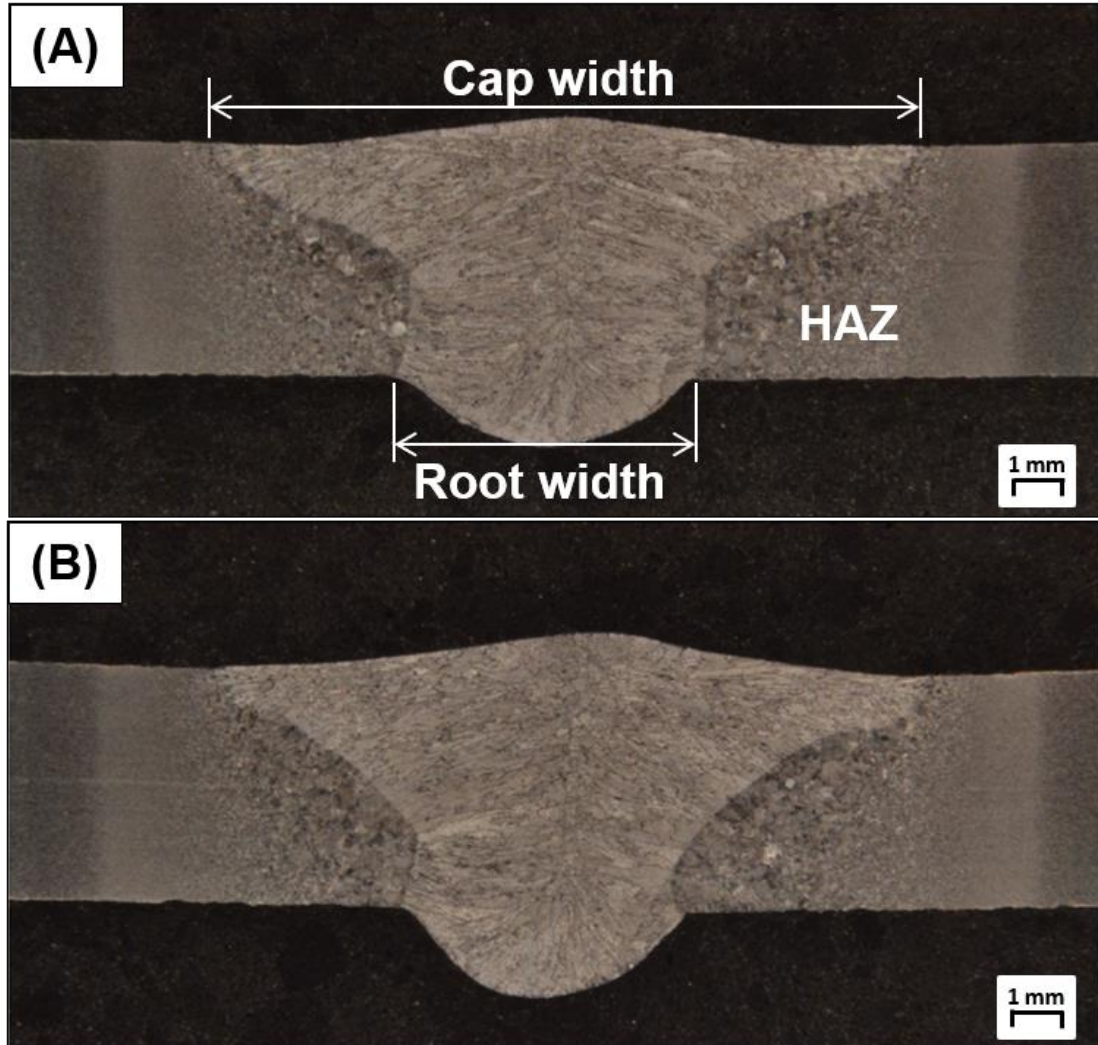


Fig. 4.6 Weld shape and HAZ comparison (etched). (A) $\text{Ø}16$ mm – 9 L/min. (B) 13 mm – 5 L/min.

Howse and Lucas [4.24] and Kaul et al. [4.25], utilising GTAW, discussed the effect of the arc constriction increasing the depth and reducing

the cap width of the weld due to the presence of an active flux. However, minor differences between measurements were found. The mean HAZ of all cases was equal to 20 mm², the mean cap width, 13.4 mm, and the mean root width, 6 mm; all averages within a maximum standard deviation of 0.3 mm² and 0.4 mm, respectively.

These findings demonstrated that it is possible to achieve a SGFR of 5 L/min without compromising the integrity of the joint, achieving savings of 4 L/min and 10 L/min when compared to the 9 L/min and 15 L/min [4.1], respectively.

4.3.4 Microstructural characterisation

The microstructure of each weld was assessed utilising an optical microscope and a scanning electron microscope. All cases provided a consistent microstructure, where neither porosity nor inclusions of significant size [4.26] were present. Besides the development of allotriomorphic ferrite (see Fig. 4.7 (A)), inclusions of approx. diameter 2.9 – 4.9 µm were observed, which worked as nucleation sites [4.26, 4.27] for the growth of acicular ferrite (see Fig. 4.7 (B)). Further analysis using the scanning electron microscope equipped with energy disperse spectroscopy has shown that inclusions were composed mainly of iron oxides (43 wt.% Fe – 33 wt.% O) and manganese oxides (19 wt.% Mn – 45 wt.% O), with a minor presence of titanium and silicon.

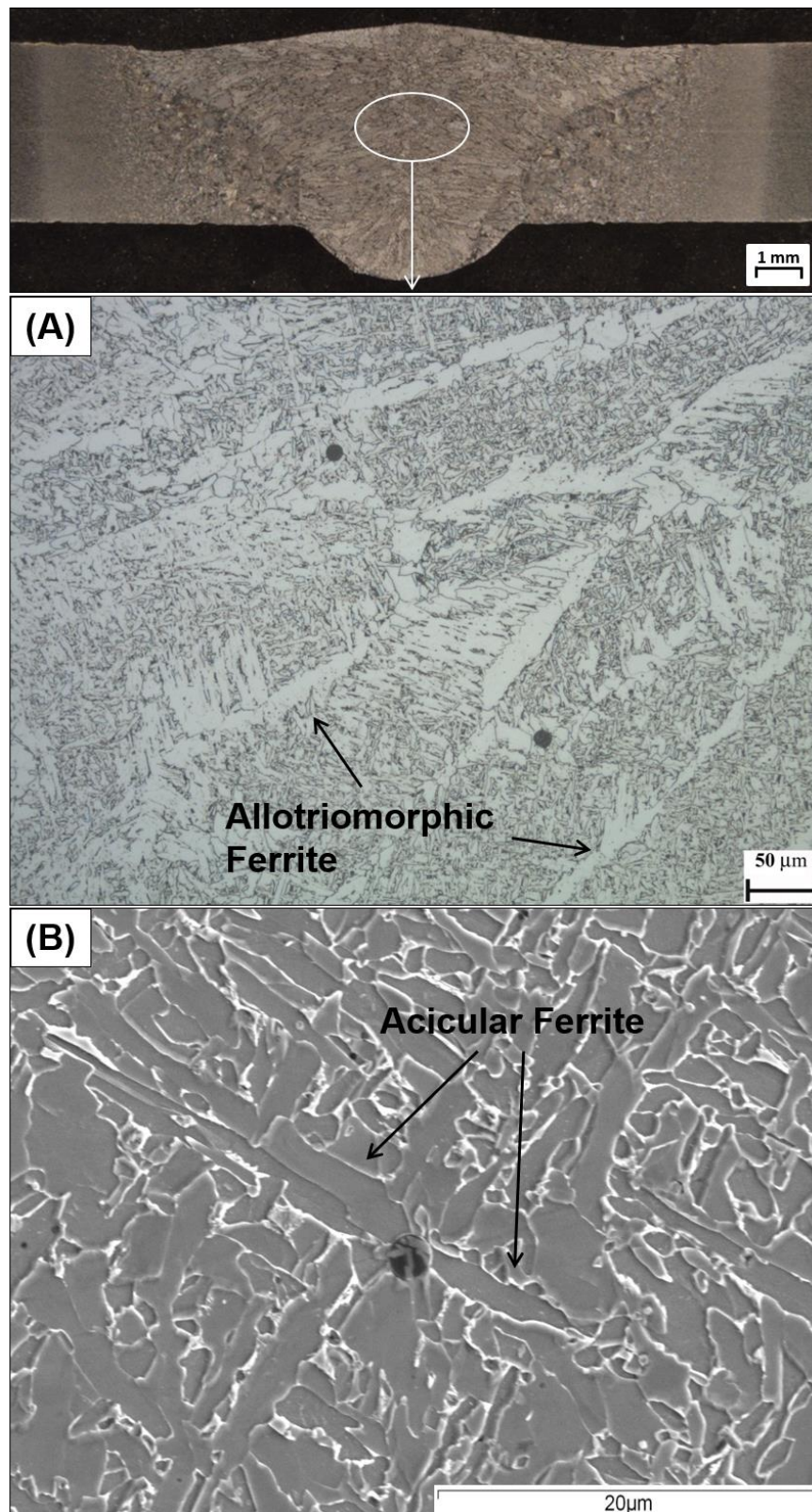


Fig. 4.7 Weld microstructure of 5L/min cases. (A) $\text{Ø}13$ mm - x200 (etched). (B) $\text{Ø}16$ mm - x3000 (etched).

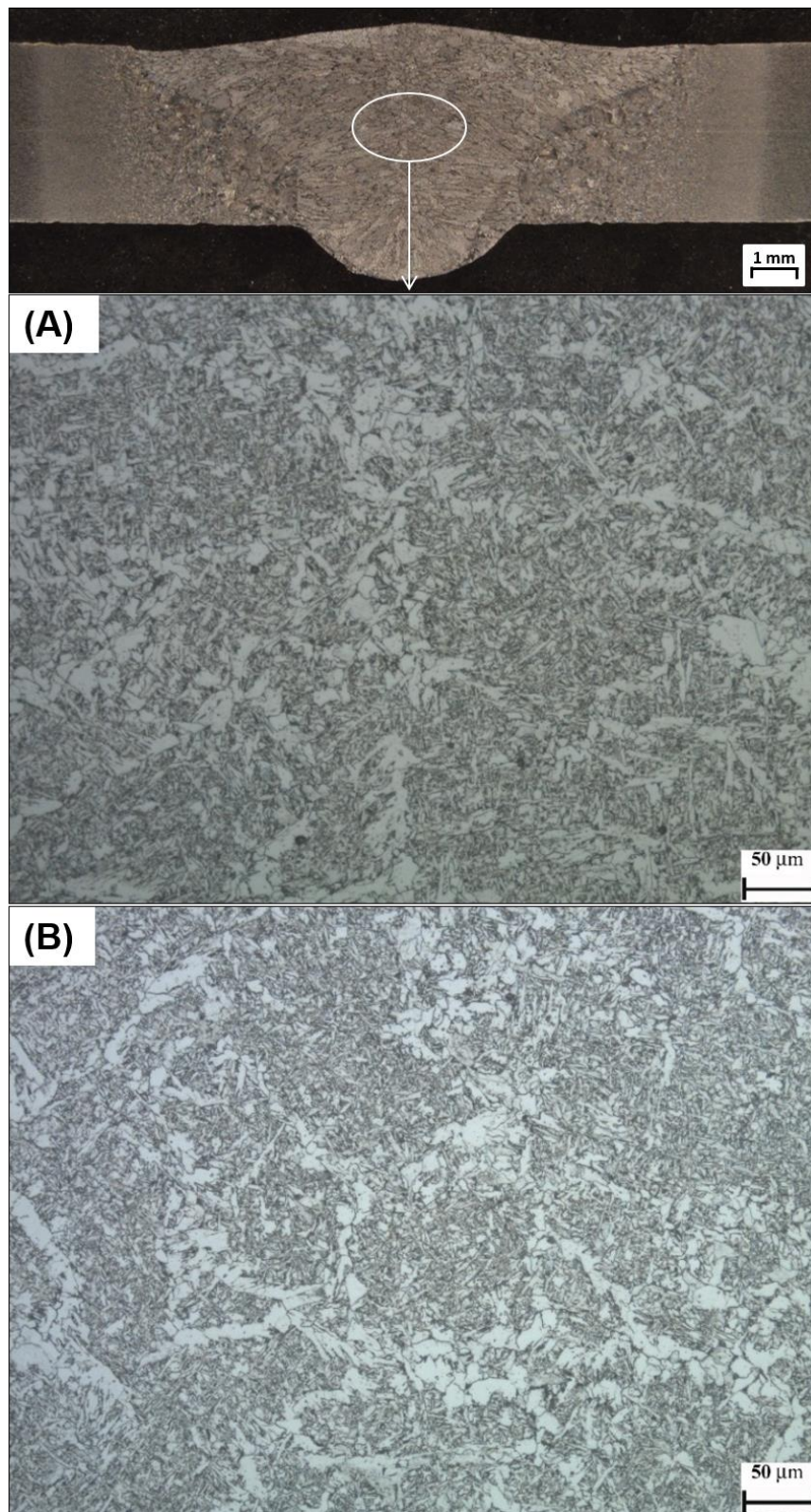


Fig. 4.8 Weld microstructure comparisons, x200 (etched). (A) $\text{Ø}13$ mm – 9 L/min. (B) $\text{Ø}16$ mm – 5 L/min.

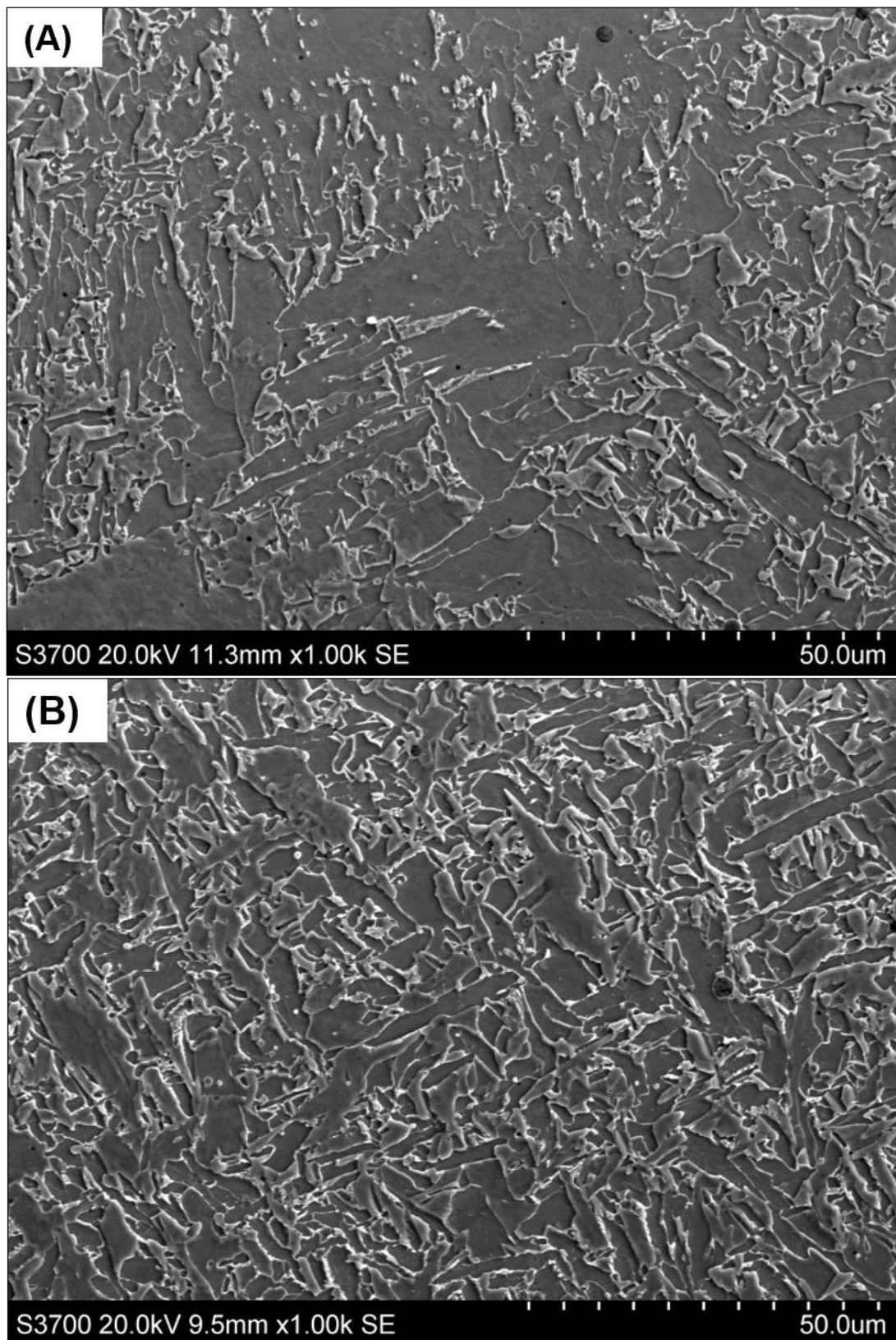


Fig. 4.9 Weld microstructure comparisons, x1000 (etched). (A) $\text{\O}16$ mm – 9 L/min. (B) $\text{\O}13$ mm – 5 L/min.

Microstructural characterisation (see Fig. 4.8 (A), (B)) has shown that all the welds were composed of very similar grain sizes. Differences in the presence of ferrite types within the weld region, for instance, were indistinguishable. This supports results from the mechanical tests (see section 4.3.6), where negligible dissimilarities were found between all joints.

Fig. 4.9 ((A), (B)) shows the microstructure of the performed welds, with the microstructural characterisation undertaken on the scanning electron microscope to identify any undesired features. The development of finer grains was expected when reducing the nozzle diameter since more metal vapour is formed [4.18], constricting the arc [4.28] and cooling the vicinity of the molten pool [4.29], i.e. less heat is absorbed by the joint (see Fig. 4.9).

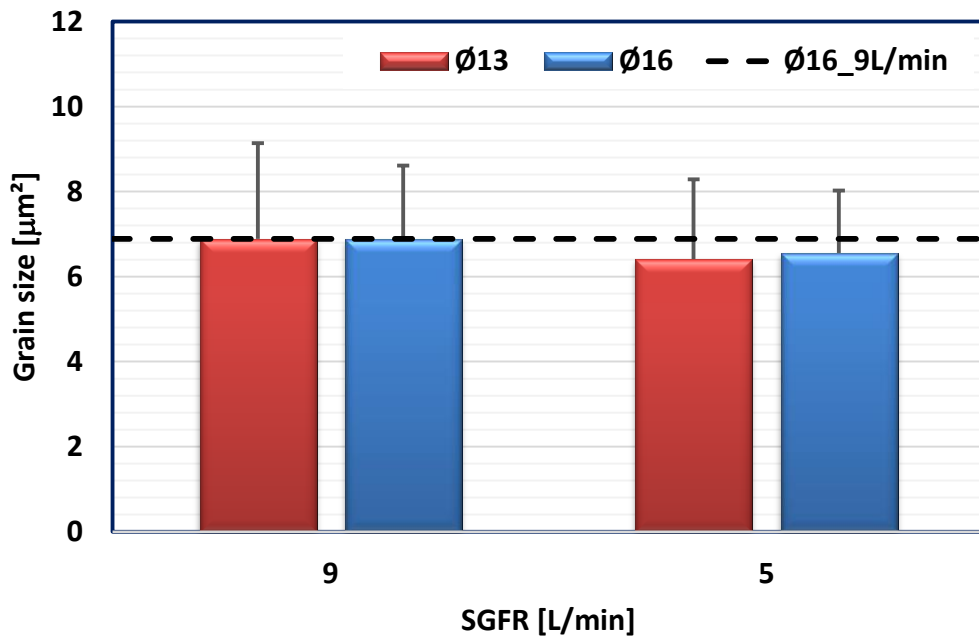


Fig. 4.10 Mean grain sizes.

To support the visual inspection of all joints in terms of grain refinement, the mean grain size of all welds was quantified [4.30] including the respective standard deviations and compared to the benchmark. A trend towards a refined microstructure when the SGFR was reduced from 9 to 5 L/min was found (see Fig. 4.10). As shown by Bitharas et al. [4.4], lowering the SGFR diminishes the potential convective heat transfer to the workpiece, also explaining the distortion findings. Constricting the nozzle by 3 mm, however, had no apparent effect on the grain size, suggesting that higher variations between the nozzle diameters are required to result in significant differences.

4.3.5 Radiography of the joints

No imperfections were found within any welds under the 9 L/min SGFR. Conversely, radiographs of some areas of the joints under the 5 L/min SGFR (see Fig. 4.11) presented imperfections, which were quantified (Table 4.2) [4.31] to assess their respective acceptance. In accordance to the radiographic interpretation guide [4.31] and the measurements undertaken using the Yenway SZMN stereomicroscope, such imperfections were negligible, i.e. their presence would not influence the weld integrity, resulting in zero-defect welds.

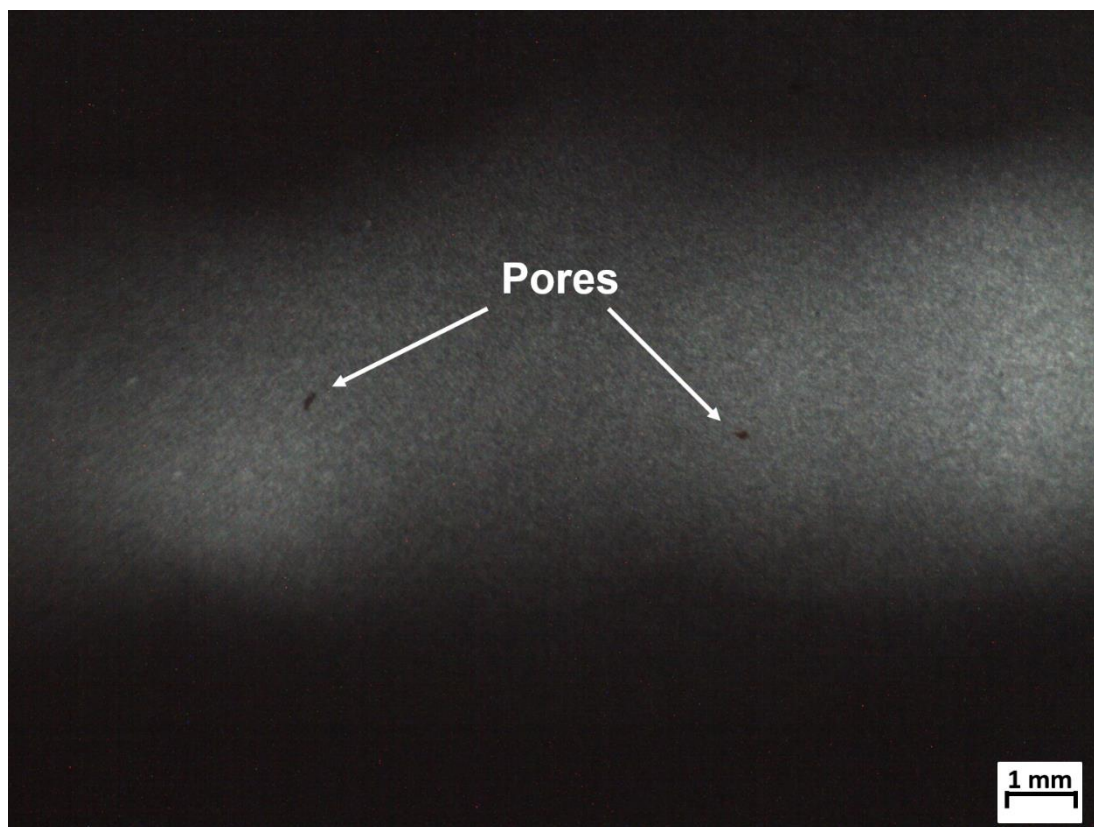


Fig. 4.11 Radiograph of a weld section ($\text{\O}16$ mm nozzle - 5 L/min SGFR).

Table 4.2 Measurements of imperfections from radiographs.

Designation	Internal Undercut (width)	External Undercut (width)	Lack of Fusion (length)	Inclusions (size)	Pores (\O)
$\text{\O}16_5\text{L}/\text{min}$	-	-	3.1 mm	0.5 mm	0.3 mm
$\text{\O}13_5\text{L}/\text{min}$	0.12 mm	0.38 mm	-	-	0.2 mm

4.3.6 Mechanical property evaluation

4.3.6.1 Hardness distribution

Micro-hardness measurements with their respective standard deviations were taken from the HAZ (see Fig. 4.12) and weld regions (see Fig. 4.13). The

collected data showed negligible changes on the hardness when modifying the nozzle diameter or SGFR due to the similar heat input from all the considered cases. This is in agreement with findings by Campbell et al. [4.1], where reducing the SGFR from 15 to 6 L/min in fillet welds had insignificant effect on the hardness of both the weld metal and the HAZ.

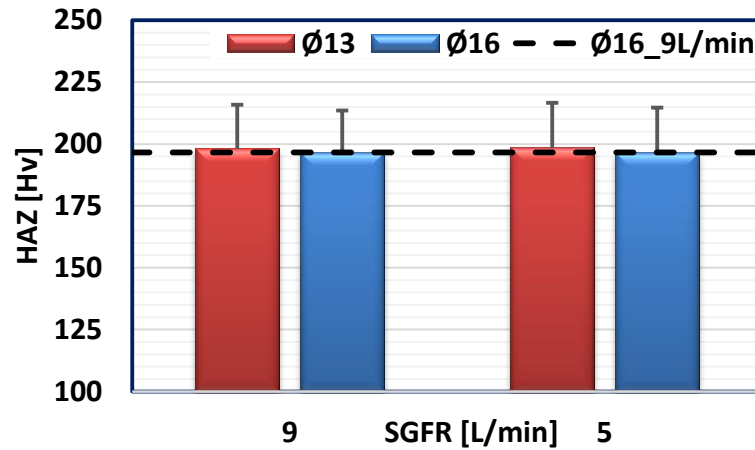


Fig. 4.12 Mean HAZ hardness measurements.

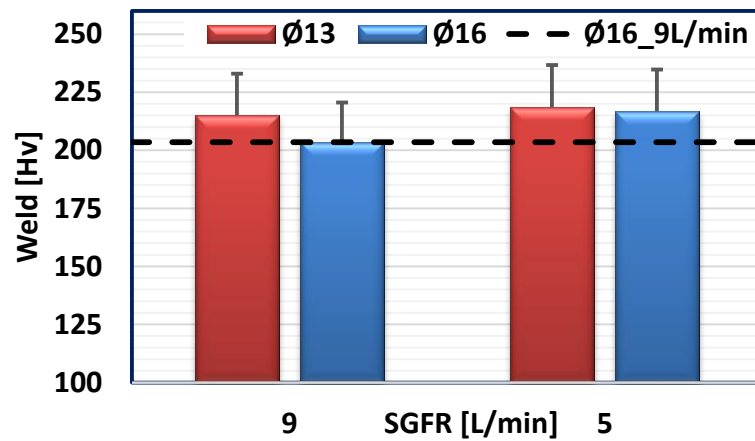


Fig. 4.13 Mean weld hardness measurements.

Yet, results suggest that a SGFR of 5 L/min or a $\text{Ø}13$ mm nozzle would improve the resistance of the weld to plastic deformation, which is in agreement with findings regarding the grain size of the weld. Additionally, a gradual hardness increase was noted when moving from the parent material towards the weld centre; a typical behaviour of most GMAW joints [4.21].

4.3.6.2 Tensile and bend tests

All the transverse tensile test specimens failed within the parent material (see Fig. 4.14 (A), (B)). When compared to the benchmark, the results of the all-weld longitudinal tensile tests exhibited no clear pattern (see Fig. 4.15).

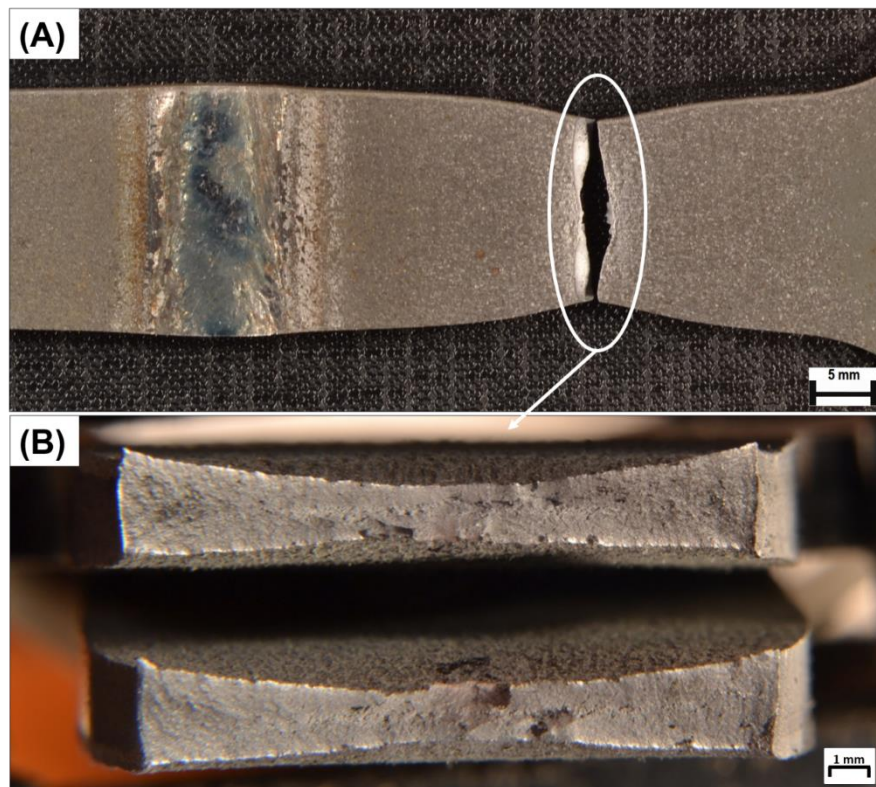


Fig. 4.14 Transverse tensile test specimen - $\text{Ø}16$ mm at 5 L/min. (A) Specimen. (B) Fracture within the parent material.

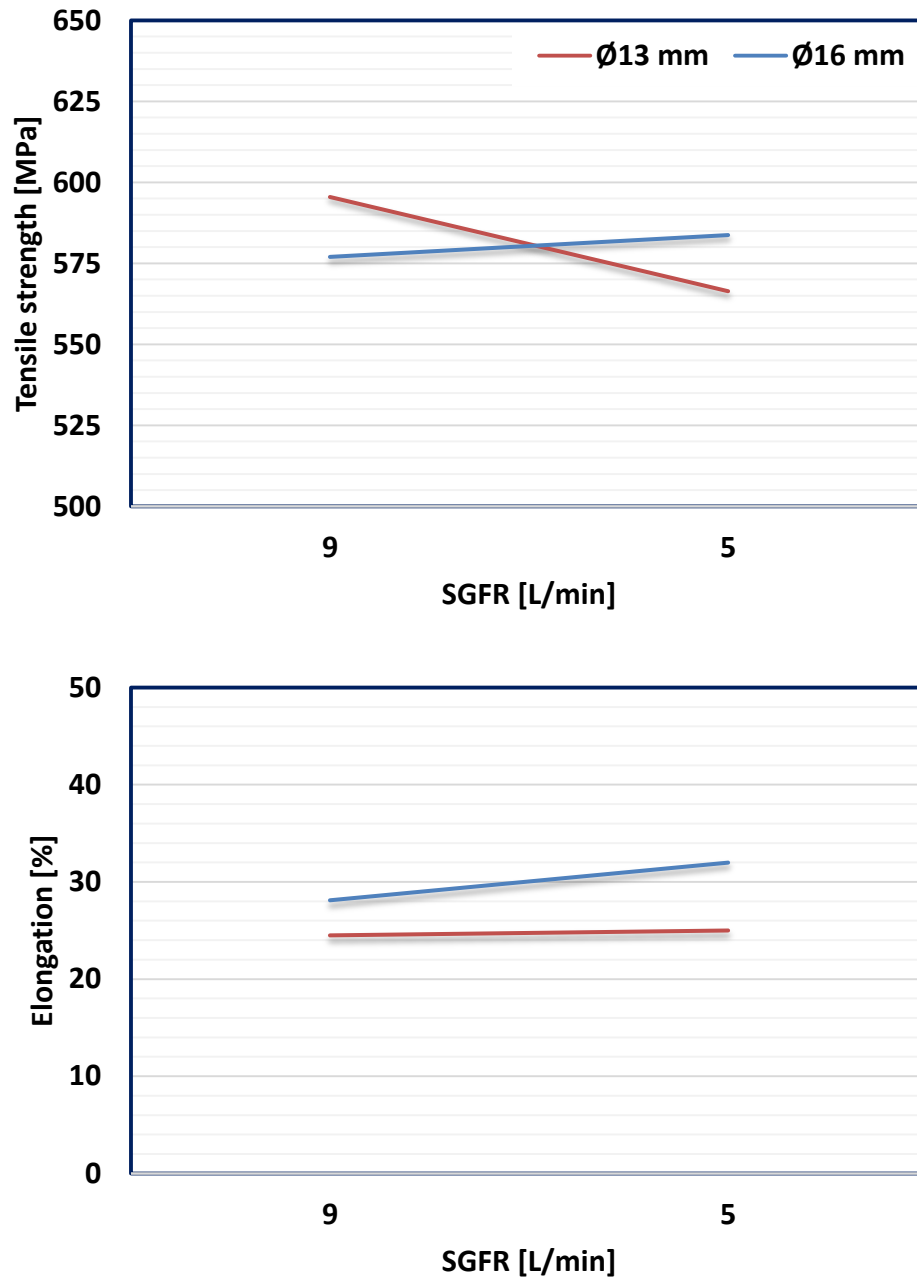


Fig. 4.15 Mean mechanical testing measurements for the all-weld tensile strength and elongation of the joints.

Changes on either the strength or the elongation of all cases were considered moderate, with insubstantial differences between welds in terms of

mechanical properties. The maximum standard deviations for each variable assessed were 31 MPa (tensile strength) and 3% (elongation).

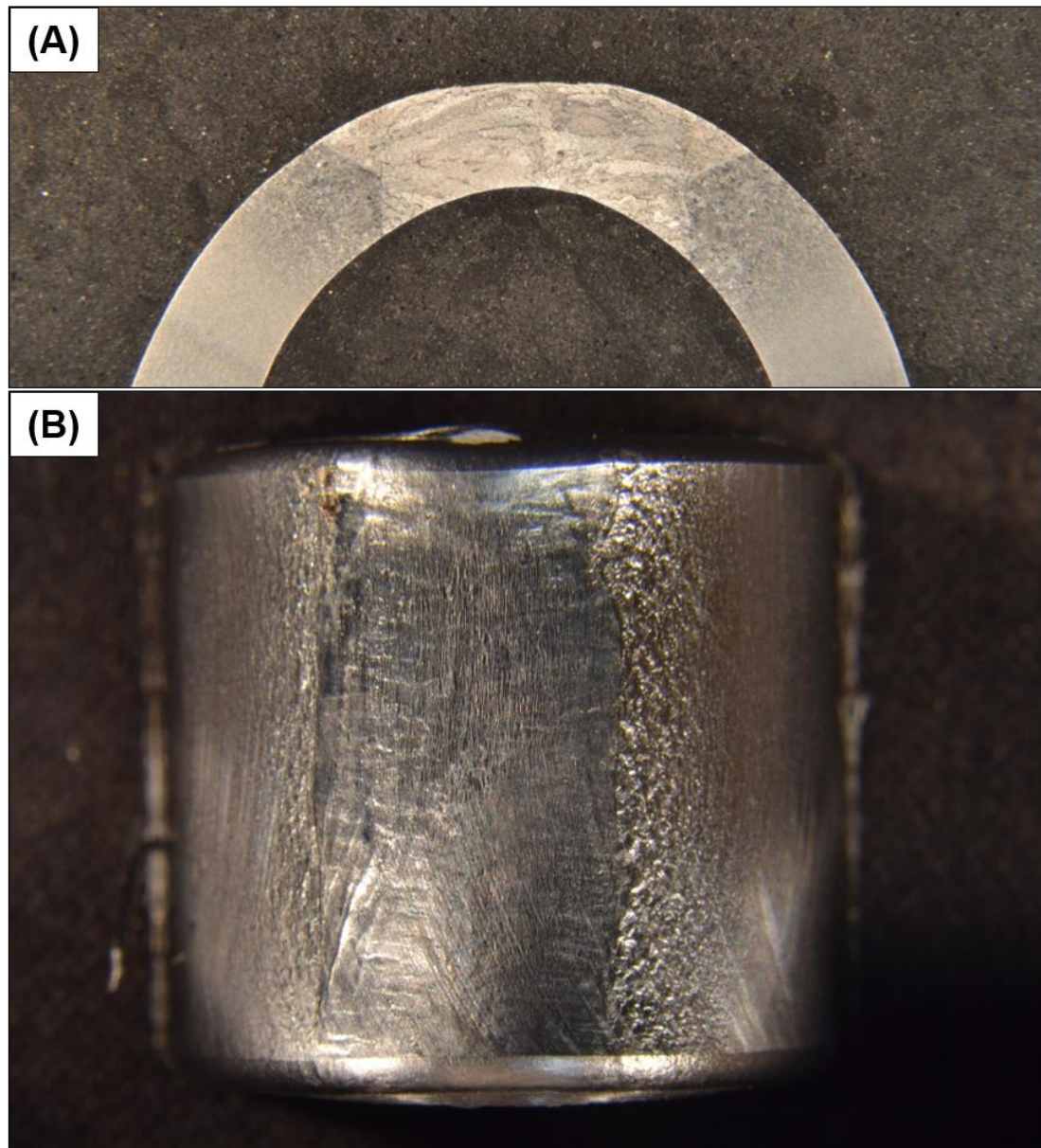


Fig. 4.16 Typical bend test specimens. (A) Cross-section. (B) Top view.

All previous sections demonstrated minor variances between the weld cases for this study. For instance, a trend was found during distortion and

temperature measurements, while no evident changes were found in terms of grain size when constricting the nozzle, which helps to explain the random performance of the mechanical properties of the weld.

The cross-section and top surfaces of the bend test specimens were analysed (see Fig. 4.16 (A), (B)). Neither irregularities nor failures were found after testing all the welds, indicating that the beneficial reduction of the SGFR is possible without compromising the joint quality.

4.4 Conclusions

This chapter has explored the reduced SGFR that would still maintain an acceptable weld using different nozzle diameters compared to a defined benchmark. From distortion and temperature measurements, radiographs, microstructural characterisation and mechanical testing, it was possible to draw some key conclusions in this preliminary study.

The microstructural assessment showed a tendency for finer grains when the SGFR was reduced to 5 L/min, without evident differences in the grain size by modifying the nozzle diameter of the torch. The SGFR was successfully reduced to 5 L/min, without apparent porosity as shown by radiographs and microscopy analysis. Inclusions of considerable size were not found, with a high integrity weld formed in a draft-free environment.

A trend where both the distortion and temperature were reduced was found by either decreasing the SGFR or increasing the nozzle diameter. However, dissimilarities between the various cases and the benchmark were negligible. In addition, no diversification was found in terms of weld shape, hardness, tensile and bend tests.

This study extended the work carried out in previous publications [4.4, 4.6, 4.19] in terms of reducing the SGFR and nozzle diameter in the GMAW process using Ar₂₀CO₂. Savings of 4 L/min were achieved by reducing the SGFR from 9 to 5 L/min, which could contribute to the decrease on CO₂ emissions, the reduction of the energy required for gas production and delivery, and the decline on shielding gas wastage, increasing productivity and permitting cost and time savings. Additionally, it was demonstrated that differences in the nozzle diameter could influence parameters such as the distortion of the workpiece and the temperature of the joint. However, to achieve evident differences in the assessed outputs, notable variations in the nozzle diameter would be required, i.e. greater than 3 mm.

The findings in this preliminary analysis regarding reductions in the SGFR when the protective gas is constantly supplied during welding will be utilised in chapter 5 and compared to the alternating shielding gas technique, aiming to better understand the benefits of employing this novel method.

4.5 Bibliography

- [4.1] S. W. Campbell, A. M. Galloway, and N. A. McPherson, “Techno-economic evaluation of reducing shielding gas consumption in GMAW whilst maintaining weld quality,” *Int. J. Adv. Manuf. Technol.*, vol. 63, no. 6–9, pp. 975–985, 2012.
- [4.2] G. M. Ramsey, A. M. Galloway, S. W. Campbell, N. A. McPherson, and T. J. Scanlon, “A computational fluid dynamic analysis of the effect of side draughts and nozzle diameter on shielding gas coverage during gas metal arc welding,” *J. Mater. Process. Technol.*, vol. 212, no. 8, pp.

1694–1699, 2012.

- [4.3] B. Mvola and P. Kah, “Effects of shielding gas control: welded joint properties in GMAW process optimization,” *Int. J. Adv. Manuf. Technol.*, vol. 88, no. 9–12, pp. 2369–2387, 2017.
- [4.4] I. Bitharas, N. A. McPherson, W. McGhie, D. Roy, and A. J. Moore, “Visualisation and optimisation of shielding gas coverage during gas metal arc welding,” *J. Mater. Process. Technol.*, vol. 255, no. December, pp. 451–462, 2018.
- [4.5] I. Bitharas, S. W. Campbell, A. M. Galloway, N. A. Mcpherson, and A. J. Moore, “Visualisation of alternating shielding gas flow in GTAW,” *Mater. Des.*, vol. 91, pp. 424–431, 2016.
- [4.6] F. H. Ley, S. W. Campbell, A. M. Galloway, and N. A. McPherson, “Effect of shielding gas parameters on weld metal thermal properties in gas metal arc welding,” *Int. J. Adv. Manuf. Technol.*, vol. 80, no. 5–8, pp. 1213–1221, 2015.
- [4.7] T. Gray, D. Camilleri, and N. McPherson, “Tools to deal with welding distortion: predictive modelling and research on in-process techniques,” in *Control of Welding Distortion in Thin-Plate Fabrication*, Woodhead Publishing Limited, 2014, pp. 39–52.
- [4.8] T. Gray, D. Camilleri, and N. McPherson, “Simulating welding distortion in butt welding of thin plates,” in *Control of Welding Distortion in Thin-Plate Fabrication*, 2014, pp. 199–232.
- [4.9] S. W. Campbell, A. M. Galloway, and N. A. McPherson, “Artificial Neural Network Prediction of Weld Geometry Performed Using GMAW with Alternating Shielding Gases,” *Weld. J.*, vol. 91, no. 6, pp. 174–181, 2012.

- [4.10] D. Deng and H. Murakawa, “Prediction of welding distortion and residual stress in a thin plate butt-welded joint,” *Comput. Mater. Sci.*, vol. 43, no. 2, pp. 353–365, 2008.
- [4.11] T. Gray, D. Camilleri, and N. McPherson, “Computational simulation of welding distortion: an overview,” in *Control of Welding Distortion in Thin-Plate Fabrication*, 2014, pp. 77–101.
- [4.12] C. Heinze, C. Schwenk, and M. Rethmeier, “The effect of tack welding on numerically calculated welding-induced distortion,” *J. Mater. Process. Technol.*, vol. 212, no. 1, pp. 308–314, 2012.
- [4.13] Y. H. P. Manurung et al., “Welding distortion analysis of multipass joint combination with different sequences using 3D FEM and experiment,” *Int. J. Press. Vessel. Pip.*, vol. 111–112, pp. 89–98, 2013.
- [4.14] T. Gray, D. Camilleri, and N. McPherson, “Understanding welding distortion: thermal fields thermo-mechanical effects,” in *Control of Welding Distortion in Thin-Plate Fabrication*, Woodhead Publishing Limited, 2014, pp. 53–76.
- [4.15] S. W. Campbell, A. M. Galloway, N. A. McPherson, and A. Gillies, “Evaluation of gas metal arc welding with alternating shielding gases for use on AA6082T6,” *Proc. Inst. Mech. Eng. Part B J. Eng. Manuf.*, vol. 226, no. 6, pp. 992–1000, 2012.
- [4.16] N. McPherson, A. Galloway, and W. McGhee, “Thin plate buckling mitigation and reduction challenges for naval ships,” *J. Mar. Eng. Technol.*, vol. 12, no. 2, pp. 3–10, 2013.
- [4.17] T. Gray, D. Camilleri, and N. McPherson, “Fabrication of stiffened thin-plate structures and the problem of welding distortion,” in *Control of Welding Distortion in Thin-Plate Fabrication*, 2014, pp. 14–38.

- [4.18] H. S. Ham, D. S. Oh, and S. M. Cho, “Measurement of arc pressure and shield gas pressure effect on surface of molten pool in TIG welding,” *Sci. Technol. Weld. Join.*, vol. 17, no. 7, pp. 594–600, 2012.
- [4.19] K. Kyohei, S. Masaya, T. Manabu, M. Akihisa, and M. Tadasuke, “Effects of a constricted nozzle on the arc phenomena in the TIG welding process,” *Weld. Int.*, vol. 30, no. 8, pp. 590–595, 2016.
- [4.20] V. Beyer, S. W. Campbell, G. M. Ramsey, A. M. Galloway, A. J. Moore, and N. A. McPherson, “Systematic study of effect of cross-drafts and nozzle diameter on shield gas coverage in MIG welding,” *Sci. Technol. Weld. Join.*, vol. 18, no. 8, pp. 652–660, 2013.
- [4.21] S. W. Campbell, A. M. Galloway, and N. A. McPherson, “Techno-economic evaluation on the effects of alternating shielding gases for advanced joining processes,” *Proc. Inst. Mech. Eng. Part B J. Eng. Manuf.*, vol. 225, no. 10, pp. 1863–1872, 2011.
- [4.22] T. Gray, D. Camilleri, and N. McPherson, “Finite-element thermo-mechanical techniques for welding distortion prediction,” in *Control of Welding Distortion in Thin-Plate Fabrication*, 2014, pp. 177–198.
- [4.23] L. D. Cozzolino, H. E. Coules, P. A. Colegrove, and S. Wen, “Investigation of post-weld rolling methods to reduce residual stress and distortion,” *J. Mater. Process. Technol.*, vol. 247, no. August 2016, pp. 243–256, 2017.
- [4.24] D. S. Howse and W. Lucas, “Investigation into arc constriction by active fluxes for tungsten inert gas welding,” *Sci. Technol. Weld. Join.*, vol. 5, no. 3, pp. 189–193, 2000.
- [4.25] R. Kaul et al., “Effect of active flux addition on laser welding of austenitic stainless steel,” *Sci. Technol. Weld. Join.*, vol. 12, no. 2, pp.

127–137, 2007.

- [4.26] Q. L. Jiang, Y. J. Li, J. Wang, and L. Zhang, “Effects of inclusions on formation of acicular ferrite and propagation of crack in high strength low alloy steel weld metal,” *Mater. Sci. Technol.*, vol. 27, no. 10, pp. 1565–1569, 2011.
- [4.27] R. Ghomashchi, W. Costin, and R. Kurji, “Evolution of weld metal microstructure in shielded metal arc welding of X70 HSLA steel with cellulosic electrodes: A case study,” *Mater. Charact.*, vol. 107, pp. 317–326, 2015.
- [4.28] H. Yu, J. Song, G. Zhang, J. Pu, H. Chen, and S. Chen, “The Effects of Arc Length on Welding Arc Characteristics in Al-Mg Alloy Pulsed Gas Tungsten Arc Welding,” in *Robotic Welding, Intelligence and Automation: Advances in Intelligent Systems and Computing.*, vol. 363, Shanghai, China: Springer, 2015, pp. 321–335.
- [4.29] Anthony B Murphy, “The effects of metal vapour in arc welding,” *J. Phys. D. Appl. Phys.*, vol. 43, no. 16, p. 165204, 2010.
- [4.30] ASTM international, “ASTM E112-13: Standard test methods for determining average grain size,” ASTM International. pp. 1–28, 2013.
- [4.31] Carestream, “Radiographic Interpretation Guide.” Carestream Inc., New York, 2014.

Chapter 5

Exploring the benefits of the alternating shielding gas technique

5.1 Introduction

As shown in chapter 4, studies regarding reductions in the shielding gas consumption have been introduced previously in arc welding processes [5.1-5.4]. Bitharas et al. [5.2], using flux cored arc welding, were able to reduce the shielding gas flow rate (SGFR) to 5 L/min without detrimental effects to the weld, such as porosity. This was due to the reaction between the remaining N₂ and O₂ in the arc surroundings with elements from the flux before the gases were absorbed by the steel. Campbell et al. [5.3] made use of the gas metal arc welding (GMAW) process in a draft-free system, decreasing the SGFR to 6 L/min, which was limited by the electromagnetic gas-saving device. Beyer et al. [5.4] induced cross-drafts during the welding procedure utilising different nozzle diameters and SGFRs. The study [5.4] showed that a SGFR of 5 L/min promoted porosity-free welds in the absence of cross-drafts, with improved protection of the molten pool by constricting the nozzle diameter. These studies, however, were limited to the premixed method, where the shielding gases were supplied in a constant manner.

Aiming to improve the weld quality and productivity and add cost savings to the welding process, methods such as the alternating shielding gas have been developed [5.3, 5.5-5.11]. However, there is limited work in terms of shielding gas reductions employing the novel alternating shielding gas technique [5.5, 5.12]. Campbell et al. [5.12] studied the effects of the alternating shielding gas method by employing a 5 L/min SGFR, which showed better protection of the weld pool compared to the premixed gas supply method due to the pressure impulse from the build-up in line pressure. Bitharas et al. [5.5], performing bead-on-plates using gas tungsten arc welding (GTAW), established that alternating Ar and He with a SGFR of 5 L/min and 2 Hz frequency was the most favourable option when comparing all the alternated cases. Such statement was a result of all welds being almost identical regardless of the SGFR employed, i.e. 10 or 5 L/min.

Despite significant contribution discussed in the previous paragraph, both studies [5.5, 5.12] were limited to the cross-daft analysis and the flow behaviour of the shielding gas using schlieren investigation. Additionally, the mixture of shielding gases within the supply hose in the latter case hindered the alternated gas delivery to the system in high frequencies [5.5]. Hence, there is opportunity to expand the examination of reduced SGFRs using the alternating shielding gas method in terms of features such as the distortion of the workpiece and microstructural and mechanical properties of the weld.

It is demonstrated in this chapter that the SGFR can be effectively reduced during the GMAW with the alternating shielding gas technique. The effects of modifying the SGFR and frequency during the weld process were addressed and contrasted with results from chapter 4. Measurements of the distortion of the workpiece and the temperature of the joint were carried out

together with analysis of the weld shape and the heat affected zone (HAZ), comparing the premixed and alternating shielding gas methods. Microstructural characterisation was performed to evaluate the presence of defects such as porosity and cracks during the solidification of the joint. Additionally, mechanical tests were conducted to clarify the influence of the alternating shielding gas technique on the weld properties when reducing the SGFR.

5.2 Experimental setup

The SGFR of each protective gas and its respective frequency were varied to assess the alternating shielding gas behaviour when reducing the gas protection. The parameters employed during welding are shown in Table 5.1. Designations are provided to ease discussion. For instance, the 15Ar-6He2 weld refers to Ar20CO₂ being supplied at 15 L/min and He at 6 L/min using a 2 Hz frequency.

Previous studies have demonstrated the advantages of using a 2 Hz frequency [5.9, 5.13] and the downside of very high frequencies, such as 8 Hz [5.5]. Hence, in this study Ar20CO₂ and He were alternated under 2 and 6 Hz frequencies, with a 50% duty cycle, i.e. both flows were supplied equally within the period of one shielding gas switching loop.

Two SGFRs were chosen: 15 and 6 L/min. The highest SGFR was set to 15 L/min based on work available in the literature [5.6, 5.8, 5.9]. As concluded in chapter 4, the 5 L/min SGFR was able to provide porosity-free welds, with good penetration and no crack development. However, by alternating the protective gases there is higher turbulence in the gas flow

[5.14]. Thus, the lowest SGFR for this study was set as 6 L/min instead. Additionally, since it is of interest to reduce the SGFR employing the alternating shielding gas method, the benchmark was set as Ø16 mm nozzle and 5 L/min SGFR (Ø16_5L/min), following the results from chapter 4.

Table 5.1 Welding parameters.

Shielding Gas	Ar20C O ₂ SGFR [L/min]	He SGFR [L/min]	Frequenc y [Hz]	Voltag e [V]	Curren t [A]	Heat Input [J/m m]	Designatio n
Ar20CO ₂ + He	15	15	2	22.52	247.29	1114	15Ar-15He2
Ar20CO ₂ + He	15	6	2	22.62	241.43	1092	15Ar-6He2
Ar20CO ₂ + He	6	15	2	22.56	250.76	1131	6Ar-15He2
Ar20CO ₂ + He	6	6	2	22.6	238.76	1079	6Ar-6He2
Ar20CO ₂ + He	15	15	6	22.56	249.33	1125	15Ar-15He6
Ar20CO ₂ + He	15	6	6	22.54	246.43	1111	15Ar-6He6
Ar20CO ₂ + He	6	15	6	22.51	238.76	1075	6Ar-15He6
Ar20CO ₂ + He	6	6	6	22.58	238.43	1077	6Ar-6He6

15Ar-6He2: Ar20CO₂ at 15 L/min, He at 6 L/min, 2 Hz frequency.

Bitharas et al. [5.5] demonstrated that a frequency of 8 Hz under a SGFR of 5 L/min when alternating Ar and He would result in a non-transitory arc behaviour due to the fully mixing of the protective gases in the supply hose. For this study, no supply hose was shared between the alternated shielding gases, which were supplied directly to the welding torch exit, as shown in chapter 3. Therefore, it is expected that the Ar20CO₂ and He

alternation and, consequently, its arc transition would still exist for a 6 L/min SGFR despite a frequency of 6 Hz.

The root gap, travel speed and wire-feed speed were set as 4 mm, 5 mm/s and 7.5 m/min, respectively. Additionally, the stand-off distance of the alternating shielding gas cases was reduced from 10 to 5 mm to assure the complete coverage of He during the welding procedure due to its low density [5.14].

5.3 Results and discussion

5.3.1 Distortion of the parent material

The distortion data was collected according to the procedure described in chapter 3. Measurements displayed a trend towards reduced distortion when decreasing the SGFR of both Ar₂₀CO₂ and He simultaneously (see Fig. 5.1). Overall, all welds, with exception of the transverse distortion of the 15Ar-15He cases, resulted in similar or lower distortion in both transverse and longitudinal directions compared to the benchmark (Ø16_5L/min). This was due to the presence of He in the system, which modified the arc properties, altering the thermal and residual stresses within the joint and impacting the distortion in both transverse and longitudinal directions [5.15, 5.16].

In the transverse direction a 2 Hz frequency provided higher distortion of the workpiece compared to the 6 Hz cases. Conversely, the distortion measured in the longitudinal direction exhibited the opposite behaviour, with most of the welds under 2 Hz presenting lower distortions. This was attributed to the residual stresses in the workpiece prior to welding as well as the

distortion developing in many directions throughout the welding procedure [5.15].

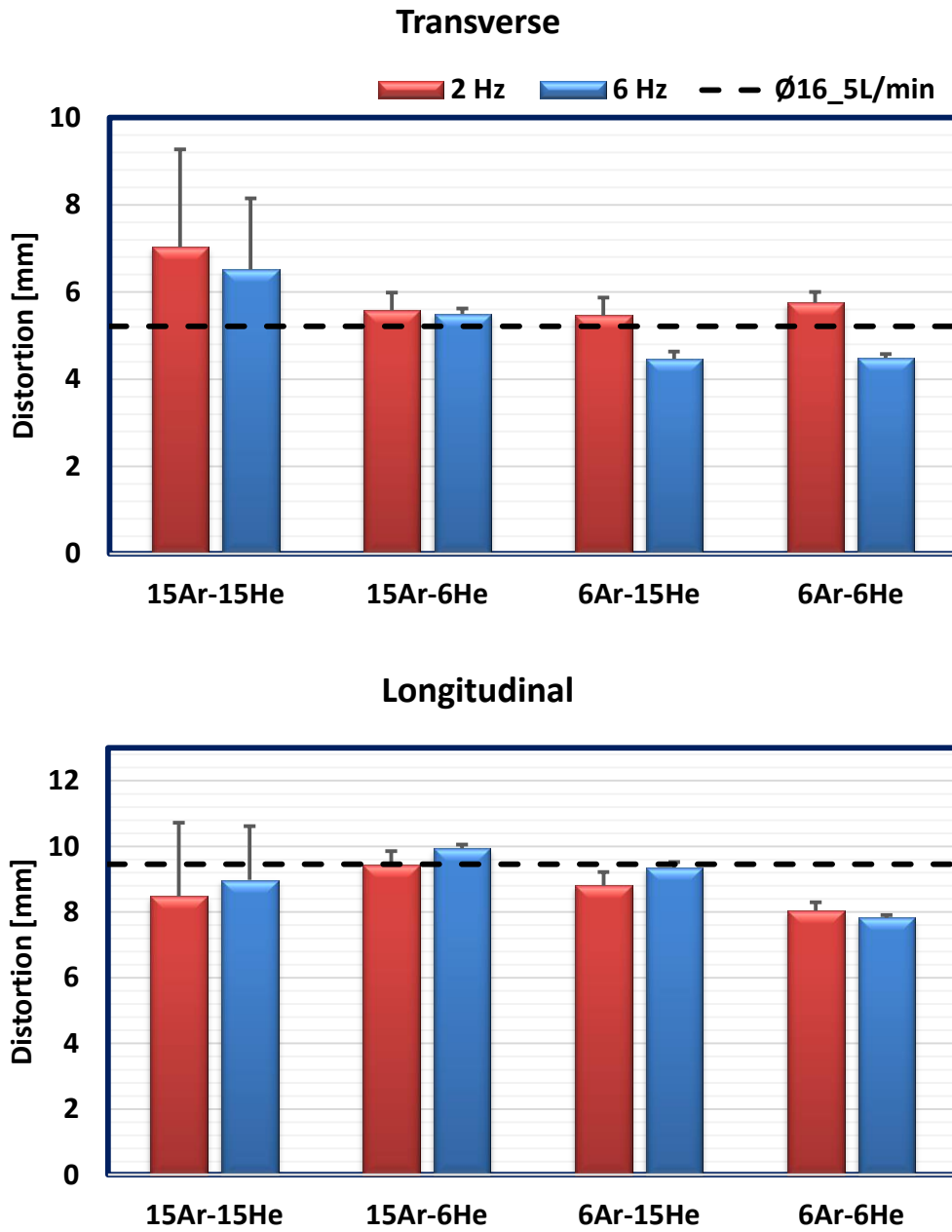


Fig. 5.1 Mean distortion measurements compared to the benchmark (Ø16_5L/min).

Despite not exhibiting a clear pattern, negligible differences in the distortion between 2 and 6 Hz welds were found in most cases. Modifying the

gas supply from 15Ar-6He to 6Ar-15He promoted a reduction in the distortion of the welded structures in both directions for the respective frequency. The reduced Ar20CO₂ SGFR and the increased presence of He (6Ar-15He case) diminished the distortion of the workpiece; a result of higher heat intensity at the base of the Ar20CO₂ arc plasma compared to the arc of pure He [5.17, 5.18].

Interestingly, results demonstrated that the overall final distortion of the welded structures was either similar or reduced even further in relation to that of the benchmark (Ø16_5L/min) by using the alternating shielding gas method. Despite a hotter arc core, this is expected due to the reduced arc plasma temperature at the arc fringe by the presence of He [5.19-5.25] during the alternating shielding gas method, which lowers the expansion-contraction effect throughout the cooling process [5.11, 5.26, 5.27].

Average distortions of 5.6 and 8.9 mm were measured in the transverse and longitudinal directions, respectively, whereas the benchmark (Ø16_5L/min) presented distortions of 5.2 (transverse) and 9.5 mm (longitudinal). The lowest distortion was found for the 6Ar-6He6 weld, with reductions of 14% (-0.72 mm) transversely and 17% (-1.63 mm) longitudinally.

5.3.2 Temperature measurements

The temperature measurements 10 mm away from the root gap of the joint (see Fig. 5.2) exhibited no significant changes between the benchmark (Ø16_5L/min) and all the alternating shielding gas cases. For the 20 mm position, the alternating shielding gas measurements demonstrated a clearer trend, where reducing the SGFR decreased the induced heat transfer to the

parent material. As demonstrated by Bitharas et al. [5.2], lowering the SGFR decreases the fluid momentum when exiting the welding nozzle, diminishing the conductive heat transfer to the joint and the distortion of the weldment.

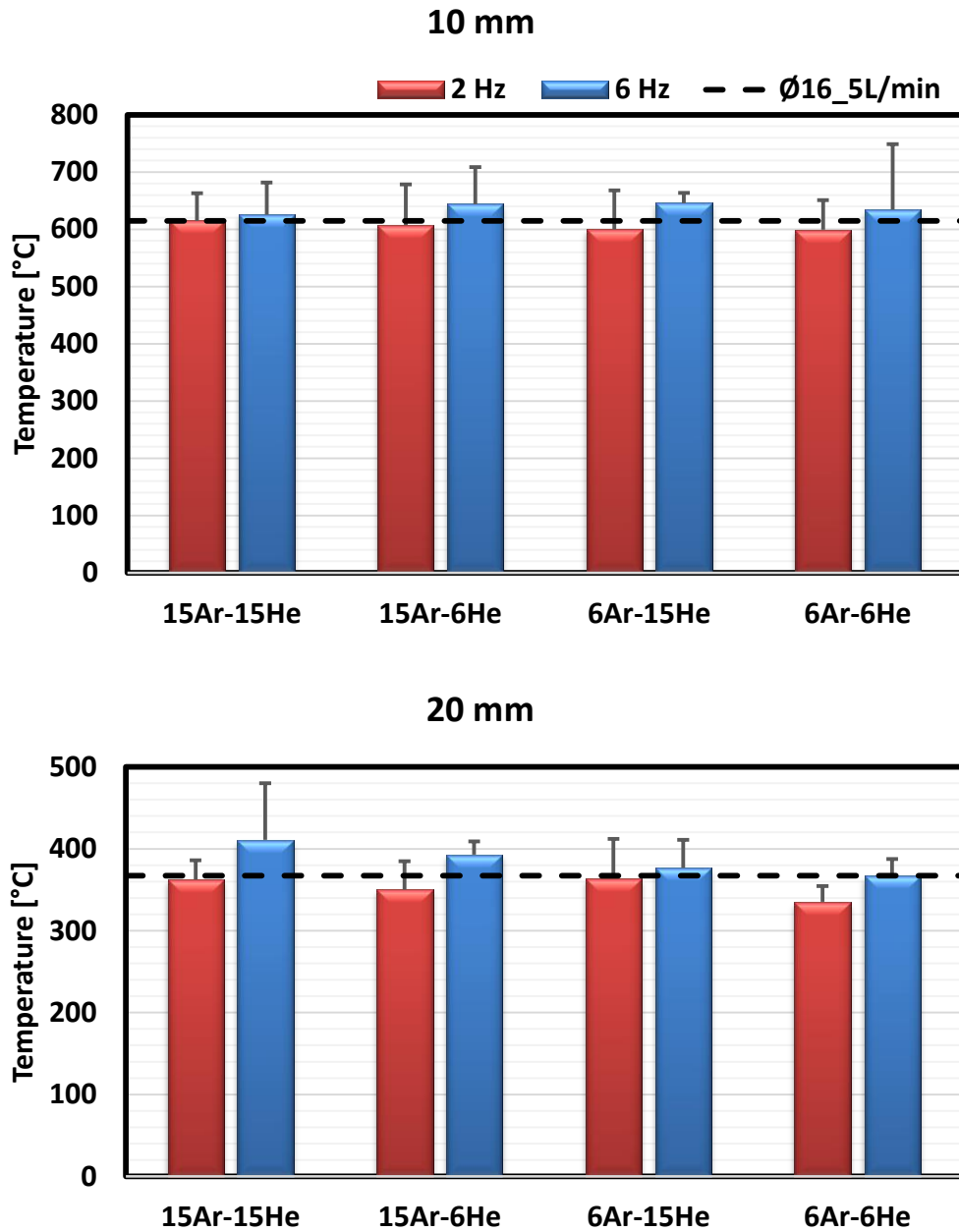


Fig. 5.2 Mean thermal data of all welds 10 and 20 mm away from the root gap compared to the benchmark (Ø16_5L/min).

For all the assessed welds, the 6 Hz frequency joints exhibited higher temperatures, which have been attributed by Ley et al. [5.11] to the higher thermal conductivity of the 6 Hz welds. This is in line with findings by Campbell et al. [5.9], where a frequency of 8 Hz led to a higher temperature of the joint. Additionally, negligible temperature variations were found between the 15Ar-6He and 6Ar-15He cases in any of the considered frequencies.

As will be shown in section 5.3.4, the higher thermal conductivity promoted by the 6 Hz frequency and the lower momentum of a 6 L/min SGFR both contribute to the refinement of the grain size in the fusion zone. Such combination would also reduce the requirement for rework, since it resulted in lower distortion of the workpiece (see Fig. 5.1).

5.3.3 Weld characteristics

The cap and root widths of all the alternating shielding gas welds have been measured to assess features such as reinforcement and penetration. Similarly, the HAZ area was quantified to better understand the influence of the alternating shielding gas on the heat input, with all welds being compared to the benchmark, i.e. Ø16_5L/min (see Fig. 5.3 (A)). In the present chapter, all welds exhibited the typical wide reinforcement narrowing towards the root of the joint.

Studies utilising the premixed method [5.2, 5.28, 5.29] in GMAW discussed the increase in heat input by reducing the stand-off distance due to the higher arc current, which is expected to promote better penetration while reducing the reinforcement height due to enhanced arc pressure [5.25, 5.30, 5.31]. By reducing the stand-off distance from 10 (Ø16_5L/min) to 5 mm and

employing the alternation of Ar₂₀CO₂ and He during the welding procedure, reductions were found in the overall reinforcement height compared to that of the benchmark (see Fig. 5.3 (A)).

Such behaviour was more evident in the 15Ar-6He welds, which exhibited a concave reinforcement (see Fig. 5.3 (B)) due to its higher arc pressure [5.30-5.32] from the greater presence of Ar₂₀CO₂. Campbell et al. [5.33] demonstrated approximate peak arc pressures at the arc centreline of 1900 N/m² for Ar and 800 N/m² for He, being even higher when applying the alternating shielding gas method.

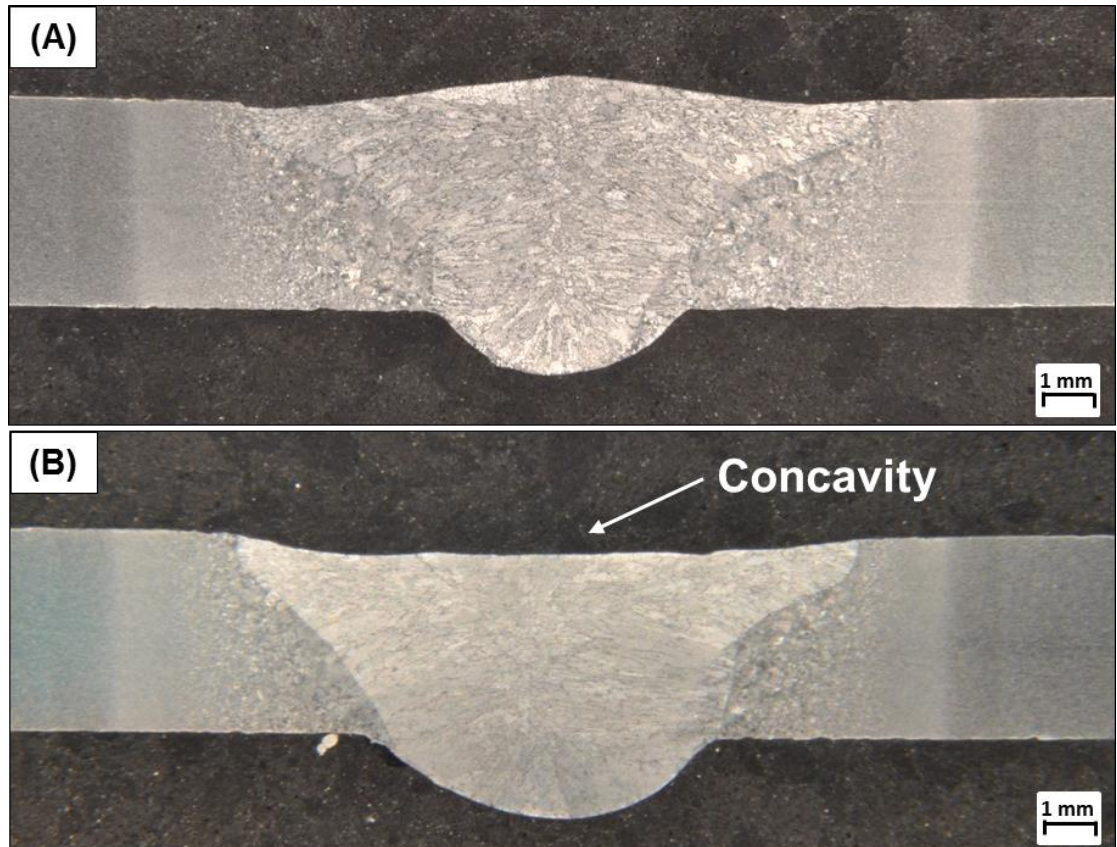


Fig. 5.3 Macrographs representing the assessed weld features (etched). (A) $\text{O}16_5\text{L}/\text{min}$ (benchmark). (B) 15Ar-6He6.

Overall, all alternated cases exhibited reduced cap width compared to the Ø16_5L/min case (see Fig. 5.4), stimulating a more uniform weld shape, which was shown by Gray et al. [5.15] to assist with reducing the weldment distortion due to a more even expansion-contraction behaviour in this direction. Negligible variations were found between the cap widths of all the alternated cases (see Fig. 5.4).

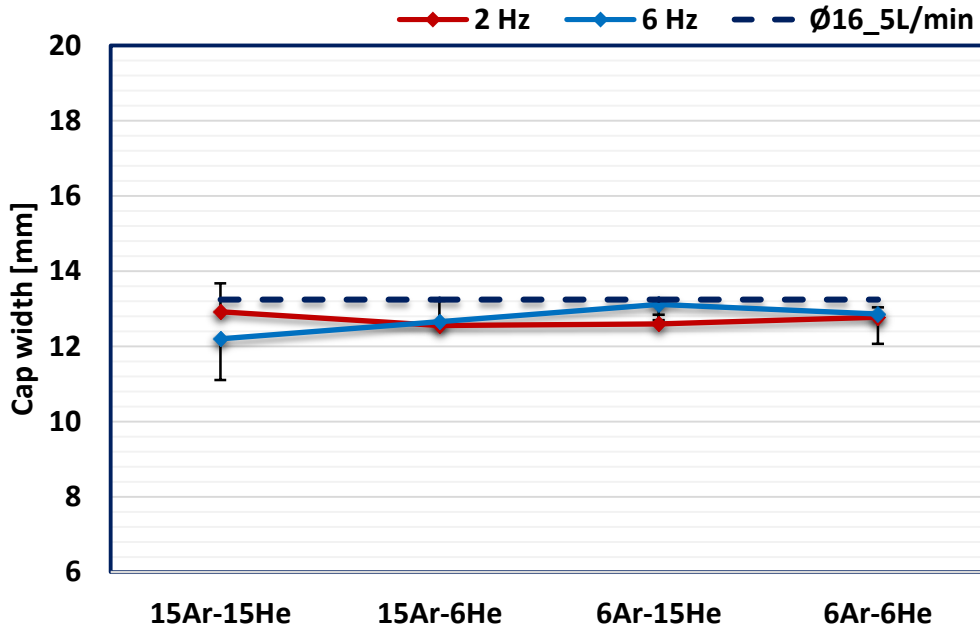


Fig. 5.4 Mean cap width measurements.

In terms of root width, the 6 Hz frequency promoted greater penetration of the joints compared to the 2 Hz joints due to a faster arc pressure transition (see Fig. 5.5) [5.8-5.10]. However, similar penetrations were found in both frequencies for the 15Ar-15He and 6Ar-15He cases, which is a result of limiting the Ar20CO_2 and He SGFRs to 6 L/min and 15 L/min, respectively, reducing the impact of the shear stress and arc pressure of Ar [5.31, 5.32, 5.34].

In this study, the alternation between the protective gases permitted greater weld penetrations than that of the benchmark, shown by Traidia and Roger [5.35] to be caused by the presence of He and its greater electromagnetic force to that of Ar [5.17, 5.35]. This is in line with findings by Bitharas et al. [5.5], where the alternating shielding gas technique increased the weld penetration by 13% on average compared to the premixed method [5.9, 5.11, 5.36]. The greater weld penetration would allow for reductions in the root gap and increments in the travel speed of the welding torch, lowering the weld metal deposition and, consequently the heat input, whilst maintaining the weld integrity.

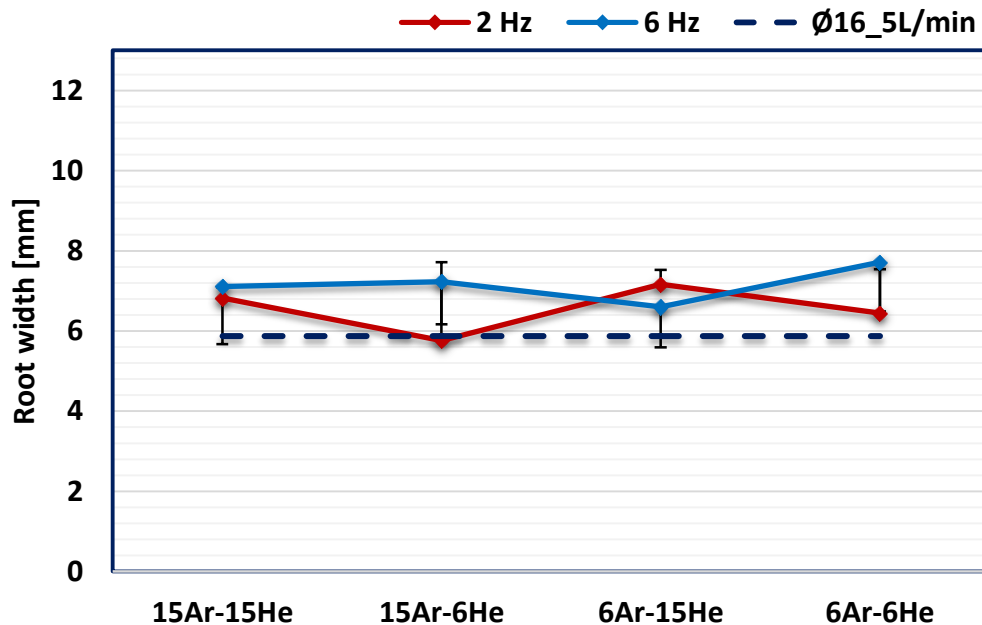


Fig. 5.5 Mean root width measurements.

Minor variances in the HAZ area were found by comparing the welds under the alternating shielding gas technique (see Fig. 5.6). However, in relation to the benchmark, significant reduction was found regarding the HAZ area of the joints when using the alternating shielding gas method. The

alternation of the protective gases allowed for overall decrements of 23% (-4.8 mm²) in the HAZ area. This was possible due to the arc transition between Ar20CO₂ and He, reducing its contact with the molten pool and, consequently, the heat transferred to the workpiece [5.6, 5.9, 5.10, 5.13, 5.37]. This behaviour is contrasting to that of the premixed method, where the Ar20CO₂ arc is in constant contact with the molten metal.

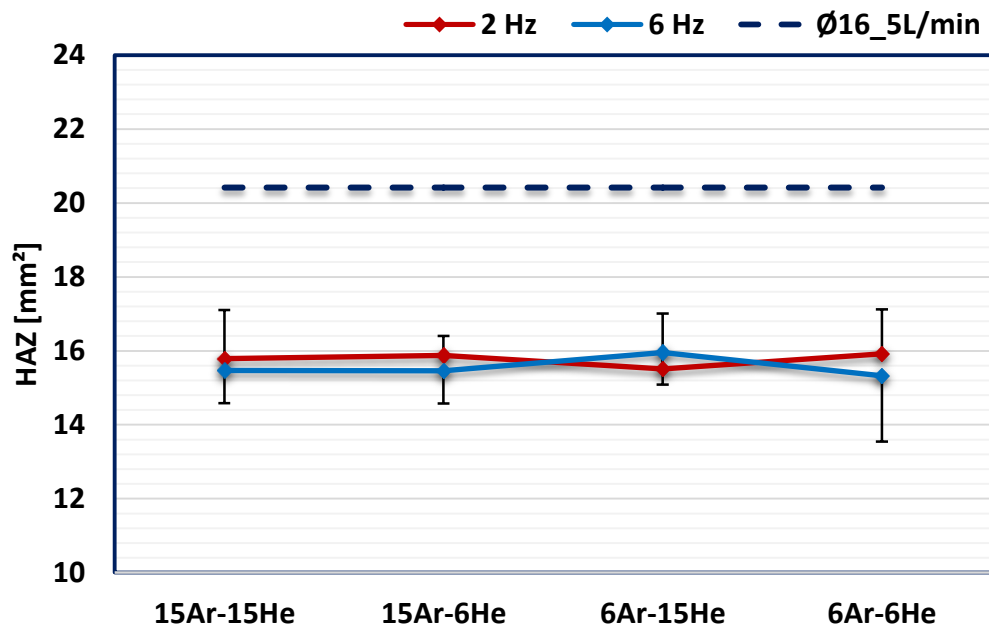


Fig. 5.6 Mean HAZ area measurements.

The HAZ area being smaller than that of the benchmark reinforces the benefits of utilising the alternating shielding gas technique. Results indicated a lower heat transferred to the joint, despite shortening the stand-off distance from 10 (benchmark) to 5 mm during the alternating shielding gas procedures and using the same travel speed for both the alternating shielding gas and premixed methods. This heat input reduction is discussed in section 5.3.4 via

the assessment of the weld and HAZ microstructures as well as measurements of the grain size in the fusion zone.

5.3.4 Microstructural characterisation

The microstructure of all welds under both the premixed and alternating shielding gas methods has been examined for undesirable features such as porosity development and slag formation. It has been shown in chapter 4 that the benchmark's weld microstructure was porosity-free, with no slag development (see Fig. 5.7 (A) - (C)).

Studies [5.6, 5.9, 5.36, 5.38] have reported the microstructural refinement of the fusion zone and HAZ regions by utilising the alternating shielding gas method. However, this outcome was the result of faster welding speeds, which were changed according to either the welding pass or the frequency [5.6, 5.9]. To better clarify the alternating shielding gas impact on the joint's microstructure, the welding speed was kept constant for all welding cases in the present study, i.e. alternating shielding gas and premixed methods. Ferrite types, namely allotriomorphic and acicular ferrites were found within the weld region (see Fig. 5.8 (A - D)) of all welds under the alternating shielding gas method, with no presence of porosity or slags. Such microstructures were developed during the cooling process, where the allotriomorphic ferrite grew from prior austenite grain boundaries [5.39-5.42] followed by the nucleation of acicular ferrite from non-metallic inclusions [5.43-4.45].

The assessment of the microstructure of the joints under the optical microscope exhibited no clear differences between the benchmark and all the

alternating shielding gas cases. Hence, all welds were further analysed in the scanning electron microscope and measurements of their respective grain sizes undertaken (see Fig. 5.9). Overall, the alternating shielding gas joints exhibited either similar or more refined grains to that of the benchmark, despite having the same travel speed and a smaller stand-off distance to that of the Ø16_5L/min case.

This indicates that by using the alternating shielding gas method there is lower heat input and, consequently, the formation of a finer grain; a correlation that has been previously discussed [5.6, 5.9, 5.36, 5.38, 5.46]. In addition, these results are in line with those from the HAZ area, which decreased by the use of the alternating shielding gas method.

Findings by Ley et al. [5.11] demonstrated greater specific heat capacity for 6 Hz than for 2 Hz when supplying Ar20CO₂ alternated with He under a 10 L/min SGFR. The specific heat capacity of the shielding gas is known to influence many parameters of the welding process, being proportional to the cooling and solidification rates of the joint [5.47-5.49], and consequently influencing the final microstructure of the fusion zone. The grain size measurements of all the alternated cases exhibited reductions of 8% (-0.5 µm²) under a 2 Hz frequency and 16% (-1.1 µm²) for the 6 Hz frequency, which is in line with findings by Ley et al. [5.11] and demonstrate the benefits of the alternating shielding gas technique in reducing the heat input.

Greater Ar20CO₂ SGFRs promoted coarser grains (see Fig. 5.9), with the 15Ar-6He joints displaying the highest grain sizes among all the alternating shielding gas cases. This was a result of the higher heat intensity of the Ar20CO₂ arc plasma compared to that of He [5.17, 5.18].

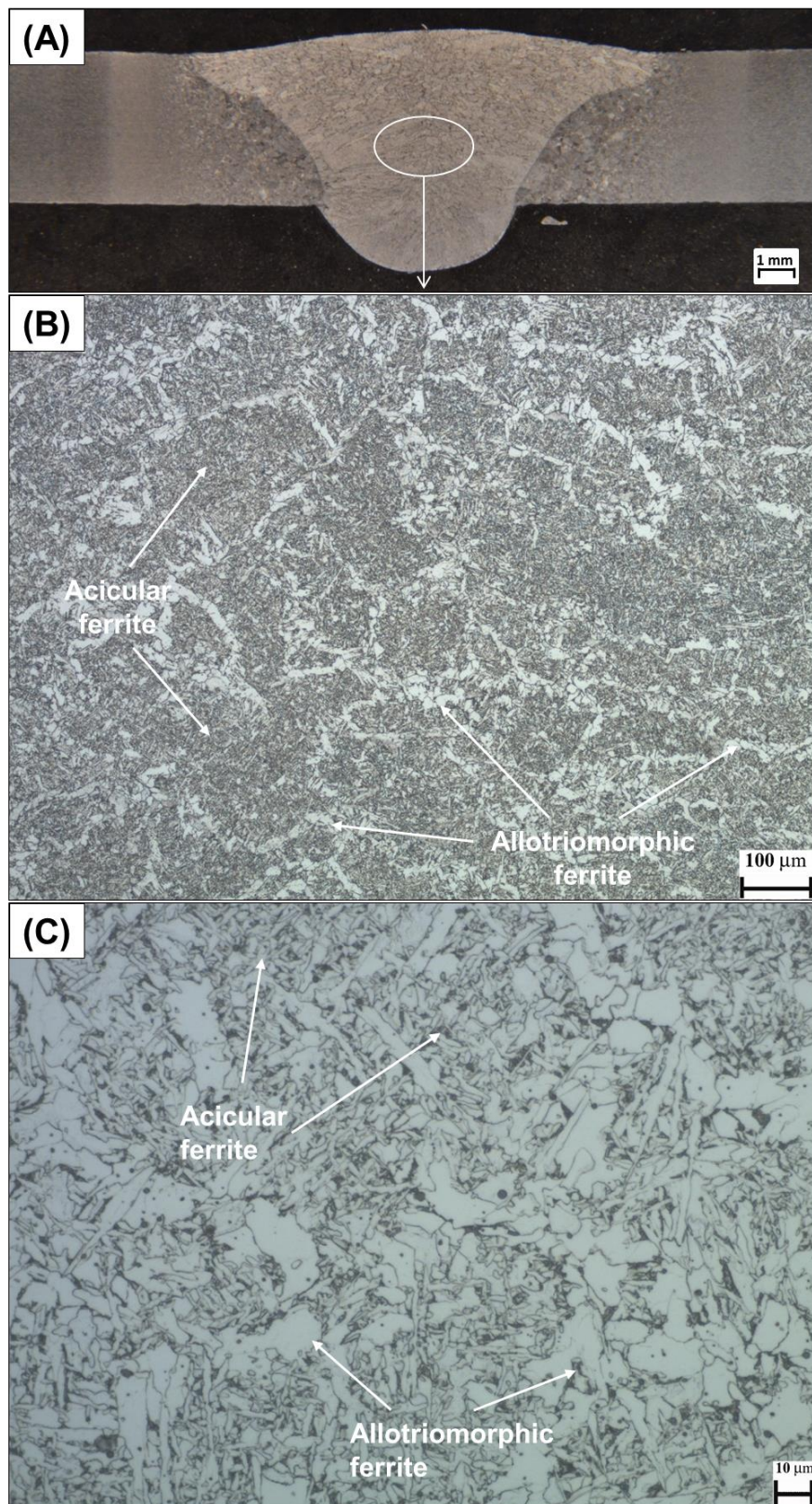


Fig. 5.7 Ø16mm - 5 L/min weld microstructure (etched). (A) Weld cross-section. (B) x100. (C) x500.

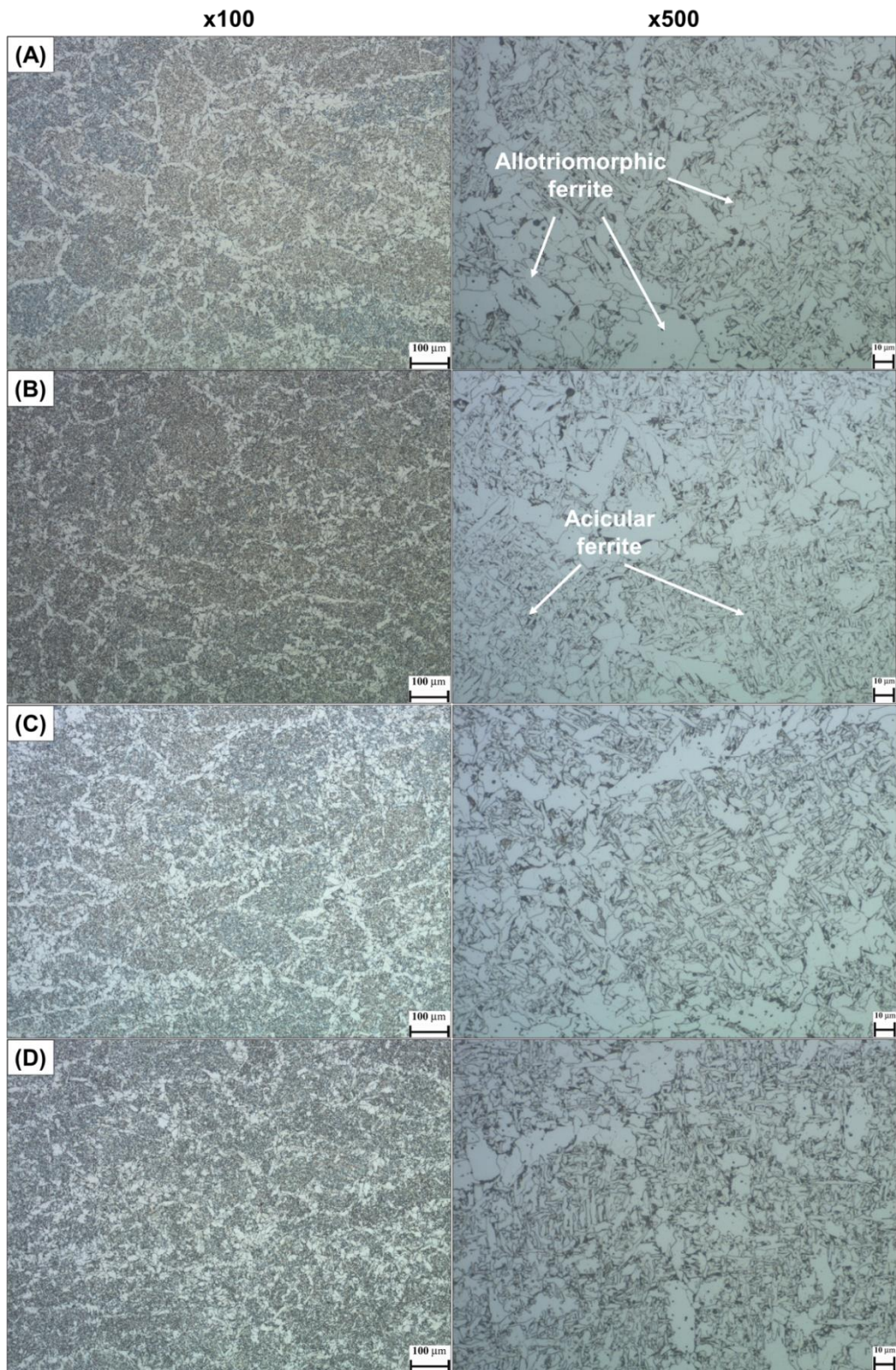


Fig. 5.8 Microstructure of the alternating shielding gas welds taken from a region comparable to that of Fig. 5.7 (A) (etched). (A) 15Ar-15He2. (B) 15Ar-15He6. (C) 6Ar-6He2. (D) 6Ar-6He6.

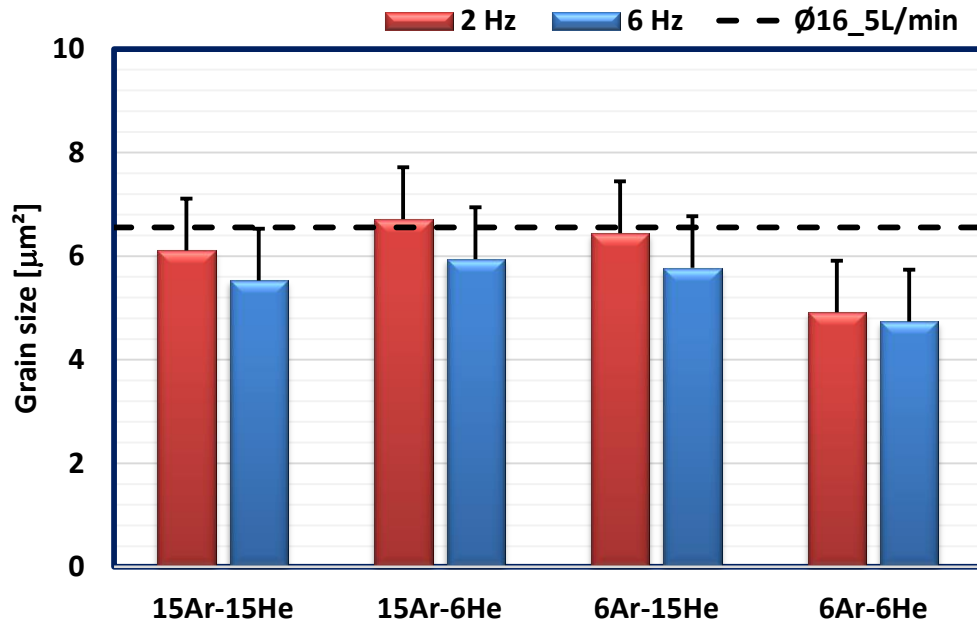


Fig. 5.9 Mean grain size of the weld region (all welds).

Negligible variations were found by modifying the Ar₂₀CO₂ + He supplies from 15Ar-6He to 6Ar-15He for the same frequency. It is inferred that, even by reducing the SGFR of Ar₂₀CO₂ to 6 L/min and increasing the SGFR of He to 15 L/min, the lower density of the latter [5.50-5.52] would hinder its ability to purge Ar₂₀CO₂ from the arc region, hence promoting minor differences in terms of heat input and, consequently, grain size for the 15Ar-6He and 6Ar-15He cases.

Reducing the SGFRs of both Ar₂₀CO₂ and He improved the grain refinement and, as discussed in chapter 4, is correlated to the lower momentum and convective heat of the protective gases exiting the nozzle towards the molten pool [5.2, 5.11]. In addition, the similar grain sizes measured for the 6Ar-6He₂ and 6Ar-6He₆ cases show that variations in the frequency have no effect when the SGFR is very low.

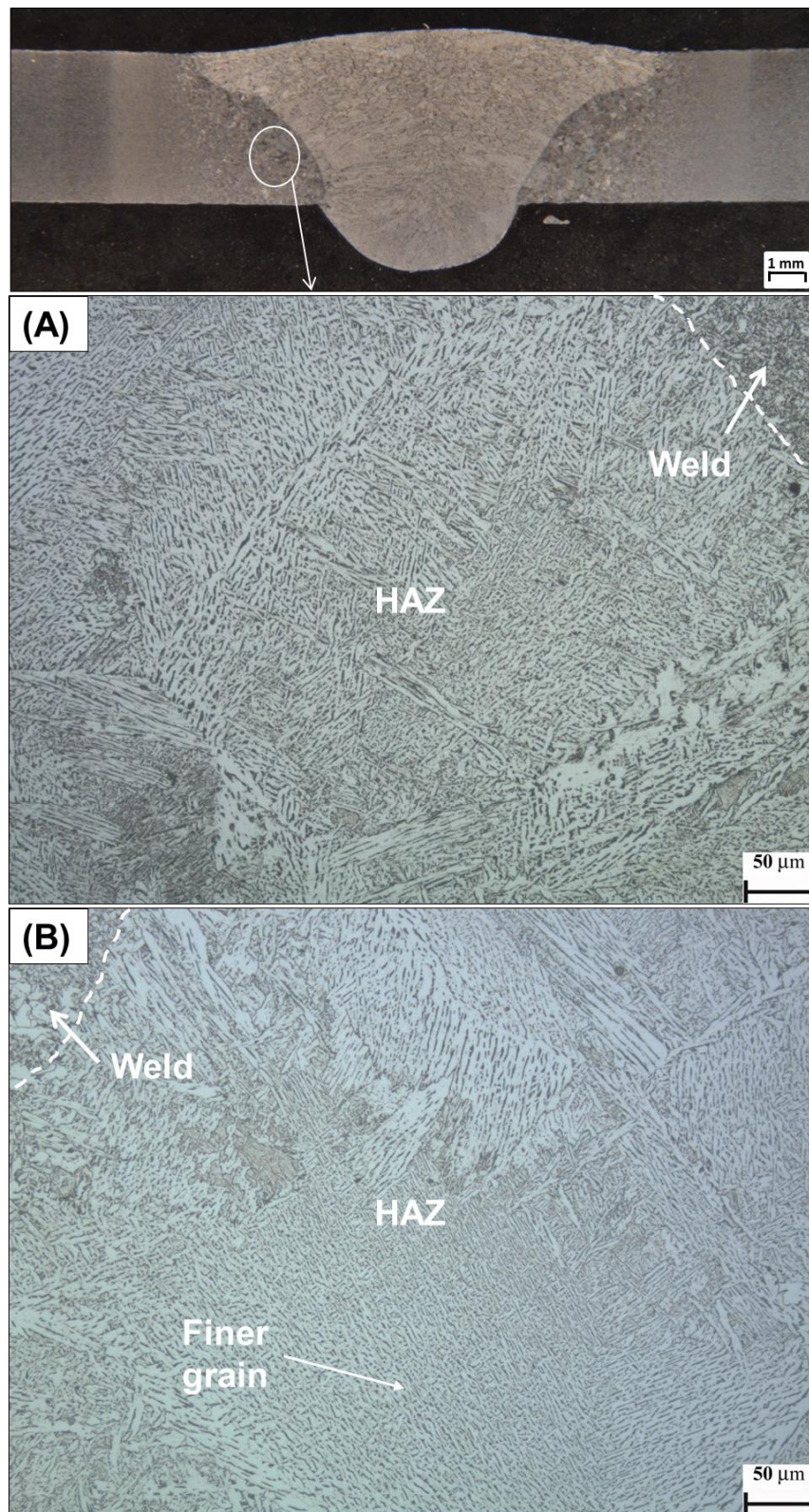


Fig. 5.10 HAZ comparison (x200 - etched). (A) Ø16_5L/min. (B) 6Ar-6He2.

A more refined HAZ microstructure by utilising the alternating shielding gas method was shown by Campbell et al. [5.9], where higher travel speeds hindered the coarsening of the grain in the HAZ area [5.6, 5.9, 5.36, 5.38]. In comparison to the benchmark (see Fig. 5.10 (A)), the presence of finer grains in some alternating shielding gas cases was observed, being more evident in the 6Ar-6He welds (see Fig. 5.10 (B)), since lower heat was transferred to the weldment.

5.3.5 Mechanical properties evaluation

Greater weld hardness is known to benefit applications where corrosion is present [5.53]. Hence, hardness measurements were undertaken to better comprehend the impact of the variations in the SGFR and frequency during the alternating shielding gas method.

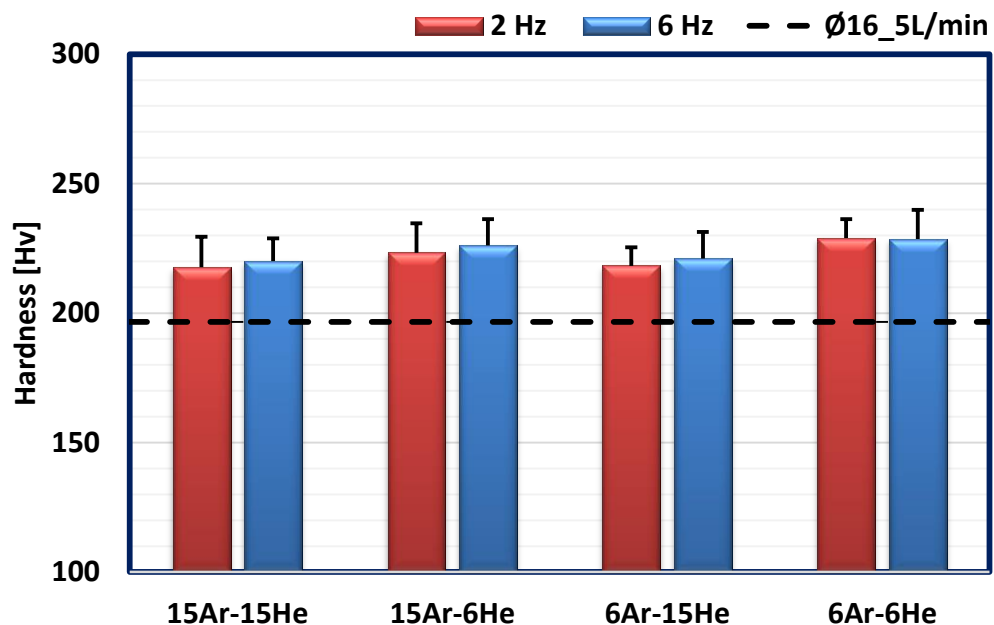


Fig. 5.11 Mean hardness measurements.

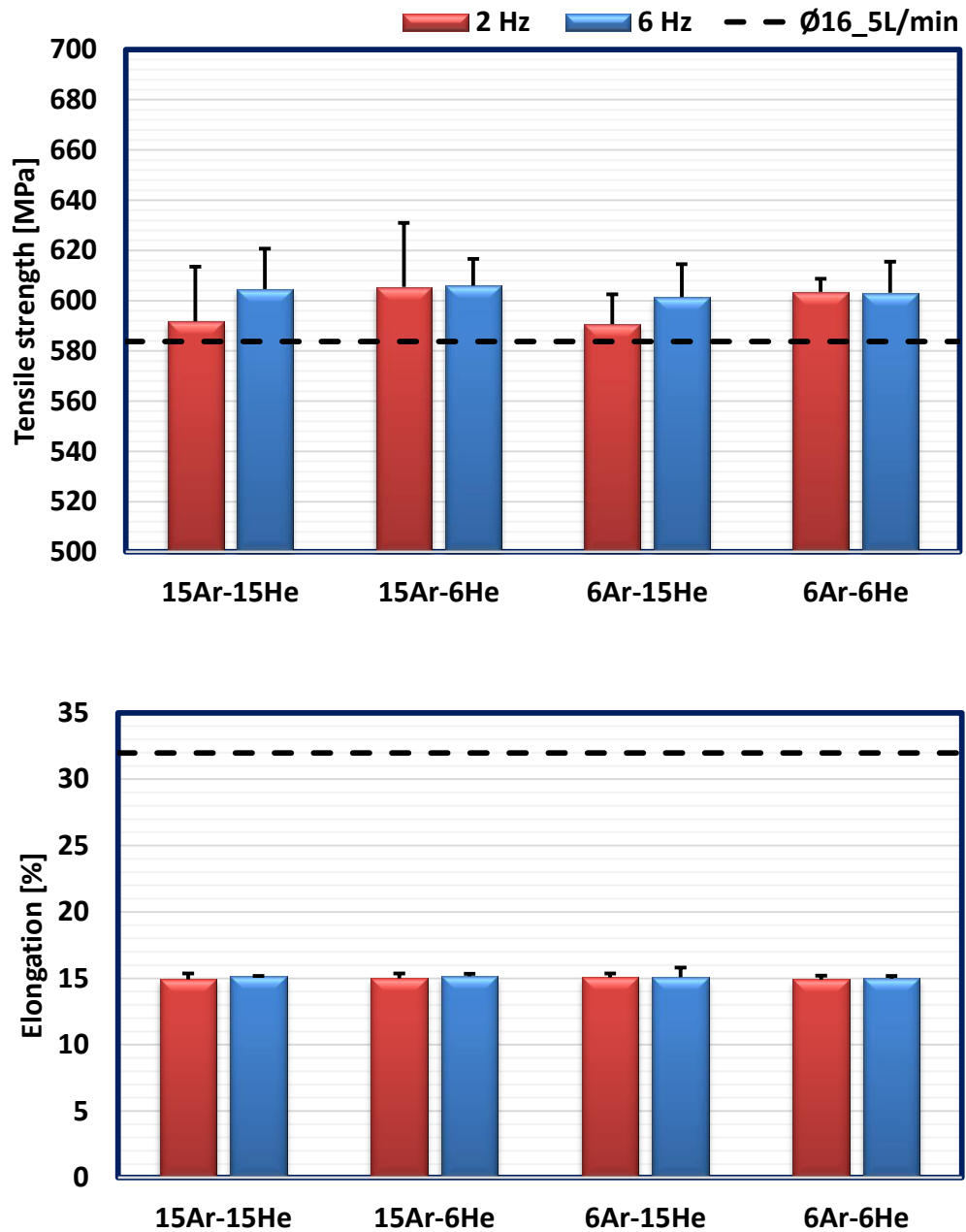


Fig. 5.12 Mean tensile strength and elongation measurements of all welds.

All the alternating shielding gas welds exhibited an average hardness of 223 Hv compared to that of the benchmark (197 Hv), with overall improvements of 13% (26 Hv). This is a result of the refinement of the grain and a more evenly distributed microstructure, which is expected to help the joint to better withstand localised plastic deformation [5.6, 5.9, 5.54, 5.55].

Additionally, these findings support data from previous sections, where the heat transferred to the joints was lowered by the use of the alternating shielding gas technique and a more refined microstructure, achieved [5.6, 5.9, 5.36, 5.38, 5.56].

Altogether, no variations in the hardness were displayed by comparing the welds under the alternating shielding gas method (see Fig. 5.11). Yet, a trend towards greater hardness was found by reducing the SGFRs of both Ar₂₀CO₂ and He, which is related to the finer grain size.

Similar to the results from chapter 4, all the samples passed the transverse tensile and bend tests. While all the transverse tensile samples failed within the parent material, no defects or porosity were found from the bend tests. The all-weld tensile tests demonstrated an average improvement in terms of strength (3%) from 584 to 601 MPa for the benchmark and the alternating shielding gas welds, respectively (see Fig. 5.12).

Conversely, the elongation of the joint was reduced to 15%, decreasing the material's ductility and, therefore, its deformation before failure. This corresponds to findings by Campbell et al. [5.9], in that higher strength and lower elongation of the joints were measured by the use of the alternating shielding gas method due to the lower heat transfer and a more refined microstructure of the weld [5.6, 5.9, 5.36, 5.38].

5.4 Conclusions

This chapter extended the knowledge regarding the novel alternating shielding gas technique. It focused on the outcomes of reducing the SGFR with

variations of both the frequency between the alternated gases and the respective SGFRs.

The alternating shielding gas technique was able to decrease the distortion of the weldment in the 6Ar-6He cases, with negligible differences in terms of temperature of the joint compared to the benchmark ($\text{Ø}16_5\text{L}/\text{min}$). It was found that the higher distortion of the workpiece does not always correlate to the greater temperature measurements, which were attributed to the higher thermal flux of the weld. Additionally, increasing the SGFR of Ar₂₀CO₂ while reducing the He presence enhanced the heat input to 1111 J/mm (15Ar-6He6) while inducing a concave reinforcement, not necessarily contributing to a greater penetration of the weld.

Despite using the same travel speed for the alternating shielding gas and premixed methods, the heat input was diminished by employing the alternating shielding gas technique. With HAZ areas reduced by 23% and grain refinements of 8 and 16% for the 2 and 6 Hz frequencies, respectively, results were in good agreement with previous studies [5.6, 5.9]. Improvements were also found from mechanical tests, with 13% greater hardness of the joint and 3% stronger welds, despite a maximum 15% elongation before failure.

Overall, the 6 Hz frequency performed better than the 2 Hz in terms of grain refinement, HAZ and root width, demonstrating a reduced heat input from 1131 J/mm (6Ar-15He2) to 1075 J/mm (6Ar-15He2), for instance. Hence, there is scope for smaller root gaps, with less metal deposition and lower heat transfer to the weldment. Furthermore, results indicate that the travel speed can be easily increased, improving the workpiece and weld microstructural and mechanical properties.

Although decreasing the stand-off distance from 10 (premixed method) to 5 mm (alternating shielding gas method), it was possible to maintain or reduce even further the impact of the arc welding heat on the joint and workpiece, with the 6Ar-6He cases as the most efficient options. These results will be utilised in chapters 6 and 7 for the sake of comparison, investigating that the replacement of CO₂ for N₂.

5.5 Bibliography

- [5.1] Loxton Industries, “New welding gas innovation,” *Australas. Weld. J.*, vol. 55, no. 1, pp. 10–11, 2010.
- [5.2] I. Bitharas, N. A. McPherson, W. McGhie, D. Roy, and A. J. Moore, “Visualisation and optimisation of shielding gas coverage during gas metal arc welding,” *J. Mater. Process. Technol.*, vol. 255, no. December, pp. 451–462, 2018.
- [5.3] S. W. Campbell, A. M. Galloway, and N. A. McPherson, “Techno-economic evaluation of reducing shielding gas consumption in GMAW whilst maintaining weld quality,” *Int. J. Adv. Manuf. Technol.*, vol. 63, no. 6–9, pp. 975–985, 2012.
- [5.4] V. Beyer, S. W. Campbell, G. M. Ramsey, A. M. Galloway, A. J. Moore, and N. A. McPherson, “Systematic study of effect of cross-drafts and nozzle diameter on shield gas coverage in MIG welding,” *Sci. Technol. Weld. Join.*, vol. 18, no. 8, pp. 652–660, 2013.
- [5.5] I. Bitharas, S. W. Campbell, A. M. Galloway, N. A. Mcpherson, and A. J. Moore, “Visualisation of alternating shielding gas flow in GTAW,” *Mater. Des.*, vol. 91, pp. 424–431, 2016.
- [5.6] S. W. Campbell, A. M. Galloway, N. A. McPherson, and A. Gillies,

- “Evaluation of gas metal arc welding with alternating shielding gases for use on AA6082T6,” *Proc. Inst. Mech. Eng. Part B J. Eng. Manuf.*, vol. 226, no. 6, pp. 992–1000, 2012.
- [5.7] N. V. Shinde and M. T. Telsang, “Effect of Alternate Supply of Shielding Gases of Tungsten Inert Gas Welding on Mechanical Properties of Austenitic Stainless Steel,” *J. Inst. Eng. Ser. C*, vol. 97, no. 3, pp. 299–307, 2016.
- [5.8] B. Y. Kang, Y. K. D. V Prasad, M. J. Kang, H. J. Kim, and I. S. Kim, “Characteristics of alternate supply of shielding gases in aluminum GMA welding,” *J. Mater. Process. Technol.*, vol. 209, no. 10, pp. 4716–4721, 2009.
- [5.9] S. W. Campbell, A. M. Galloway, and N. A. McPherson, “Techno-economic evaluation on the effects of alternating shielding gases for advanced joining processes,” *Proc. Inst. Mech. Eng. Part B J. Eng. Manuf.*, vol. 225, no. 10, pp. 1863–1872, 2011.
- [5.10] Y. H. Chang, “Improve GMAW and GTAW with alternating shield gases,” *Weld. J.*, vol. 85, no. 2, pp. 41–43, 2006.
- [5.11] F. H. Ley, S. W. Campbell, A. M. Galloway, and N. A. McPherson, “Effect of shielding gas parameters on weld metal thermal properties in gas metal arc welding,” *Int. J. Adv. Manuf. Technol.*, vol. 80, no. 5–8, pp. 1213–1221, 2015.
- [5.12] S. W. Campbell, F. H. Ley, A. M. Galloway, and N. A. McPherson, “Artificial neural network optimisation of shielding gas flow rate in gas metal arc welding subjected to cross drafts when using alternating shielding gases,” *Proc. Inst. Mech. Eng. Part B J. Eng. Manuf.*, vol. 229, no. 1, pp. 122–129, 2015.

- [5.13] B. Y. Kang, Y. K. D. V Prasad, M. J. Kang, H. J. Kim, and I. S. Kim, “The effect of alternate supply of shielding gases in austenite stainless steel GTA welding,” *J. Mater. Process. Technol.*, vol. 209, no. 10, pp. 4722–4727, 2009.
- [5.14] S. W. Campbell, A. M. Galloway, G. M. Ramsey, and N. A. McPherson, “A potential solution to GMAW gas flow optimisation,” in *ASM Proceedings of the International Conference: Trends in Welding Research*, 2012.
- [5.15] T. Gray, D. Camilleri, and N. McPherson, “Understanding welding distortion: thermal fields thermo-mechanical effects,” in *Control of Welding Distortion in Thin-Plate Fabrication*, Woodhead Publishing Limited, 2014, pp. 53–76.
- [5.16] T. Gray, D. Camilleri, and N. McPherson, “Simulating welding distortion in butt welding of thin plates,” in *Control of Welding Distortion in Thin-Plate Fabrication*, 2014, pp. 199–232.
- [5.17] L. L. Wang, F. G. Lu, H. P. Wang, A. B. Murphy, and X. H. Tang, “Effects of shielding gas composition on arc profile and molten pool dynamics in gas metal arc welding of steels,” *J. Phys. D. Appl. Phys.*, vol. 47, no. 46, p. 465202 (14pp), 2014.
- [5.18] A. B. Murphy, M. Tanaka, K. Yamamoto, S. Tashiro, T. Sato, and J. J. Lowke, “Modelling of thermal plasmas for arc welding: the role of the shielding gas properties and of metal vapour,” *J. Phys. D. Appl. Phys.*, vol. 42, no. 19, p. 194006 (20pp), 2009.
- [5.19] S. Tashiro et al., “Plasma properties of helium gas tungsten arc with metal vapour,” *Sci. Technol. Weld. Join.*, vol. 12, no. 3, pp. 202–207, 2007.

- [5.20] Anthony B Murphy, “The effects of metal vapour in arc welding,” *J. Phys. D. Appl. Phys.*, vol. 43, no. 16, p. 165204, 2010.
- [5.21] K. Yamamoto et al., “Metal vapour behaviour in thermal plasma of gas tungsten arcs during welding,” *Sci. Technol. Weld. Join.*, vol. 13, no. 6, pp. 566–572, 2008.
- [5.22] M. Schnick et al., “Numerical Investigations of the Influence of Metal Vapour in GMA Welding,” *Weld. World*, vol. 55, no. 11–12, pp. 114–120, 2011.
- [5.23] S. Kodama, K. Sugiura, S. Nakanishi, Y. Tsujimur, M. Tanaka, and A. B. Murphy, “Effect of plasma heat source characteristics on nitrogen absorption in gas tungsten arc weld metal,” *Weld. World*, vol. 57, no. 6, pp. 925–932, 2013.
- [5.24] S. Kodama et al., “Nitrogen absorption phenomenon of GTA welding with nitrogen-mixed shielding gases: effect of plasma characteristics on nitrogen content in GTA welded metal,” *Weld. Int.*, vol. 29, no. 4, pp. 262–269, 2015.
- [5.25] L. L. Wang, H. P. Wang, F. G. Lu, A. B. Murphy, and B. E. Carlson, “Numerical analysis of Al vapour effects in gas metal arc welding of Al alloys,” *Sci. Technol. Weld. Join.*, vol. 19, no. 5, pp. 361–368, 2014.
- [5.26] E. Armentani, R. Esposito, and R. Sepe, “The effect of thermal properties and weld efficiency on residual stresses in welding,” *Manuf. Eng.*, vol. 20, no. 1–2, pp. 319–322, 2007.
- [5.27] P. Michaleris, L. Zhang, S. R. Bhide, and P. Marugabandhu, “Evaluation of 2D, 3D and applied plastic strain methods for predicting buckling welding distortion and residual stress,” *Sci. Technol. Weld. Join.*, vol. 11, no. 6, pp. 707–716, 2006.

- [5.28] T. P. Quinn, R. B. Madigan, and T. A. Siewert, “An Electrode Extension Model for Gas Metal Arc Welding,” *Weld. J.*, vol. 73, no. 10, p. 10, 1994.
- [5.29] Y. Kim and S. Rhee, “A Study of Heat Input Distribution on the Surface during Torch Weaving in Gas Metal Arc Welding,” *Japan Soc. Mech. Eng. J.*, vol. 48, no. 3, pp. 144–150, 2005.
- [5.30] H. S. Ham, D. S. Oh, and S. M. Cho, “Measurement of arc pressure and shield gas pressure effect on surface of molten pool in TIG welding,” *Sci. Technol. Weld. Join.*, vol. 17, no. 7, pp. 594–600, 2012.
- [5.31] S. W. Campbell, A. M. Galloway, and N. A. McPherson, “Arc pressure and fluid flow during alternating shielding gases. Part 2: arc force determination,” *Sci. Technol. Weld. Join.*, vol. 18, no. 7, pp. 597–602, 2013.
- [5.32] A. B. Murphy, M. Tanaka, S. Tashiro, T. Sato, and J. J. Lowke, “A computational investigation of the effectiveness of different shielding gas mixtures for arc welding,” *J. Phys. D. Appl. Phys.*, vol. 42, p. 115205, 2009.
- [5.33] S. W. Campbell, A. M. Galloway, and N. A. McPherson, “Arc pressure and weld metal fluid flow while using alternating shielding gases. Part 1: arc pressure measurement,” *Sci. Technol. Weld. Join.*, vol. 18, no. 7, pp. 591–596, 2013.
- [5.34] J. Norrish, *Advanced Welding Processes*. Springer Netherlands, 1992.
- [5.35] A. Traidia and F. Roger, “A computational investigation of different helium supplying methods for the improvement of GTA welding,” *J. Mater. Process. Technol.*, vol. 211, no. 9, pp. 1553–1562, 2011.
- [5.36] R. G. Tazetdinov, O. M. Novikov, A. S. Persidskii, B. A. Khasyanov, E.

- N. Ivanov, and L. T. Plaksina, “Arc welding in shielding gases with alternate pulsed supply of dissimilar gases,” *Weld. Int.*, vol. 7116, no. May 2015, pp. 1–4, 2012.
- [5.37] T. Gray, D. Camilleri, and N. McPherson, “Fabrication of stiffened thin-plate structures and the problem of welding distortion,” in *Control of Welding Distortion in Thin-Plate Fabrication*, 2014, pp. 14–38.
- [5.38] N. S. Barabokhin et al., “Technological special features of welding 1460 high-strength aluminium alloy,” *Weld. Int.*, vol. 14, no. 6, pp. 468–470, 2000.
- [5.39] R. Ghomashchi, W. Costin, and R. Kurji, “Evolution of weld metal microstructure in shielded metal arc welding of X70 HSLA steel with cellulosic electrodes: A case study,” *Mater. Charact.*, vol. 107, pp. 317–326, 2015.
- [5.40] H. Bhadeshia and R. Honeycombe, *Steels: Microstructure and Properties*, 4th ed. Elsevier Ltd., 2017.
- [5.41] G. Thewlis, J. A. Whiteman, and D. J. Senogles, “Dynamics of austenite to ferrite phase transformation in ferrous weld metals,” *Mater. Sci. Technol.*, vol. 13, no. 3, pp. 257–274, 1997.
- [5.42] T. Koseki, “A Review on Inclusion-Assisted Microstructure Control in C-Mn and Low-Alloy Steel Welds,” *Weld. World*, vol. 49, no. 5–6, pp. 22–28, 2005.
- [5.43] A. F. Gourgues, H. M. Flower, and T. C. Lindley, “Electron backscattering diffraction study of acicular ferrite, bainite, and martensite steel microstructures,” *Mater. Sci. Technol.*, vol. 16, no. 1, pp. 26–40, 2000.
- [5.44] W. L. Costin, O. Lavigne, and A. Kotousov, “A study on the

- relationship between microstructure and mechanical properties of acicular ferrite and upper bainite,” *Mater. Sci. Eng. A*, vol. 663, pp. 193–203, 2016.
- [5.45] I. Madariaga, I. Gutiérrez, C. García-De Andrés, and C. Capdevila, “Acicular ferrite formation in a medium carbon steel with a two stage continuous cooling,” *Scr. Mater.*, vol. 41, no. 3, pp. 229–235, 1999.
- [5.46] D. Min, J. Shen, S. Lai, and J. Chen, “Effect of heat input on the microstructure and mechanical properties of tungsten inert gas arc butt-welded AZ61 magnesium alloy plates,” *Mater. Charact.*, vol. 60, no. 12, pp. 1583–1590, 2009.
- [5.47] *Welding and brazing: ASM metals handbook*, 8th ed., vol. 6. ASM International.
- [5.48] S. W. Campbell, “Shielding Gas Parameter Optimisation in Arc Welding Processes,” University of Strathclyde, 2015.
- [5.49] ASM, “Welding, Brazing and Soldering,” in *ASM metals handbook*, 8th ed., vol. 6, Ohio, 1993, pp. 37–38.
- [5.50] British Standard Institution, “BS EN ISO 14175:2008. Welding consumables — Gases and gas mixtures for fusion welding and allied processes.” BSI, London, 2008.
- [5.51] P. Kah and J. Martikainen, “Influence of shielding gases in the welding of metals,” *Int. J. Adv. Manuf. Technol.*, vol. 64, no. 9–12, pp. 1411–1421, 2013.
- [5.52] B. Mvola and P. Kah, “Effects of shielding gas control: welded joint properties in GMAW process optimization,” *Int. J. Adv. Manuf. Technol.*, vol. 88, no. 9–12, pp. 2369–2387, 2017.
- [5.53] N. Bailey, “Joint integrity,” in *Weldability of Ferritic Steels*, 1994, p.

286.

- [5.54] P. K. Ghosh, S. R. Gupta, and H. S. Randhawa, “Characteristics of a Pulsed-Current, Vertical-Up Gas Metal Arc Weld in Steel,” *Metall. Mater. Trans. A*, vol. 31, no. 9, pp. 2247–2259, 2000.
- [5.55] Y. Zheng et al., “An experimental study of nitrogen gas influence on the 443 ferritic stainless steel joints by double-shielded welding,” *Int. J. Adv. Manuf. Technol.*, vol. 87, no. 9–12, pp. 3315–3323, 2016.
- [5.56] J. Wang, Y. Li, and P. Liu, “Effect of weld heat input on toughness and structure of HAZ of a new super-high strength steel,” *Bull. Mater. Sci.*, vol. 26, no. 3, pp. 301–305, 2003.

“Successful and unsuccessful people do not vary greatly in their abilities.

They vary in their desires to reach their potential”

John Maxwell

Chapter 6

Exploring the use of N₂ in the alternating shielding gas technique

6.1 Introduction

As discussed in chapter 2, gases such as Ar, CO₂, N₂ and He are chosen in different welding processes according to their particular properties and outputs that are required [6.1-6.4]. In gas metal arc welding (GMAW), the pure Ar arc plasma, for example, permits an easier arc initiation compared to He, which provides a better penetration of the joint due to its higher arc energy [6.1, 6.4-6.7]. Different gas mixtures are also possible, combining the benefits of the various shielding gases [6.8-6.11]. For instance, in gas tungsten arc welding (GTAW) Nage et al. [6.8] demonstrated that additions of N₂ to Ar were able to enhance mechanical properties such as strength and hardness of the weld, related to the strengthening of the austenitic phase when welding 317L and 904L steels. Lu et al. [6.11] also showed that the arc ignitability and stability of He in GTAW was improved by additions of Ar to the shielding gas.

While extensive work has been published [6.12-6.17] utilising gas mixtures of Ar, CO₂ and He to weld steels such as DH36, mixtures with N₂ present a greater challenge considering its reactive behaviour in high temperatures [6.1-6.3]. The N₂ shielding gas is known to dissociate into its monatomic form within the high-temperature arc domain during welding,

where it is then absorbed into the molten pool [6.3, 6.18, 6.19]. Since the equilibrium solubility of N in the molten pool diminishes during the solidification of the weld, its excess is released to the atmosphere, creating blowholes and precipitation of nitrides coupled with the solidification of N in interstitial solid solution [6.1, 6.19]. The amount of N in welds should not exceed 80 ppm, which decreases toughness and promotes the development of blowholes [6.18, 6.20]. For instance, mixing 1% of N₂ in premixed Ar20CO₂ shielding gas during GMAW increases the N content in the weld metal to 200 - 300 ppm [6.18].

Kodama et al. [6.3], using premixed shielding gases such as Ar1N₂, He1N₂, Ar7H₂1N₂, and ArHe1N₂, showed that increasing the arc voltage decreased the N content within the weld due to the development of metal vapour, which cooled the arc fringe. Olson et al. [6.21] explored the influence of the wire-feed speed and the travel speed in the N solubility and concluded that it is possible to eliminate the presence of porosity by setting parameters such as voltage and torch speed accordingly. The influence of alloying elements in the N content within the weld and consequent blowholes development has been well documented [6.1, 6.2, 6.22-6.25]. Littleton et al. [6.25] examined the reduction in porosity content within the weld bead when increasing the travel speed and using denitrating elements such as Ti and Al. Kodama et al. [6.18] correlated the heat input and N absorption within the molten pool when welding mild and stainless steel using GTAW. The study [6.18] compared Ar1N₂ and He1N₂ and results exhibited a reduction in the N content within the solidified weld when increasing the welding current. In addition, the same study [6.18] discussed the importance that He has in diminishing the N amount by lowering the plasma temperature due to the higher presence of metal

vapour, hindering the N₂ dissociation and its consequent absorption by the molten pool. Despite the promising results in terms of porosity elimination delivered by N₂, the gas supply was constant in all the aforementioned studies, with non-existent research utilising the alternating shielding gas technique.

In this chapter, a novel approach to the reduction of N absorption within the weld bead is attempted. Alternating Ar5N₂ + He is investigated in terms of higher travel speeds and wire-feed speeds, so to promote the elimination of the porosity caused by the presence of N₂. In addition, and as a qualitative observation, the produce fumes were significantly reduced. Non-destructive tests such as radiography together with mechanical testing helped identifying important properties of this advanced joining process whereas heat transfer analysis assisted with the understanding of how the N content decreased according to the chosen parameters.

6.2 Experimental setup

6.2.1 Determining suitable parameters for defect free welds

Bead-on-plate welds were performed as a first step to define the suitable welding parameters for butt welds. An increase in the N content within the molten pool and, consequent porosity, was expected by changing the SGFR from 9 to 15 L/min due to the greater amount of supplied N₂ in contact with the liquid metal [6.18, 6.26]. However, the greater wire-feed speed, travel speed and voltage eliminated the formation of blowholes (see Fig. 6.1 (A)) on the weld surface, despite unacceptable levels of spatter on the edges of the joint (see Fig. 6.1 (B)).

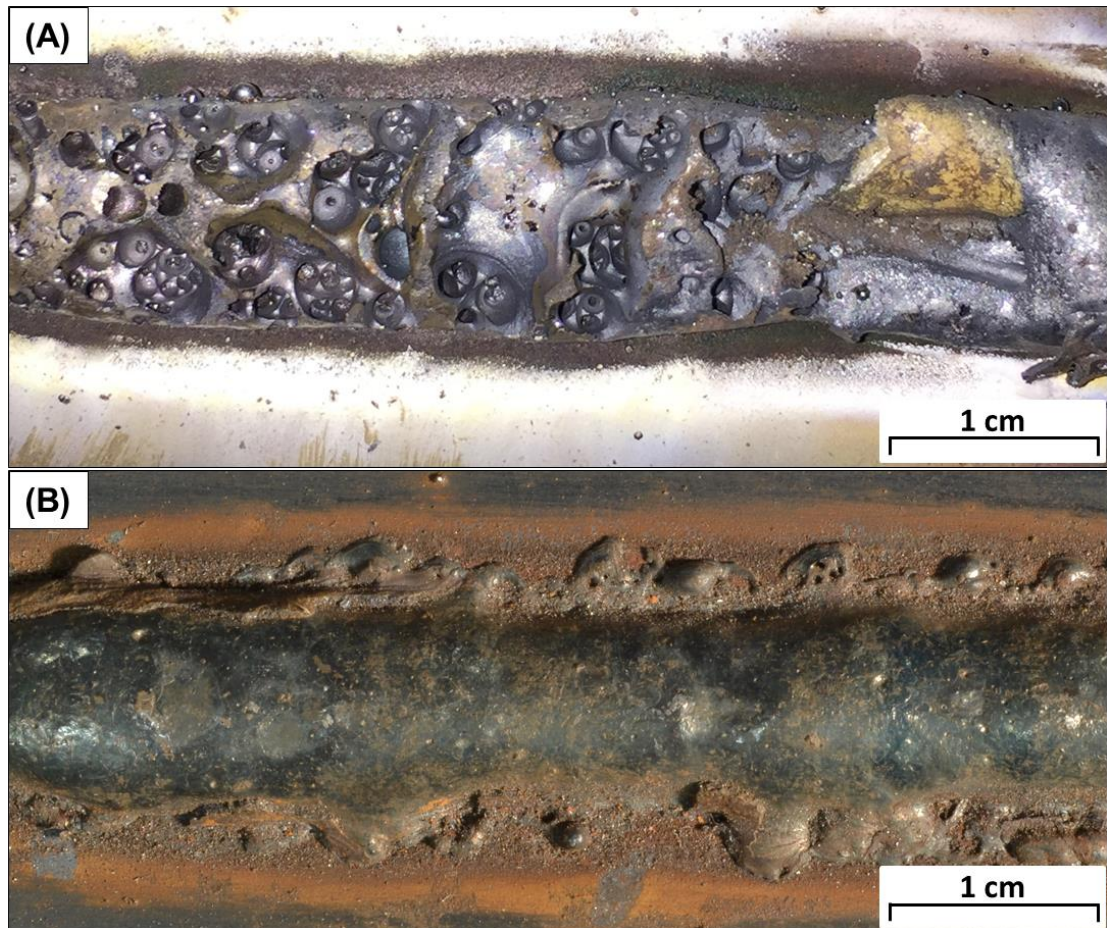


Fig. 6.1 Bead-on-plate welds. (A) SGFR: 9 L/min - Travel speed: 3 mm/s - Wire-feed speed: 7.5 m/min (Ar5N₂ - 25 V). (B) SGFR: 15 L/min - Travel speed: 7 mm/s - Wire-feed speed: 14 m/min (Ar5N₂ - 26 V).

While the greater wire-feed speeds and, consequently, enhanced arc current and heat input decreased the cooling rate of the joint, allowing more time for the N desorption [6.18, 6.27, 6.28], the higher travel speeds hindered the porosity formation by reducing the time available for the N absorption from the protective gas [6.25]. In terms of voltage, its increase stimulated the formation of metal vapour, reducing the arc plasma temperature and the N₂ dissociation [6.3, 6.29].

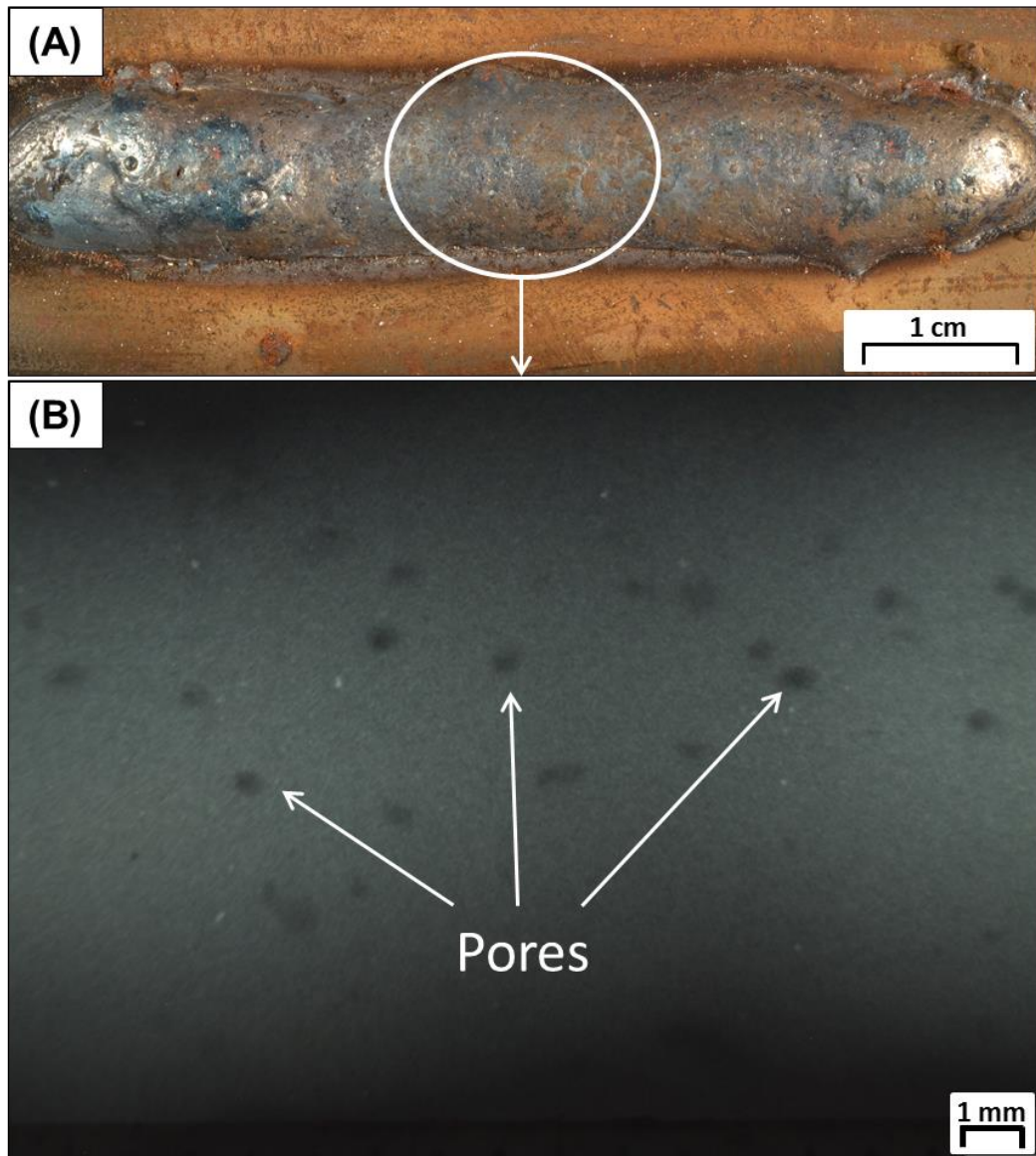


Fig. 6.2 Bead-on-plate (A) and radiograph (B) with pores. SGFR: 15 L/min - Travel speed: 5 mm/s - Wire-feed speed: 10 m/min (Ar5N₂ - 26 V).

The inner region of all bead-on-plate welds was also assessed utilising radiography (see Fig. 6.2 and 6.3). Porosity elimination was evident when increasing the travel speed from 5 to 7 mm/s and the wire-feed speed from 10 to 14 m/min. The addition of He as a shielding gas (see Fig. 6.3) was expected to reduce the arc plasma temperature [6.3, 6.18, 6.29-6.33] and contribute to

the porosity elimination in the alternated case by hindering the N₂ dissociation.

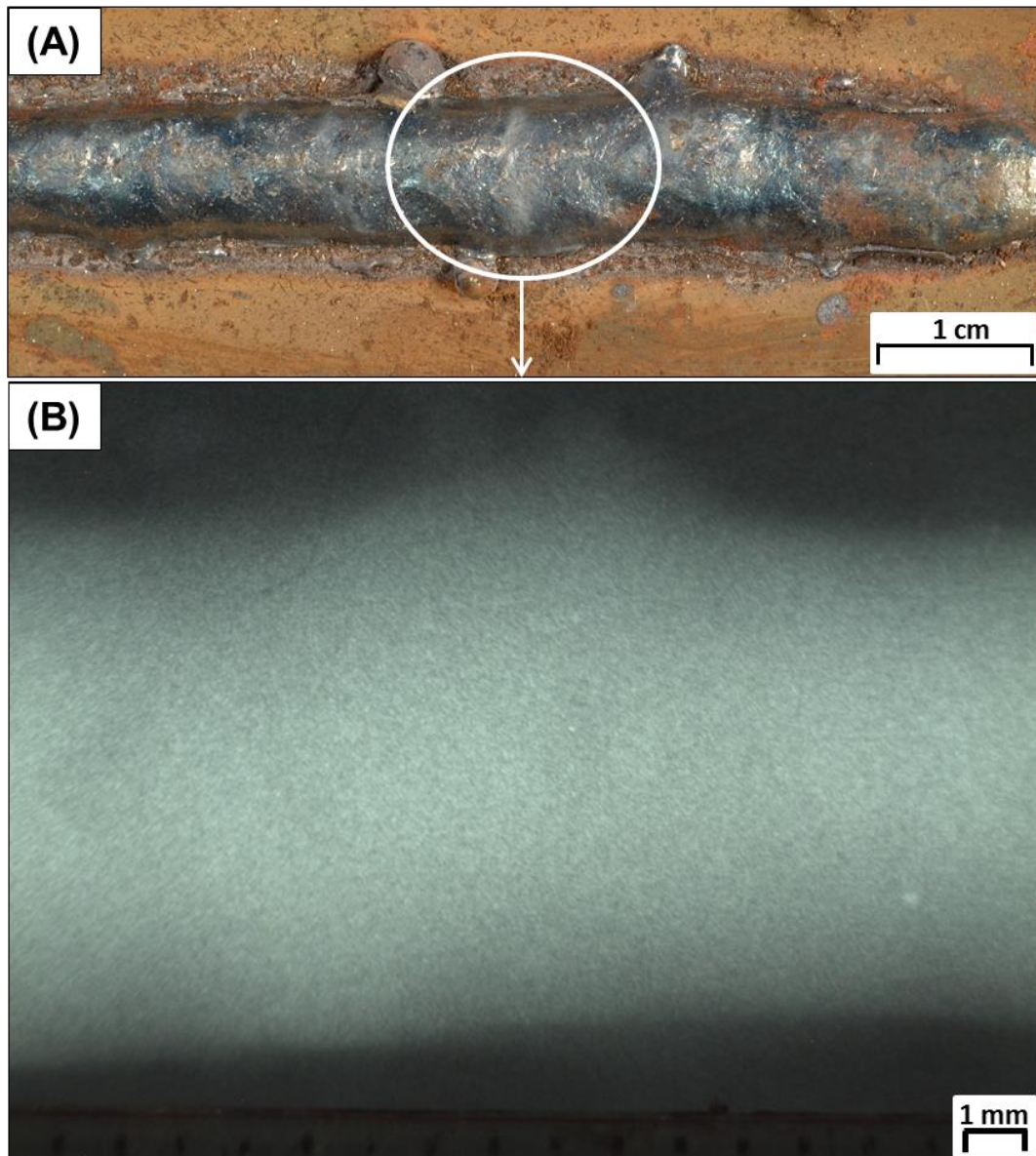


Fig. 6.3 Porosity-free bead-on-plate (A) and radiograph (B). SGFR: 15 L/min - Travel speed: 7 mm/s - Wire-feed speed: 14 m/min (Ar5N₂ + He - 26 V).

Porosity-free welds were performed within a 12 to 16.6 m/min range for the wire-feed speed and 7 to 9 mm/s for the travel speed, where both cases had

a SGFR of 15 L/min. Hence, based on the results from the bead-on-plate trials, the SGFR utilised during the butt welds was also 15 L/min, whilst wire-feed speed values were set as 12, 14 and 16.6 m/min and the travel speeds as 7, 8 and 9 mm/s.

6.2.2 Welding process

The wire-feed speeds utilised were 7.5, 12, 14 and 16.6 m/min. The benchmark was chosen to be an alternated supply of Ar₂₀CO₂ + He with a 2 Hz frequency, according to the work by Campbell et al. [6.17], and was designated as 7.5W-5T (see Table 6.2). The stand-off distance was reduced from 10 to 5 mm compared to that from chapter 4, since it was found elsewhere [6.27, 6.34] to increase N desorption.

Table 6.1 Mean welding parameters used during experiments.

Shielding Gas	Voltage [V]	Current [A]	Wire-feed speed [m/min]	Travel speed [mm/s]	Heat Input [J/mm]	Designation
Ar ₅ N ₂	22.6	252.1	12	9	633	12W-9TP
Ar ₅ N ₂	22.3	297.8	14	8	830	14W-8TP
Ar ₅ N ₂	22.2	339.8	16.6	7	1078	16.6W-7TP

To better understand the impact of alternating Ar₅N₂ + He, the premixed supply of Ar₅N₂ was also assessed and compared to the alternating shielding gas cases. Within the range of parameters chosen for this study, three cases were considered (see Table 6.1), since they represent the extremes of each

range as well as the values of the input variables in between the respective ranges.

Table 6.2 Mean welding parameters used during experiments.

Shielding Gas	Frequency [Hz]	Voltage [V]	Current [A]	Wire-feed speed [m/min]	Travel speed [mm/s]	Heat Input [J/mm]	Designation
Ar5N ₂ + He	2	22.6	267.6	12	7	864	12W-7T
Ar5N ₂ + He	2	22.6	264.9	12	8	748	12W-8T
Ar5N ₂ + He	2	22.6	264.9	12	9	665	12W-9T
Ar5N ₂ + He	2	22.5	306	14	7	984	14W-7T
Ar5N ₂ + He	2	22.5	303.1	14	8	852	14W-8T
Ar5N ₂ + He	2	22.5	300.7	14	9	752	14W-9T
Ar5N ₂ + He	2	22.3	343.7	16.6	7	1095	16.6W-7T
Ar5N ₂ + He	2	22.3	337.6	16.6	8	941	16.6W-8T
Ar5N ₂ + He	2	22.3	346.2	16.6	9	858	16.6W-9T
Ar20CO ₂ + He	-	22.5	247.3	7.5	5	1114	7.5W-5T (benchmark)

12W-9T: wire-feed speed of 12 m/min, travel speed of 9 mm/s.

Replacing CO₂ with N₂ is expected to improve the arc constriction, increasing the arc power density and the concentration of heat flux close to the workpiece [6.35]. Thus, the root gap was set as 3 mm for the Ar5N₂ + He supply and 4 mm for all the other cases.

Each set of parameters is presented in Table 6.2 together with the recorded data for the voltage and current. Designations were provided for each combination of input parameters. Hence, a 12W-9TP case represents a weld with a wire-feed speed of 12 m/min and a travel speed of 9 mm/s, where P stands for a premixed gas supply.

6.3 Results and discussion

6.3.1 Distortion of the parent material

As discussed in chapter 3, all the distortion measurements were taken using an optical distance sensor attached to the rig. Overall, all welded plates presented a lower longitudinal distortion in relation to the benchmark for the Ar5N₂ + He cases (see Fig. 6.4), whereas distortion measurements in the transverse direction were greater for all cases under a 7 mm/s travel speed. In general, improved control of the distortion of the welded structures was found in the transverse direction by reducing the wire-feed speed (Ar5N₂ + He case), which was a result of the lower arc current and, therefore, lower heat input [6.36, 6.37].

The allowable increase in the travel speed by utilising the alternating shielding gas technique reduced the heat input and the distortion of the workpiece, which is in line with studies presented elsewhere [6.5, 6.38, 6.39]. For instance, a travel speed of 9 mm/s produced an overall heat input of 758 J/mm, which is 31% lower than that of the benchmark (1114 J/mm). With less material and heat transferred to the joint, the expansion-contraction effect was reduced during the cooling process and, consequently, the residual stresses that cause the distortion of the workpiece [6.40-6.42].

The welds from the premixed supply of Ar5N₂ exhibited similar distortion behaviour to that of its respective alternated cases in terms of travel speed and wire-feed speed (see Fig. 6.5). Despite the lower distortion in the transverse direction, supplying Ar5N₂ increased the distortion of the workpiece longitudinally compared to Ar5N₂ + He.

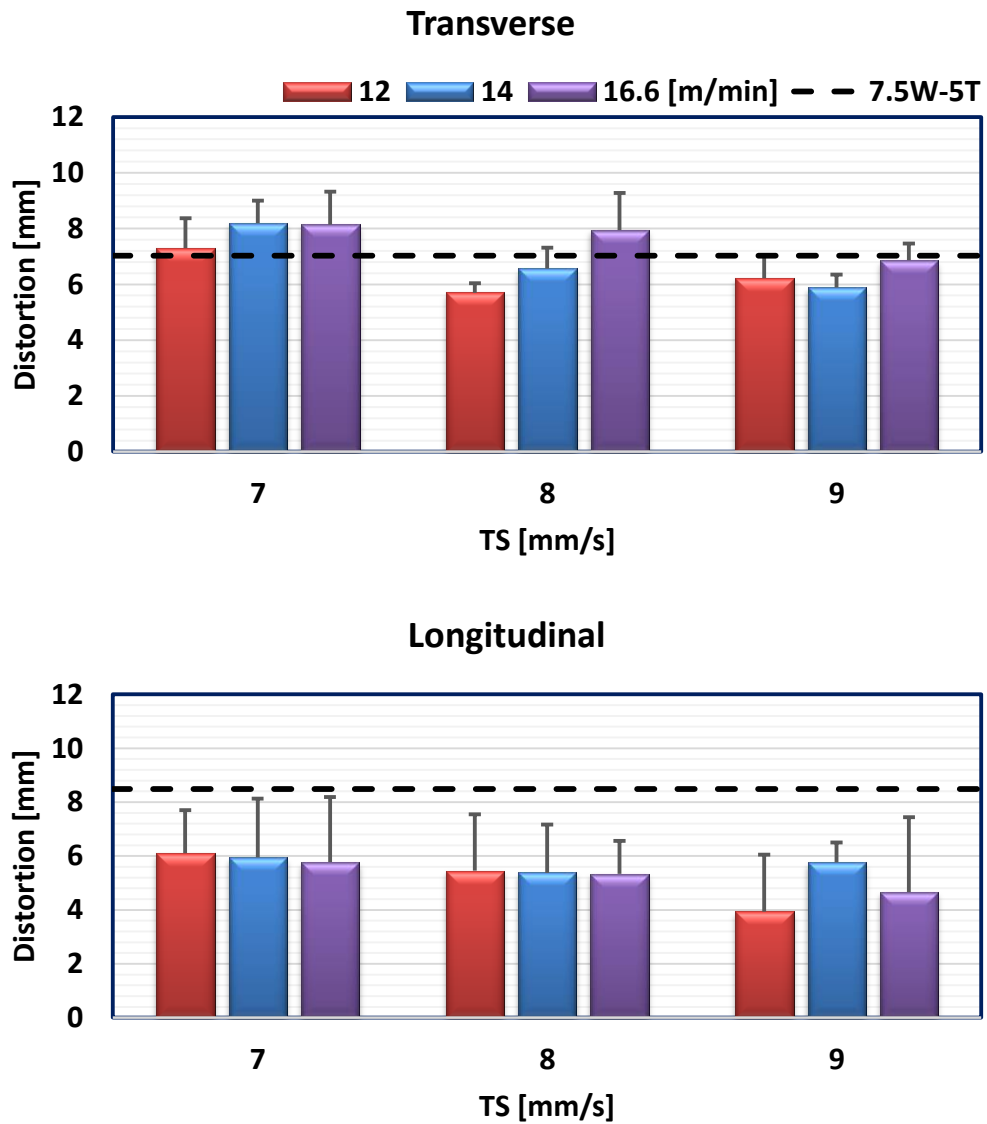


Fig. 6.4 Mean distortion of all the alternating shielding gas and benchmark welded workpieces.

By employing the alternating shielding gas method, the distortion of the workpiece was reduced, mainly due to the increased travel speeds. The alternating shielding gas technique also exhibited workpieces with lower distortion compared to their respective premixed method cases, which was attributed to the presence of He, which reduced the heat input due to the development of metal vapour [6.3, 6.18].

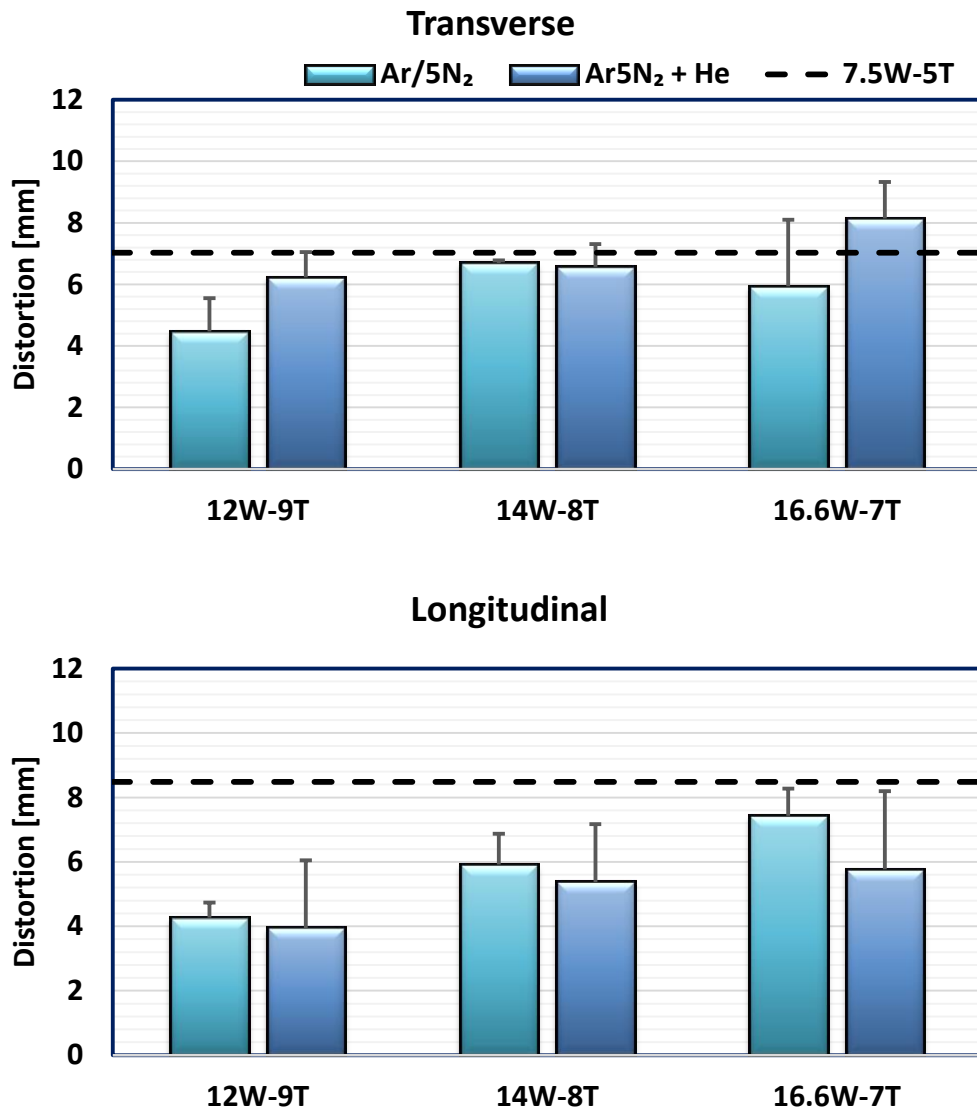


Fig. 6.5 Mean distortion of the benchmark, premixed cases and their respective alternated welds.

6.3.2 Temperature measurements

The temperature was recorded during the GMAW process using pre-calibrated K-type thermocouples (see chapter 3) to clarify the impact of the alternated Ar5N₂ + He on the joint (see Fig. 6.6). Measurements were in line with results for the distortion of the workpiece in the transverse direction, where the measured temperatures were higher for low travel speeds and high wire-feed speeds. Replacing CO₂ with N₂ in the Ar mixture reduced the peak temperature of the joint, which is explained by the lower temperature at the base of the Ar5N₂ arc [6.35] compared to that of the Ar20CO₂ arc [6.43]. Negligible variations in the peak temperatures were found when modifying the gas supply from Ar5N₂ + He to Ar5N₂ (see Fig. 6.7).

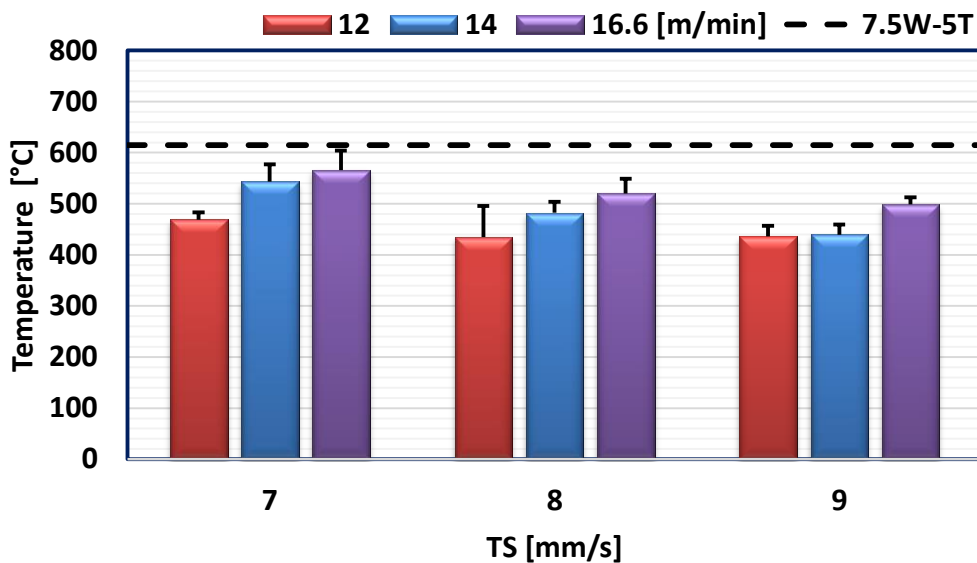


Fig. 6.6 Mean peak temperature of all the alternating shielding gas and benchmark welds.

These findings demonstrated that replacing CO₂ for N₂ was enough to reduce the weld temperature. Reducing the heat input is important, since it will contribute to the refinement of the grain in the fusion zone and HAZ, as

will be discussed in section 6.3.4. Additionally, it influences the distortion of the workpiece as explored in section 6.3.1.

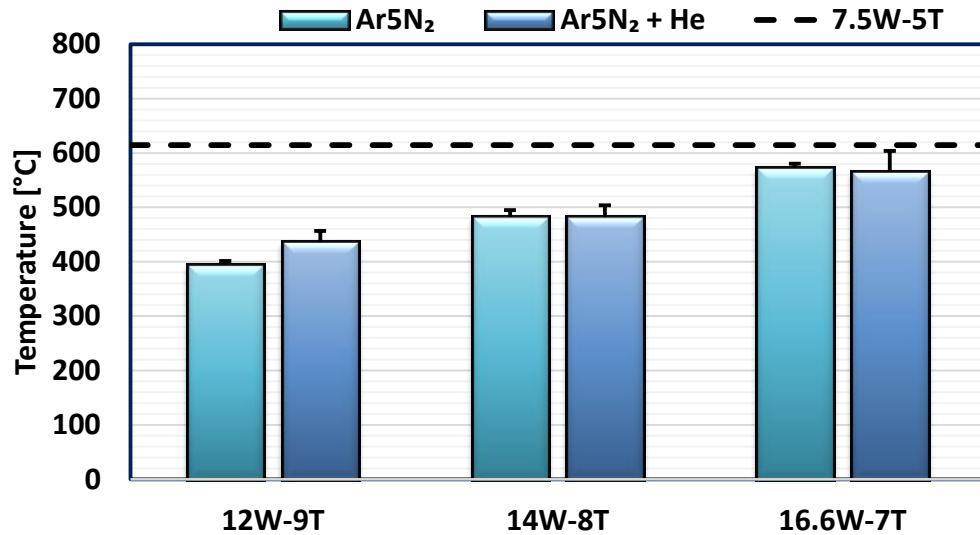


Fig. 6.7 Mean temperature of the benchmark, premixed cases and their respective alternated welds.

6.3.3 Weld characteristics

Macrographs of the cross-section of each weld were taken (see Fig. 6.8) to verify the influence of the alternating shielding gas method and the addition of N₂ as a shielding gas on the weld features. Gray et al. [6.39] showed the importance of having a uniform weld shape, since significant differences between the cap width and the root width of the weld would increase the angular distortion of the workpiece. Hence, measurements were taken from all welds, with the root to cap ratio displayed in Fig. 6.9.

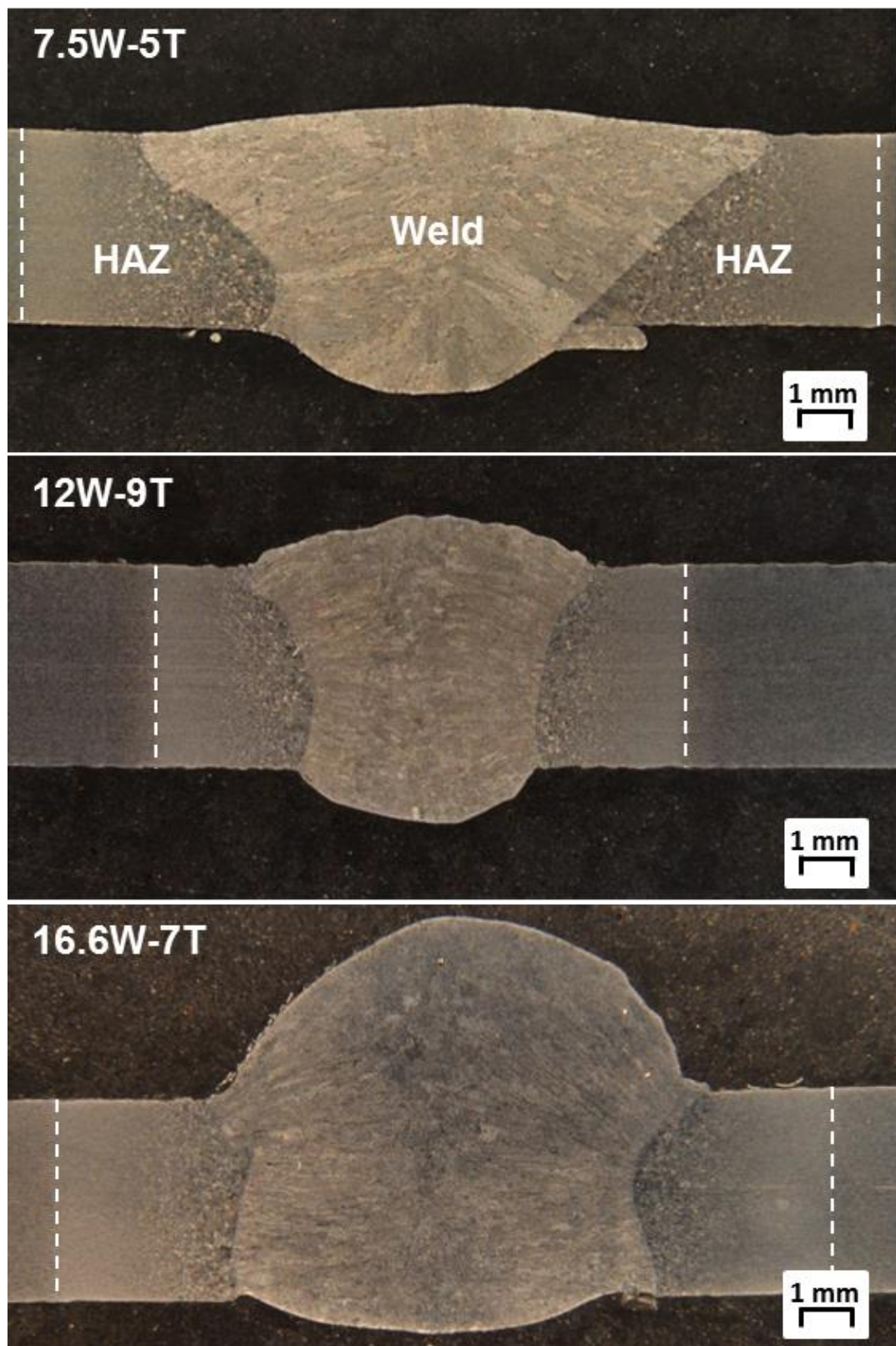


Fig. 6.8 Analysis of the weld shape: dashed lines delineate the HAZ.

While the increase in the travel speed for the Ar5N₂ + He cases presented negligible differences in terms of weld shape, the greater wire-feed speed improved the root to cap ratio of the weld, promoting a more even appearance from the reinforcement towards the root, with similar dimensions of the cap and root widths. Compared to the benchmark, the use of Ar5N₂ + He raised the root to cap ratio, promoting the development of greater root widths and penetration.

As a shielding gas, pure N₂ promotes a more constricted arc plasma compared to pure Ar [6.44, 6.45]. A study by Murphy et al. [6.35] showed that additions of N₂ to Ar contributed to the constriction of the arc plasma due to the thermal pinch effect. Hence, this higher arc energy from the Ar5N₂ mixture during the alternating shielding gas process was able to promote greater root widths of the joint to that of the Ar20CO₂ + He.

Apart from the 14W-8TP case, the premixed supply of Ar5N₂ exhibited a more uniform weld shape than their respective alternated cases, with the 16.6W-7TP weld presenting a 1.1 root to cap ratio (see Fig. 6.10). This was attributed to the addition and constant supply of N₂ as a shielding gas, shown by Tanaka et al. [6.10] to have a more concentrated arc energy and velocity profile compared to Ar and He, contributing to a deeper penetration and smaller reinforcement widths.

The root to cap ratio findings helped to understand the distortion behaviour in the transverse direction of the workpiece. With a more even shape from the cap of the joint towards its root the expansion-contraction residual stresses are more equally distributed, assisting with the reduction of the workpiece's distortion, as discussed by Gray et al. [6.39]. This trend was found when comparing Fig. 6.4 and Fig. 6.9, showing that the greater travel speed

promoted a lower distortion of the weldment and a higher root to cap ratio of the joint.

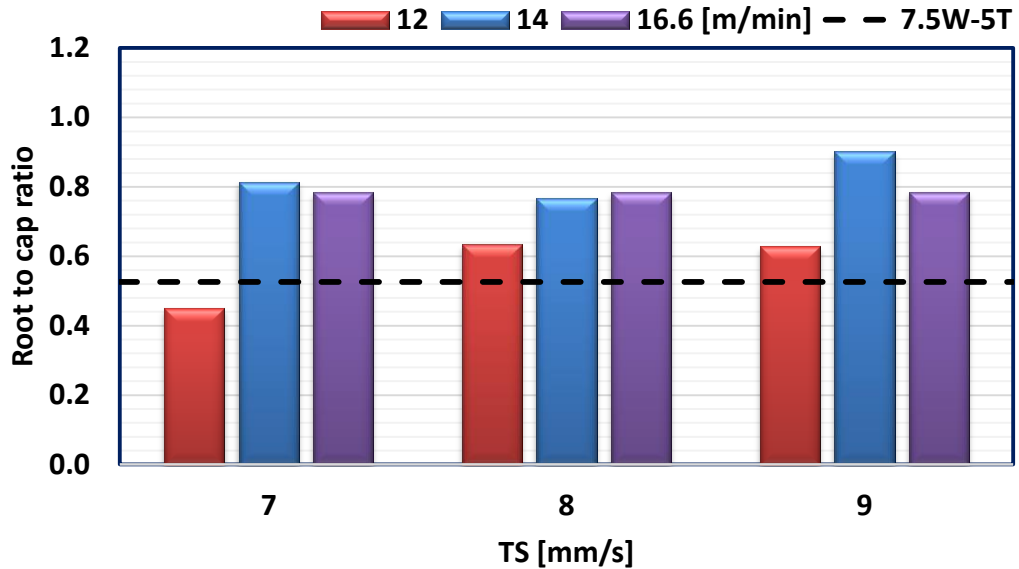


Fig. 6.9 Mean root to cap ratio of all the alternating shielding gas and benchmark welds.

The reduction in the heat affected zone (HAZ) area was evident when moving from Ar₂₀CO₂ + He to Ar₅N₂ + He (see Fig. 6.8) due to lower heat input from the increased travel speed [6.5, 6.17, 6.46] and the presence of N₂ compared to CO₂ [6.35, 6.43]. However, the increase in the wire-feed speed in the 16.6W-7T weld, despite generating a more uniform weld shape compared to the 7.5W-5T weld, did not result in better penetration depth, which was shallower than the 12W-9T and benchmark welds.

Measurements demonstrated that the benchmark presented the highest HAZ area, while decreasing the wire-feed speed and increasing the travel speed provided lower values when alternating Ar₅N₂ + He (see Fig. 6.11). This increase in the travel speed was possible due to the pressure peaks developed

within the alternating shielding gas arc system [6.5, 6.47] and the consequent higher temporary forces coupled with the arc constriction from He, hence diminishing both the heat input and the HAZ areas [6.5, 6.6, 6.17].

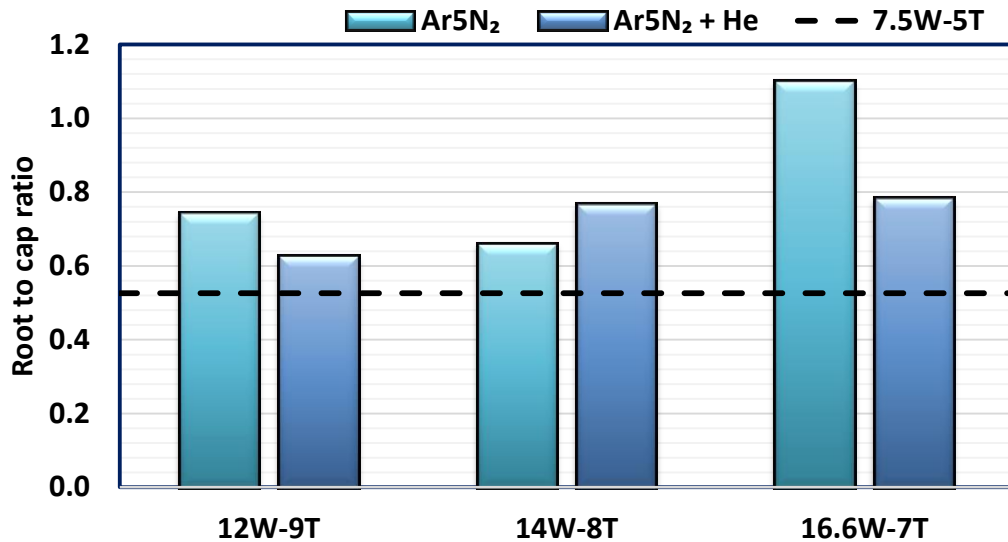


Fig. 6.10 Comparison between the root to cap ratios of the premixed, alternated and benchmark welds.

The premixed supply of Ar5N₂ generated slightly higher HAZ areas than its respective alternating shielding gas cases (see Fig. 6.12). This is explained by the lower heat transferred to the workpiece from alternating Ar5N₂ + He. Additions of N₂ to the Ar shielding gas have been reported by Tseng et al. [6.48] to increase the heat input to the joint. Furthermore, since the alternating shielding gas method reduced the contact time between the Ar5N₂ arc plasma with the molten metal and is assisted by the presence of He, the HAZ area is expected to decrease due to the lower heat transfer [6.3, 6.18, 6.29].

It was qualitative observed that the produced fumes were significantly reduced during the welding procedure when changing the gas supply from

Ar20CO₂ + He to Ar5N₂ and Ar5N₂ + He. This is directly related to the higher travel speeds and the decreased amount of CO₂ present as a shielding gas in the system [6.49, 6.50].

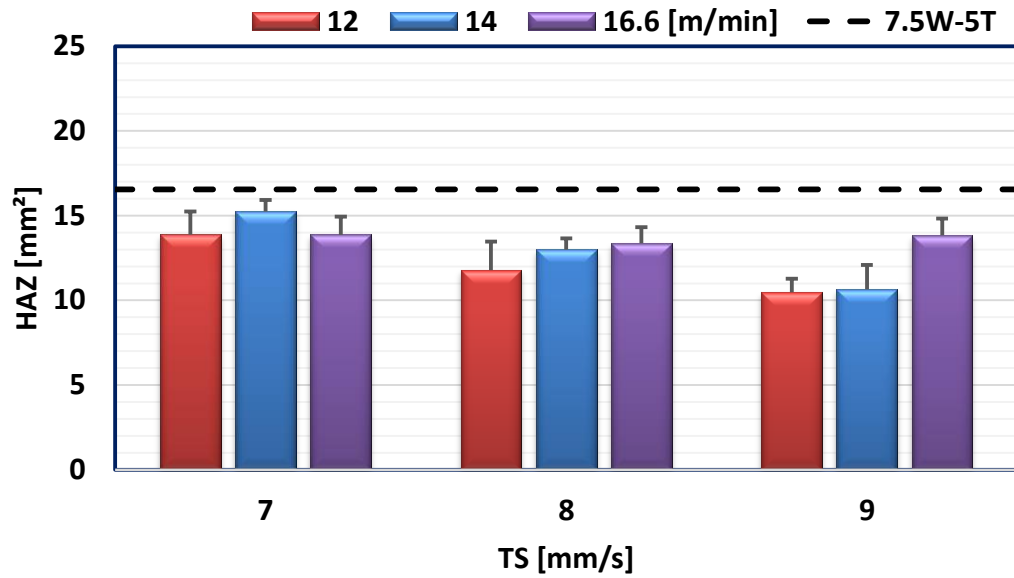


Fig. 6.11 Mean HAZ area of all the alternating shielding gas and benchmark welds.

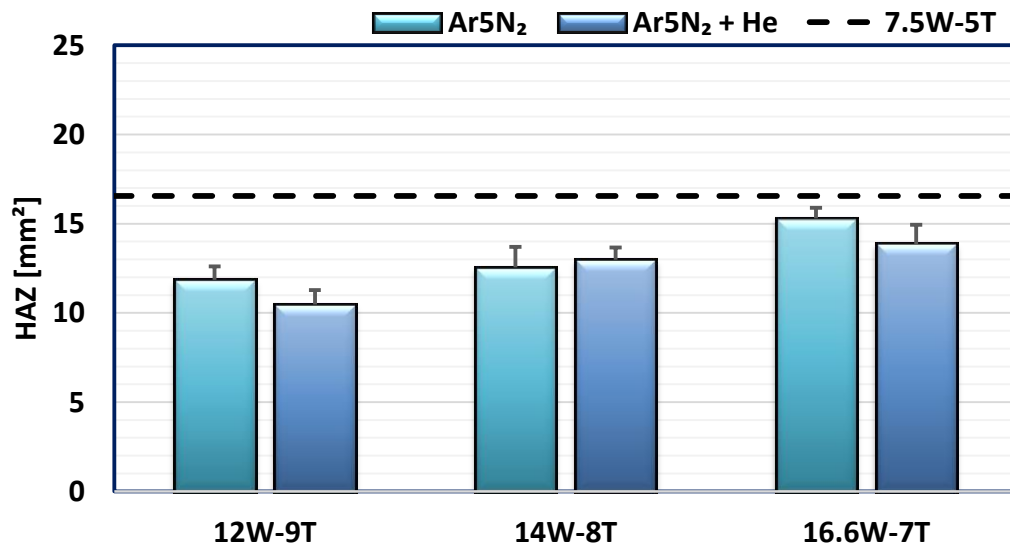


Fig. 6.12 Mean HAZ area of the benchmark, premixed cases and their respective alternated welds.

6.3.4 Microstructural characterisation

Grain refinement was found by using the alternating shielding gas method under Ar5N₂ + He (see Fig. 6.13 (C), (D)) compared to the benchmark (see Fig. 6.13 (A), (B)). Images of the fusion zone exhibited a clear reduction of the allotriomorphic ferrite development and greater, more evenly distributed acicular ferrite formation (see Fig. 6.13 (B)) due to the higher travel speeds.

The measurements of the grain size of all welds (see Fig. 6.15) have shown a similar behaviour to that of the distortion and temperature data, i.e. the higher the heat input the higher the grain size. The 7.5W-5T weld led to an average grain size of 6.2 μm², while 4.6 μm² (12W-9T) and 8 μm² (16.6W-7T) average grain sizes were found to be the lowest and highest calculated values, respectively.

It has been shown that the interstitial N helps to refine the grain microstructure and, up to certain levels, improve the mechanical properties of the joint [6.1, 6.51, 6.52]. In addition, elements like Ti and Al stimulate the formation of nitrides during the GMAW process and, to some extent, have helped promoting the acicular ferrite development during the cooling process of the weld, as mentioned by Wegrzyn [6.20].

The overall decreased heat input of 862 J/mm from higher travel speeds reduced the average grain size within the joint [6.5, 6.17, 6.53, 6.54]. Changing from 7.5W-5T to 12W-9T increased the travel speed by 4 mm/s, which balanced the greater wire-feed speed (12 m/min) and the consequent higher heat input. As shown in section 6.3.2, the measured peak temperature of the 12W-9T weld was found to be lower than that of 7.5W-5T, increasing the

cooling rate of the weld metal and decreasing the driving forces for grain boundary migration and coarsening.

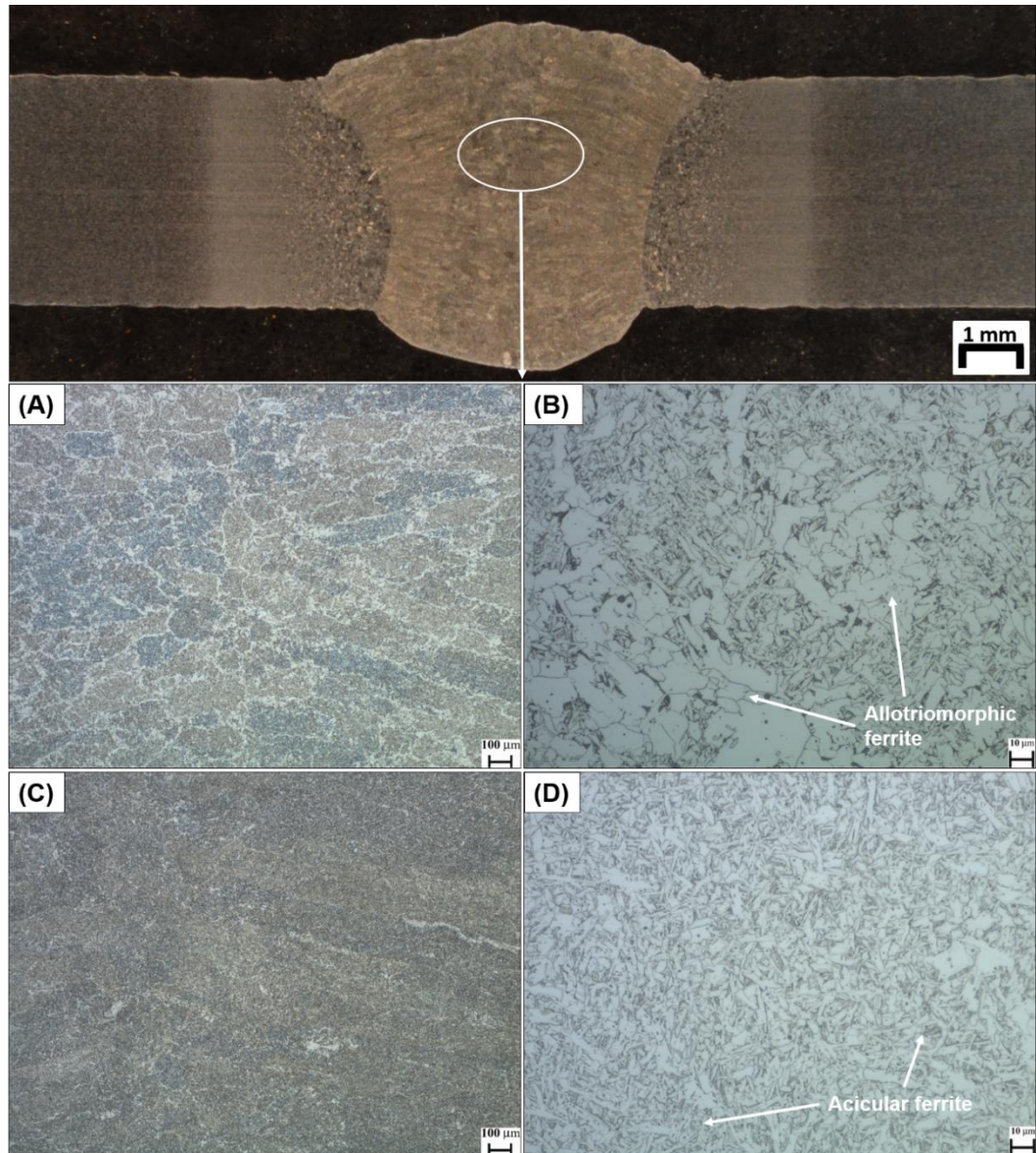


Fig. 6.13 Comparison between the weld microstructures of 7.5W-5T and 12W-9T (etched). (A) 7.5W-5T, x50. (B) 7.5W-5T, x500. (C) 12W-9T, x50. (D) 12W-9T, x500.

Previous studies [6.5, 6.17] have shown the use of the alternating shielding gas method as beneficial to the HAZ, refining its grain size due to the

lower heat input from the reduced contact between the arc plasma with the molten pool, which has been confirmed in chapter 5.

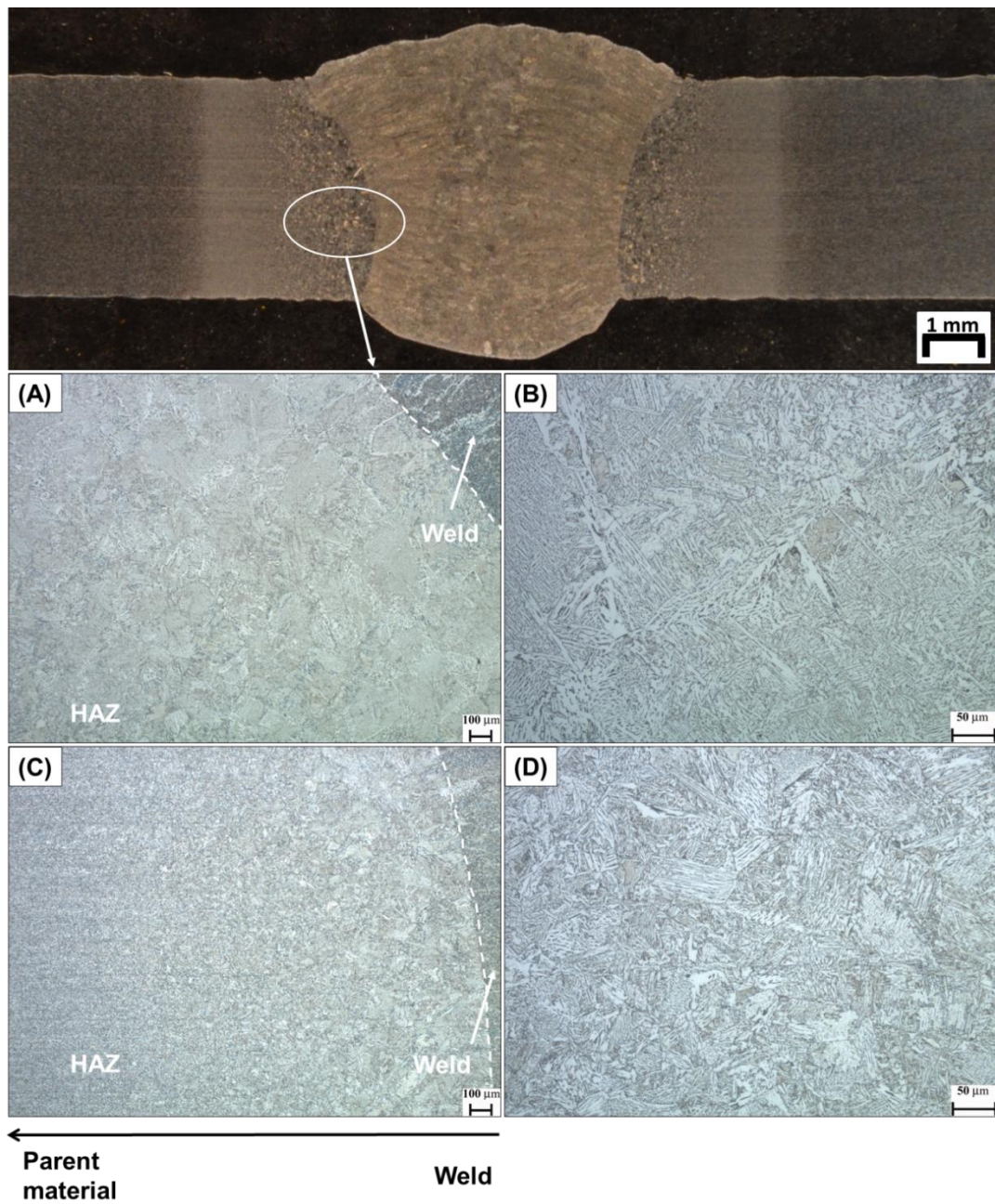


Fig. 6.14 Comparison between HAZ microstructures of 7.5W-5T and 12W-9T (etched). (A) 7.5W-5T, x50. (B) 7.5W-5T, x200. (C) 12W-9T, x50. (D) 12W-9T, x200.

Analysis of the HAZ region (see Fig. 6.14 (A)) presented a faster grain refinement from the weld towards the parent material for the 12W-9T weld in comparison to the 7.5W-5T case and correlates to the lower heat transferred to the former. A greater volume of coarse prior austenite grains was found within the 7.5W-5T HAZ, while the 12W-9T case exhibited a more interlocking and refined grain structure (see Fig. 6.14 (B)). It is appreciated, however, that the presence of coarser grains in the HAZ region compared to its surrounding regions and a sudden microstructural change in the transition from the weld region towards the parent material weaken the joint, as will be discussed in section 6.3.5.

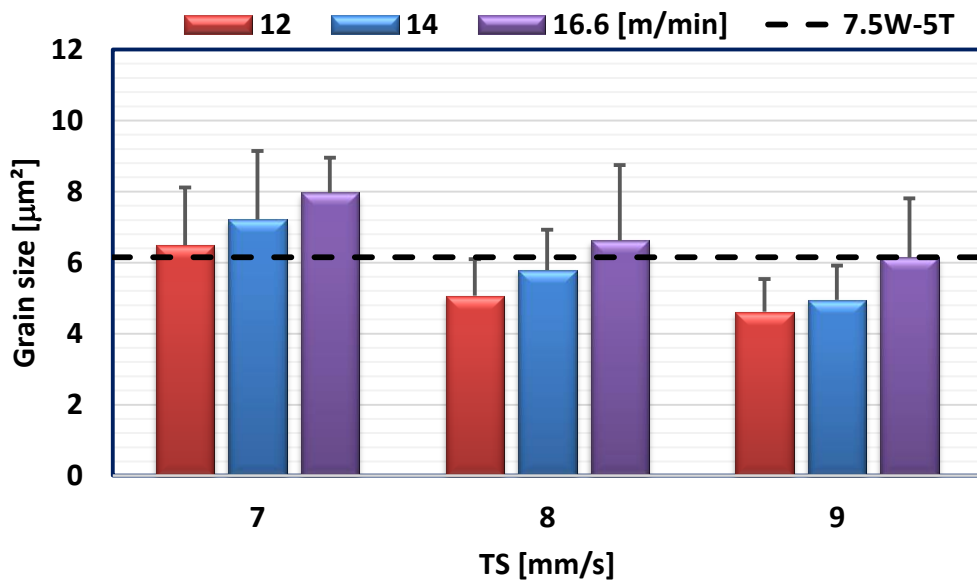


Fig. 6.15 Mean grain size of all the alternating shielding gas and benchmark welds.

The welds under the premixed gas supply of Ar5N₂ presented average grain sizes of 8.3 μm² (16.6W-7TP), 7.4 μm² (14W-8TP) and 5.3 μm² (12W-9TP). By alternating Ar5N₂ + He, the average grain size was reduced

compared to their respective premixed supply cases (see Fig. 6.16). For instance, the average grain size of 14W-8T decreased by 21% (1.6 μm^2). This is in line with findings in chapter 5 and in the literature [6.5, 6.17, 6.38, 6.55], where the use of the alternating shielding gas method allowed for a lower heat transfer to the weld and hindered grain growth.

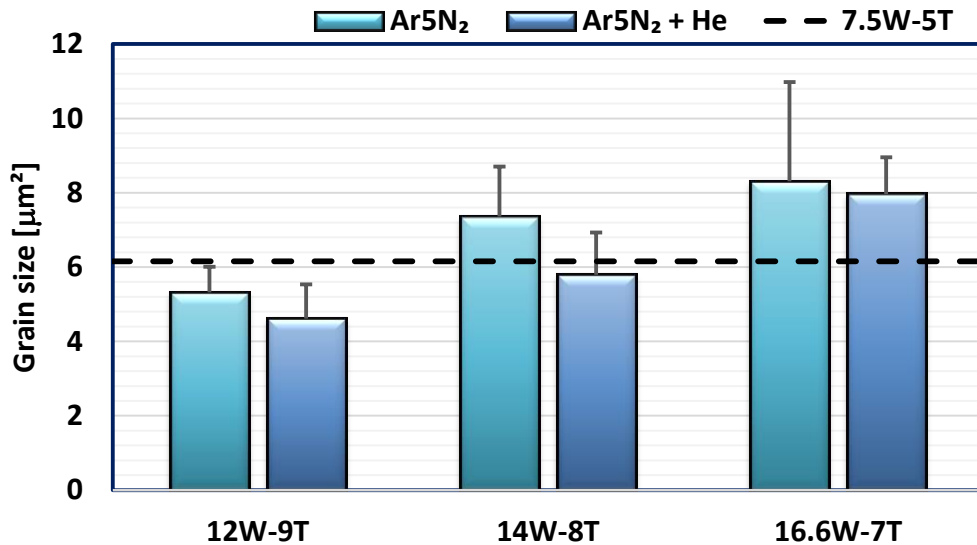


Fig. 6.16 Mean grain sizes of the benchmark, premixed cases and their respective alternated welds.

The alternating shielding gas not only allowed for lower heat input and grain size reductions, but also permitted the use of N₂ in the shielding gas mixture without compromising the microstructure of the weld. This microstructural refinement is important, since it hinders the crack propagation and consequent failure of the joint. As will be demonstrated in the next section, it will promote a stronger joint compared to that of the benchmark (7.5W-5T).

6.3.5 Mechanical property evaluation

6.3.5.1 Hardness distribution

Measurements presented slightly greater hardness by using Ar5N₂ + He compared to the benchmark (see Fig. 6.17) since the heat input (862 J/mm) was reduced and a finer microstructure developed. This improvement in the hardness of the joint was found by either increasing the travel speed or decreasing the wire-feed speed. Additionally, the hardness was increased by the interstitial existence of N within the weld microstructure, which also contributed to the grain refinement [6.1, 6.2, 6.8, 6.9, 6.22, 6.55].

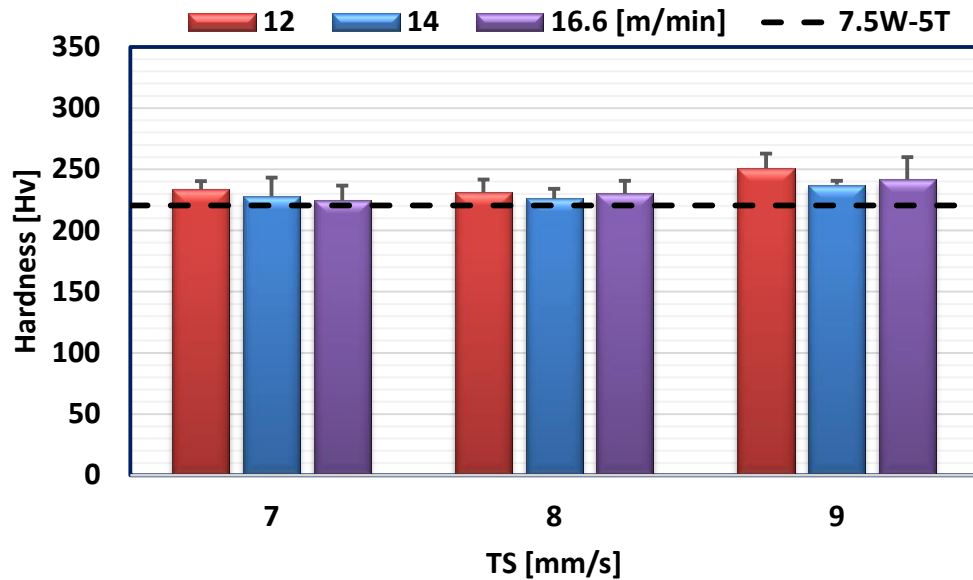


Fig. 6.17 Mean hardness of all the alternating shielding gas and benchmark welds.

Compared to the Ar5N₂ supply, Ar5N₂ + He enhanced the resistance of the weld to indentations (see Fig. 6.18), which is in line with the grain size measurements, i.e. the finer the grain the harder the microstructure [6.17, 6.51, 6.56]. Additionally, such findings are in agreement with previous studies [6.17,

6.57], where the use of the alternating shielding gas technique reduced the heat input to the joint, improving the hardness of both the weld metal and HAZ due to the grain refinement.

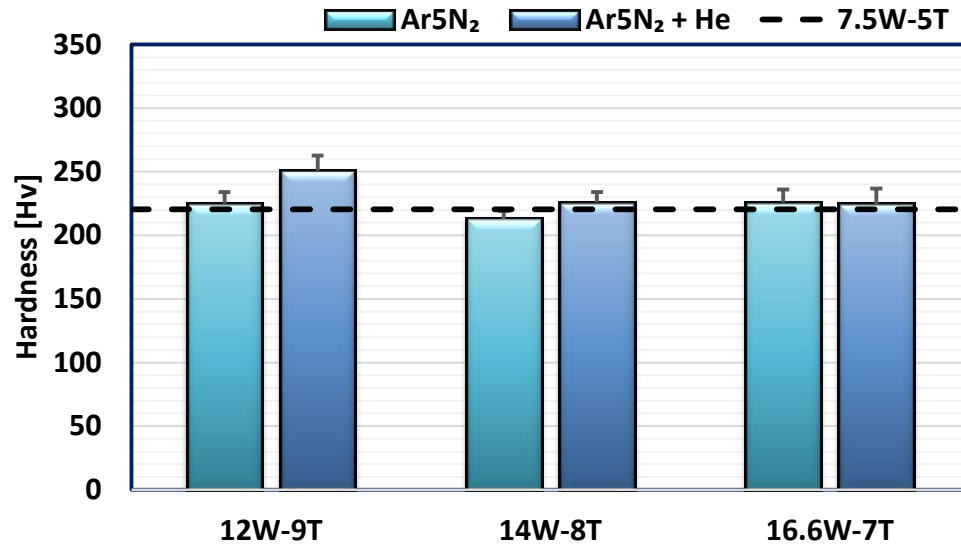


Fig. 6.18 Mean hardness of the benchmark, premixed cases and their respective alternated welds.

6.3.5.2 Tensile testing

As in previous chapters, all the transverse tensile tests failed within the parent material. Regarding the all-weld tensile tests, improvements in the mechanical properties of the welds were found, with enhanced weld strength compared to the benchmark when supplying either alternating (see Fig. 6.19) or premixed (see Fig. 6.20) shielding gases. Such behaviour has been shown previously [6.1, 6.2, 6.8], where the presence of N₂ improved the tensile strength and hardness of the weld.

Increasing the travel speed from 7 to 9 mm/s enhanced the mechanical strength of the joint by diminishing the heat transfer and developing a finer

microstructure. A similar trend was found when the wire-feed speed increased, which was attributed to the greater nitride content within the weld. No variations were found in terms of elongation (see Fig. 6.21-6.22) when comparing the alternating shielding gas welds to the benchmark (7.5W-5T). This is in line with previous studies [6.34, 6.58-6.60], where the increase in the N content within the fusion zone had no impact in the weld ductility.

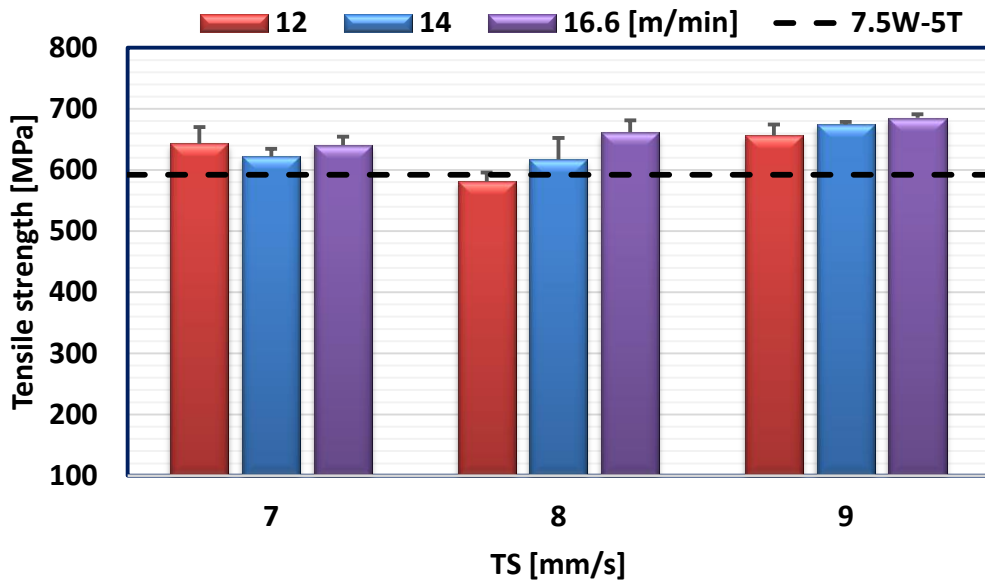


Fig. 6.19 Mean tensile strength of all the alternating shielding gas and benchmark welds.

While the 7.5W-5T, 12W-9TP, 14W-8TP, and 16.6W-7TP cases presented slag-free tensile samples (all-weld cases), some of the welds under the alternating shielding gas supply exhibited voids caused by slag formation and developed during the solidification of the joint (see Fig. 6.23-6.25). The analysis of the slags (see Fig. 6.26 (B)) using a scanning electron microscope equipped with energy dispersive spectroscopy showed that they were composed by oxides, with high content of elements such as O (32.1 wt.%), Ti (21.2

wt.%), Mn (5.9 wt.%), Zr (3.9 wt.%) and Al (3.4 wt.%), with a minor presence of Si, Mg, Zn and Na (see Fig. 6.26 (A)).

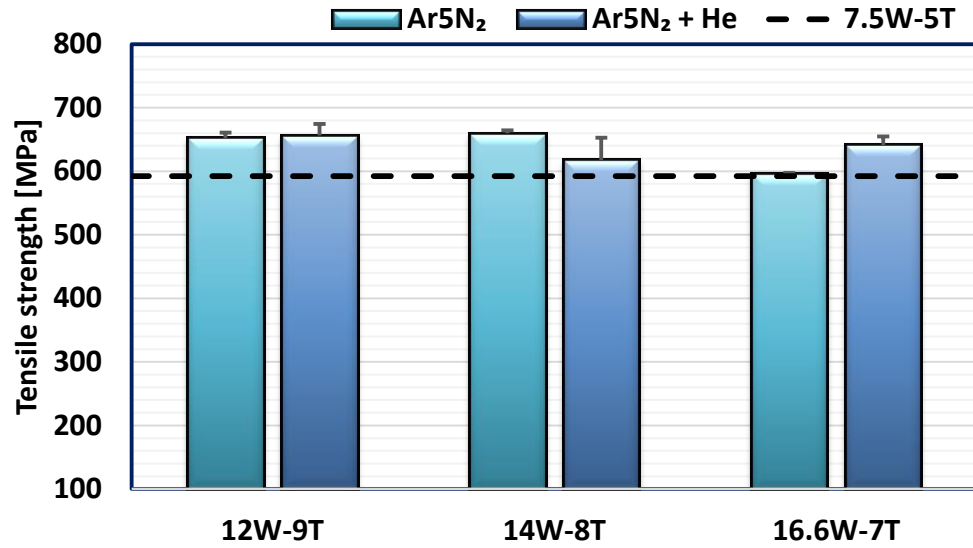


Fig. 6.20 Mean tensile strength of the benchmark, premixed cases and their respective alternated welds.

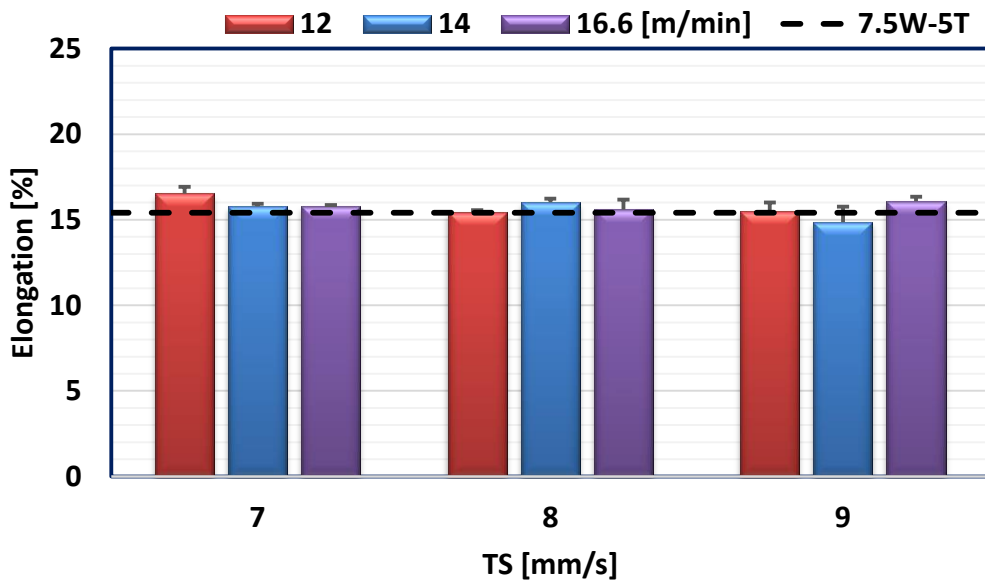


Fig. 6.21 Mean elongation of all the alternating shielding gas and benchmark welds.

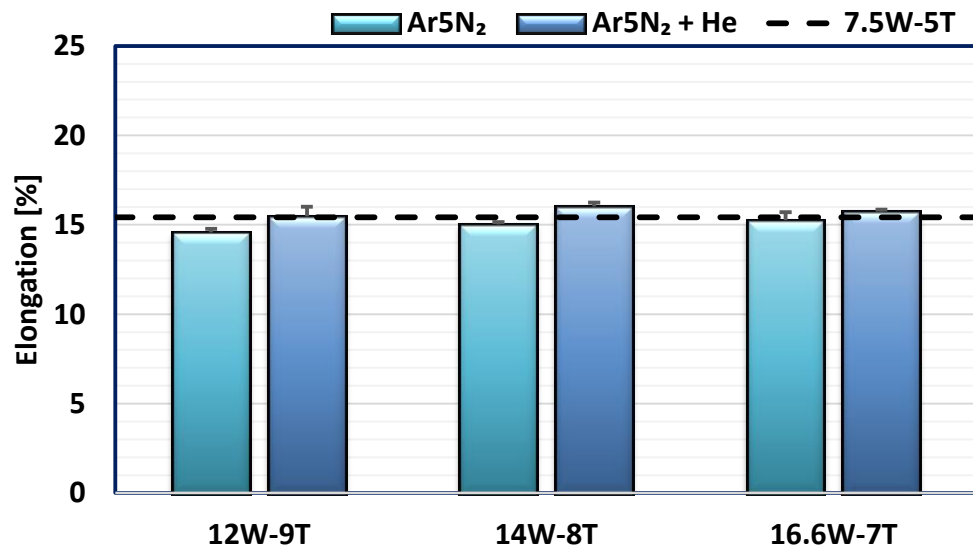


Fig. 6.22 Mean elongation of the benchmark, premixed cases and their respective alternated welds.

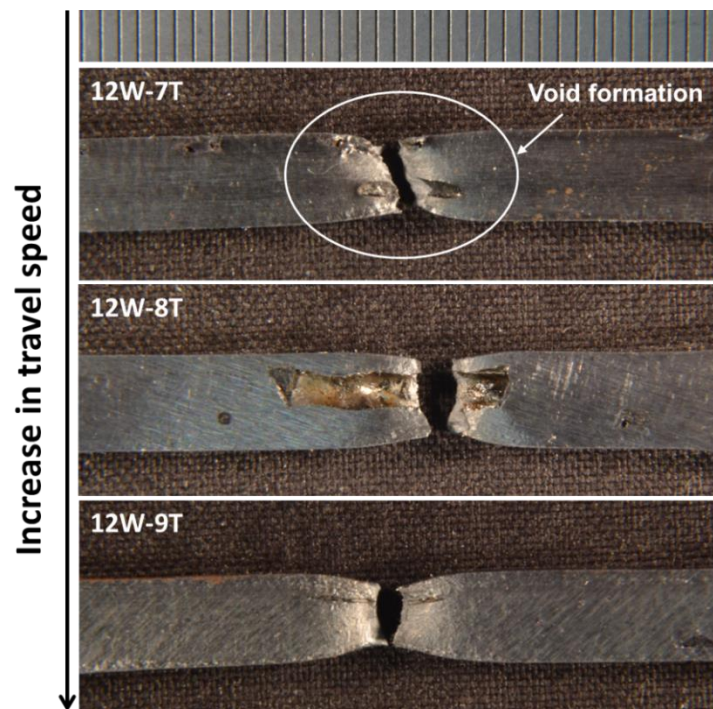


Fig. 6.23 Void formation within all-weld tensile samples of 12 m/min wire-feed speed welds.

Elements like Ti and Al, as strong denitrifiers, bond N, forming nitrides such as TiN and AlN after the weld solidification [6.2, 6.25]. Above certain amounts, such compounds cause porosity, weakening the weld metal [6.61]. The presence of O (a surface-active element [6.60, 6.62]) in the gas atmosphere increases the N content within the weld, promoting the formation of nitric oxides [6.2, 6.19, 6.60] and, above a certain threshold, blowholes. Therefore, a great amount of O during the welding process can be detrimental to the joint, since it impacts directly the N absorption by the molten pool.

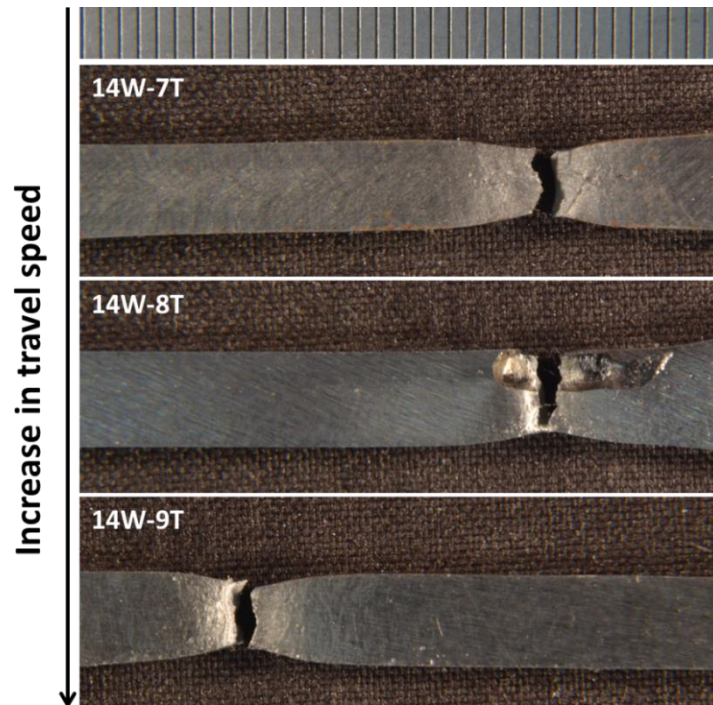


Fig. 6.24 Void formation within all-weld tensile samples of 14 m/min wire-feed speed welds.

Previous studies [6.63-6.65] demonstrated that not only N, but O is also responsible for porosity development due to the formation of oxides from the flux-cored wire elements. Studies [6.18, 6.27, 6.28] using GTAW have shown that increasing the wire-feed speed allows more time for N desorption due to

the greater arc current and heat input, lowering the cooling rate of the joint. Conversely, the increase in the arc current enhances the O in the molten pool, where the electrode tip and metal droplet are the major sites for oxygen absorption [6.64, 6.66]. This is due to a more prevalent flux decomposition with the increase in the arc temperature, stimulating higher development of oxides.

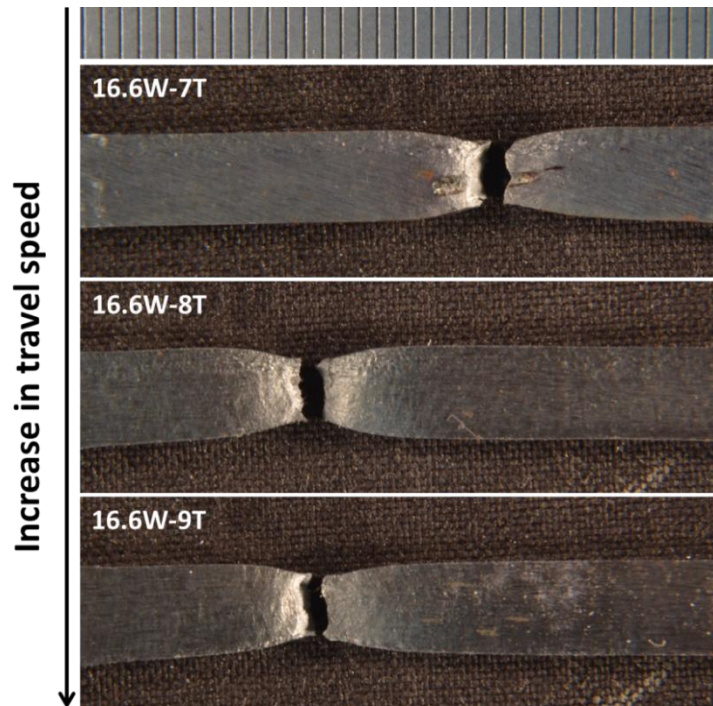


Fig. 6.25 Void formation within all-weld tensile samples of 16.6 m/min wire-feed speed welds.

While increasing the wire-feed speed promotes the flux decomposition, it also allows for greater heat input. This increased heat transfer to the weld reduces its cooling rate and allows more time for the slag to raise to the surface. Increasing the travel speed is also beneficial, since it reduces the amount of material being deposited and, consequently, the chances of slag entrapment. This behaviour is evident in Fig. 6.23-6.25, where the greater wire-feed speeds coupled with higher travel speeds produced slag free welds.

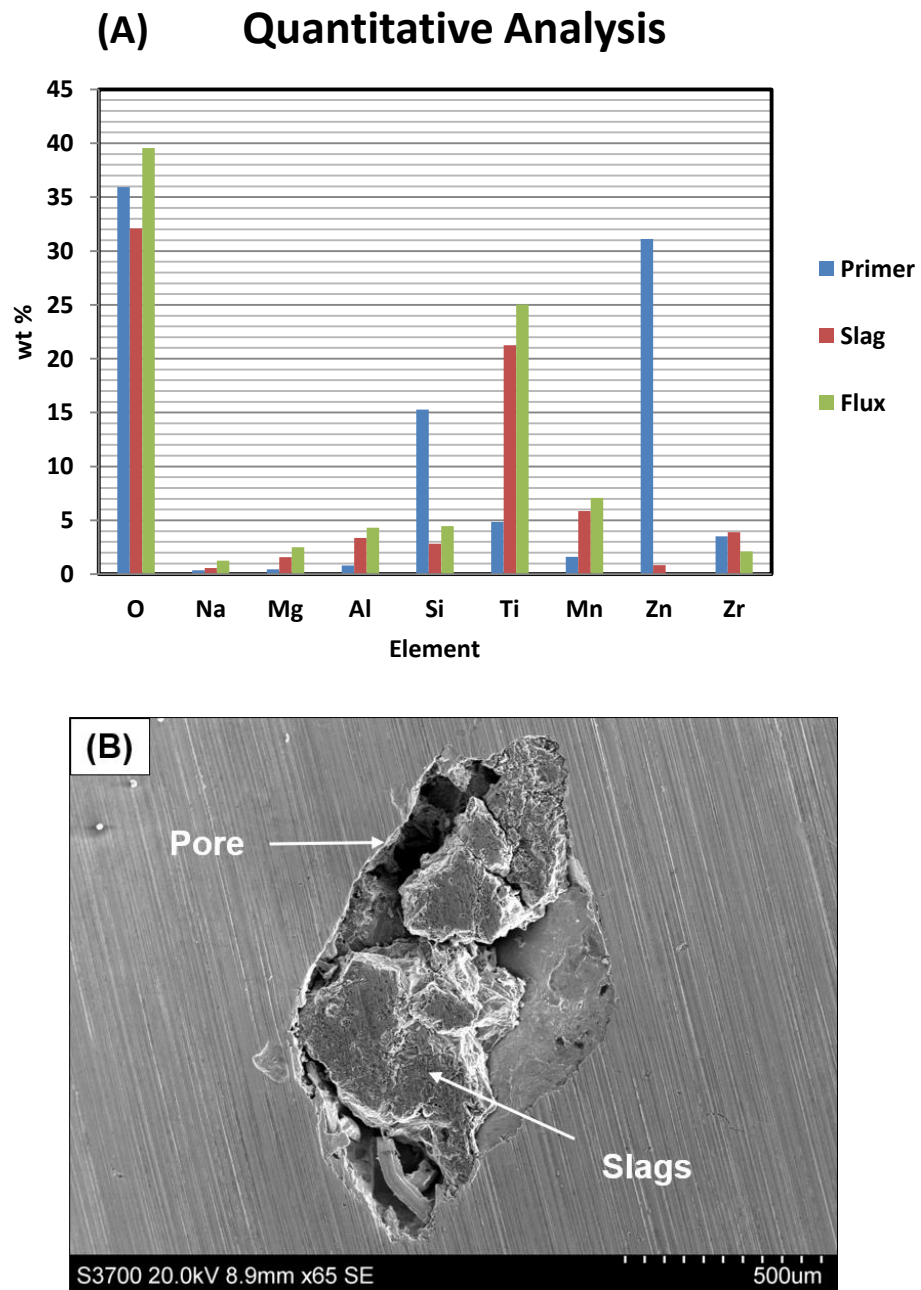


Fig. 6.26 Quantitative and qualitative analysis of elements. (A) Mean values of elements via energy disperse spectroscopy analysis. (B) Porosity and slugs (etched - scanning electron microscope).

The addition of He to the gas supply suppresses the N₂ dissociation and decreases its proportion within the joint [6.3, 6.18] due to the greater metal

vapour presence. However, it increases the arc energy as well as the arc temperature near the electrode tip [6.29, 6.35], stimulating a higher content of O within the molten pool and increasing the formation of oxides [6.64, 6.66]. This explains the lack of oxides within the all-weld tensile samples when the premixed method of Ar5N₂ was used during the welding process compared to the alternating shielding gas technique (Ar5N₂ + He).

The quantitative analysis in Fig. 6.26 (A) demonstrates that both the primer and the weld flux contributed significantly to the amount of O and Ti in the slag (see Fig. 6.26 (B)). Thus, either grinding off the primer near the root gap before welding or changing the electrode type would assist with eliminating the development of oxides within the joints.

6.3.5.3 Bend testing

As in the all-weld tensile specimens, the presence of slags within some of the joints was evident from the investigation of the bend test samples (see Fig. 6.27), with most of the rejected specimens being root-type.

Similarly to the all-weld tensile samples (see section 6.3.5.2), the welds under the premixed method as well as the 14W-9T, 16.6W-8T and 16.6W-9T (Fig. 6.28), under the alternating shielding gas method, passed the bend test without evident presence of oxides. The increase in the travel speed reduced O absorption, hindering the formation of voids within the joints.

To better clarify the cause of failure throughout the joint, specimens 12W-9T and 14W-7T were cross-sectioned (see Fig. 6.29 (A)). The 12W-9T images show that cracks initiated in the voids, caused by the oxides and propagated between the weld and the HAZ up to a certain limit (see Fig. 6.29

(B)). As discussed in section 6.3.4, the narrow HAZ region was weakened by its coarser grains [6.67-6.72], which were surrounded by a finer microstructure. Likewise, the 14W-7T sample exhibited a rupture caused by slag entrapment between the weld and the HAZ region (see Fig. 6.29 (C)), demonstrating why slags are undesirable within the joint in terms of mechanical properties.

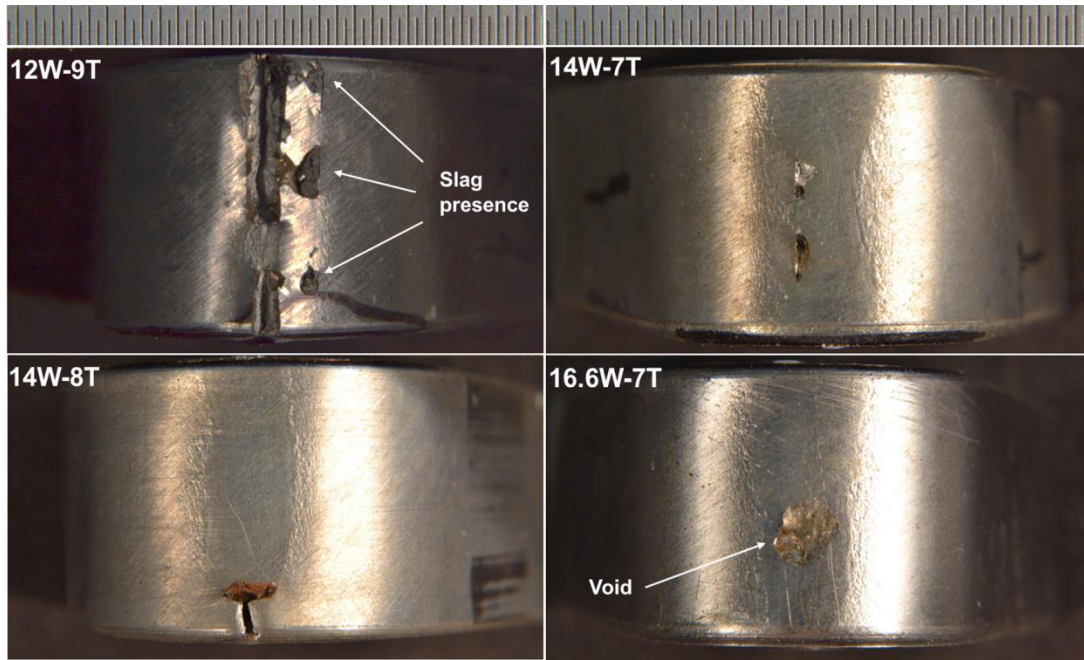


Fig. 6.27 Failed bend test samples (root).

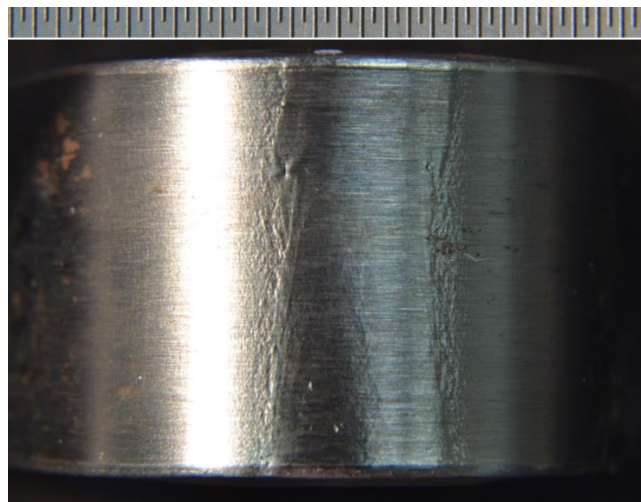


Fig. 6.28 Pass weld bend test sample: 16.6W-9T (root).

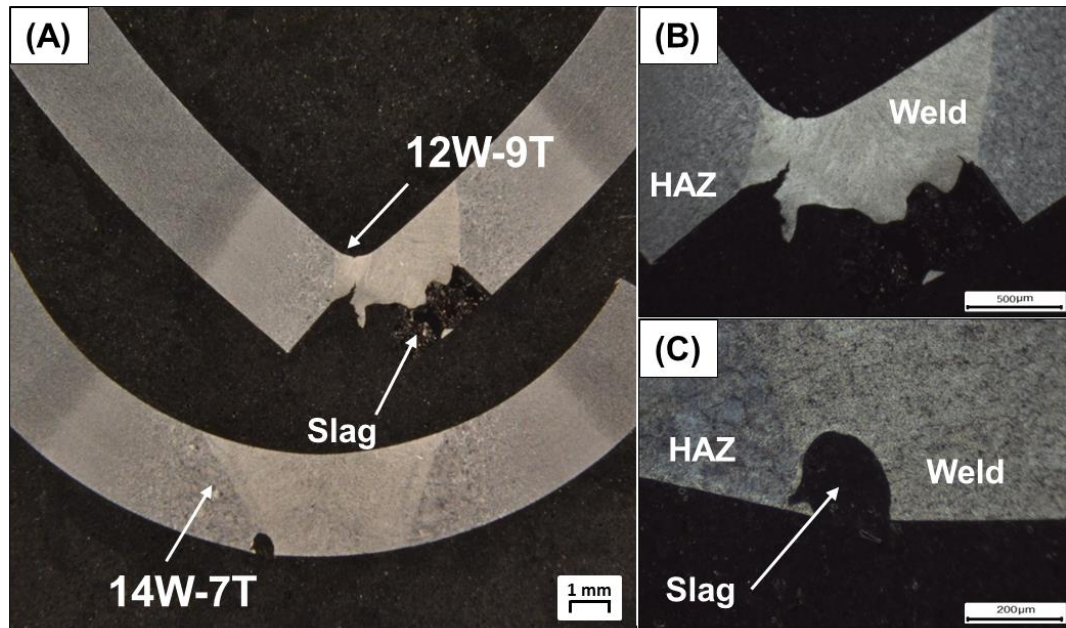


Fig. 6.29 Inspection of the weld after the bend test. (A) 12W-9T and 14W-7T specimens (etched). (B) 12W-9T (etched). (C) 14W-7T (etched).

The inspection of the 12W-9T specimen using the scanning electron microscope (see Fig. 6.30) demonstrated the clear influence of the oxides and cavities in the propagation of the crack (see Fig. 6.30 (A), (B)). Within the joint, areas of typical dimple fracture (see Fig. 6.30 (C)) and lack of appreciable ductility with some apparent cleavage (see Fig. 6.30 (D)) were found.

The brittleness development was caused by a high travel speed and reduced wire-feed speed together with the added N₂ as a shielding gas. Hence, despite reducing the N desorption within the molten pool, a too high travel speed coupled with a low wire feed speed can be detrimental to the joint integrity and must be set accordingly.

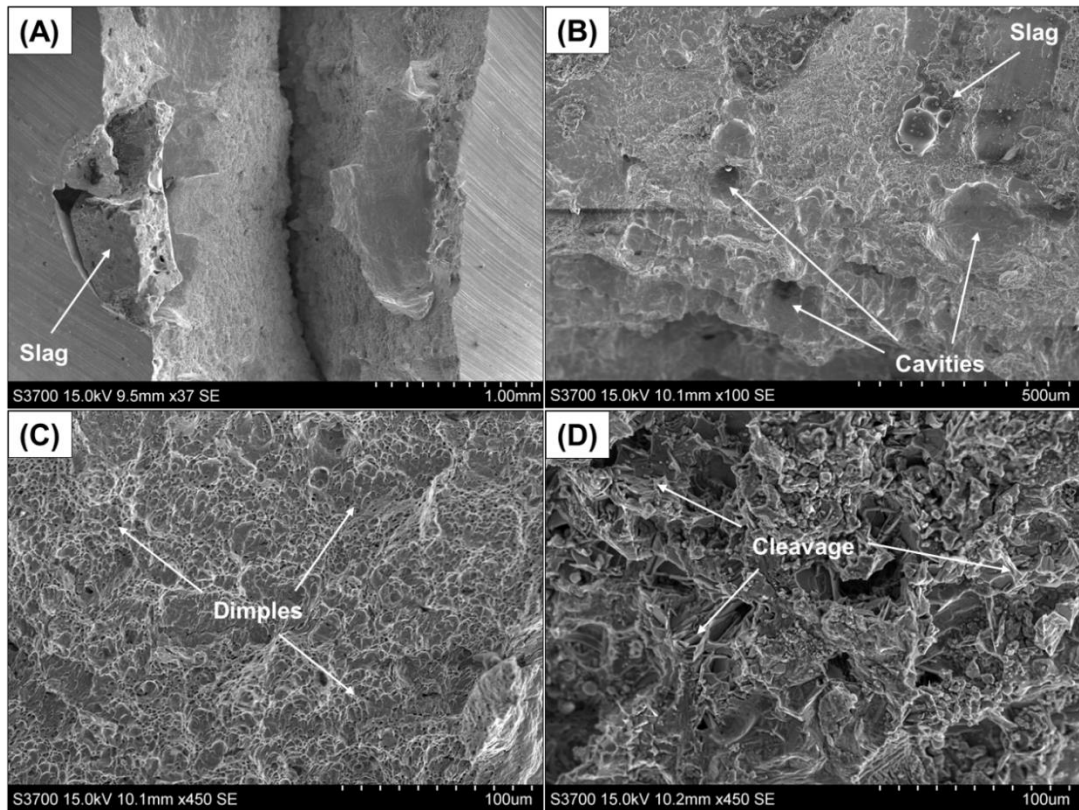


Fig. 6.30 Scanning electron microscope analysis of the 12W-9T weld. (A) Slag influence on the crack propagation. (B) Cavities and slag presence within the joint. (C) Ductile-like rupture area. (D) Quasi-cleavage rupture area.

6.4 Conclusions

An extended investigation in the use of the alternating shielding gas method and N₂ as a shielding gas in the GMAW process was carried out. Based on results discussed throughout this study, additions of N₂ as a shielding gas could be used as an alternative during GMAW.

Replacing Ar20CO₂ + He for either Ar5N₂ + He or Ar5N₂ enhanced weld properties and promoted a qualitative decrease in the fume development during the welding process. Overall, reductions of 22% (140 °C) in the weld temperature (see Fig. 6.6) and 20% (1.6 mm) in the workpiece distortion (see

Fig. 6.5) were evident compared to the benchmark, which could assist with reduced straightening requirements after welding. However, there was no evident difference between the distortion and temperature measurements of the Ar5N₂ + He and Ar5N₂ cases.

The overall strength of the alternated welds increased by 8% (50 MPa) while premixed cases presented joints 7% (44 MPa) stronger from the addition of N₂ and greater travel speeds, despite the development of slags in some of the joints. Negligible difference was found between the mechanical properties of the Ar5N₂ + He and Ar5N₂ welds. In particular, the premixed supply of Ar5N₂ promoted porosity-free welds with strength similar to their respective alternated cases. Furthermore, the additional assessment of the slags demonstrated that either changing the electrode type or removing the primer near the root gaps before the welding procedure could hinder the slag development by the reducing O within the system.

Increased wire-feed speeds and travel speeds of Ar5N₂ + He promoted similar ductility to that of the benchmark (7.5W-5T) joint as well as slag-free welds, despite fracture in some of the joints during the bend tests. Additionally, the Ar5N₂ + He promoted increased resistance of the joint to plastic deformation in contrast to the 7.5W-5T weld and negligible differences between Ar5N₂ + He and Ar5N₂ were found, with only 12W-9T having higher hardness than its respective premixed case.

The achievable increase in the travel speed to 9 mm/s by employing the alternating shielding gas method reduced/ eliminated the porosity formation, refined the grain profile of the weld and limited the HAZ extent. Consequently, welding processes approximately twice as fast can be achieved, enhancing productivity and lowering costs, for instance, by reducing changeover of gas

cylinders and increasing the number of workpieces welded. Such comprehensive improvements were also possible by the premixed Ar5N₂ gas supply, with minor differences compared to its respective alternating shielding gas cases.

Hence, this study extended the protective gas options by demonstrating the potential of N₂ mixtures to weld DH36 steel plates, further improving features such as distortion, heat input and microstructural and mechanical properties. The findings in this chapter are explored in chapter 7, with optimisation methods developed to refine the input parameters that would yield high integrity welds under N₂ mixtures.

6.5 Bibliography

- [6.1] P. Kah and J. Martikainen, “Influence of shielding gases in the welding of metals,” *Int. J. Adv. Manuf. Technol.*, vol. 64, no. 9–12, pp. 1411–1421, 2013.
- [6.2] T. Wegrzyn, “An attempt at the classification of steel weld metals and arc-welding methods on the basis of nitrogen concentration in the weld metal,” *Weld. Int.*, vol. 13, no. 3, pp. 173–179, 1999.
- [6.3] S. Kodama, K. Sugiura, S. Nakanishi, Y. Tsujimur, M. Tanaka, and A. B. Murphy, “Effect of plasma heat source characteristics on nitrogen absorption in gas tungsten arc weld metal,” *Weld. World*, vol. 57, no. 6, pp. 925–932, 2013.
- [6.4] American Welding Society, “Choosing Shielding Gases for Gas Metal Arc Welding,” in *Welding Handbook*, vol. 2, no. May, 2008, pp. 32–35.
- [6.5] S. W. Campbell, A. M. Galloway, N. A. McPherson, and A. Gillies, “Evaluation of gas metal arc welding with alternating shielding gases for

- use on AA6082T6,” *Proc. Inst. Mech. Eng. Part B J. Eng. Manuf.*, vol. 226, no. 6, pp. 992–1000, 2012.
- [6.6] P. G. Jönsson, T. W. Eagar, and J. Szekely, “Heat and Metal Arc Metal Transfer Welding Using in Gas Argon and Helium,” *Metall. Mater. Trans. B*, vol. 26, no. 2, pp. 383–395, 1995.
- [6.7] J. J. Lowke, M. Tanaka, and M. Ushio, “Mechanisms giving increased weld depth due to a flux,” *J. Phys. D. Appl. Phys.*, vol. 38, no. 18, pp. 3438–3445, 2005.
- [6.8] D. D. Nage, V. S. Raja, and R. Raman, “Effect of nitrogen addition on the microstructure and mechanical behavior of 317L and 904L austenitic stainless steel welds,” *J. Mater. Sci.*, vol. 41, no. 7, pp. 2097–2112, 2006.
- [6.9] H. Y. Huang, “Effects of shielding gas composition and activating flux on GTAW weldments,” *Mater. Des.*, vol. 30, no. 7, pp. 2404–2409, 2009.
- [6.10] M. Tanaka, S. Tashiro, T. Satoh, A. B. Murphy, and J. J. Lowke, “Influence of shielding gas composition on arc properties in TIG welding,” *Sci. Technol. Weld. Join.*, vol. 13, no. 3, pp. 225–231, 2008.
- [6.11] S. Lu, H. Fujii, and K. Nogi, “Arc ignitability, bead protection and weld shape variations for He-Ar-O₂ shielded GTA welding on SUS304 stainless steel,” *J. Mater. Process. Technol.*, vol. 209, no. 3, pp. 1231–1239, 2009.
- [6.12] I. Bitharas, N. A. McPherson, W. McGhie, D. Roy, and A. J. Moore, “Visualisation and optimisation of shielding gas coverage during gas metal arc welding,” *J. Mater. Process. Technol.*, vol. 255, no. December, pp. 451–462, 2018.
- [6.13] G. M. Ramsey, A. M. Galloway, S. W. Campbell, N. A. McPherson, and T. J. Scanlon, “A computational fluid dynamic analysis of the effect

- of side draughts and nozzle diameter on shielding gas coverage during gas metal arc welding,” *J. Mater. Process. Technol.*, vol. 212, no. 8, pp. 1694–1699, 2012.
- [6.14] S. W. Campbell, A. M. Galloway, and N. A. McPherson, “Artificial Neural Network Prediction of Weld Geometry Performed Using GMAW with Alternating Shielding Gases,” *Weld. J.*, vol. 91, no. 6, pp. 174–181, 2012.
- [6.15] S. W. Campbell, A. M. Galloway, G. M. Ramsey, and N. A. McPherson, “A potential solution to GMAW gas flow optimisation,” in *ASM Proceedings of the International Conference: Trends in Welding Research*, 2012.
- [6.16] V. Beyer, S. W. Campbell, G. M. Ramsey, A. M. Galloway, A. J. Moore, and N. A. McPherson, “Systematic study of effect of cross-drafts and nozzle diameter on shield gas coverage in MIG welding,” *Sci. Technol. Weld. Join.*, vol. 18, no. 8, pp. 652–660, 2013.
- [6.17] S. W. Campbell, A. M. Galloway, and N. A. McPherson, “Techno-economic evaluation on the effects of alternating shielding gases for advanced joining processes,” *Proc. Inst. Mech. Eng. Part B J. Eng. Manuf.*, vol. 225, no. 10, pp. 1863–1872, 2011.
- [6.18] S. Kodama et al., “Nitrogen absorption phenomenon of GTA welding with nitrogen-mixed shielding gases: effect of plasma characteristics on nitrogen content in GTA welded metal,” *Weld. Int.*, vol. 29, no. 4, pp. 262–269, 2015.
- [6.19] H. Kokawa, “Nitrogen absorption and desorption by steels during arc and laser welding,” *Weld. Int.*, vol. 18, no. Issue 4, pp. 277–287, 2004.
- [6.20] T. Wegrzyn, “The Classification of Metal Weld Deposits in Terms of

- the Amount of Nitrogen,” in Proceedings of the Tenth (2000) International Offshore and Polar Engineering Conference, 2000, vol. IV, pp. 130–134.
- [6.21] D. L. Olson, R. D. Dixon, and A. L. Liby, *Welding: Theory and Practice*. 1990.
- [6.22] H. Sekiguchi, I. Masumoto, H. Konishi, and I. Suzuki, “Use of Nitrogen in Welding Atmosphere (Report 1),” *J. Japan Weld. Soc.*, vol. 34, no. 2, pp. 128–136, 1965.
- [6.23] T. Kobayashi, T. Kuwana, and R. Kiguchi, “Effect of Alloying Elements on Nitrogen Content of Steel Weld Metals (Report 2),” *J. Japan Weld. Soc.*, vol. 41, no. 4, pp. 415–424, 1972.
- [6.24] T. Kobayashi, T. Kuwana, and R. Kiguchi, “Effect of Alloying Elements on Nitrogen Content of Steel Weld Metals (Report 1),” *J. Japan Weld. Soc.*, vol. 41, no. 3, pp. 308–321, 1972.
- [6.25] J. Littleton, J. Lammas, and M. F. Jordan, “Nitrogen Porosity in Gas Shielded Arc Welding of Copper,” *Weld. J.*, vol. 12, pp. 561–565, 1974.
- [6.26] R. Sasidharan, S. Rajendra Boopathy, and S. R. Koteswara Rao, “Effects of nitrogen added argon gas flow rate on the mechanical and corrosion properties of duplex stainless steel gas tungsten arc welds,” *J. Corros. Sci. Eng.*, vol. 17, pp. 1–17, 2014.
- [6.27] W. Chuaiphan and L. Srijaroenpramong, “The Behaviour of Nitrogen on the Welding Parameters of the Dissimilar Weld Joints between AISI 304 and AISI 316L Austenitic Stainless Steels Produced by Gas Tungsten Arc Welding,” *Appl. Mech. Mater.*, vol. 248, pp. 395–401, 2013.
- [6.28] L. Zhao, Z. L. Tian, and Y. Peng, “Control of nitrogen content and porosity in gas tungsten arc welding of high nitrogen steel,” *Sci. Technol.*

- Weld. Join., vol. 14, no. 1, pp. 87–93, 2008.
- [6.29] K. Yamamoto et al., “Metal vapour behaviour in thermal plasma of gas tungsten arcs during welding,” *Sci. Technol. Weld. Join.*, vol. 13, no. 6, pp. 566–572, 2008.
- [6.30] S. Tashiro et al., “Plasma properties of helium gas tungsten arc with metal vapour,” *Sci. Technol. Weld. Join.*, vol. 12, no. 3, pp. 202–207, 2007.
- [6.31] Anthony B Murphy, “The effects of metal vapour in arc welding,” *J. Phys. D. Appl. Phys.*, vol. 43, no. 16, p. 165204, 2010.
- [6.32] M. Schnick et al., “Numerical Investigations of the Influence of Metal Vapour in GMA Welding,” *Weld. World*, vol. 55, no. 11–12, pp. 114–120, 2011.
- [6.33] L. L. Wang, H. P. Wang, F. G. Lu, A. B. Murphy, and B. E. Carlson, “Numerical analysis of Al vapour effects in gas metal arc welding of Al alloys,” *Sci. Technol. Weld. Join.*, vol. 19, no. 5, pp. 361–368, 2014.
- [6.34] A. M. Galloway, N. A. McPherson, and T. N. Baker, “An evaluation of weld metal nitrogen retention and properties in 316LN austenitic stainless steel,” *Proc. Inst. Mech. Eng.*, vol. 225, no. 2, pp. 61–69, 2011.
- [6.35] A. B. Murphy, M. Tanaka, S. Tashiro, T. Sato, and J. J. Lowke, “A computational investigation of the effectiveness of different shielding gas mixtures for arc welding,” *J. Phys. D. Appl. Phys.*, vol. 42, p. 115205, 2009.
- [6.36] A. Haelsing, M. Kusch, and P. Mayr, “Calorimetric analyses of the comprehensive heat flow for gas metal arc welding,” *Weld. World*, vol. 59, no. 2, pp. 191–199, 2014.
- [6.37] Z. H. Rao, J. Zhou, and H. L. Tsai, “Determination of equilibrium wire-

- feed-speeds for stable gas metal arc welding,” *Int. J. Heat Mass Transf.*, vol. 55, no. 23–24, pp. 6651–6664, 2012.
- [6.38] Y. H. Chang, “Improve GMAW and GTAW with alternating shield gases,” *Weld. J.*, vol. 85, no. 2, pp. 41–43, 2006.
- [6.39] T. Gray, D. Camilleri, and N. McPherson, “Understanding welding distortion: thermal fields thermo-mechanical effects,” in *Control of Welding Distortion in Thin-Plate Fabrication*, Woodhead Publishing Limited, 2014, pp. 53–76.
- [6.40] F. H. Ley, S. W. Campbell, A. M. Galloway, and N. A. McPherson, “Effect of shielding gas parameters on weld metal thermal properties in gas metal arc welding,” *Int. J. Adv. Manuf. Technol.*, vol. 80, no. 5–8, pp. 1213–1221, 2015.
- [6.41] E. Armentani, R. Esposito, and R. Sepe, “The effect of thermal properties and weld efficiency on residual stresses in welding,” *Manuf. Eng.*, vol. 20, no. 1–2, pp. 319–322, 2007.
- [6.42] P. Michaleris, L. Zhang, S. R. Bhide, and P. Marugabandhu, “Evaluation of 2D, 3D and applied plastic strain methods for predicting buckling welding distortion and residual stress,” *Sci. Technol. Weld. Join.*, vol. 11, no. 6, pp. 707–716, 2006.
- [6.43] L. L. Wang, F. G. Lu, H. P. Wang, A. B. Murphy, and X. H. Tang, “Effects of shielding gas composition on arc profile and molten pool dynamics in gas metal arc welding of steels,” *J. Phys. D. Appl. Phys.*, vol. 47, no. 46, p. 465202 (14pp), 2014.
- [6.44] S. Lu, W. Dong, D. Li, and Y. Li, “Numerical study and comparisons of gas tungsten arc properties between argon and nitrogen,” *Comput. Mater. Sci.*, vol. 45, no. 2, pp. 327–335, 2009.

- [6.45] B. Zorc, “Automatic TIG welding of austenitic stainless steels in nitrogen and nitrogen-based gas mixtures,” *Rev. Metal.*, vol. 47, no. 1, pp. 29–37, 2011.
- [6.46] R. Weber, “Determination of the Effect of Current and Travel Speed of Gas Metal-Arc Welding on the Mechanical Properties of A36, A516, and A514 Steels,” 1980.
- [6.47] I. Bitharas, S. W. Campbell, A. M. Galloway, N. A. Mcpherson, and A. J. Moore, “Visualisation of alternating shielding gas flow in GTAW,” *Mater. Des.*, vol. 91, pp. 424–431, 2016.
- [6.48] K. H. Tseng and C. P. Chou, “Effect of nitrogen addition to shielding gas on residual stress of stainless steel weldments,” *Sci. Technol. Weld. Join.*, vol. 7, no. 1, pp. 57–62, 2002.
- [6.49] N. T. Jenkins, P. F. Mendez, and T. W. Eagar, “Effect of Arc Welding Electrode Temperature on Vapor and Fume Composition,” *Trends Weld. Res. Proc. 7th Int. Conf.*, no. 2, 2005.
- [6.50] K. R. Carpenter, B. J. Monaghan, and J. Norrish, “Influence of shielding gas on fume formation rate for gas metal arc welding (GMAW) of plain carbon steel,” *ASM Proc. Int. Conf. Trends Weld. Res.*, vol. 49, no. 3, pp. 436–442, 2009.
- [6.51] Y. Zheng et al., “An experimental study of nitrogen gas influence on the 443 ferritic stainless steel joints by double-shielded welding,” *Int. J. Adv. Manuf. Technol.*, vol. 87, no. 9–12, pp. 3315–3323, 2016.
- [6.52] J. R. Davis, “Structure / Property Relationships in Irons and Steels,” *Met. Handb. Desk, Second Ed.*, pp. 153–173, 1998.
- [6.53] N. S. Barabokhin et al., “Technological special features of welding 1460 high-strength aluminium alloy,” *Weld. Int.*, vol. 14, no. 6, pp. 468–470,

2000.

- [6.54] R. G. Tazetdinov, O. M. Novikov, A. S. Persidskii, B. A. Khasyanov, E. N. Ivanov, and L. T. Plaksina, “Arc welding in shielding gases with alternate pulsed supply of dissimilar gases,” *Weld. Int.*, vol. 7116, no. May 2015, pp. 1–4, 2012.
- [6.55] N. V. Shinde and M. T. Telsang, “Effect of Alternate Supply of Shielding Gases of Tungsten Inert Gas Welding on Mechanical Properties of Austenitic Stainless Steel,” *J. Inst. Eng. Ser. C*, vol. 97, no. 3, pp. 299–307, 2016.
- [6.56] P. K. Ghosh, S. R. Gupta, and H. S. Randhawa, “Characteristics of a Pulsed-Current, Vertical-Up Gas Metal Arc Weld in Steel,” *Metall. Mater. Trans. A*, vol. 31, no. 9, pp. 2247–2259, 2000.
- [6.57] J. Wang, Y. Li, and P. Liu, “Effect of weld heat input on toughness and structure of HAZ of a new super-high strength steel,” *Bull. Mater. Sci.*, vol. 26, no. 3, pp. 301–305, 2003.
- [6.58] J. W. Simmons, “Overview: High-nitrogen alloying of stainless steels,” *Mater. Sci. Eng. A*, vol. 207, no. 2, pp. 159–169, 1996.
- [6.59] E. A. Metzbower, J. J. DeLoach, S. H. Lalam, and H. K. D. H. Bhadeshia, “Analysis of toughness of welding alloys for high strength low alloy shipbuilding steels,” *Sci. Technol. Weld. Join.*, vol. 6, no. 6, pp. 368–374, 2014.
- [6.60] M. Du Toit and P. C. Pistorius, “Nitrogen Control during Autogenous Arc Welding of Stainless Steel- Part 1: Experimental Observations,” *Weld. J.*, vol. 82, no. 8, p. 219/S-224/S, 2003.
- [6.61] H. Kokawa, E. Tsory, and T. H. North, “Nitride Precipitation in Duplex Stainless Steel Weld Metal,” *ISIJ Int.*, vol. 35, no. 10, pp. 1277–1283,

1995.

- [6.62] C. Heiple, J. Roper, R. Stagner, and R. Aden, “Surface active element effects on the shape of GTA, laser and electron beam welds,” *Weld. J.*, no. March, pp. 72–77, 1983.
- [6.63] T. Lau, G. C. Weatherly, and A. McLean, “Gas/Metal/Slag Reactions in Submerged Arc Welding Using CaO-Al₂O₃ Based Fluxes,” *Weld. Res. Supplement*, no. February, pp. 31–38, 1986.
- [6.64] T. Lau, G. C. Weatherly, and A. McLean, “The sources of oxygen and nitrogen contamination in submerged arc welding using CaO-Al₂O₃ based fluxes,” *Weld. J.*, no. December, p. 343s–348s, 1985.
- [6.65] Q. Wei, Q. Hu, F. Guo, and D. J. Xiong, “A Study of Weld Pore Sensitivity of Self-Shielded, Flux Cored Electrodes,” *Weld. J.*, no. June, pp. 90–94, 2002.
- [6.66] J. Amanie, “Effect of Submerged Arc Welding Parameters on the Microstructure of SA516 and A709 Steel Welds,” University of Saskatchewan, 2011.
- [6.67] I. Madariaga, I. Gutiérrez, C. García-De Andrés, and C. Capdevila, “Acicular ferrite formation in a medium carbon steel with a two stage continuous cooling,” *Scr. Mater.*, vol. 41, no. 3, pp. 229–235, 1999.
- [6.68] J. Du, M. Strangwood, and C. L. Davis, “Effect of TiN Particles and Grain Size on the Charpy Impact Transition Temperature in Steels,” *J. Mater. Sci. Technol.*, vol. 28, no. 10, pp. 878–888, 2012.
- [6.69] H. K. D. H. Bhadeshia, “Bainite in Steels: transformations, microstructure and properties.” IOM Communications, London, 2001.
- [6.70] M. Díaz-Fuentes, A. Iza-Mendia, and I. Gutiérrez, “Analysis of different acicular ferrite microstructures in low-carbon steels by electron

- backscattered diffraction. Study of their toughness behavior,” *Metall. Mater. Trans. A Phys. Metall. Mater. Sci.*, vol. 34 A, no. 11, pp. 2505–2516, 2003.
- [6.71] R. A. Farrar and P. L. Harrison, “Acicular ferrite in carbon-manganese weld metals: An overview,” *J. Mater. Sci.*, vol. 22, no. 11, pp. 3812–3820, 1987.
- [6.72] W. Wang, W. Yan, L. Zhu, P. Hu, Y. Shan, and K. Yang, “Relation among rolling parameters, microstructures and mechanical properties in an acicular ferrite pipeline steel,” *Mater. Des.*, vol. 30, no. 9, pp. 3436–3443, 2009.

*“If I had asked people what they wanted,
they would have said faster horses”*

Henry Ford

Chapter 7

Heuristic and mathematical optimisation of the GMAW process

7.1 Introduction

The importance of decreasing the heat input towards the joint has been discussed in previous chapters, hence minimising the distortion of the workpiece and guaranteeing the weld integrity. While it was possible to effortlessly measure outcomes such as distortion and peak temperature, a more accurate assessment of the joint required destructive methods, namely sectioning, to evaluate features like the grain size, heat affected zone (HAZ) and weld shape. However, material availability, preparation of the workpiece, and metallographic preparations like polishing and etching can be demanding and time consuming, whilst not always an available option.

Aiming to overcome these limitations, mathematical modelling and search methods, e.g. regression analysis, neural networks, genetic algorithms, response surface methodology and desirability functions, have been applied to welding procedures to efficiently predict the welding outcomes [7.1-7.12]. For instance, techniques such as regression analysis and neural networks were widely used to predict the arc welding features [7.1, 7.2, 7.5-7.10]. Yet, these techniques are prone to success only when the welding parameters are chosen near the optimal conditions [7.11, 7.13]. The regression analysis alone was not

able to describe the welding process accordingly, due to nonlinear characteristics and complexity of the system. Despite the many advantages compared to the linear regression method, neural networks can be demanding in terms of time and cost, and over-fitting may happen when a limited sample size with too much noise (irregular fluctuations that are not part of the system) is provided [7.1].

Different from other heuristic approaches, genetic algorithms only require the values of the objective functions for optimisation of the process and not the respective derivatives [7.1, 7.12, 7.14]. This technique has been widely employed to optimise and mostly to define the weld shape characteristics [7.7, 7.11, 7.12, 7.15]. Correia et al. [7.16] refined control variables (voltage, wire-feed speed and travel speed) based on four responses: deposition efficiency, bead width, depth of penetration and reinforcement. Kumar and Debroy [7.17] simulated heat transfer and fluid-flow models, further creating many optimal combinations of arc current, arc voltage, wire-feed speed and travel speed coupled with targeted features of the weld geometry (leg length, penetration and throat). Jia et al. [7.18] improved high speed rotating arc welding sensor parameters, presenting the genetic algorithm as an effective method to predict the target weld shape. Thao et al. [7.19] employed multiple regression models and the genetic algorithm method, correlating coefficients such as the contact-tip-to-work distance, shielding gas flow rate (SGFR), travel speed, arc current and arc voltage via linear, curvilinear and intelligent models to understand the impact of control variables on the top width of the joint.

Additionally, Bag and De [7.14] presented the benefits of using the genetic algorithm approach to assist a finite element based three-dimension numerical heat transfer model, relating input and output variables during the

gas tungsten arc welding process, whereas Prasad et al. [7.13] achieved optimum conditions in terms of grain size, hardness and strength of the weld via the genetic algorithm technique.

The response surface methodology and desirability function approaches have also been used systematically with genetic algorithms [7.3, 7.4, 7.20]. Correia et al. [7.3] compared the response surface methodology and genetic algorithm by optimising the gas metal arc welding (GMAW) process, with the best values of arc voltage, wire-feed speed and travel speed defined based on process responses, e.g. deposition efficiency, bead width, depth of penetration and reinforcement. Results indicated both methods as being capable of finding optimum conditions using a relatively small number of experiments. Shahi and Pandey [7.20] utilised the response surface methodology to check the effects of the wire-feed speed, arc voltage, travel speed, electrode stick-out, and preheating current on the welding current. The study [7.20] compared both the GMAW and universal GMAW processes, where the latter was defined by utilising a specially designed torch to preheat the filler wire independently, before its emergence from the torch. Kim and Rhee [7.4] defined desirability functions as objective functions followed by the wire-feed speed and travel speed optimisation and weld penetration assessment.

Despite important contributions, the research involving genetic algorithms, response surface methodology and desirability function approaches to predict and improve weld features were all limited to the constant supply of pure CO₂ and ArCO₂. Furthermore, discussions were mostly focused on the weld shape, missing predictions of the workpiece distortion and the impact of the alternating shielding gas technique on the grain size of the fusion zone. Thus, the lack of heuristic modelling and search studies optimising the

alternating shielding gas method in the GMAW process coupled with the possibility of adding further improvements to the joint under the supply of N_2 offer an opportunity to extend the scientific knowledge in this area.

This chapter combines the genetic algorithm heuristic, the response surface methodology approach and the desirability function technique to extend and optimise the welding conditions presented in chapter 6. Experiments using the genetic algorithm narrowed the search region, followed by the development of regression models using the response surface methodology to predict the responses from welding. The desirability function was further introduced and effectively enhanced the multiple responses related to the input variables.

7.2 Methodology

7.2.1 Experimental setup

Aiming to optimise the welding conditions based on results from chapter 6, the welds carried out in this chapter had $Ar5N_2 + He$ as the protective gas, supplied at a 15 L/min SGFR and a frequency of 2 Hz. A stand-off distance of 10 mm and a root gap of 3 mm were chosen, assisting with the heat input reduction. The dimensions and positioning of the workpiece are as described in chapter 3.

7.2.2 Optimisation process

A search technique and mathematical models were established according to those suggested by Kim et al [7.1], namely the genetic algorithm, the response surface methodology and the desirability function. Java programming

was developed in the IntelliJ IDEA software for the genetic algorithm search and desirability function optimisation, whilst RStudio software assisted with the creation of a R code to define the central composite design equations correlating control variables and responses in the response surface methodology. The respective codes are available in Appendix B.

Three control variables were considered, namely wire-feed speed, voltage and travel speed, since they influence directly the N absorption/desorption [7.21-7.24] in the welding process. The search space was broadened based on results from chapter 6, with a respective range given to each input variable (see Table 7.1). The responses analysed were the grain size of the microstructure of each joint, the distortion on the extremes of the workpiece in the transverse direction and the peak temperature 10 mm away from the root gap.

Table 7.1 Range and respective number of bits of the considered input variables.

Input variable	Range	Units	Number of bits
Wire-feed speed [m/min]	12 to 16.6	-	4
Voltage	21 to 25	V	4
Travel speed	7 to 12	mm/s	3

The objective in this chapter was to minimise the output variables, reducing the heat input during the welding process, the slag development and the porosity in the fusion zone. Each weld was considered as being a chromosome, i.e. an individual of a randomly generated population, composed of either the input variables or both the control variables and responses. Thus,

the latter will be referred to as the global chromosome whilst the former, input chromosome.

The optimisation process can be summarised as follow:

- 1) Twelve initial input chromosomes are created utilising a L_{12} orthogonal array based on the search space in Table 7.1 (see section 7.3.1);
- 2) Using the input chromosomes generated, experiments are carried out to produce the respective outputs of interest and population (see section 7.3.2);
- 3) The genetic operators fitness, crossover and mutation from the genetic algorithm are employed on each global chromosome of the created population, generating another 12 input chromosomes (see sections 7.3.2 and 7.3.3);
- 4) Steps 2) and 3) are performed until population 3 is achieved (see Table 7.5);
- 5) The input chromosome with the highest fitness is selected from population 3 and works as the origin for a new, narrower search space (see Table 7.6), with the response surface methodology utilised to create 15 input chromosomes (see section 7.4);
- 6) Experiments are carried out using the 15 input chromosomes, creating the respective responses and population 4 (see Table 7.7);
- 7) Population 4 is utilised to create the mathematical models (see equations 7.1, 7.2 and 7.3) to predict the responses of interest;

- 8) Three independent simulations are performed using the mathematical models to predict the responses of interest, where the genetic algorithm coupled with the desirability function refined the search space by generating 51 populations per simulation (see section 7.5);
- 9) The best input chromosome from population 51 in each of the three simulations is selected and validated by comparing their respective predicted and experimental responses (see section 7.6), hence assessing the performance of the optimisation process.

In addition, populations created during the simulation phase will be referred to as generations. According to studies by Kim et al. [7.1] and Grefenstette [7.25], the number of individuals, the crossover rate and the mutation rate (described in chapter 2) were 12, 0.95 and 0.01, respectively, during the genetic algorithm phase.

7.3 The genetic algorithm phase

7.3.1 Systematic initialisation: orthogonal arrays

The input parameters of any first population are usually initialised in a random manner [7.1, 7.26]. However, a systematic initialisation was demonstrated by Reeves [7.26] to produce a more favourable search space for a small number of individuals. Thus, the Taguchi method [7.27, 7.28] was applied using binary strings of a L_{12} orthogonal array (see Table 7.2), with each line of the matrix representing an individual composed by three inputs.

$$I_k = r_k^{min} + \frac{bin}{(2^{inbits} - 1)} (r_k^{max} - r_k^{min}) \quad 7.1$$

Table 7.2 A typical L_{12} orthogonal array based on the Taguchi method.

	Wire-feed speed				Voltage				Travel speed		
	1	2	3	4	5	6	7	8	9	10	11
	Chromosome	1	0	0	0	0	0	0	0	0	0
2	0	0	0	0	0	1	1	1	1	1	1
3	0	0	1	1	1	0	0	0	1	1	1
4	0	1	0	1	1	0	1	1	0	0	1
5	0	1	1	0	1	1	0	1	0	1	0
6	0	1	1	1	0	1	1	0	1	0	0
7	1	0	1	1	0	0	1	1	0	1	0
8	1	0	1	0	1	1	1	0	0	0	1
9	1	0	0	1	1	1	0	1	1	0	0
10	1	1	1	0	0	0	0	1	1	0	1
11	1	1	0	1	0	1	0	0	0	1	1
12	1	1	0	0	1	0	1	0	1	1	0

Four bits were assigned to the wire-feed speed and voltage and three bits to the travel speed during the decoding process (see Table 7.1). Each binary string (k) was decoded according to equation 7.1 [7.15, 7.16], which changed the binary bits to an actual initial input value (I_k). The maximum and minimum range numbers of each control variable were represented by r_k^{max} and r_k^{min} , respectively. Equation 7.1 also considered the number of bits for each input parameter (*inbits*) and the converted binary section (*bin*)

according to the respective input variable chosen. Therefore, the set of control variables to compose population 1 was systematically generated.

It is important to highlight that according to the number of bits in Table 7.1, two-level factorial experiments [7.29] would require 2048 search points; a substantial sample space. Conversely, the genetic algorithm approach was able to cover such space more efficiently, reducing the number of welds required to optimise the process.

7.3.2 Fitness stage

Subsequently, welds were performed and the grain size (g), distortion (d), and temperature (t) responses, measured. As explained in chapter 2, the genetic algorithm technique selects individuals based on the respective fitness (see equation 7.2), which was obtained from an objective function (see equation 7.3) [7.1, 7.16, 7.29]. The objective function was a composition of the normalised differences between each of the measured responses and the minimum, where *min* and *max* indicate the lowest and highest values of a certain response within a specific population.

Global chromosomes from population 1 are shown in Table 7.3 with their respective fitness. The global chromosomes 1.2, followed by 1.10 and 1.12 were the most desirable cases since the grain size, workpiece distortion and temperature were the lowest. Therefore, the chances of the aforementioned being selected for the next population were high compared to the other individuals in population 1.

Once the objective function and fitness of all responses were calculated, the most feasible input chromosomes were selected to compose the matrix for

the next population. The fitness method was then applied as described in chapter 2, followed by the crossover and mutation processes, which occurred in a random manner.

$$f_k = \left[(1 + OF_k) \sum_{k=1}^{12} OF_k \right]^{-1} \quad 7.2$$

$$OF_k = \frac{(d_k - d_{min})}{(d_{max} - d_{min})} + \frac{(t_k - t_{min})}{(t_{max} - t_{min})} + \frac{(g_k - g_{min})}{(g_{max} - g_{min})} \quad 7.3$$

Table 7.3 Population 1: control variables, responses and fitness.

	Wire-feed speed [m/min]	Voltage [V]	Travel speed [mm/s]	Grain size [μm^2]	Distortion [mm]	Temperature [$^{\circ}\text{C}$]	Fitness
1.1	12.2	21.0	7.0	8.5	4.1	507.9	6.7%
1.2	12.2	22.9	12.0	5.3	3.4	386.1	14.6%
1.3	13.0	23.1	12.0	7.9	4.0	391.7	9.8%
1.4	13.8	23.9	7.7	6.8	5.1	536.4	5.4%
1.5	14.0	24.5	8.4	13.4	4.8	509.6	5.0%
1.6	14.2	22.6	9.9	11.1	4.3	450.1	6.6%
1.7	15.5	21.8	8.4	8.9	4.0	435.9	8.1%
1.8	15.0	24.7	7.7	17.9	4.6	568.6	4.2%
1.9	14.8	24.5	9.9	7.5	3.3	482.2	9.3%
1.10	16.4	21.3	10.6	5.7	3.7	407.3	11.6%
1.11	15.9	22.1	9.1	6.8	3.9	500.0	7.6%
1.12	15.7	23.7	11.3	5.9	3.6	419.8	11.0%

7.3.3 Crossover and mutation stages

The single-point crossover procedure [7.16, 7.29] was chosen for this study and applied to the entire population. In this method, two parents (see

Fig. 7.1) were randomly selected in turns based on the crossover rate. Since each input chromosome was composed by three control variables, the assigned crossover point was either 1 or 2, chosen arbitrarily. This number sectioned both parents and all bits to the right were swapped, resulting in a new offspring.

Table 7.4 Population 2: control variables, responses and fitness.

	Wire-feed speed [m/min]	Voltage [V]	Travel speed [mm/s]	Grain size [μm^2]	Distortion [mm]	Temperature [$^{\circ}\text{C}$]	Fitness
2.1	14.2	22.6	12.0	4.4	3.7	397.2	10.3%
2.2	12.2	22.9	9.9	5.6	4.2	429.1	6.8%
2.3	13.0	23.1	12.0	5.5	3.5	391.4	10.2%
2.4	13.0	23.1	12.0	5.3	3.6	394.7	9.6%
2.5	15.7	23.7	12.0	6.4	4.2	436.5	6.4%
2.6	13.0	23.1	11.3	5.8	3.5	441.6	8.4%
2.7	13.0	24.5	8.4	8.4	3.9	504.5	5.5%
2.8	14.0	23.1	12.0	6.3	4.0	391.6	7.6%
2.9	16.4	22.6	9.9	7.0	3.6	491.0	6.8%
2.10	14.2	21.3	10.6	3.5	3.3	413.6	13.6%
2.11	15.0	21.3	10.6	3.9	3.4	432.6	10.9%
2.12	16.4	24.7	7.7	10.4	4.5	603.3	3.8%

In the mutation process, values between 0 and 100% were randomly assigned to each bit within the input chromosomes. If the value was lower than 1%, mutation occurred and a random number between r_k^{max} and r_k^{min} replaced the bit of the respective control variable. However, due to the very low mutation rate, such operation was rare.

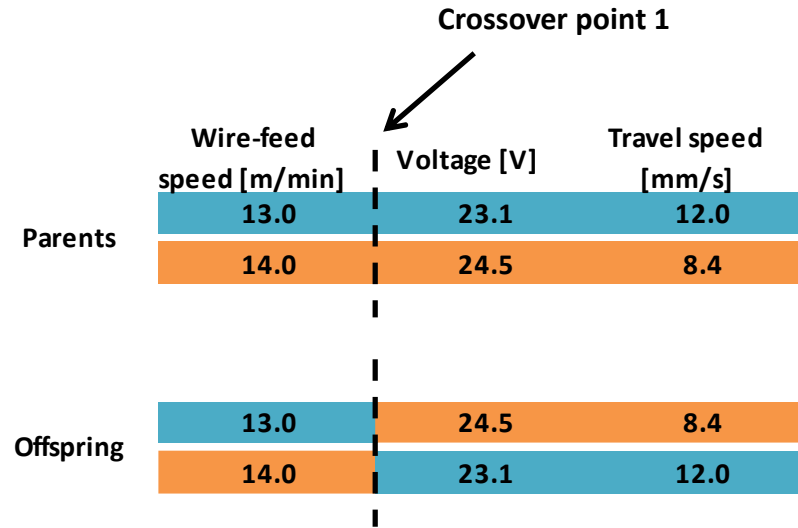


Fig. 7.1 Crossover example during the genetic algorithm refinement with chromosomes 1.3 and 1.5 as parents

Table 7.5 Population 3: control variables, responses and fitness.

	Wire-feed speed [m/min]	Voltage [V]	Travel speed [mm/s]	Grain size [μm^2]	Distortion [mm]	Temperature [$^{\circ}\text{C}$]	Fitness
3.1	13.0	23.1	11.3	4.7	3.7	414.8	9.3%
3.2	13.0	23.1	11.3	6.0	3.9	418.2	7.3%
3.3	15.0	21.3	10.6	5.4	3.8	441.6	7.7%
3.4	15.0	21.3	10.6	4.7	3.0	426.5	11.9%
3.5	13.0	23.1	11.0	6.7	3.7	460.8	6.7%
3.6	14.2	21.3	10.6	4.2	3.7	607.6	7.3%
3.7	14.2	21.3	10.6	3.9	3.3	499.7	10.6%
3.8	14.0	23.1	12.0	4.6	4.3	430.4	7.8%
3.9	14.2	22.6	12.0	5.5	3.6	383.4	9.1%
3.10	12.2	22.9	9.9	5.0	4.4	429.4	7.1%
3.11	13.0	23.1	11.3	6.3	3.9	426.1	7.0%
3.12	12.2	22.9	9.9	6.9	3.5	339.0	8.1%

A total of four populations were generated: population 1 (see Table 7.3), population 2 (see Table 7.4), population 3 (see Table 7.5) and population 4 (see Table 7.7). Limiting the population number to three during the genetic algorithm phase was reasonable, since results in population 3 started to converge, i.e. input chromosomes 3.1-3.2, 3.3-3.4, 3.6-3.7, and 3.10-3.12 were composed by the same control variables.

7.4 The response surface methodology phase

The response surface methodology was employed subsequently to the generation of population 3, since extending experiments using the genetic algorithm technique turned to be ineffective due to convergence. As demonstrated by Kim et al. [7.1], this would prevent loss of performance and allow for the generation of mathematical models between the input and output parameters.

The input chromosome 3.4 was the most favourable in terms of control variables, i.e. with the highest fitness. Hence, it was defined as the origin in the new search region during the response surface methodology. As suggested by Kim et al. [7.1], the central composite design approach [7.3, 7.30] was utilised as the experimental design to create regression models correlating input and output parameters.

Table 7.6 shows the factors and levels employed in the response surface methodology phase. Table 7.7 exhibits population 4, with values of all control variables considered to develop the regression models as well as the respective coded units and measured responses from experiments. For better comprehension, designations were given to each variable, where I_1 (wire-feed

speed), I_2 (voltage), and I_3 (travel speed) represent the natural units and i_1 (wire-feed speed), i_2 (voltage), and i_3 (travel speed), the coded units (see Table 7.7).

Table 7.6 Factor and levels employed in the central composite design method.

Factor	Level		
	-1	0	1
Wire-feed speed [m/min]	14.2	15	15.7
Voltage [V]	20.8	21.3	21.8
Travel speed [mm/s]	8.6	10.6	12.6

The second-order regression models, namely equations 7.4, 7.5 and 7.6, to predict the grain size, distortion, and temperature responses were originated from data in Table 7.7. The coefficient of multiple determinations (R^2) were 0.7012 (grain size), 0.87 (distortion), and 0.9431 (temperature), designating a strong positive correlation from the temperature data, a good correlation from the distortion measurements and a reasonable correlation from the grain size responses [7.31, 7.32].

$$\begin{aligned}
 g = & 5.58231 + 0.27601i_1 + 0.31936i_2 - 0.05182i_3 + 0.19176(i_1)^2 \\
 & - 0.65099(i_2)^2 - 0.23089(i_3)^2 - 0.58423i_1i_2 \\
 & - 0.19163i_1i_3 + 0.72140i_2i_3 + 0.11655i_1i_2i_3
 \end{aligned} \tag{7.4}$$

$$\begin{aligned}
 d = & 3.34205 + 0.08010i_1 + 0.17610i_2 - 0.64684i_3 + 0.16581(i_1)^2 \\
 & - 0.08209(i_2)^2 - 0.33519(i_3)^2 - 0.09723i_1i_2 \\
 & + 0.56715i_1i_3 - 0.11838i_2i_3 + 0.14443i_1i_2i_3
 \end{aligned} \tag{7.5}$$

$$\begin{aligned}
 t = & 422.493 + 9.530i_1 + 7.360i_2 - 44.350i_3 + 30.183(i_1)^2 \\
 & - 17.667(i_2)^2 + 10.183(i_3)^2 - 12.400i_1i_2 \\
 & + 6.775i_1i_3 + 0.525i_2i_3 - 5.950i_1i_2i_3
 \end{aligned} \tag{7.6}$$

Table 7.7 Central composite design and weld measurements (population 4).

Weld	Natural units			Coded units			Responses		
	I_1	I_2	I_3	i_1	i_2	i_3	g	d	t
1	14.2	20.8	8.6	-1	-1	-1	4.1	3.7	483.9
2	15.7	20.8	8.6	1	-1	-1	6.0	3.5	493.8
3	14.2	21.8	8.6	-1	1	-1	5.2	4.6	501.9
4	15.7	21.8	8.6	1	1	-1	4.2	3.5	486.0
5	14.2	20.8	12.6	-1	-1	1	3.3	1.6	365.1
6	15.7	20.8	12.6	1	-1	1	4.0	3.1	425.9
7	14.2	21.8	12.6	-1	1	1	6.8	1.5	409.0
8	15.7	21.8	12.6	1	1	1	5.6	3.2	396.4
9	14.2	21.3	10.6	-1	0	0	4.6	4.0	425.9
10	15.7	21.3	10.6	1	0	0	7.0	3.1	479.0
11	15.0	20.8	10.6	0	-1	0	5.5	2.9	380.1
12	15.0	21.8	10.6	0	1	0	4.3	3.7	429.1
13	15.0	21.3	8.6	0	0	-1	5.7	3.4	469.6
14	15.0	21.3	12.6	0	0	1	5.0	2.7	395.3
15	15.0	21.3	10.6	0	0	0	5.6	3.2	423.4

7.5 The desirability function phase

The second-order regression models were able to predict the desired responses. However, as described by Kim et al. [7.1], it was possible that the narrowed search region did not include input combinations that satisfied many responses simultaneously. Therefore, it was important to also optimise the output parameters, so the control variables could, at least, produce acceptable responses.

The desirability function [7.33-7.35] was used as the objective function during the simulation process. As shown elsewhere [7.36-7.38], it permits the analysis of each output parameter individually, further considering their overall impact on the quality of the control variables. In the present work, the response type small-is-best (SIB) was used as the objective function (see equation 7.7) to minimise all three output variables [7.33, 7.34]. Since the search space has been narrowed, a linear objective function was chosen, i.e. $s = 1$.

$$d_r = \begin{cases} 1 & , \quad y \leq T \\ \left(\frac{y-U}{T-U}\right)^s & , \quad T < y < U \\ 0 & , \quad y \geq U \end{cases} \quad 7.7$$

The median value of each group of responses in Table 7.7 was chosen as the target (T), considering that the search was within the optimal region and that lower values could result in experimental difficulties, e.g. impractical welds. The upper limit (U) was set as the highest measurement from each response group (see Table 7.8).

Table 7.8 Upper limits and targets according to the respective responses.

Response	U	T
g	7.0001	5.1600
d	4.6401	3.1991
t	501.9	425.9

The genetic algorithm was employed in this final stage since the desirability function had non-differentiable points in the search region and

required a derivative-free optimisation algorithm [7.1, 7.29]. The search region for each control variable was limited between levels -1 and 1. Considering that the search process was within the optimal region (see Table 7.6), the number of individuals (welds) and generations were increased to 30 and 51, respectively, during the simulations. The crossover rate was maintained as 95% and the mutation rate as 1%.

7.6 Results and discussion

7.6.1 Welding process optimisation

In this study, the search technique utilised aimed to decrease the heat input during welding. This was demonstrated gradually during the optimisation process by the grain refinement of the joint, reductions in the distortion of the workpiece and lower peak temperatures of the weld (see Fig. 7.2).

The best input chromosome from the 51st generation of each of the three independent simulations was selected and validated. These will be discussed in section 7.6.2, but their average is shown in Fig. 7.2 for comparison with welds from populations 1, 2, 3 and 4. The joints that presented the best outcomes in chapters 4 ($\text{Ø}16_5\text{L}/\text{min}$), 5 (6Ar-6He6) and 6 (14W-9T) are also considered to better demonstrated the impact of the optimisation process in reducing the heat input.

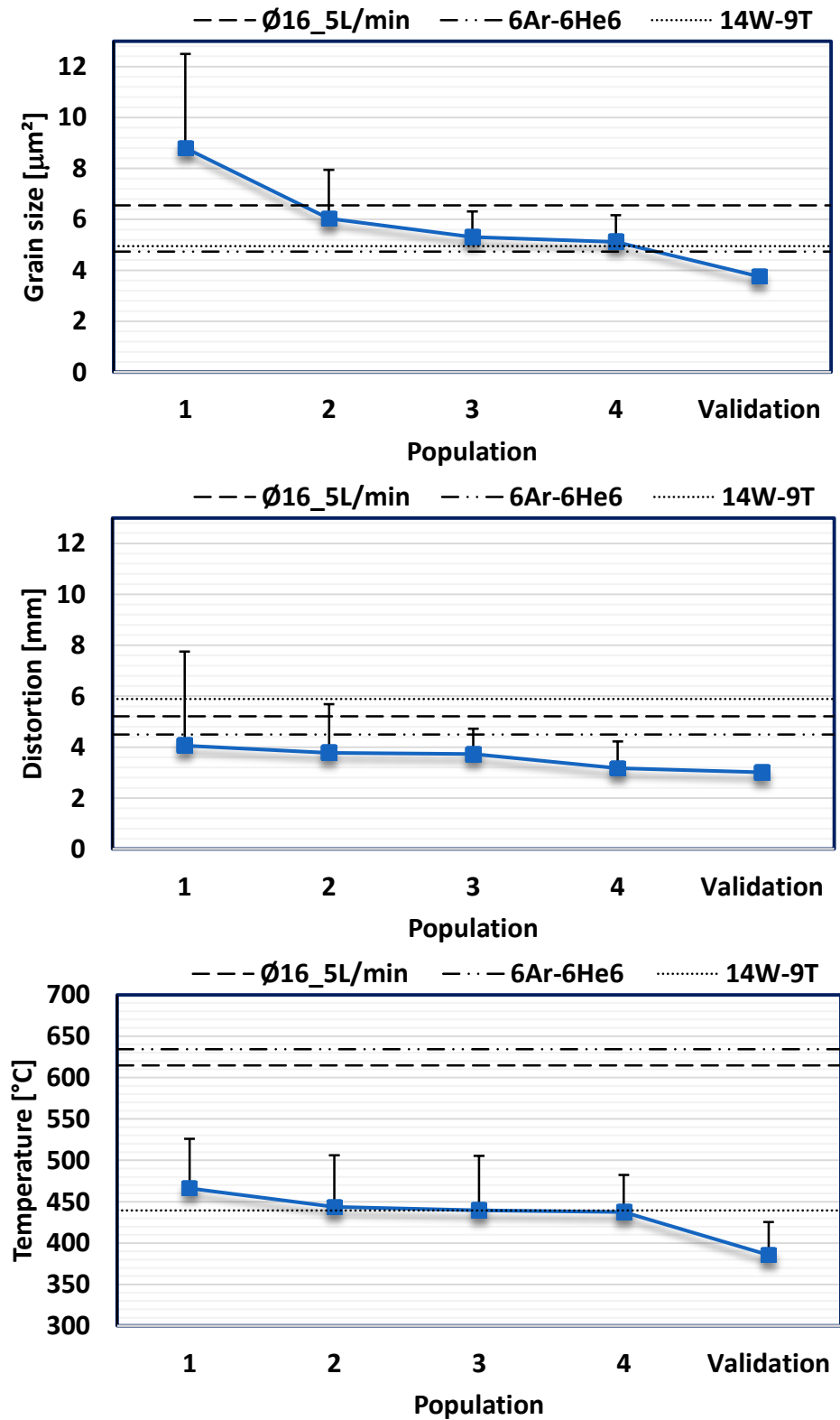


Fig. 7.2 Mean experimental values of responses measured for populations 1, 2, 3 and 4 and for the validation procedure.

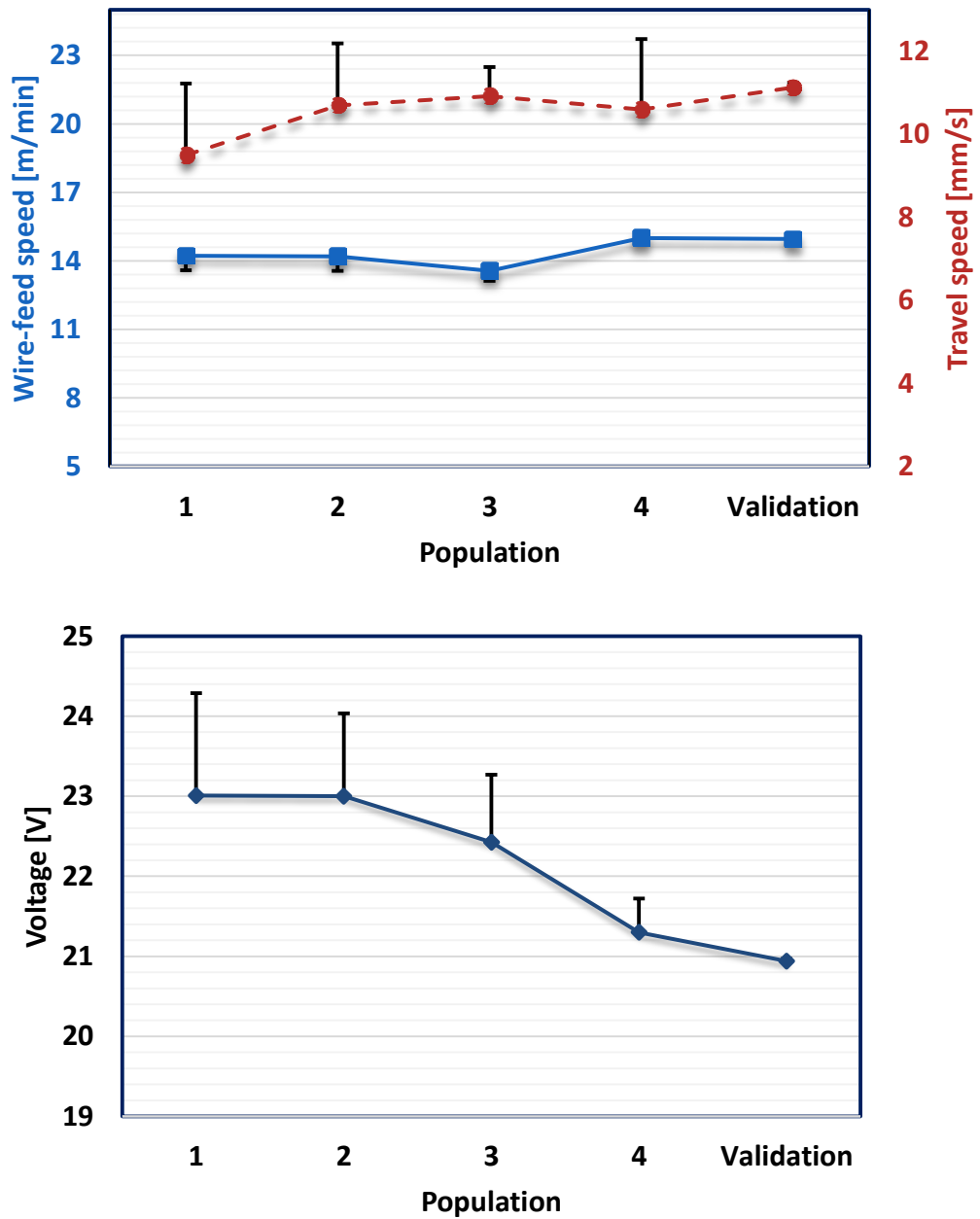


Fig. 7.3 Mean values of control variables employed during experiments for populations 1, 2, 3 and 4 and for the validation procedure.

Table 7.9 Generation 1 - simulation 1.

Weld	I_1	I_2	I_3	g	d	t	Desirability function
1	14.86	21.3	11.26	5.55	3.05	408.54	0.92
2	15.63	21.5	12.02	5.76	3.29	427.27	0.85
3	15.13	21.1	9.08	5.61	3.50	459.72	0.69
4	14.71	21.1	10.98	5.02	3.05	405.38	1.00
5	14.27	21.6	10.91	5.84	3.32	439.69	0.78
6	15.03	21.2	12.36	5.15	2.53	390.13	1.00
7	14.47	21.5	11.25	5.81	3.05	424.40	0.86
8	15.01	21.8	9.61	4.96	3.73	438.47	0.81
9	14.70	21.0	9.48	5.11	3.57	444.49	0.83
10	14.93	21.7	11.61	5.64	2.94	397.17	0.90
11	15.50	21.1	11.06	5.58	3.31	429.37	0.88
12	15.65	21.3	9.83	6.08	3.55	472.65	0.53
13	15.47	20.8	9.25	5.75	3.28	451.87	0.75
14	15.03	21.7	11.83	5.62	2.87	392.58	0.91
15	14.63	21.3	10.91	5.43	3.18	420.97	0.95
16	15.39	21.5	9.20	5.42	3.57	466.30	0.67
17	15.31	21.3	9.31	5.71	3.53	462.25	0.66
18	15.68	21.4	9.62	5.97	3.55	480.82	0.49
19	14.47	21.3	9.57	5.31	3.82	460.93	0.65
20	15.03	21.4	8.74	5.33	3.69	473.40	0.61
21	15.25	21.0	9.27	5.64	3.39	451.20	0.76
22	15.18	21.3	11.52	5.59	3.07	408.90	0.92
23	15.16	21.1	9.86	5.60	3.44	439.32	0.80
24	15.21	21.4	9.10	5.45	3.61	464.78	0.66
25	15.52	21.7	12.24	5.61	3.04	402.88	0.91
26	14.93	21.0	10.92	5.07	3.10	404.54	1.00
27	14.91	21.6	10.82	5.59	3.33	416.01	0.89
28	15.18	21.2	10.90	5.52	3.24	418.07	0.92
29	15.59	21.4	9.76	5.88	3.55	466.23	0.60
30	14.47	21.3	10.89	5.45	3.21	426.90	0.94

Table 7.10 Generation 51 - simulation 1.

Weld	I_1	I_2	I_3	g	d	t	Desirability function
1	14.63	21.0	11.25	4.57	2.84	395.14	1.00
2	14.63	21.0	11.25	4.57	2.84	395.14	1.00
3	14.63	21.0	11.25	4.57	2.84	395.14	1.00
4	14.63	21.0	11.25	4.57	2.84	395.14	1.00
5	14.63	21.0	11.25	4.57	2.84	395.14	1.00
6	14.63	21.0	10.91	4.65	3.02	403.16	1.00
7	14.63	21.0	11.25	4.57	2.84	395.14	1.00
8	14.63	21.2	11.25	5.19	2.94	408.71	1.00
9	14.63	21.0	11.25	4.57	2.84	395.14	1.00
10	14.63	21.0	11.25	4.57	2.84	395.14	1.00
11	14.63	21.0	11.25	4.57	2.84	395.14	1.00
12	14.63	21.0	11.25	4.57	2.84	395.14	1.00
13	14.63	21.0	11.25	4.57	2.84	395.14	1.00
14	14.63	21.0	11.25	4.57	2.84	395.14	1.00
15	14.63	21.0	11.25	4.57	2.84	395.14	1.00
16	14.63	21.2	11.25	5.19	2.94	408.71	1.00
17	14.63	21.0	11.25	4.66	2.85	397.13	1.00
18	15.67	21.0	11.25	5.59	3.40	443.37	0.80
19	14.63	21.0	11.25	4.57	2.84	395.14	1.00
20	14.63	21.0	11.25	4.57	2.84	395.14	1.00
21	14.63	21.2	11.25	5.19	2.94	408.71	1.00
22	15.67	21.0	11.25	5.59	3.40	443.37	0.80
23	14.63	21.6	11.25	5.80	3.06	418.55	0.87
24	14.63	21.0	11.25	4.57	2.84	395.14	1.00
25	14.63	21.0	11.25	4.57	2.84	395.14	1.00
26	15.67	21.0	11.25	5.59	3.40	443.37	0.80
27	14.63	21.0	11.25	4.57	2.84	395.14	1.00
28	14.63	21.0	11.25	4.57	2.84	395.14	1.00
29	14.63	21.0	11.25	4.57	2.84	395.14	1.00
30	14.63	21.0	11.25	4.57	2.84	395.14	1.00

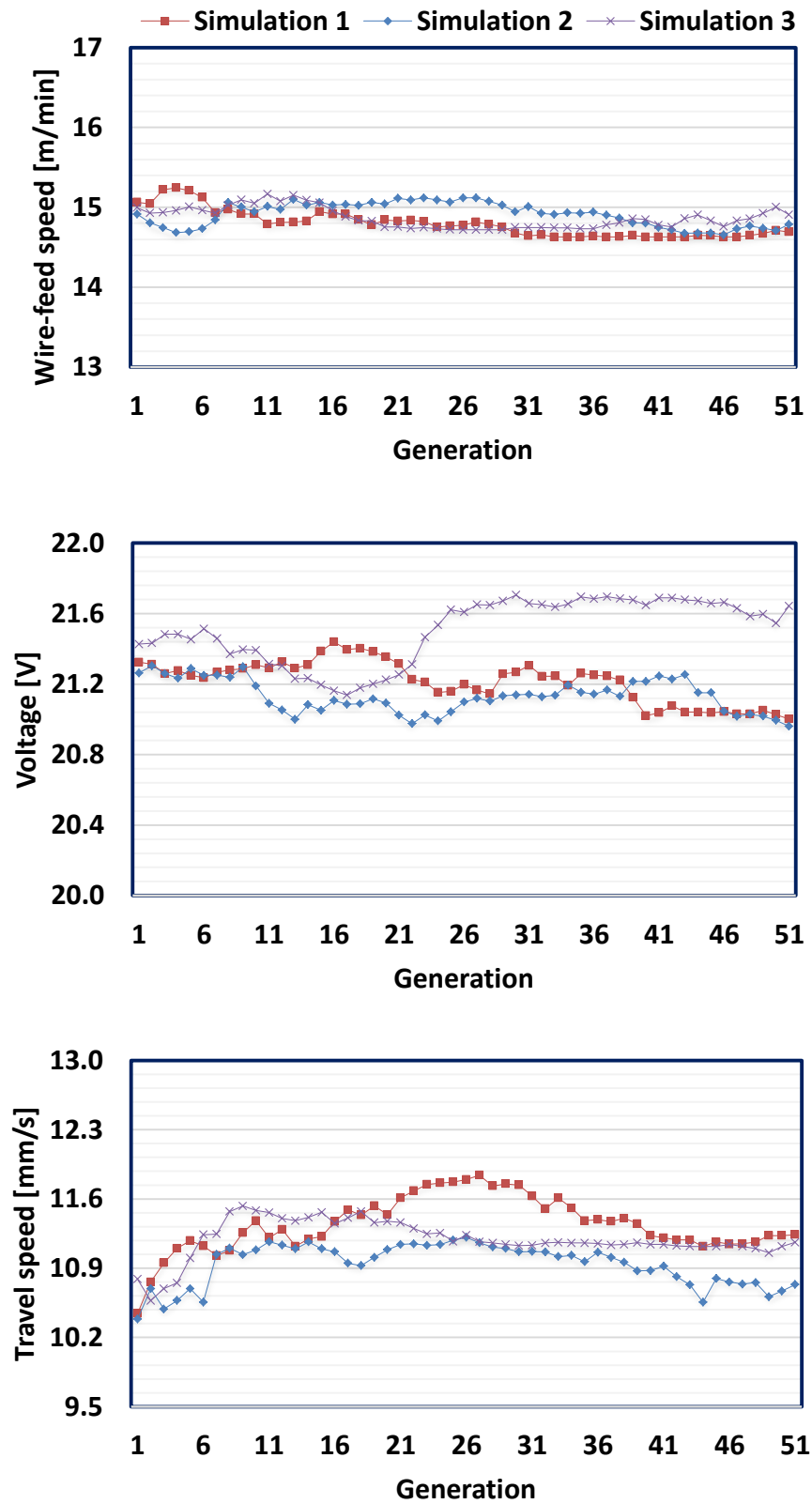


Fig. 7.4 Comparison between genetic algorithm simulations using the desirability function for the wire-feed speed, voltage and travel speed.

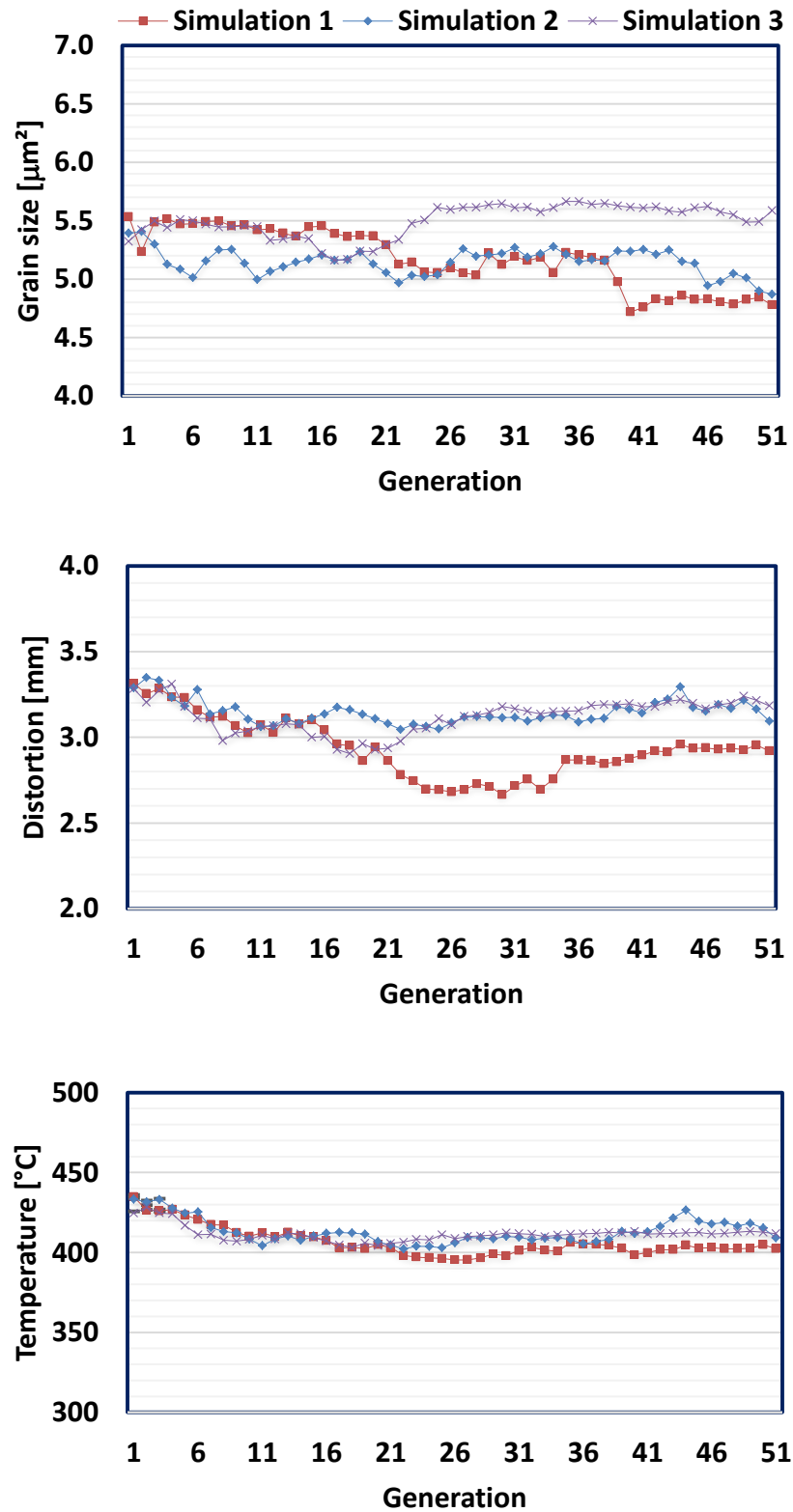


Fig. 7.5 Comparison between genetic algorithm simulations using the desirability function for the grain size, distortion and temperature.

When comparing the mean results from the validation welds with the mean values from population 1, the grain size was diminished by 57%, the temperature by 17%, and the distortion by 26%. The final welds generated by the optimisation process presented the lowest grain size, distortion, and temperature in contrast to the $\text{Ø}16_5\text{L}/\text{min}$, 6Ar-6He6 and 14W-9T welds. These findings clarify how satisfactory both the mathematical models and search method were when optimising the responses, minimising the overall heat input in all cases.

It is known that the welding parameters influence the heat input to the weld and are important factors to be controlled [7.39-7.44]. For instance, increasing the travel speed permits a lower volume of weld metal and heat transfer to the workpiece [7.41, 7.42]. The optimisation process allowed for an overall 17% (1.6 mm/s) improvement in the travel speed when comparing the population 1 and the validation welds (see Fig. 7.3), e.g. a productivity 14% greater was achieved for a 500 mm length weld. Furthermore, a travel speed of 11 mm/s was utilised in the validation welds, which is 2.2 times faster in comparison to that of the $\text{Ø}16_5\text{L}/\text{min}$ weld (5 mm/s).

Significant improvement was found throughout simulations based on the desirability function results. For instance, moving from the 1st (see Table 7.9) to the 51st (see Table 7.10) generation in simulation 1 exhibited a greater amount of desirable responses overall, with the mean desirability function increasing from 0.80 (1st generation) to 0.98 (51st generation).

To better analyse the optimisation process, all three simulations were compared by calculating the mean value per generation of each column of the input and output variables (see Fig. 7.4 and 7.5). Overall, all simulations decreased the grain size of the weld, the distortion of the workpiece and the

peak temperature. No significant variations were found between simulations in terms of wire-feed speed.

The mean voltage measurements increased and converged after generation 21 in simulation 3, influencing negatively the grain size of the joint. Such behaviour was a result of a smaller number of mutations throughout the generations, inducing convergence of the search space. Hence, it is important to properly choose the number of generations and population size as well as having the crossover and mutation genetic operators [7.12, 7.45], avoiding premature convergence.

7.6.2 Experimental validation

The impact of the second-order regression models in predicting the weld responses was assessed through three simulations. Once all simulations were finished, the global chromosome (input and output combination) with the highest desirability function in the 51st generation from each simulation was selected (see Table 7.11) and experimentally validated.

A comparison between the predicted and experimental results is shown in Fig. 7.6. The combination of control variables and responses selected from each simulation was able to produce predicted output values close to the defined target. The average prediction measurements were found to be up to 6% lower than the target. This demonstrates the advantage of using the genetic algorithm method together with the desirability function as optimising tools when predicting output parameters based on predefined equations.

Table 7.11 Chromosomes with the best desirability function from the 51st generation of each simulation.

Simulation	I_1	I_2	I_3	g	d	t	Desirability function
1	14.6	21.0	11.25	4.57	2.84	395.14	1.00
2	14.9	21.0	11.02	4.85	3.02	397.83	1.00
3	15.4	20.9	11.12	5.19	3.19	416.88	0.99

Similarly, the experimental measurements exhibited values close to the predefined target. The mean grain size from the measured outputs provided a 27% ($1.4 \mu\text{m}^2$) lower grain size compared to the chosen target. In terms of distortion of the workpiece, the mean experimental value was found to be 27% (0.86 mm) lower compared to the respective target, whilst the mean measured temperature was only 3% (13 °C) below the target.

The accuracy of measurements is related to the R^2 [7.31, 7.32], which explains the greater difference between the target and experimental responses when using the grain size and distortion regression models. The 70% (grain size) and 87% (distortion) R^2 values were a result of the complex behaviour of the developed microstructure and plate distortion compared to that of the temperature, hindering accurate predictions when using linear objective functions, i.e. $s = 1$.

However, since the objective was to minimise the output variables, the mathematical models were capable of producing input variables that reduced the experimental responses even further. These findings support the strength of coupling both the mathematical models and search methods. Additionally, the second-order regression models can be modified and adapted accordingly in future experiments.

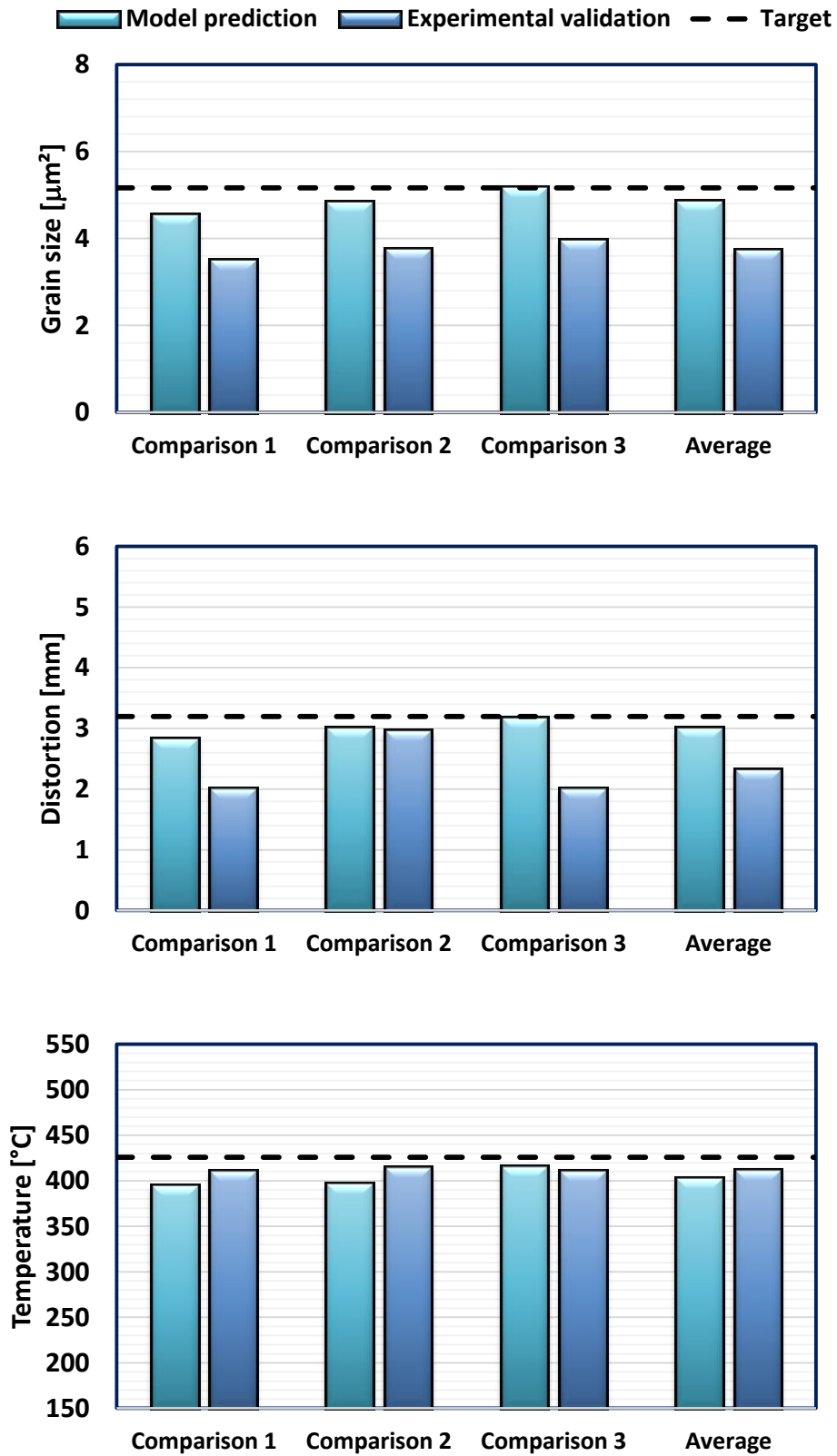


Fig. 7.6 Comparison between the predicted and experimental responses of the optimal global chromosomes for each simulation case.

7.6.2.1 Weld characteristics

The search method using the genetic algorithm reduced the HAZ area, afterwards increased during the response surface methodology phase and subsequently reduced through the simulation under the desirability function optimisation (see Fig. 7.7). This increase in the HAZ during the response surface methodology phase is explained by the expansion of the search space in population 4, where some input parameters developed greater HAZ areas. Analysis of the cross-section of all welds presented an overall reduction of 26% in the HAZ area when comparing the population 1 and validation joints. There was also a clear reduction of the HAZ area in contrast to the $\text{\O}16_5\text{L}/\text{min}$, 6Ar-6He6 and 14W-9T welds.

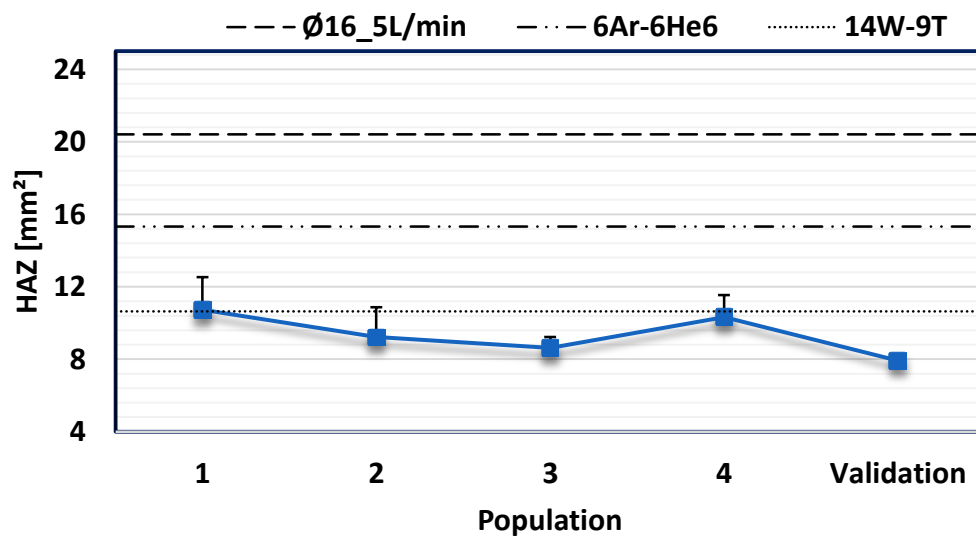


Fig. 7.7 Measured values and mean data per population of the HAZ areas during the optimisation process.

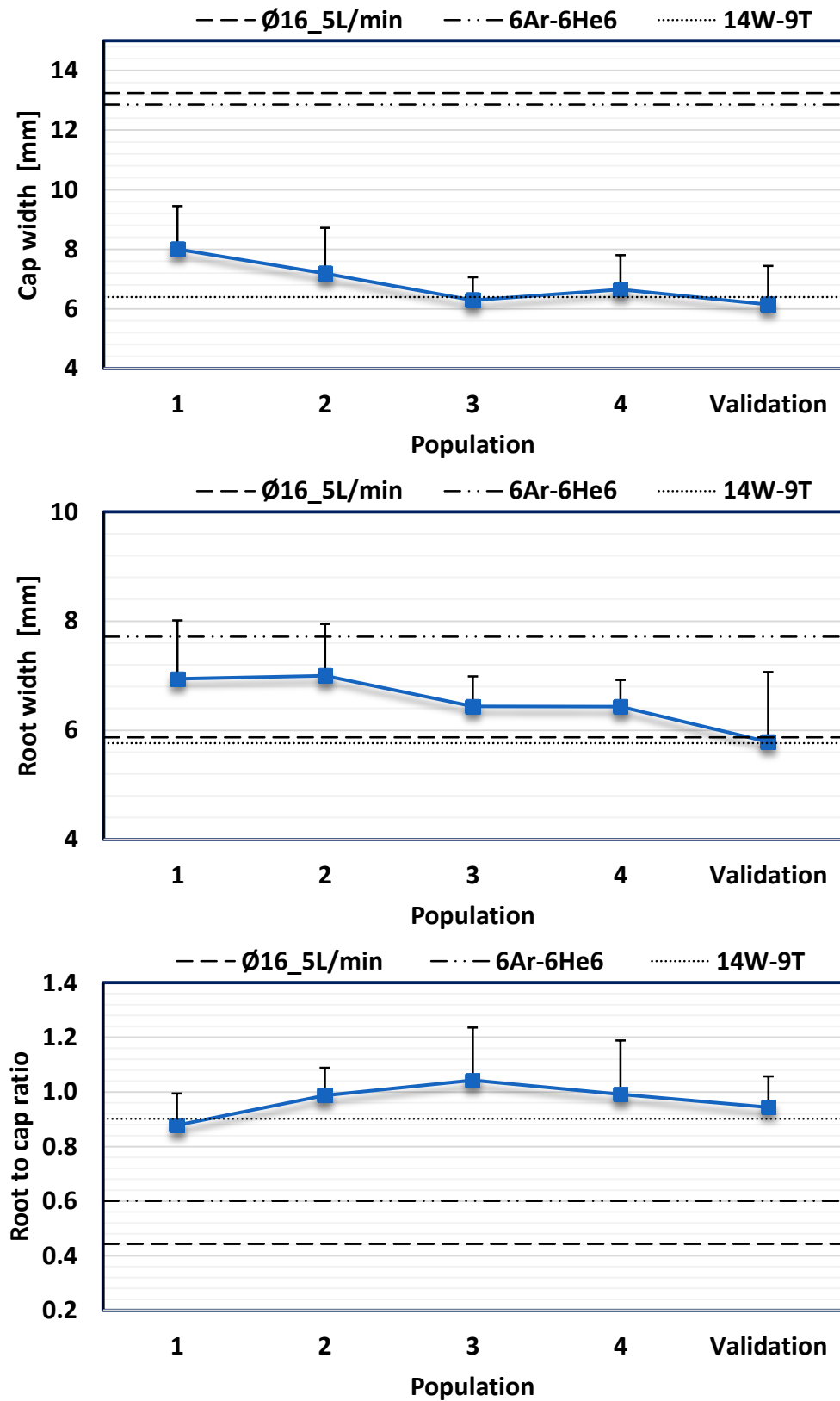


Fig. 7.8 Measured values and mean data per population of the root to cap ratios during the optimisation process.

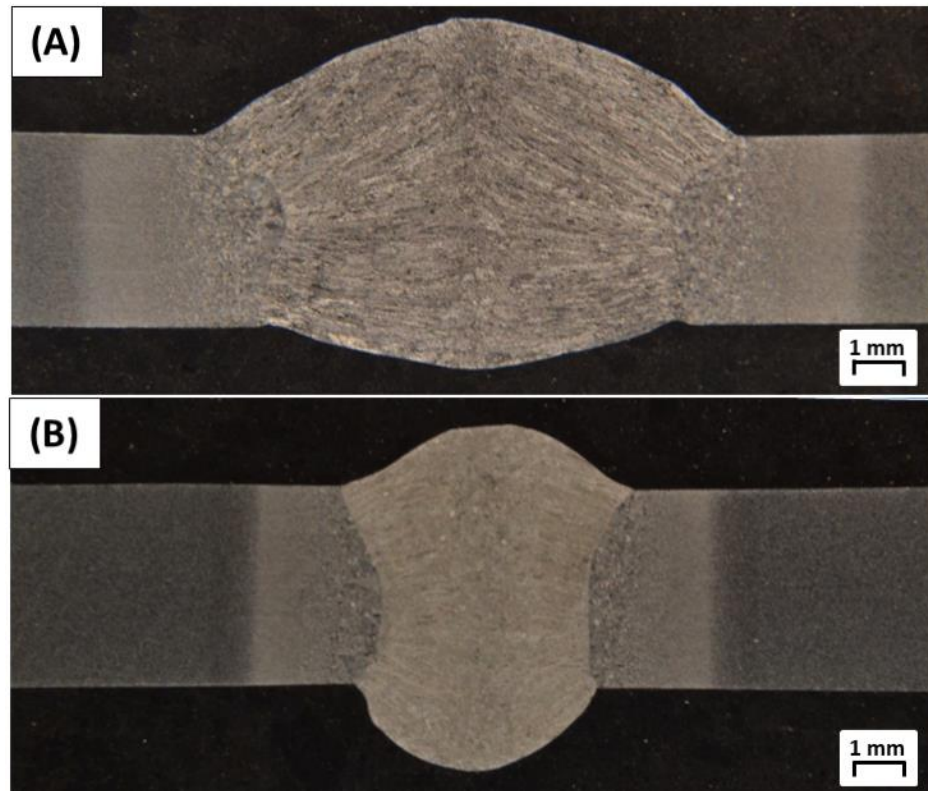


Fig. 7.9 Weld shape (etched). (A) Weld 1.8. (B) Validation from simulation 1.

As discussed in chapter 6, uniformity in the weld shape is desirable, i.e. a root to cap ratio closer to 1, since it influences the angular distortion of the workpiece [7.46]. Hence, the cap width, root width and root to cap ratio were also assessed (see Fig. 7.8). The mean cap width and root width from the validation welds were lower by 1.9 (23%) and 1.2 mm (17%), respectively, compared to population 1. By applying the central composite design method and the simulation process, the validation results presented a higher overall cap width, reducing the root to cap ratio. The root to cap ratios calculated in this chapter were the highest compared to the $\text{Ø}16_5\text{L}/\text{min}$, 6Ar-6He6 and 14W-9T welds, increasing from 0.88 in population 1 to 1.04 in population 3 and maintaining its ratio around 1 afterwards.

An example of the improvements achieved from the optimisation process is presented in Fig. 7.9. The 1.8 weld exhibited a 12.9 mm² HAZ area, a 10.7 mm cap width and an 8.72 mm root width, whilst the validation weld from simulation 1 presented a HAZ area, cap width and root width of 8.5 mm², 5.6 mm and 5.1 mm, respectively. Therefore, the utilised search method and mathematical models were able to define control parameters in the search space that produced welds with a more evenly distributed shape throughout the cross-section of the workpiece (see Fig. 7.9 (B)). The penetration in the validation weld from simulation 1 was improved and can be correlated to the reduced voltage and increased travel speed [7.44, 7.47, 7.48], with significant reduction in the weld metal deposition (see Fig. 7.9 (B)).

7.6.2.2 Weld microstructure

The analysis of the microstructure of all welds and HAZs using the optical microscope indicated a clear reduction in the grain size due to the diminished heat input [7.41, 7.42, 7.49]. For instance, examination showed a greater presence of coarse prior austenite grains in the HAZ region of the 1.8 joint compared to the weld from simulation 3. The modification of parameters throughout the optimisation process produced a reduced HAZ region (see Fig. 7.10), which is correlated to the lower voltage and increased travel speed [7.44, 7.47, 7.48].

Heat input reduction was also evident when assessing the weld microstructure (see Fig. 7.11). Higher content of Widmanstätten ferrite and allotriomorphic ferrite was found in welds of population 1, which is exemplified by the microstructure of the 1.8 case (see Fig. 7.11 (A)).

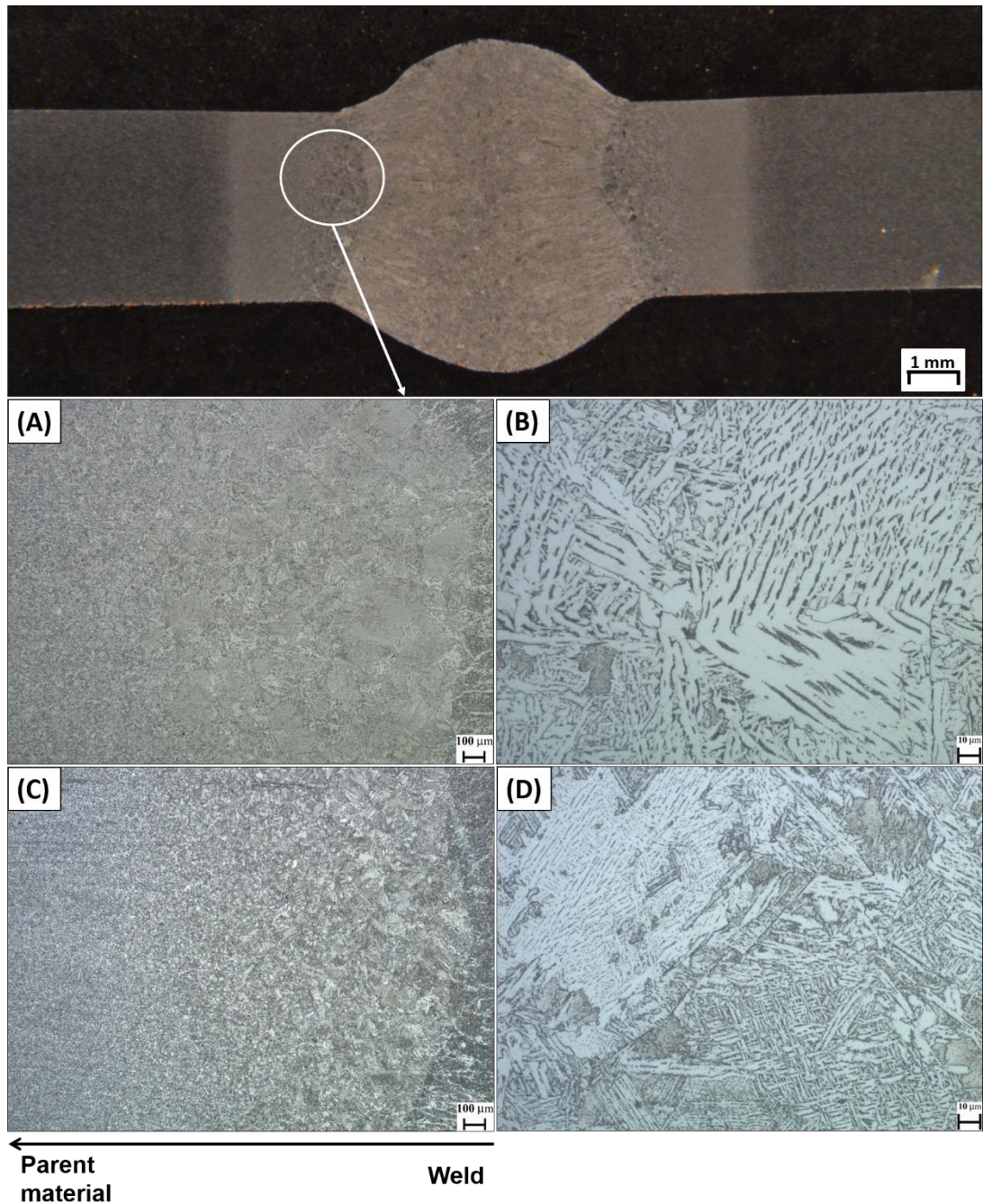


Fig. 7.10 Comparison between HAZ microstructures (etched). Weld 1.8 from population 1: (A) x50. (B) x500. Weld from simulation 3: (C) x50. (D) x500.

The development of acicular ferrite was more significant in the joint from simulation 3 (see Fig. 7.11 (B)), which presented minor presence of

allotriomorphic ferrite. Additionally, further analysis utilising the scanning electron microscope exhibited porosity-free welds (see Fig. 7.12), with the development of a more interlocking microstructure.

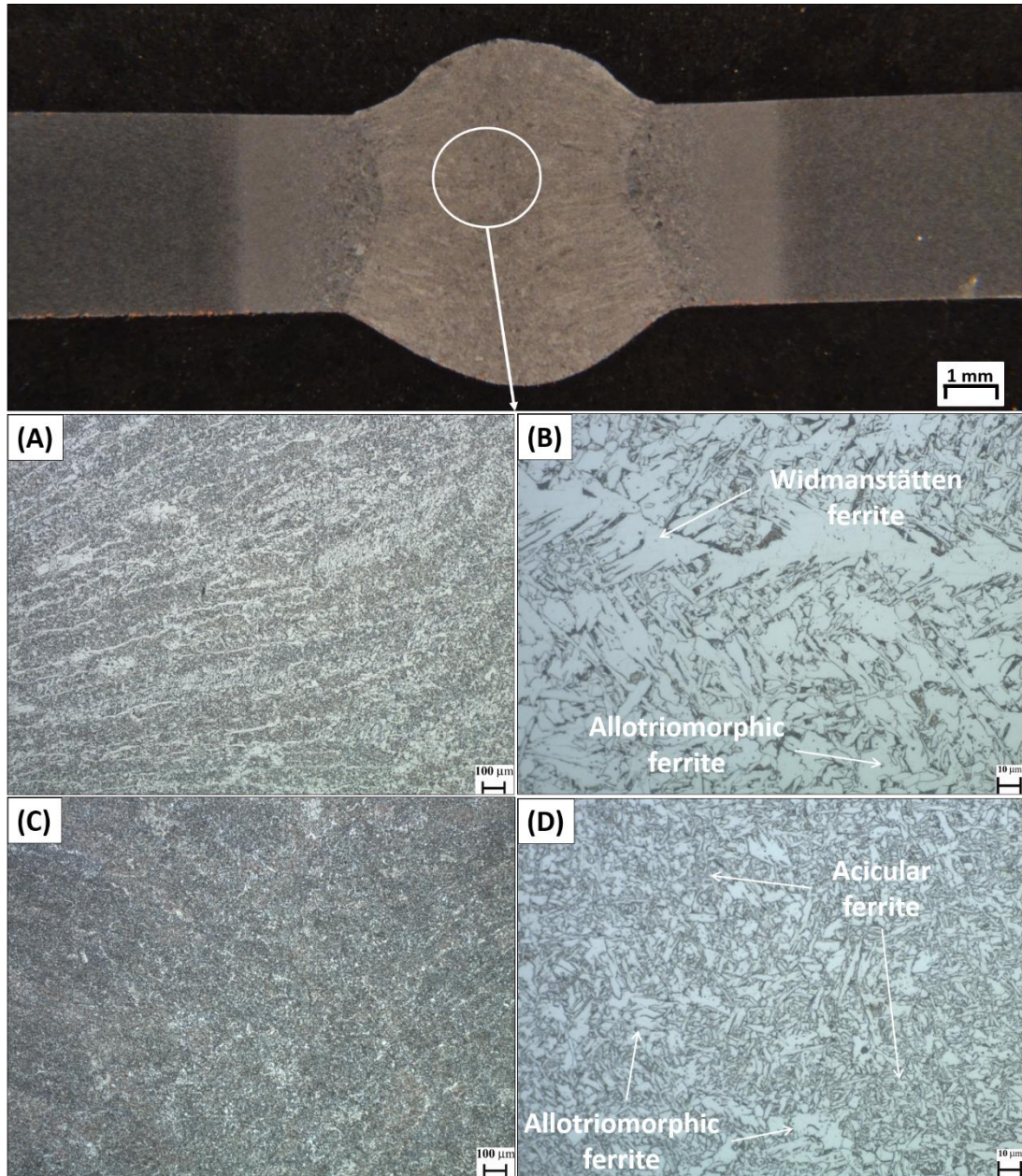


Fig. 7.11 Comparison between weld microstructures of the population 1 and validation procedure (etched). (A) Weld 1.8 from population 1. (B) Weld from simulation 3.

The achieved travel speed of 11 mm/s coupled with a voltage of 21 V were able to refine the grain microstructure due to an increased cooling rate of the joint, decreasing the driving forces for grain boundary mitigation and coarsening [7.41, 7.42, 7.50, 7.51]. This finer microstructure is beneficial to the joint, since it hinders crack propagation, mainly with the development of acicular ferrite [7.52-7.57]. Additionally, the results presented in this section are the best compared to the $\text{Ø}16_5\text{L}/\text{min}$, 6Ar-6He6 and 14W-9T welds, which are the most favourable conditions from chapters 4, 5 and 6, respectively.

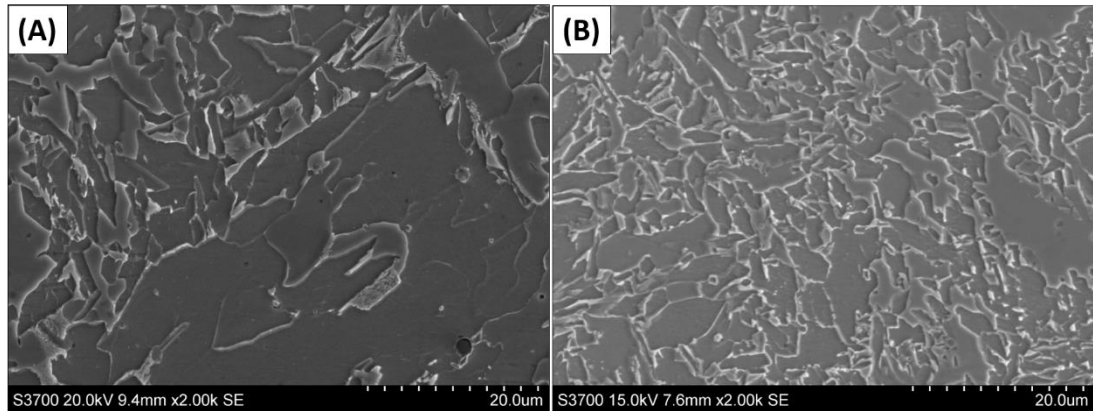


Fig. 7.12 Weld microstructure comparisons, x2000 (etched). (A) Weld 1.8. (B) Weld 3 from the validation process.

7.6.2.3 Mechanical properties

The mean hardness was increased from 234 (population 1) to 253 Hv (validation welds) during the optimisation process (see Fig. 7.13). It has been discussed in chapter 6 that the presence of nitrogen as well as the alternating shielding gas technique improved mechanical properties of the joint such as its hardness [7.41, 7.58-7.61].

For the present study however, the increase in the travel speed and voltage reduction during the optimisation process had a more significant impact on the overall hardness of the joint. This was due to the reduced heat input, with consequent grain refinement of the fusion zone and greater resistance of the welds to localised indentation [7.41, 7.42, 7.50, 7.51, 7.62].

All-weld tensile tests were carried out for the selected weld in simulation 1 (validation 1) to assess the tensile strength, yield strength and elongation of the joint (see Fig. 7.14). This mechanical test was not performed in welds from simulations 2 and 3, since they were expected to present similar results due to the negligible differences between the input parameters. Aiming to evaluate the impact of the optimisation process in the joint, results were compared to the most favourable welds in chapters 4 ($\text{Ø}16_5\text{L}/\text{min}$), 5 (6Ar-6He6) and 6 (14W-9T).

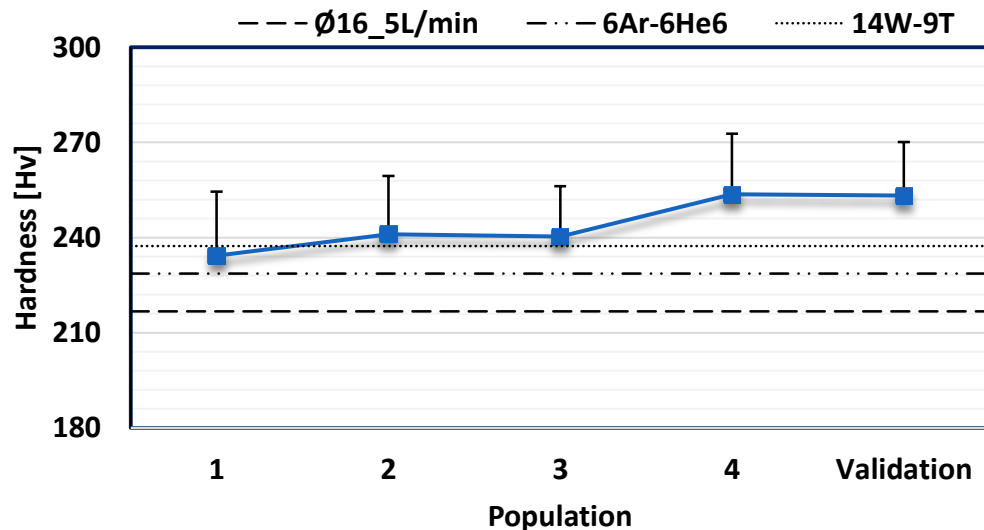


Fig. 7.13 Measured values and mean data per population of the hardness during the optimisation process.

The mean strength of the weld was clearly ameliorated, with the tensile strength increasing from 593 ($\text{\O}16_5\text{L}/\text{min}$) to 736 MPa (Validation 1) and the yield strength, from 522 ($\text{\O}16_5\text{L}/\text{min}$) to 588 MPa (Validation 1). These improvements were correlated to the lower heat input and consequent refined microstructure of the joint from the optimisation process [7.52, 7.63-7.66]. However, a decrement of 71% (from 32 to 9%) in the elongation was found between the $\text{\O}16_5\text{L}/\text{min}$ and validation 1 welds, which was attributed to the improved weld strength [7.67, 7.68]. Hence, it is clear that the presence of N_2 coupled with higher travel speeds of the welding torch was able to produce a joint with significant strength compared to the studied cases in chapter 4.

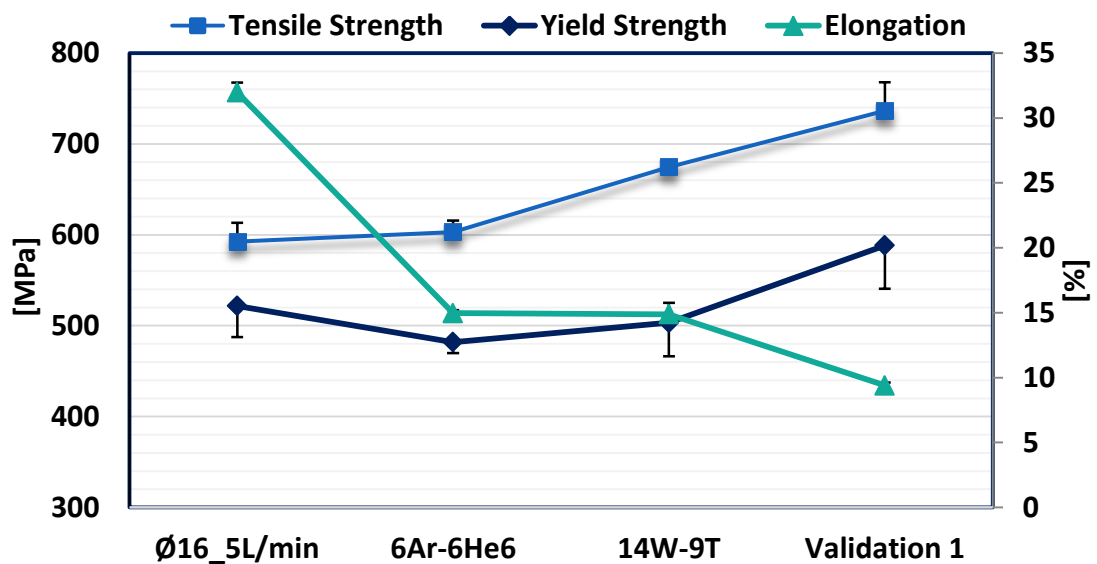


Fig. 7.14 Mean mechanical properties from all-weld tensile tests on the $\text{\O}16_5\text{L}/\text{min}$, 6Ar-6He6, 14W-9T and validation 1 welds.

7.7 Conclusions

This chapter permitted analysing different combinations of input and output variables using Ar5N₂ + He as the shielding gas. The main objective was to minimise the heat transfer to the workpiece by employing mathematical models. These were developed based on results from the genetic algorithm as a search method and allowed for the correlation between control variables and responses.

The use of the genetic algorithm, response surface methodology and desirability function produced welds with an overall 37% lower peak temperature, 42% decreased distortion and 43% smaller grains compared to the most favourable weld in chapter 4 (Ø16_5L/min), reducing the requirements for the workpiece straightening after welding. The higher travel speeds and lower voltages promoted a more efficient process, with a 2.2 times faster welding procedure and reduced heat input.

The genetic algorithm heuristic was able to refine the search space and further create generations that ameliorated the welding conditions. For instance, simulation 1 promoted a mean desirability function of 0.98 in generation 51, demonstrating the positive contribution of the genetic algorithm heuristic in refining the responses and control variables. However, the importance of properly setting up parameters such as the crossover and mutation rates was evident based on the convergence of the voltage results found in simulation 3.

The negligible differences between the model predictions, with a maximum error of 6% compared to the target, and the experimental responses demonstrated the significance of this optimisation process, which can be

extended to various welding processes. There is also potential to reduce the requirement for experiments in the search space of interest and, consequently, lower cost and time.

Analysis of the root to cap ratio exhibited an improved weld shape, where the relation between the root and cap widths was increased and maintained to approximately 1. Overall reductions of 54% in the cap width and 61% in the HAZ compared to the Ø16_5L/min weld promoted a more even weld shape with lower heat input, which benefits the welded structure by reducing its distortion.

Higher travel speeds permitted lower material deposition as well as porosity elimination within the fusion zone, which was verified from the microstructural characterisation analysis. This also allowed for the refinement of the grain microstructure, the decrease of the HAZ area and the development of a more interlocking microstructure, with greater presence of acicular ferrite within the joint. Furthermore, the presence of N coupled with the grain refinement improved the strength of the weld and its resistance to plastic deformation, which was evident from the hardness measurements.

7.8 Bibliography

- [7.1] D. Kim, S. Rhee, and H. Park, “Modelling and optimization of a GMA welding process by genetic algorithm and response surface methodology,” *Int. J. Prod. Res.*, vol. 40, no. 7, pp. 1699–1711, 2002.
- [7.2] S. W. Campbell, F. H. Ley, A. M. Galloway, and N. A. McPherson, “Artificial neural network optimisation of shielding gas flow rate in gas metal arc welding subjected to cross drafts when using alternating

- shielding gases,” *Proc. Inst. Mech. Eng. Part B J. Eng. Manuf.*, vol. 229, no. 1, pp. 122–129, 2015.
- [7.3] D. S. Correia, C. V. Gonçalves, S. S. Da Cunha, and V. A. Ferraresi, “Comparison between genetic algorithms and response surface methodology in GMAW welding optimization,” *J. Mater. Process. Technol.*, vol. 160, no. 1, pp. 70–76, 2005.
- [7.4] D. Kim and S. Rhee, “Optimization of a gas metal arc welding process using the desirability function and the genetic algorithm,” *J. Eng. Manuf.*, vol. 218, pp. 35–41, 2004.
- [7.5] K. Andersen, G. E. Cook, G. Karsai, and K. Ramaswamy, “Artificial neural networks applied to arc welding process modeling and control,” *IEEE Trans. Ind. Appl.*, vol. 26, no. 5, pp. 824–830, 1990.
- [7.6] S. W. Campbell, A. M. Galloway, and N. A. McPherson, “Artificial Neural Network Prediction of Weld Geometry Performed Using GMAW with Alternating Shielding Gases,” *Weld. J.*, vol. 91, no. 6, pp. 174–181, 2012.
- [7.7] S. Mishra and T. DebRoy, “Tailoring gas tungsten arc weld geometry using a genetic algorithm and a neural network trained with convective heat flow calculations,” *Mater. Sci. Eng. A*, vol. 454–455, pp. 477–486, 2007.
- [7.8] L. Carrino, U. Natale, L. Nele, M. L. Sabatini, and L. Sorrentino, “A neuro-fuzzy approach for increasing productivity in gas metal arc welding processes,” *Int. J. Adv. Manuf. Technol.*, vol. 32, no. 5–6, pp. 459–467, 2007.
- [7.9] S. Yamane, T. Yoshida, Y. Kaneko, H. Yamamoto, and K. Oshima, “Estimation of wire extension length using neural network in MIG

- welding,” *Weld. Int.*, vol. 23, no. 7, pp. 510–516, 2009.
- [7.10] S. Bhattacharya, K. Pal, and S. K. Pal, “Multi-sensor based prediction of metal deposition in pulsed gas metal arc welding using various soft computing models,” *Appl. Soft Comput. J.*, vol. 12, no. 1, pp. 498–505, 2012.
- [7.11] D. Kim, M. Kang, and S. Rhee, “Determination of Optimal Welding Conditions with a Controlled Random Search Procedure,” *Weld. J.*, no. August, pp. 125–130, 2005.
- [7.12] P. Sathiya, P. M. Ajith, and R. Soundararajan, “Genetic algorithm based optimization of the process parameters for gas metal arc welding of AISI 904 L stainless steel,” *J. Mech. Sci. Technol.*, vol. 27, no. 8, pp. 2457–2465, 2013.
- [7.13] K. S. Prasad, C. S. Rao, and D. N. Rao, “Optimization of fusion zone grain size, hardness, and ultimate tensile strength of pulsed current micro plasma arc welded Inconel 625 sheets using genetic algorithm,” *Acta Metall. Sin. (English Lett.)*, vol. 25, no. 3, pp. 179–189, 2012.
- [7.14] S. Bag and A. De, “Development of efficient numerical heat transfer model coupled with genetic algorithm based optimisation for prediction of process variables in GTA spot welding,” *Sci. Technol. Weld. Join.*, vol. 14, no. 4, pp. 333–345, 2009.
- [7.15] D. Kim and S. Rhee, “Optimization of Arc Welding Process Parameters Using a Genetic Algorithm,” *Weld. J.*, vol. 80, no. 7, p. 184s–189s, 2001.
- [7.16] D. S. Correia, C. V. Gonçalves, S. S. C. Junior, and V. A. Ferraresi, “GMAW welding optimization using genetic algorithms,” *J. Brazilian Soc. Mech. Sci. Eng.*, vol. 26, no. 1, pp. 28–32, 2004.
- [7.17] A. Kumar and T. DebRoy, “Tailoring complex weld geometry through

- reliable heat-transfer and fluid-flow calculations and a genetic algorithm,” *Metall. Mater. Trans. A*, vol. 36A, no. October, pp. 2725–2735, 2005.
- [7.18] J. P. Jia, H. Zhang, and H. Huang, “Optimization of Welding Process Parameters for Rotating Arc Welding Sensor Based on Genetic Algorithm,” *Mater. Sci. Forum*, vol. 575–578, pp. 769–773, 2008.
- [7.19] D. T. Thao, I. S. Kim, H. H. Na, S. M. Jung, and J. Y. Shim, “Development of mathematical model with a genetic algorithm for automatic GMA welding process,” *Int. J. Adv. Manuf. Technol.*, pp. 837–847, 2014.
- [7.20] A. S. Shahi and S. Pandey, “Welding current prediction in GMAW and UGMAW processes using response surface methodology,” *Sci. Technol. Weld. Join.*, vol. 11, no. 3, pp. 341–346, 2006.
- [7.21] D. L. Olson, R. D. Dixon, and A. L. Liby, *Welding: Theory and Practice*. 1990.
- [7.22] S. Kodama, K. Sugiura, S. Nakanishi, Y. Tsujimur, M. Tanaka, and A. B. Murphy, “Effect of plasma heat source characteristics on nitrogen absorption in gas tungsten arc weld metal,” *Weld. World*, vol. 57, no. 6, pp. 925–932, 2013.
- [7.23] J. Littleton, J. Lammas, and M. F. Jordan, “Nitrogen Porosity in Gas Shielded Arc Welding of Copper,” *Weld. J.*, vol. 12, pp. 561–565, 1974.
- [7.24] S. Kodama et al., “Nitrogen absorption phenomenon of GTA welding with nitrogen-mixed shielding gases: effect of plasma characteristics on nitrogen content in GTA welded metal,” *Weld. Int.*, vol. 29, no. 4, pp. 262–269, 2015.
- [7.25] J. J. Grefenstette, “Optimization of control parameters for genetic algorithm,” *IEEE Trans. Syst. Man. Cybern.*, vol. 16, no. 1, pp. 122–128,

1986.

- [7.26] C. R. Reeves, "Using Genetic Algorithms With Small Populations," in Using genetic algorithms with small populations. Proceedings of the 5th International Conference on Genetic Algorithms, 1993, pp. 92–99.
- [7.27] A. Pat, "On Construction of a Class of Orthogonal Arrays (Thesis)," no. May, 2012.
- [7.28] Y. S. Tarng and W. H. Yang, "Optimisation of the weld bead geometry in gas tungsten arc welding by the taguchi method," *Int. J. Adv. Manuf. Technol.*, vol. 14, no. 8, pp. 549–554, 1998.
- [7.29] R. Malhotra, N. Singh, and Y. Singh, "Genetic Algorithms: Concepts, Design for Optimization of Process Controllers," *Comput. Inf. Sci.*, vol. 4, no. 2, pp. 39–54, 2011.
- [7.30] P. Angelopoulos, H. Evangelaras, and C. Koukouvinos, "Small , balanced , efficient and near rotatable central composite designs," *J. Stat. Plan. Inference*, vol. 139, no. 6, pp. 2010–2013, 2008.
- [7.31] M. P. Allen, "The coefficient of determination in multiple regression," in *Understanding Regression Analysis*, 1997, pp. 91–95.
- [7.32] C. L. Cheng, Shalabh, and G. Garg, "Coefficient of determination for multiple measurement error models," *J. Multivar. Anal.*, vol. 126, pp. 137–152, 2014.
- [7.33] B. A. Öztürk, G. W. Weber, and G. Köksal, "Desirability Functions in Multiresponse Optimization," in *Communications in Computer and Information Science*, vol. 499, 2015, pp. 129–146.
- [7.34] N. R. Costa, J. Lourenço, and Z. L. Pereira, "Desirability function approach: A review and performance evaluation in adverse conditions," *Chemom. Intell. Lab. Syst.*, vol. 107, no. 2, pp. 234–244, 2011.

- [7.35] G. Derringer and R. Suich, “Simultaneous Optimization of Several Response Variables,” *J. Qual. Technol.*, vol. 12, no. 4, pp. 214–219, 1980.
- [7.36] I. García, L. A. Sarabia, M. C. Ortiz, and J. M. Aldama, “Optimization of the chromatographic conditions for the determination of hormones by gas chromatography with mass spectrometry detection,” *Anal. Chim. Acta*, vol. 544, no. 1–2 SPEC. ISS., pp. 26–35, 2005.
- [7.37] M. E. Rueda, L. A. Sarabia, A. Herrero, and M. C. Ortiz, “Optimisation of a flow injection system with electrochemical detection using the desirability function: Application to the determination of hydroquinone in cosmetics,” *Anal. Chim. Acta*, vol. 479, no. 2, pp. 173–184, 2003.
- [7.38] L. V. Candioti, J. C. Robles, V. E. Mantovani, and H. C. Goicoechea, “Multiple response optimization applied to the development of a capillary electrophoretic method for pharmaceutical analysis,” *Talanta*, vol. 69, no. 1, pp. 140–147, 2006.
- [7.39] B. Y. Kang, Y. K. D. V Prasad, M. J. Kang, H. J. Kim, and I. S. Kim, “The effect of alternate supply of shielding gases in austenite stainless steel GTA welding,” *J. Mater. Process. Technol.*, vol. 209, no. 10, pp. 4722–4727, 2009.
- [7.40] Y. H. Chang, “Improve GMAW and GTAW with alternating shield gases,” *Weld. J.*, vol. 85, no. 2, pp. 41–43, 2006.
- [7.41] S. W. Campbell, A. M. Galloway, and N. A. McPherson, “Techno-economic evaluation on the effects of alternating shielding gases for advanced joining processes,” *Proc. Inst. Mech. Eng. Part B J. Eng. Manuf.*, vol. 225, no. 10, pp. 1863–1872, 2011.
- [7.42] S. W. Campbell, A. M. Galloway, N. A. McPherson, and A. Gillies, “Evaluation of gas metal arc welding with alternating shielding gases for

- use on AA6082T6,” *Proc. Inst. Mech. Eng. Part B J. Eng. Manuf.*, vol. 226, no. 6, pp. 992–1000, 2012.
- [7.43] T. Gray, D. Camilleri, and N. McPherson, “Fabrication of stiffened thin-plate structures and the problem of welding distortion,” in *Control of Welding Distortion in Thin-Plate Fabrication*, 2014, pp. 14–38.
- [7.44] A. Haelsig, M. Kusch, and P. Mayr, “Calorimetric analyses of the comprehensive heat flow for gas metal arc welding,” *Weld. World*, vol. 59, no. 2, pp. 191–199, 2014.
- [7.45] D. E. Goldberg, *Genetic Algorithms in Search, Optimization and Machine Learning*. Boston: Addison-Wesley Longman, 1989.
- [7.46] T. Gray, D. Camilleri, and N. McPherson, “Understanding welding distortion: thermal fields thermo-mechanical effects,” in *Control of Welding Distortion in Thin-Plate Fabrication*, Woodhead Publishing Limited, 2014, pp. 53–76.
- [7.47] S. Lathabai, “Joining of aluminium and its alloys,” in *Fundamentals of Aluminium Metallurgy: Production, Processing and Applications*, Woodhead Publishing Limited, 2010, pp. 607–654.
- [7.48] D. S. Naidu, S. Ozcelik, and K. L. Moore, “Gas Metal Arc Welding: Modeling,” in *Modeling, Sensing and Control of Gas Metal Arc Welding*, 2003, pp. 9–93.
- [7.49] D. Min, J. Shen, S. Lai, and J. Chen, “Effect of heat input on the microstructure and mechanical properties of tungsten inert gas arc butt-welded AZ61 magnesium alloy plates,” *Mater. Charact.*, vol. 60, no. 12, pp. 1583–1590, 2009.
- [7.50] N. S. Barabokhin et al., “Technological special features of welding 1460 high-strength aluminium alloy,” *Weld. Int.*, vol. 14, no. 6, pp. 468–470,

2000.

- [7.51] R. G. Tazetdinov, O. M. Novikov, A. S. Persidskii, B. A. Khasyanov, E. N. Ivanov, and L. T. Plaksina, “Arc welding in shielding gases with alternate pulsed supply of dissimilar gases,” *Weld. Int.*, vol. 7116, no. May 2015, pp. 1–4, 2012.
- [7.52] I. Madariaga, I. Gutiérrez, C. García-De Andrés, and C. Capdevila, “Acicular ferrite formation in a medium carbon steel with a two stage continuous cooling,” *Scr. Mater.*, vol. 41, no. 3, pp. 229–235, 1999.
- [7.53] J. Du, M. Strangwood, and C. L. Davis, “Effect of TiN Particles and Grain Size on the Charpy Impact Transition Temperature in Steels,” *J. Mater. Sci. Technol.*, vol. 28, no. 10, pp. 878–888, 2012.
- [7.54] H. K. D. H. Bhadeshia, “Bainite in Steels: transformations, microstructure and properties.” IOM Communications, London, 2001.
- [7.55] M. Díaz-Fuentes, A. Iza-Mendia, and I. Gutiérrez, “Analysis of different acicular ferrite microstructures in low-carbon steels by electron backscattered diffraction. Study of their toughness behavior,” *Metall. Mater. Trans. A Phys. Metall. Mater. Sci.*, vol. 34 A, no. 11, pp. 2505–2516, 2003.
- [7.56] R. A. Farrar and P. L. Harrison, “Acicular ferrite in carbon-manganese weld metals: An overview,” *J. Mater. Sci.*, vol. 22, no. 11, pp. 3812–3820, 1987.
- [7.57] W. Wang, W. Yan, L. Zhu, P. Hu, Y. Shan, and K. Yang, “Relation among rolling parameters, microstructures and mechanical properties in an acicular ferrite pipeline steel,” *Mater. Des.*, vol. 30, no. 9, pp. 3436–3443, 2009.
- [7.58] D. D. Nage, V. S. Raja, and R. Raman, “Effect of nitrogen addition on

- the microstructure and mechanical behavior of 317L and 904L austenitic stainless steel welds,” *J. Mater. Sci.*, vol. 41, no. 7, pp. 2097–2112, 2006.
- [7.59] T. Wegrzyn, “An attempt at the classification of steel weld metals and arc-welding methods on the basis of nitrogen concentration in the weld metal,” *Weld. Int.*, vol. 13, no. 3, pp. 173–179, 1999.
- [7.60] H. Y. Huang, “Effects of shielding gas composition and activating flux on GTAW weldments,” *Mater. Des.*, vol. 30, no. 7, pp. 2404–2409, 2009.
- [7.61] P. Kah and J. Martikainen, “Influence of shielding gases in the welding of metals,” *Int. J. Adv. Manuf. Technol.*, vol. 64, no. 9–12, pp. 1411–1421, 2013.
- [7.62] J. Wang, Y. Li, and P. Liu, “Effect of weld heat input on toughness and structure of HAZ of a new super-high strength steel,” *Bull. Mater. Sci.*, vol. 26, no. 3, pp. 301–305, 2003.
- [7.63] H. Bhadeshia and R. Honeycombe, “Acicular Ferrite,” in *Steels: Microstructure and Properties*, 4th ed., Elsevier Ltd, 2017, pp. 203–216.
- [7.64] H. Bhadeshia and R. Honeycombe, *Steels: Microstructure and Properties*, 4th ed. Elsevier Ltd., 2017.
- [7.65] W. L. Costin, O. Lavigne, and A. Kotousov, “A study on the relationship between microstructure and mechanical properties of acicular ferrite and upper bainite,” *Mater. Sci. Eng. A*, vol. 663, pp. 193–203, 2016.
- [7.66] R. A. Ricks, P. R. Howell, and G. S. Barritte, “The nature of acicular ferrite in HSLA steel weld metals,” *J. Mater. Sci.*, vol. 17, no. 3, pp. 732–740, 1982.
- [7.67] S. Ragu Nathan, V. Balasubramanian, S. Malarvizhi, and a. G. Rao, “Effect of welding processes on mechanical and microstructural

characteristics of high strength low alloy naval grade steel joints,” Def. Technol., vol. 11, no. 3, pp. 308–317, 2015.

- [7.68] J. R. Davis, “Structure / Property Relationships in Irons and Steels,” Met. Handb. Desk, Second Ed., pp. 153–173, 1998.

“Thoughts become words, which become habits that define your values.

Values become character, and your character, your destiny”

Mahatma Gandhi

Chapter 8

Thesis conclusion

8.1 Final remarks

This thesis was able to introduce significant findings and contribute to a better understanding of the alternating shielding gas technique in the gas metal arc welding (GMAW) process. Benefits of this novel method permitted to reduce the shielding gas consumption even further, accelerate the welding procedure, lower the heat input, expand the shielding gas options by adding introducing N₂ during welding, and optimise the welding process.

Analyses of the reduced shielding gas flow rate (SGFR) under the premixed method in chapter 4 demonstrated that modifications in the nozzle diameter as well as on the SGFR were not capable of influencing significantly the weld properties. For instance, hardness and tensile strength as well as the weld shape were constant despite modifying the SGFR and nozzle diameter. Yet, mild improvements in terms of grain size, distortion, and temperature were found when decreasing the shielding gas flow rate from 9 to 5 L/min. Hence, it is clear that it is possible to reduce the SGFR to 5 L/min while maintaining the weld integrity, achieving savings of 4 L/min.

Subsequently, the alternating shielding gas method was introduced in chapter 5 to assess its benefits under a lower SGFR. Improvements were found in terms of heat input and microstructural and mechanical properties of the

weld. For instance, the heat-affected zone (HAZ) was lower by 23%, grains were finer by 16%, and welds stronger by 3% compared to the Ø16_5L/min case. Reduced deformation of the workpiece and better penetration of the joint were observed, where the most favourable option was a SGFR of 6 L/min under a 6 Hz frequency. Additionally, results indicated that increased travel speeds could be easily introduced, diminishing the heat input, improving the weld properties even further, and controlling the gas wastage.

Since the alternating shielding gas technique has been limited to Ar, CO₂ and He as protective gases, N₂ was investigated in chapter 6. Replacing CO₂ with N₂ in the welding system promoted reductions in the fume development, weld temperature and workpiece distortion. Greater travel speeds were achieved, decreasing the heat input and improving the strength of the joint, despite the development of slags in few cases. Analysis showed that the slag formation could be reduced by either choosing a different electrode type or removing the primer from the root gap edges prior to welding. Furthermore, the two times faster welding procedures allowed for evident microstructural refinement, which was beneficial to the weld strength due to the greater density of acicular ferrite in welds under the presence of N₂. However, the comparison between the Ar5N₂ + He (alternated supply) and Ar5N₂ (premixed supply) joints demonstrated negligible differences, which implies that He as a protective could be removed, adding to cost savings.

An attempt was carried out in chapter 7 to explore further combinations of input variables that could yield good quality welds under the Ar5N₂ + He gas supply, utilising the genetic algorithm heuristic coupled with mathematical models. Compared to results in chapters 4, 5 and 6, this systematic approach was beneficial in terms of refinement of the grain size in

the weld microstructure, promoting the acicular ferrite development as well as lower temperatures of the joint and deformation of the workpiece. The developed mathematical models were able to produce a more even weld shape throughout the weld cross-section as well as a reduced HAZ and greater penetration, contributing to a lower distortion of the workpiece. These models consistently predicted the output parameters, which is important in manufacturing industries, since it reduces the requirement for experimental work. In addition, the optimisation process eliminated the porosity formation within the fusion zone from the presence of N_2 and required less material deposition due to the faster welding speeds, hence stimulating decreased heat transfer to the welded structures.

Clear improvements were achieved throughout this thesis work by modifying the supply method from premixed to alternated, replacing the $Ar20CO_2$ shielding gas for $Ar20CO_2 + He$, $Ar5N_2$ or $Ar5N_2 + He$, and increasing the travel speeds of the welding torch. Compared to the initial parameters used in this work (chapter 4), the optimised control variables (chapter 7) were able to present an overall decrement of 46% (2.6 mm) in the workpiece distortion, 37% (228 °C) in the joint temperature, 54% (7.2 mm) in the top width, and 61% (12.3 mm²) in the HAZ area, whereas the strength of the joint was enhanced by 26% (152.4 MPa) and the hardness by 18% (39 Hv).

This research work was capable of further reducing the heat input to the joints, refine the microstructure of the fusion zone with greater presence of acicular ferrite, and enhance the performance of the arc plasma, adding to the scientific knowledge regarding the alternating shielding gas technique and the GMAW. Such findings, besides adding positive contribution to the welding field, demonstrated that the alternating shielding gas technique can be

employed to varied welding conditions, ameliorating the weld properties and reducing costs by hastening the welding process. Additionally, it was shown that it is possible to use N_2 mixtures to weld the high strength DH36 low alloy steel without compromising the joint quality, potentially diminishing the fume development and shielding gas usage.

8.2 Future contributions

The research work generated important findings to the welding field in advanced manufacturing. However, new challenges have been identified in different welding aspects, where further research is essential to enhance the scientific knowledge, as follow:

- The alternating shielding gas method utilising $Ar5N_2 + He$ could be employed using other types of steel besides the DH36 grade and the SF-1A electrodes. This would extend the material options available by assessing ways of eliminating the porosity formation and evaluating its development.
- In chapter 6 it was demonstrated for specific cases that the premixed supply of $Ar5N_2$ provided similar outcomes compared to that of the $Ar5N_2 + He$ welds. Therefore, analysis using the premixed method ($Ar5N_2$) could be extended and compared to other $Ar5N_2 + He$ cases, focusing on the elimination of He as a protective gas due to its expensive cost.
- The N_2 percentage in the ArN_2 mixture was fixed to 5%. Yet, other ratios could be considered using the alternating shielding gas technique to determine thresholds in the N_2 absorption by

the joint as well as optimal conditions based on the amount of N_2 in the Ar mixture.

- It was suggested that the alternating shielding gas method assisted with the reduction of porosity within the joint, which was expected from the presence of N and O. Therefore, investigations could be performed to measure the N and O content within the weld, verifying the impact of He, the influence of the various travel speeds, and the effect of the alternating shielding gas process.
- Simulations using ArN_2 mixtures alternated with different shielding gases could be carried out to assist with understanding how the presence of N_2 influences the joint during the alternating shielding gas process. Furthermore, such simulations could consider the presence of metal vapour in the arc plasma and the development of the molten pool during welding, examining their influence on the N absorption/ desorption when utilising the alternating shielding gas method.
- Considering the distance between the nozzle exit and the gas cylinder, it was possible that some mixing between the shielding gases occurred during their alternation. Hence, the alternation technique can be ameliorated by reducing the hose length, for instance.

Appendix A

LabVIEW: visual programming

Introduction

For this study it was essential to control and precisely measure certain features of the welding system. Considering its wide industrial and academic application, the LabVIEW software was chosen as a tool to measure the distortion of the workpiece, define the speed of the welded structure underneath the welding torch and record data regarding the temperature of the joint.

LabVIEW utilises graphical programming syntax, allowing reduced programming time [A.1]. It is an environment to develop sophisticated measurement tools and test and control systems. Two main visual programs were developed in order to control the welding process. 1) to measure the distortion of the structure before and after welding. 2) to simultaneously move the plate under the torch and measure the temperature of the weld.

Distortion measurement

The path followed by the laser throughout the distortion data acquisition has been shown in chapter 3. Fig. A 1 shows the panel used to control the distortion measurements. A frequency that could vary between 500

and 7500 Hz was provided, controlling the stepper motors speed and, consequently, the speed of the laser. Dimensions of the workpiece were given for both the transverse and longitudinal directions coupled with the distance (desired precision) between paths in the longitudinal direction. In case the transverse dimension was lower than the desired precision, the software would stop the measurements and a warning sign would flash. In addition, the panel provided updated values of the distance read by the laser in mm, the voltage, and the time elapsed.

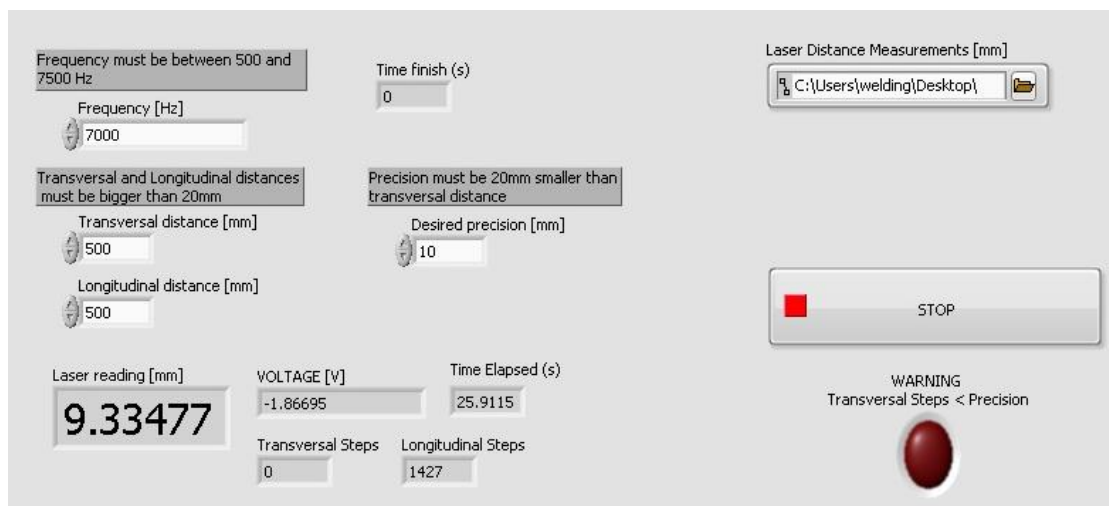


Fig. A 1 Panel to control the parameters of window to set up the laser position.

Voltage signals from the laser readings were translated as the distance between the laser and the surface of the workpiece, given in mm. The final distortion at a certain point of the workpiece would be the difference between points located at the same position before and after the welding procedure. Fig. A 2 exhibits the first half of the block diagram with case structures to control, for instance, the laser movement. Fig. A 3 shows the second half of the block

diagram in Fig. A 2, where the system converted the voltage signals to distance.

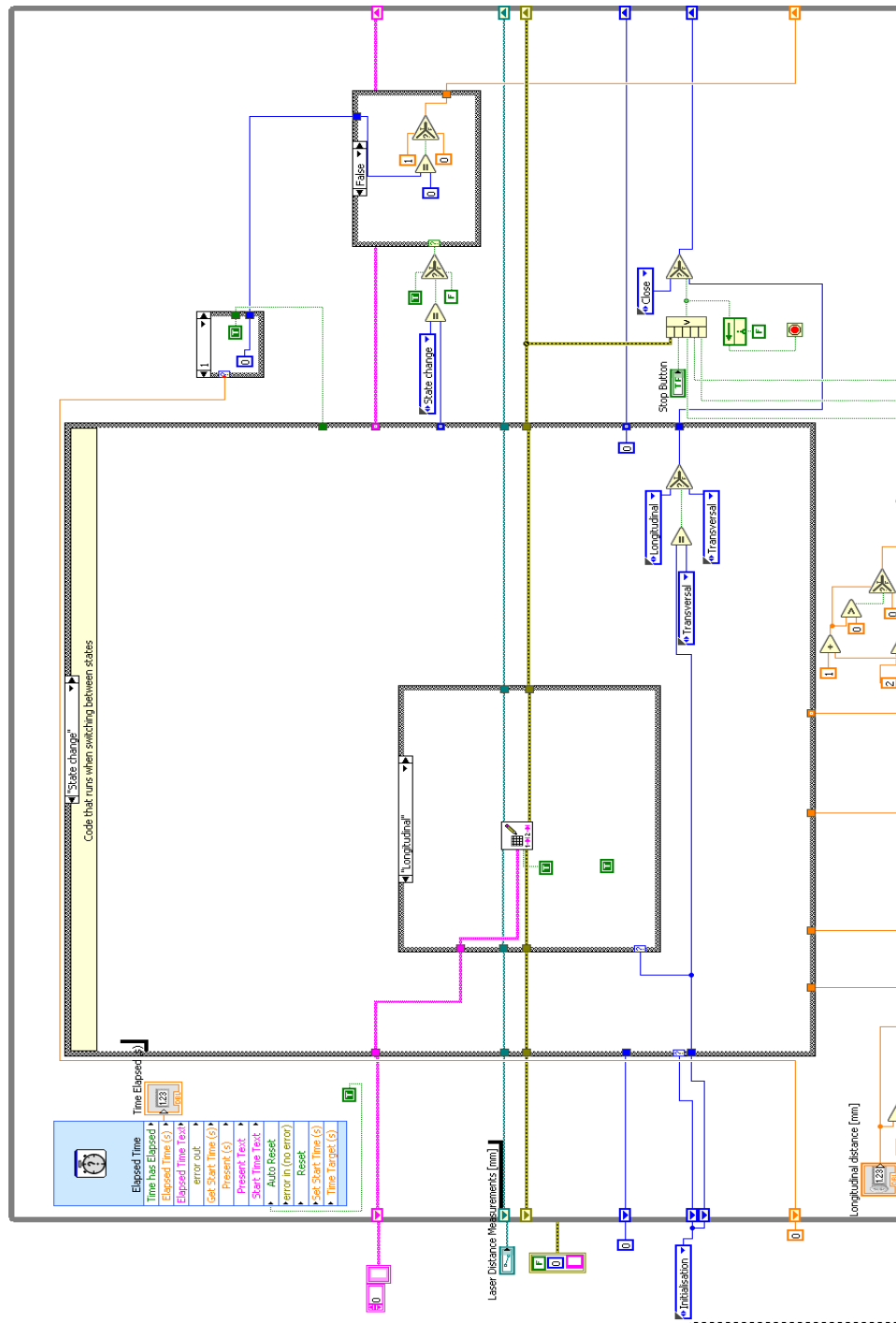


Fig. A 2 First half of the block diagram to measure the workpiece's distortion.

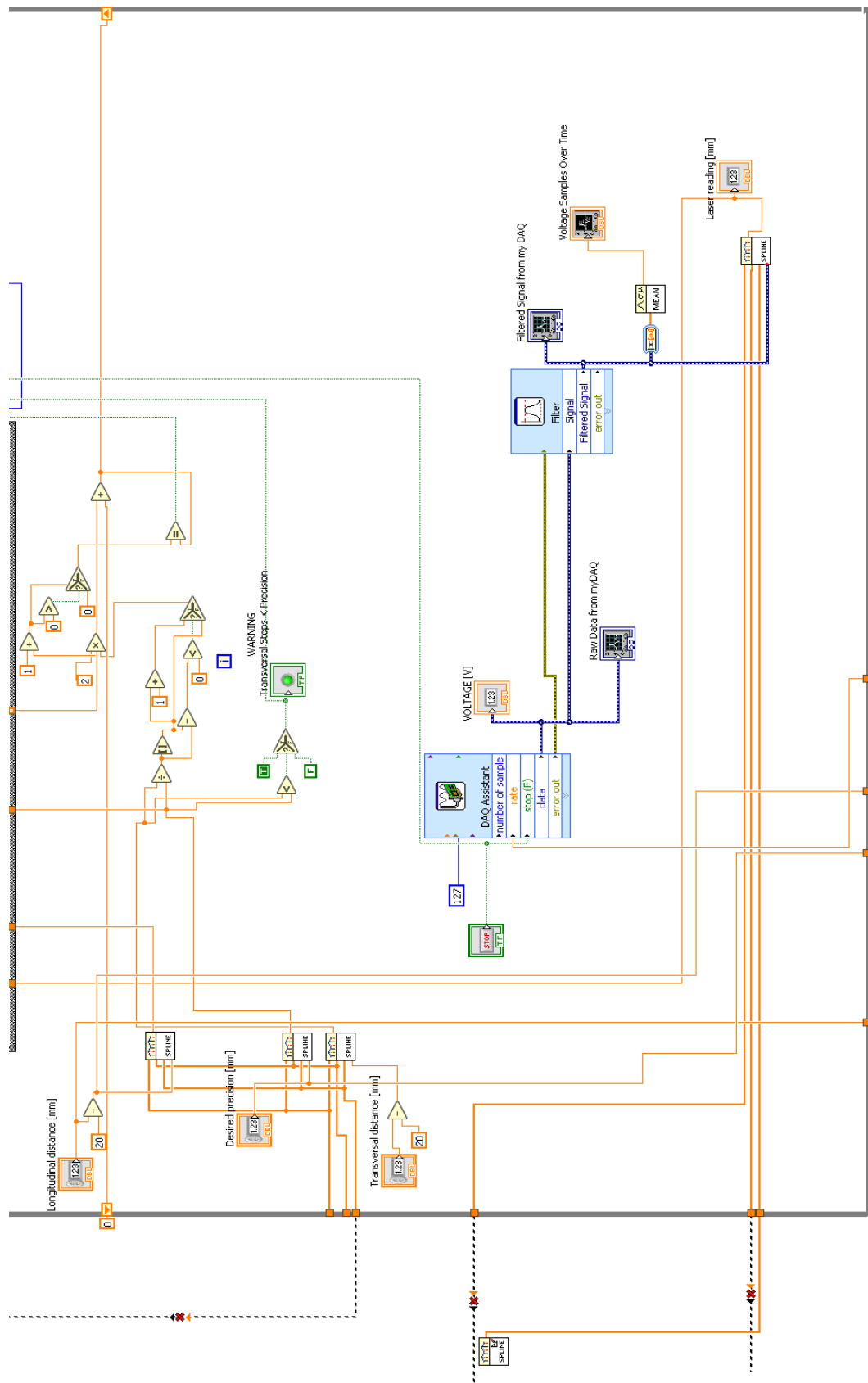


Fig. A 3 Second half of the block diagram to measure the workpiece's distortion.

Five case structures were created within the while loop. 1) Initialisation. 2) Transverse direction. 3) Longitudinal direction. 4) State change. 5) Close. In the *Initialisation* case structure, an excel file of choice was initialised, with all its previous data being deleted and the current distortion values, recorded. Subsequently, the laser was required to move in the longitudinal and transverse directions, reading values on the plate's surface. The *State change* case structure was responsible to modify the directions of the laser, whilst the *Close* one ended the running once the entire plate was read.

Plate movement and temperature measurements

The movement of the workpiece as well as the recording of the temperature during the welding procedure were concurrent. In the control panel (see Fig. A 4) it was possible to define the speed of the workpiece, select the welding direction and specify an excel file to record the temperature data. The *STOP Welding* button was used when the welding process was complete to stop the workpiece's movement without interrupting the temperature measurements, stopped after 45 minutes (*STOP Temperature* button). In addition, the *Waveform Chart* showed the temperature in real-time, with the time elapsed being constantly visible during the entire process.

In the block diagram created to control the movement of the workpiece (see Fig. A 5), the input speed was converted into steps to move the stepper motors. Once the workpiece started moving the welding torch activated to start the welding process. With the welding procedure finished, the STOP Welding button was activated, leaving the thermocouples measuring the temperature during the next 45 minutes.

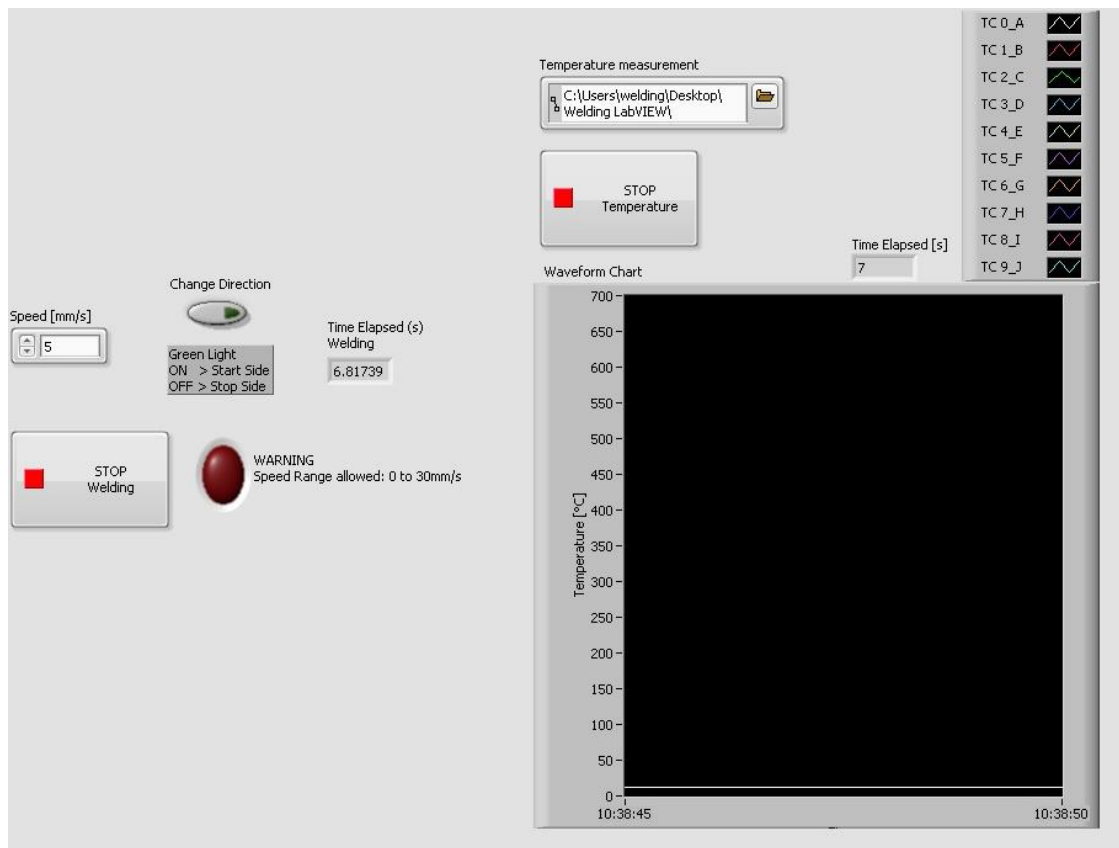


Fig. A 4 Front panel to control the welding movement and the temperature measurement.

The virtual circuit developed to monitor and record data from thermocouples is shown in Fig. A 6. The system was able to record data from up to 10 thermocouples. The signal from the temperature measurements was first filtered and then recorded by blocks, which represented a specific thermocouple. Finally, data was sent to and recorded in an excel spreadsheet for further analysis.

Appendix B

Coding in Java and R

Programming languages

Part of the optimisation procedure in chapter 7 was carried out by coding in Java and R languages. While Java is class-based, object-oriented, and designed to reduce the number of implementation dependencies, R was developed for statistical computing and graphics. This thesis section discusses the code developed aiming to optimise the welding inputs, resulting in high-quality welds and reduced heat input.

The genetic algorithm phase

The genetic algorithm to create populations 1, 2 and 3 was initially implemented in three classes: *TestingGA*, *GA*, and *SolutionGA*. While *GA* was a subclass of *TestingGA*, *SolutionGA* was a subclass of *GA* (see Fig. B 1).

In the *TestingGA* class the user was firstly asked which generation (population) would be analysed. In case that was the first population, the class would access the method *initialG* in the subclass *GA* and build the first matrix with input variables for experiments. Conversely, if the population to be analysed was not the first one, the class would access methods such as the *subsequentG* to analyse data provided by the user.

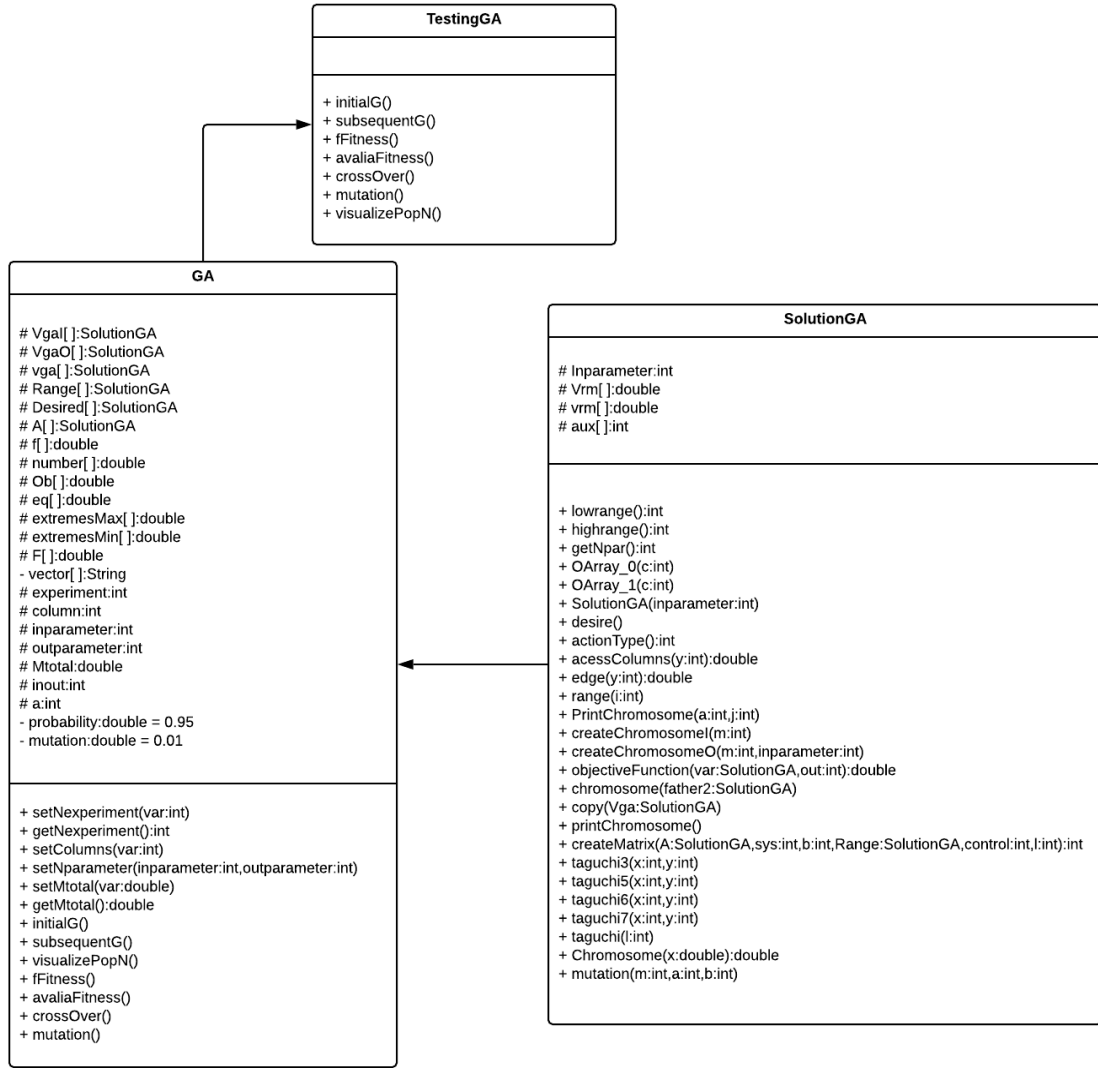


Fig. B 1 Unified Modeling Language diagram representation of the genetic algorithm classes.

After gathering the required information, the *TestingGA* class accessed the *GA* subclass. If the first population was the considered case, the Taguchi matrix was generated and used to create a matrix of input variables to be utilised for the first set of experiments (*initialG* method). Otherwise, the user would provide additional information by accessing the *subsequentG* method, namely the number of welds performed and the number of responses. Additionally, the input and output variables would be manually inserted to allow for the assessment of all welds.

The matrix containing combinations of input and output variables was evaluated and refined through the fitness, crossover and mutation operators using the *fFitness* and *avaliaFitness*, *crossover*, and *mutation* methods, respectively. The new population after the assessment stage was printed by the *visualizePopN* method, exhibiting only the optimised input variables that would be employed in the next set of experiments.

Among the various methods developed in the *SolutionGA* subclass the main ones include the *range* method to allocate the range of the input variables, the *desire* method to assist with the response objective (minimise, maximise, or target), and the *copy* method to swap values between chromosomes based on the crossover point chosen.

The response surface methodology phase

As discussed in chapter 7, second-order regression models were required to predict the three responses being minimised. To create the mathematical models based on findings in population 4, a R code was employed, where the coded units for the control variables were correlated to the respective responses.

The desirability function phase

The second-order regression models were employed in simulations for the final refinement of the welding parameters. Java programming was utilised with the genetic algorithm as the searching method and the desirability function as the objective function. The desirability function phase was similar

to that of the genetic algorithm. For the simulation, *RSM* was a subclass of *TestingRSM* (main class), while *SolutionRSM* was a subclass of *RSM* (see Fig. B 2).

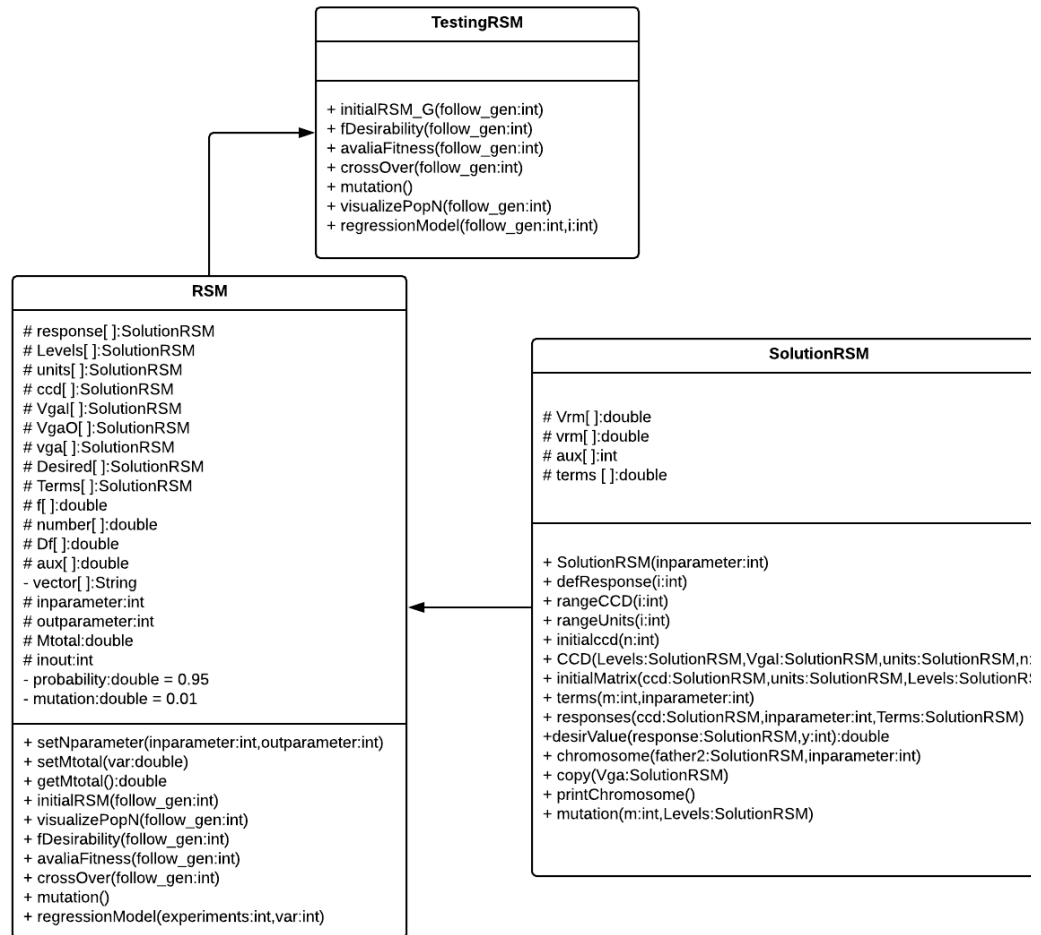


Fig. B 2 Unified Modeling Language diagram representation of the response surface methodology and desirability function classes.

In the *TestingRSM* class the user was required to specify the number of generations that would be created and the respective number of experiments. Subsequently, the method *initialRSM_G* initialised the first generation, followed by the *fDesirability* method that created the desirability numbers.

Other methods accessed by the *TestingRSM* class included the *avaliaFitness*, *crossOver*, and *mutation*.

Once the *TestingRSM* class accessed the *RSM* subclass the number of input and output variables were required in the *initialRSM_G* method. Hence, the first generation would be created utilising the second-order regression models to predict the respective responses.

The response objective (minimise, maximise, or target) was displayed by accessing the subclass *SolutionRSM*. In this study, the minimise option was selected, which prompted requests for the upper and target values of each response (*defResponse* method). In the *rangeCCD* method the user was required to input the ranges for each control variable based on the CCD levels. The *initialccd* method initialised the coded input variables, translated by the *CCD* method, which allowed for the development of a first matrix in the *initialMatrix* method. The method *terms* was utilised to specify each term of the regression model in the respective equation, while *responses* created responses based on the coded units and regression models. Additionally, the *desirValue* method defined the desirability of a certain chromosome according to the response objective.

Testing GA class

```
import java.util.Scanner;

public class TestingGA
{
    public static void main(String args[ ])
    {
        GA w1 = new GA( );

        Scanner in = new Scanner (System.in);

        System.out.printf("Is it the first generation? YES/NO \n");
        String gen = in.nextLine( );
    }
}
```

```

        int variable = 1;
        if (gen.toUpperCase( ).equals("YES") ||
gen.toUpperCase( ).equals("NO"))
            {variable = 0;}

        if (variable == 1)
        {
            do
            {
                System.out.println("Not a valid choice!\n Please try
again...\n");
                System.out.printf("Is it the first generation? YES/NO \n");
                gen = in.nextLine( );

                if (gen.toUpperCase( ).equals("YES") ||
gen.toUpperCase( ).equals("NO"))
                    {variable = 0;}

                else
                    {variable = 1;}
            } while (variable == 1);
        }

        if (variable == 0)
        {
            switch (gen.toUpperCase( )) {
                case "YES":
                    w1.initialG( );
                    break;
                case "NO":
                    w1.subsequentG( );
                    w1.fFitness( );
                    w1.avaliaFitness( );
                    w1.crossOver( );
                    w1.mutation( );
                    w1.visualizePopN( );
                    break;
            }
        }
    }
}

```

GA subclass

```

import java.util.Scanner;
import java.util.Random;

public class GA extends TestingGA
{
    protected SolutionGA VgaI[ ]; //Object to access
    subclass - input parameters
    protected SolutionGA VgaO[ ]; //Object to access
    subclass - output parameters
    protected SolutionGA vga[ ]; //Object to store new
    population for exchange during crossover
    protected SolutionGA Range[ ]; //Object to define
    ranges from input parameters
    protected SolutionGA Desired[ ]; //Object to define
    desired output parameters
    protected int experiment; //Number of experiments
    done
    protected int column; //Number of columns for

```

```

Orthogonal Array
    protected int inparameter;           //Number of input
parameters
    protected int outparameter;         //Number of output
parameters
    private double probability = 0.95;   //Probability of
Crossover
    private double mutation = 0.01;     //Probability of Mutation
    protected double f [ ];             //Storage of the
percentage of a Chromosome in the Roulette
    protected double number [ ];        //Probability of a
Chromosome to be selected for the New Generation
    protected double Mtotal;            //Storage of the sum of
all Objective Function values
    protected int inout;                //Sum of total parameters
to be analysed
    protected double Ob [ ];           //Storage of Objective
Function values
    protected double eq [ ];           //Calculating values
based on equation 1/(1+x)
    protected double extremesMax [ ];   //Allocating the maximum
value of a specific output column
    protected double extremesMin [ ];   //Allocating the minimum
value of a specific output column
    protected double F [ ];            //Storage of Fitness
values
    protected int a;                    //Variable to assist
Auxiliar Matrix Construction
    protected SolutionGA A[ ];         //Object to access
Auxiliar Matrix
    private String vector [ ];         //Array to control
titles of columns in the matrices created

//Validating number of experiments
public void setNexperiment(int var)
{experiment = var;}

//Returning number of experiments
public int getNexperiment( )
{return experiment;}

//Validating number of columns - Orthogonal Array
public void setColumns(int var)
{column = var;}

//Validating number of parameters
public void setNparameter(int inparameter, int outparameter)
{inout = inparameter+outparameter;}

//Sum of all values from Objective function to build the roulette
public void setMtotal(double var)
{Mtotal = var;}

//Returning sum of all values from Objective function to build the
roulette
public double getMtotal( )
{return Mtotal;}

//Generating initial population
public void initialG( )
{
    Scanner in = new Scanner (System.in);

    System.out.println("Please insert the number of input parameters: 2
or 3.");

```

```

    inparameter = in.nextInt( );

    int variable = 1;

    if (inparameter == 2 || inparameter == 3)
    {variable = 0;}

    if (variable == 1)
    {
        do
        {
            System.out.println("Not a valid choice!\n Please try
again...\n");
            System.out.printf("Please insert the number of input
parameters: 2 or 3.\n");
            inparameter = in.nextInt( );

            if (inparameter == 2 || inparameter == 3)
            {variable = 0;}

            else
            {variable = 1;}
        } while (variable == 1);
    }

    if(variable == 0)
    {
        setNexperiment (inparameter*4);
        setColumns (inparameter*4-1);

        if (inparameter == 1)
        {a=2;}
        if (inparameter == 2)
        {a=3;}
        if (inparameter == 3)
        {a=4;}

        VgaI = new SolutionGA[getNexperiment( )];
        VgaO = new SolutionGA[getNexperiment( )];
        vga = new SolutionGA[getNexperiment( )+1];
        Range = new SolutionGA[inparameter];
        Desired = new SolutionGA[1];
        A = new SolutionGA[getNexperiment( )];

        for (int i=0; i<getNexperiment( ); i++)
        {
            VgaI[i] = new SolutionGA(inparameter);
            vga[i] = new SolutionGA(inparameter);
            A[i] = new SolutionGA(inparameter);
        }

        for (int i=0; i<Range.length; i++)
        {
            int aux = 2;
            Range[i] = new SolutionGA(aux);
        }

        for (int i=0; i<Range.length; i++)
        {Range[i].range(i);System.out.printf("\n");}

        for (int c=0; c<a; c++)
        {
            if(c==0)
            {
                for (int l=0; l<A.length/2; l++)

```

```

        {A[l].OArray_0(c);
        for (int l=A.length/2; l<A.length; l++)
        {A[l].OArray_1(c);}
    }

    if(c==1)
    {
        for (int l=0; l<A.length/4; l++)

{A[l].OArray_0(c);A[l+(A.length/4)].OArray_1(c);A[l+(2*A.length/4)].OArray_0
(c);A[l+(3*A.length/4)].OArray_1(c);}

        if(inparameter==1)
        {
            int x1 = 0; int x2 = 1;
            for (int l = 0; l < A.length; l++)
            {A[l].taguchi3(x1, x2);}
        }

    if(c==2)
    {
        c+=1;

        if(inparameter==2)
        {
            for (int l=0; l<A.length/2; l++)
            {A[2*l].OArray_0(c);A[1+2*l].OArray_1(c);}

            int x1 = 0; int x2 = 1; int x3 = 3; int x4 = 2;
            for (int l = 0; l < A.length; l++)
            {A[l].taguchi3(x1, x2); A[l].taguchi5(x1, x3);
A[l].taguchi6(x2, x3); A[l].taguchi7(x4, x3);}
        }

        if(inparameter==3)
        {
            for (int l=0; l<A.length; l++)
            {A[l].taguchi(1);}
        }
    }

    System.out.print("*****TAGUCHI's MATRIX *****\n");

    int n = A.length-1;
    for (int j=0; j<A.length; j++)
    {A[j].PrintChromosome(n,j);}
    System.out.printf("\n\n");

    //Generating initial population
    for (int i=0; i<inparameter; i++)
    {
        int control, cel = 0;
        for (int l=0; l<A.length; l++)
        {
            for (int sys=0; sys<inparameter; sys++)
            {
                int b;
                control = cel;

                if (sys == 0 && inparameter == 1 || sys == 1 &&
inparameter == 2 || sys == 2 && inparameter == 3)
                {b = 3;}
            }
        }
    }

```

```

        else
        {b = 4;}

        cel = VgaI[1].createMatrix(A[1],sys,b,Range[sys],1,
control);
    }
    cel = 0;
}
}

//Showing initial population
System.out.print("*****INITIAL POPULATION *****\n");

//Defining an array to control strings
vector = new String [6];
vector[0] = "Input 1"; vector[1] = "Input 2"; vector[2] = "Input
3";
vector[3] = "Output 1"; vector[4] = "Output 2"; vector[5] =
"Output 3";

String format = "%15s";
String format1 = "%12s";

System.out.printf(format,vector[0]);

for(int m = 1; m<inparameter; m++)
{System.out.printf(format1,vector[m]);}

System.out.printf("\n");

for(int m = 0; m<getNexperiment( ); m++)
{
    System.out.printf("Row %d:",m+1);
    VgaI[m].printChromosome( );
    System.out.printf("\n");
}
System.out.printf("\n");
}
}

//Generating subsequent population
public void subsequentG( )
{
    Scanner in = new Scanner (System.in);
    System.out.println("Please choose the number of experiments done: 4,
8 or 12.");
    experiment = in.nextInt( );

    int variable = 1;

    if (experiment == 4 || experiment == 8 || experiment == 12)
    {variable = 0;}

    if (variable == 1)
    {
        do
        {
            System.out.println("Not a valid choice!\n Please try
again...\n");
            System.out.printf("Please choose the number of experiments
done: 4, 8 or 12. \n");
            experiment = in.nextInt( );

            if (experiment == 4 || experiment == 8 || experiment == 12)
            {variable = 0;}

```

```

        else
            {variable = 1;}
    } while (variable == 1);
}

setNexperiment(experiment);

if(variable == 0)
{
    System.out.println("Please insert the number of input
parameters: 2 or 3.");
    inparameter = in.nextInt( );

    int inp = 1;

    if (inparameter == 2 || inparameter == 3)
    {inp = 0;}

    if (inp == 1)
    {
        do
        {
            System.out.println("Not a valid choice!\n Please try
again...\n");
            System.out.printf("Please insert the number of input
parameters: 2 or 3. \n");
            inparameter = in.nextInt( );

            if (inparameter == 2 || inparameter == 3)
            {inp = 0;}

            else
            {inp = 1;}
        } while (inp == 1);
    }

    if(inp == 0)
    {
        System.out.println("Please insert the number of output
parameters: 1, 2 or 3.");
        outparameter = in.nextInt( );

        int outp = 1;

        if (outparameter == 1 || outparameter == 2 || outparameter
== 3)
        {outp = 0;}

        if (outp == 1)
        {
            do
            {
                System.out.println("Not a valid choice!\n Please try
again...\n");
                System.out.printf("Please insert the number of
output parameters: 1, 2 or 3. \n");
                outparameter = in.nextInt( );

                if (outparameter == 1 || outparameter == 2 ||
outparameter == 3)
                {outp = 0;}

                else
                {outp = 1;}
            }

```



```

    } while (outp == 1);
}

if(outp == 0)
{
    setNparameter(inparameter,outparameter);

    VgaI = new SolutionGA[getNexperiment( )];
    VgaO = new SolutionGA[getNexperiment( )];
    vga = new SolutionGA[getNexperiment( )+1];
    Range = new SolutionGA[inparameter];
    Desired = new SolutionGA[1];

    for (int i=0; i<getNexperiment( ); i++)
    {
        VgaI[i] = new SolutionGA(inparameter);
        VgaO[i] = new SolutionGA(outparameter);
        vga[i] = new SolutionGA(inparameter);
    }

    for (int i=0; i<Range.length; i++)
    {
        int aux = 2;
        Range[i] = new SolutionGA(aux);
    }

    System.out.printf("\n");
    for (int i=0; i<Range.length; i++)
    {Range[i].range(i);System.out.printf("\n");}

    Desired[0] = new SolutionGA(outparameter);
    Desired[0].desire( );

    System.out.printf("\n");
    System.out.println("Please insert values for the matrix
as asked:");

    for(int m = 0; m<getNexperiment( ); m++)
    {
        VgaI[m].createChromosomeI(m);
        VgaO[m].createChromosomeO(m,inparameter);
    }
    System.out.print("\n");
}
}

//Showing new population
public void visualizePopN( )
{
    System.out.print("*****NEW POPULATION *****\n");

    System.out.printf("\n");
    String format = "%15s";
    String format1 = "%12s";
    System.out.printf(format,vector[0]);

    for(int m = 1; m<inparameter; m++)
    {System.out.printf(format1,vector[m]);}

    System.out.printf("\n");

    for(int m = 0; m<getNexperiment( ); m++)
    {

```

```

        System.out.printf("Row %d:",m+1);
        VgaI[m].printChromosome( );
        System.out.printf("\n");
    }
    System.out.printf("\n");
}

//Applying fitness
public void fFitness( )
{
    double var = 0.0;
    int aT = Desired[0].actionType( );

    f = new double[getNexperiment( )+1];
    number = new double[getNexperiment( )];

    //Defining objective function values
    Ob = new double [getNexperiment( )];

    //Defining the maximum/ minimum output value from a certain column
    based on a specific output population (output column)
    extremesMax = new double [outparameter];
    extremesMin = new double [outparameter];

    //Defining values based on 1/(1+x) equation
    eq = new double [experiment];

    //Defining fitness values
    F = new double [experiment];

    for(int a=0; a<f.length; a++)
    {f[a]=0.0;}

    for(int k=0; k<number.length; k++)
    {number[k]=0.0;}

    for(int k=0; k<Ob.length; k++)
    {Ob[k]=0.0;}

    for(int a=0; a<extremesMax.length; a++)
    {extremesMax[a]=0.0;extremesMin[a]=0.0;}

    if(aT == 1)
    {
        //Defining the maximum and minimum in an output column
        for(int y = 0; y<outparameter; y++)
        {
            extremesMax [y] = VgaO[0].edge(y);
            System.out.printf("\textremesMax[%d]:
%5.2f",y,extremesMax[y]);

            for(int x = 0; x<VgaO.length; x++)
            {
                if(extremesMax [y] < VgaO[x].edge(y))
                {extremesMax [y] =
VgaO[x].edge(y);System.out.printf("\textremesMax[%d]:
%5.2f",y,extremesMax[y]);}
            }

            extremesMin [y] = extremesMax [y];
            System.out.printf("\textremesMin[%d]:
%5.2f",y,extremesMin[y]);

            for(int x = 0; x<VgaO.length; x++)
            {

```

```

        if(extremesMin [y] > VgaO[x].edge(y) &&
VgaO[x].edge(y) != 0)
        {extremesMin [y] =
VgaO[x].edge(y);System.out.printf("\textremesMin[%d]:
%5.2f",y,extremesMin[y]);}
    }

    //Sum up of differences between the maximum and a specific
output value
    for(int i = 0; i<VgaO.length; i++)
    {
        for(int j = 0; j<outparameter; j++)
        {
            System.out.printf("\tOb[%d]: %5.2f",i,Ob[i]);
            if(VgaO[i].accessColumns(j) == 0)
            {Ob[i] += 0;System.out.printf("\tOb[%d]:
%5.2f",i,Ob[i]);}

            else
            {Ob[i] += extremesMax[j] -
VgaO[i].accessColumns(j);System.out.printf("\tOb[%d]: %5.2f",i,Ob[i]);}
        }
    }

    //Changing zeros for maximums in a specific objective function
column
    Double Max = 0.0;

    for(int i = 0; i<VgaO.length; i++)
    {
        if(Max < Ob[i])
        {Max = Ob[i];}
    }

    for(int i = 0; i<VgaO.length; i++)
    {
        int y = 0;
        if(Ob[i] == 0 && VgaO[i].edge(y) == 0)
        {Ob[i] = Max*1.5;}
    }

    for(int v = 0; v<VgaO.length; v++)
    {eq[v] = (1/(1+Ob[v]));}

    double eqSum = 0.0;
    for(int n = 0; n<Ob.length; n++)
    {eqSum += eq[n];}

    //Calculating fitness
    for(int m = 0; m<F.length; m++)
    {F[m] = 100*(eq[m]/eqSum);var += F[m];setMtotal(var);}
}

if(aT == 0)
{
    //Defining the maximum and minimum in an output column
    for(int y = 0; y<outparameter; y++)
    {
        extremesMax [y] = VgaO[0].edge(y);
        System.out.printf("\textremesMax[%d]:
%5.2f",y,extremesMax[y]);

        for(int x = 0; x<VgaO.length; x++)
        {

```

```

        if(extremesMax [y] < VgaO[x].edge(y))
        {extremesMax [y] =
VgaO[x].edge(y);System.out.printf("\textremesMax[%d]:
%5.2f",y,extremesMax[y]);}
    }

    extremesMin [y] = extremesMax [y];
    System.out.printf("\textremesMin[%d]:
%5.2f",y,extremesMin[y]);

    for(int x = 0; x<VgaO.length; x++)
    {
        if(extremesMin [y] > VgaO[x].edge(y) &&
VgaO[x].edge(y) != 0)
        {extremesMin [y] =
VgaO[x].edge(y);System.out.printf("\textremesMin[%d]:
%5.2f",y,extremesMin[y]);}
    }
}

//Sum up of differences between a specific output value and the
minimum
for(int i = 0; i<VgaO.length; i++)
{
    for(int j = 0; j<outparameter; j++)
    {
        System.out.printf("\tOb[%d]: %5.2f",i,Ob[i]);
        if(VgaO[i].accessColumns(j) == 0)
        {Ob[i] += 0;System.out.printf("\tOb[%d]:
%5.2f",i,Ob[i]);}

        else
        {Ob[i] += VgaO[i].accessColumns(j) -
extremesMin[j];System.out.printf("\tOb[%d]: %5.2f",i,Ob[i]);}
    }
}

//Changing zeros for maximums in a specific objective function
column
Double Max = 0.0;

for(int i = 0; i<VgaO.length; i++)
{
    if(Max < Ob[i])
    {Max = Ob[i];}
}

for(int i = 0; i<VgaO.length; i++)
{
    int y = 0;
    if(Ob[i] == 0 && VgaO[i].edge(y) == 0)
    {Ob[i] = Max*1.5;}
}

for(int v = 0; v<VgaO.length; v++)
{eq[v] = (1/(1+Ob[v]));}

double eqSum = 0.0;
for(int n = 0; n<Ob.length; n++)
{eqSum += eq[n];}

//Calculating fitness
for(int m = 0; m<F.length; m++)
{F[m] = 100*(eq[m]/eqSum);var += F[m];setMtotal(var);}
}

```

```

if(aT == 2)
{
    for(int x = 0; x<Ob.length; x++)
    {
        double aux=0.0;
        if(VgaO[x].Chromosome(aux) != 0.0)
        {Ob[x]=VgaO[x].objectiveFunction(Desired[0],outparameter);}
    }

    double sup1 = 0.0;double sup2 = 0.0;
    for(int m = 0; m<getNexperiment( ); m++)
    {
        if(sup1<Ob[m])
        {sup1=Ob[m];}

        sup2 = sup1*1.5;
    }

    for(int m = 0; m<getNexperiment( ); m++)
    {
        double aux = 0.0;
        if(VgaO[m].Chromosome(aux) == 0.0)
        {Ob[m]=sup2;}
    }

    for(int m = 0; m<F.length; m++)
    {F[m] = (1/(Ob[m]+1));var = var+F[m];setMtotal(var);}
}

System.out.print("*****INITIAL GLOBAL MATRIX *****\n");

String format = "%15s";
String format1 = "%12s";
String format2 = "%9s";

//Defining an array to control strings
vector = new String [6];
vector[0] = "Input 1"; vector[1] = "Input 2"; vector[2] = "Input 3";
vector[3] = "Output 1"; vector[4] = "Output 2"; vector[5] = "Output
3";

String OF = "OFunction";String fitness = "Fitness";

System.out.printf("\n");

System.out.printf(format,vector[0]);

for(int m = 1; m<inparameter; m++)
{System.out.printf(format1,vector[m]);}

for(int m = 3; m<outparameter+3; m++)
{System.out.printf(format1,vector[m]);}

System.out.printf(format1,OF);
System.out.printf(format2,fitness);
System.out.printf("\n");

for(int m = 0; m<getNexperiment( ); m++)
{
    System.out.printf("Row %d:",m+1);
    VgaI[m].printChromosome( );
    VgaO[m].printChromosome( );
    System.out.printf("\t%5.2f",Ob[m]);
    System.out.printf("\t%5.2f",F[m]);
}

```

```

        System.out.printf("\n");
    }
    System.out.printf("\n");

    f[0] = ((double)F[0]/getMtotal( ))*100;
    System.out.printf("f[0] = %.1f\n",f[0]);
    number[0] = (Math.random( ) *100);
    System.out.printf("Number[0] = %.1f\n\n",number[0]);

    for(int d=1; d<number.length; d++)
    {
        number[d] = (Math.random( ) *100);
        f[d] = ((double)F[d]/getMtotal( ))*100 + f[d-1];

        System.out.printf("f[%d] = %.2f\n",d,f[d]);
        System.out.printf("Number[%d] = %.2f\n\n",d,number[d]);
    }
}

//Choosing chromosomes for new generation based on the roulette
public void avaliaFitness( )
{
    //Selecting chromosomes
    for(int e=0; e<number.length; e++)
    {
        vga[e] = new SolutionGA(inparameter);
        if(number[e]<=f[0])
        {
            vga[e].copy(VgaI[0]);
            System.out.printf("** Applying Fitness (%.2f < %.2f)
**\n",number[e],f[0]);
            System.out.printf("Chromosome 1 selected: ");
            VgaI[0].printChromosome( );
            System.out.printf("\n\n");
        }
        else
        {
            for(int a=0; a<f.length-1; a++)
            {
                if(number[e]>f[a] && number[e]<=f[a+1])
                {
                    vga[e].copy(VgaI[a+1]);
                    System.out.printf("** Applying Fitness (%.2f < %.2f)
**\n",number[e],f[a+1]);
                    System.out.printf("Chromosome %d selected: ",a+2);
                    VgaI[a+1].printChromosome( );

                    System.out.printf("\n\n");
                }
            }
        }
    }

    System.out.printf("\n");

    //Generating new population
    for(int i=0; i<VgaI.length; i++)
    {VgaI[i].copy(vga[i]);}

    System.out.printf("*****POPULATION AFTER FITNESS
*****\n");

    System.out.printf("\n");
    String format = "%15s";

```

```

String format1 = "%12s";

System.out.printf(format,vector[0]);

for(int m = 1; m<inparameter; m++)
{System.out.printf(format1,vector[m]);}

System.out.printf("\n");

for(int g=0; g<VgaI.length; g++)
{
    System.out.printf("Row %d:",g+1);
    VgaI[g].printChromosome( );
    System.out.printf("\n");
}
System.out.printf("\n");
}

//Applying Crossover
public void crossOver( )
{
    int father1=0, father2, first = 0;
    double x;

    Random randomNumbers = new Random( );

    for(int i=0; i<getNexperiment( ); i++)
    {
        x = randomNumbers.nextDouble( );
        father2 = i;
        if(x < probability)
        {
            first++;
            if(first % 2 == 0)
            {
                System.out.printf("** Applying Crossover (%.2f <
%.2f)**",x,probability);
                System.out.println("\nFather1: "+(father1+1));
                VgaI[father1].printChromosome( );
                System.out.println(" ");
                System.out.println("Father2: "+(father2+1));
                VgaI[father2].printChromosome( );
                System.out.println("");
                System.out.printf("\n");
                System.out.printf("**%.2f < %.2f**\n",x,probability);
                VgaI[father1].chromosome(VgaI[father2]);
            }
            else father1 = i;
        }
    }
}

//Applying Mutation
public void mutation( )
{
    Random randomNumbers = new Random( );
    double x;

    for(int i=0; i<VgaI.length; i++)
    {
        for(int m=0; m<Range.length; m++)
        {
            x = randomNumbers.nextDouble( );
            if(x < mutation)
            {

```

```

        System.out.printf("\n** Mutation (%.2f < %.2f) -
Chromosome %d**",x,mutation,i+1);
        System.out.printf("\nBefore Mutation: ");
        VgaI[i].printChromosome( );

VgaI[i].mutation(m,Range[m].lowrange( ),Range[m].highrange( ));

        System.out.printf("\nAfter Mutation: ");
        VgaI[i].printChromosome( );
        System.out.printf("\n");
    }
}
System.out.printf("\n\n");
}
}

```

SolutionGA subclass

```

import java.util.Scanner;
import java.util.Random;

public class SolutionGA extends GA
{
    protected int Inparameter; //Defining the number of input values
    protected double Vrm[ ]; //Vector that allows access from GA
    Class
    protected int vrm[ ]; //Vector that allows creation of
    Orthogonal Array
    protected int aux [ ]; //Auxiliar vector for the Orthogonal
    Array Matrix

    //Defining range - minimum value
    public int lowrange( )
    {int aux = (int)this.Vrm[0]; return aux;}

    //Defining range - maximum value
    public int highrange( )
    {int aux = (int)this.Vrm[1]; return aux;}

    //Retorning number of columns for the Chromosome
    public int getNpar( )
    {return Inparameter;}

    //Zeros for Auxiliar Matrix
    public void OArray_0(int c)
    {this.aux[c]=0;}

    //Ones for Auxiliar Matrix
    public void OArray_1(int c)
    {this.aux[c]=1;}

    //Constructor with parameters
    public SolutionGA(int inparameter)
    {
        Inparameter = inparameter;
        Vrm = new double [Inparameter];
        vrm = new int [Inparameter];
    }
}

```



```

        aux = new int [Inparameter*4-1];

        for(int j=0; j<Vrm.length; j++)
        {this.Vrm[j]=0;}

        for(int j=0; j<vrm.length; j++)
        {this.vrm[j]=0;}
    }

    //Defining desired values for output parameters
    public void desire( )
    {
        Scanner in = new Scanner (System.in);

        System.out.printf("Please define the desired type action on output
parameters: 'Maximise', 'Minimise' or 'Target is best!' \n");
        String gen = in.nextLine( );

        int variable = 0;

        if (gen.toUpperCase( ).equals("MAXIMISE") ||
gen.toUpperCase( ).equals("MINIMISE") || gen.toUpperCase( ).equals("TARGET
IS BEST"))
        {variable = 1;}

        if (variable == 0)
        {
            do
            {
                System.out.println("Not a valid choice!\n Please try
again...\n");
                System.out.printf("Please define the desired type action on
output parameters: 'Maximise', 'Minimise' or 'Target is best!' \n");
                gen = in.nextLine( );

                if (gen.toUpperCase( ).equals("MAXIMISE") ||
gen.toUpperCase( ).equals("MINIMISE") || gen.toUpperCase( ).equals("TARGET
IS BEST"))
                    {variable = 1;}

                else
                    {variable = 0;}
            } while (variable == 0);
        }

        if (variable == 1)
        {
            switch(gen.toUpperCase( ))
            {
                case "MAXIMISE":
                    this.Vrm [0] = 1;
                    break;
                case "MINIMISE":
                    this.Vrm [0] = 0;
                    break;
                case "TARGET IS BEST":
                    for (int i=0; i<Vrm.length; i++)
                    {
                        System.out.printf("Please insert the desired value
for output parameter %d\n",i+1);
                        Vrm [i] = in.nextDouble( );
                        System.out.printf("\n");
                    }
                    break;
            }
        }
    }
}

```

```

    }
}

//Defining the action type for output parameters
public int actionType( )
{
    int aT;
    if (this.Vrm [0] == 1)
    {aT = 1;}
    else
    {
        if (this.Vrm [0] == 0)
        {aT = 0;}
        else
        {aT = 2;}
    }

    return aT;
}

//Sum of values for outputs
public double accessColumns(int y)
{double a = this.Vrm[y]; return a;}

//Allocating either the maximum or minimum output value from a certain
output population (output column)
public double edge(int y)
{double edge = this.Vrm[y];return edge;}

//Defining ranges for input parameters
public void range(int i)
{
    Scanner in = new Scanner (System.in);
    System.out.printf("Please insert the range for input parameter
%d.\n", i+1);
    System.out.printf("From: ");
    this.Vrm [0] = in.nextFloat( );
    System.out.printf("To: ");
    this.Vrm [1] = in.nextFloat( );
    System.out.printf("\n");

    int variable = 1;

    if (this.Vrm[0] < this.Vrm[1])
    {variable = 0;}

    if (variable == 1)
    {
        do
        {
            System.out.printf("Not a valid choice! %.2f equal or bigger
than %.2f.\n Please try again...\n\n", this.Vrm[0], this.Vrm[1]);
            System.out.printf("Please insert the range for input
parameter %d\n", i+1);
            System.out.printf("From: ");
            this.Vrm [0] = in.nextFloat( );
            System.out.printf("To: ");
            this.Vrm [1] = in.nextFloat( );
            System.out.printf("\n");

            if (this.Vrm[0] < this.Vrm[1])
            {variable = 0;}

            else
            {variable = 1;}
        }
    }
}

```

```

    } while (variable == 1);
}

public void PrintChromosome(int a, int j)
{
    for(int i=0; i<a; i++)
    {
        if (j==0)
            {System.out.printf("\t %d",i+1);}
    }
    System.out.printf("\n");

    for(int i=0; i<a; i++)
        {System.out.printf("\t %d",this.aux[i]);}
}

//Generating population to be analysed - Input values
public void createChromosomeI(int m)
{
    Scanner in = new Scanner (System.in);
    for (int i=0; i<Vrm.length; i++)
    {
        System.out.printf("M[%d] [%d]",m+1,i+1);
        Vrm [i] = in.nextDouble( );
    }
}

//Generating population to be analysed - Output values
public void createChromosomeO(int m,int inparameter)
{
    Scanner in = new Scanner (System.in);
    for (int i=0; i<Vrm.length; i++)
    {
        System.out.printf("M[%d] [%d]",m+1,i+inparameter+1);
        Vrm [i] = in.nextDouble( );
    }
}

//Defining values for Objective Function
public double objectiveFunction(SolutionGA var,int out)
{
    double ob = 0.0;
    double a;

    for (int i=0; i<out; i++)
    {
        a = Math.pow(var.Vrm[i]-this.Vrm[i],2);
        ob+= a;
    }
    return ob;
}

//Crossover in SolutionGA
public void chromosome(SolutionGA father2)
{
    int point;
    double son1[ ] = new double[getNpar( )];
    double son2[ ] = new double[getNpar( )];

    if(getNpar( ) == 2)
        point = 1;
    else
        do
            {point = (int) (Math.random( ) * getNpar( ));}
}

```

```

        while(point==0);

        System.out.printf("Point: %d",point);

        for(int i = 0; i<point; i++)
        {
            son1[i] = this.Vrm[i];
            son2[i] = father2.Vrm[i];
        }

        for(int i = point; i<Vrm.length; i++)
        {
            son1[i] = father2.Vrm[i];
            son2[i] = this.Vrm[i];
        }

        for(int i=0; i<Vrm.length; i++)
        {
            this.Vrm[i] = son1[i];
            father2.Vrm[i] = son2[i];
        }

        System.out.printf("\nSon1::::: ");
        this.printChromosome( );
        System.out.printf("\n");
        System.out.printf("Son2::::: ");
        father2.printChromosome( );
        System.out.printf("\n");
    }

    //Copy method for Crossover
    public void copy(SolutionGA Vga)
    {
        for(int i=0; i<Vrm.length; i++)
        {this.Vrm[i]=Vga.Vrm[i];}
    }

    //Printing Chromosome
    public void printChromosome( )
    {
        for(int i=0; i<Vrm.length; i++)
        {System.out.printf("\t %3.1f\t",this.Vrm[i]);}
    }

    //Creating matrix from Taguchi's method
    public int createMatrix(SolutionGA A, int sys, int b, SolutionGA Range,
    int control, int l)
    {
        double bin = 0;
        double d;
        int bits = (int) Math.pow(2,b)-1;
        int a = control, extra = 0;

        for(int i = control; i < a+b; i++)
        {
            d = A.aux[i]*(int) Math.pow(2,(b-extra-1));
            bin += d;
            control ++; extra++;
        }

        this.Vrm[sys] = Range.Vrm[0] + ((bin/bits)*(Range.Vrm[1]-
        Range.Vrm[0]));
        return control;
    }
}

```

```

//Method to fill coulumn 3 of taguchi's matrix L8
public void taguchi3(int x, int y)
{
    if(this.aux[x]==this.aux[y])
    {this.aux[2]=0;}
    else
        this.aux[2]=1;
}

//Method to fill coulumn 5 of taguchi's matrix L8
public void taguchi5(int x, int y)
{
    if(this.aux[x]==this.aux[y])
    {this.aux[4]=0;}
    else
        this.aux[4]=1;
}

//Method to fill coulumn 6 of taguchi's matrix L8
public void taguchi6(int x, int y)
{
    if(this.aux[x]==this.aux[y])
    {this.aux[5]=0;}
    else
        this.aux[5]=1;
}

//Method to fill coulumn 7 of taguchi's matrix L8
public void taguchi7(int x, int y)
{
    if(this.aux[x]==this.aux[y])
    {this.aux[6]=0;}
    else
        this.aux[6]=1;
}

//Method to fill coulums of taguchi's matrix L12
public void taguchi(int l)
{
    if(l==0)

{this.aux[2]=this.aux[3]=this.aux[4]=this.aux[5]=this.aux[6]=this.aux[7]=this.aux[8]=this.aux[9]=this.aux[10]=0;}
    if(l==1)
    {this.aux[2]=this.aux[3]=this.aux[4]=0;
this.aux[5]=this.aux[6]=this.aux[7]=this.aux[8]=this.aux[9]=this.aux[10]=1;}
    if(l==2)
    {this.aux[5]=this.aux[6]=this.aux[7]=0;
this.aux[2]=this.aux[3]=this.aux[4]=this.aux[8]=this.aux[9]=this.aux[10]=1;}
    if(l==3)
    {this.aux[2]=this.aux[5]=this.aux[8]=this.aux[9]=0;
this.aux[3]=this.aux[4]=this.aux[6]=this.aux[7]=this.aux[10]=1;}
    if(l==4)
    {this.aux[2]=this.aux[4]=this.aux[5]=this.aux[7]=this.aux[9]=1;
this.aux[3]=this.aux[8]=this.aux[6]=this.aux[10]=0;}
    if(l==5)
    {this.aux[4]=this.aux[7]=this.aux[9]=this.aux[10]=0;
this.aux[2]=this.aux[3]=this.aux[8]=this.aux[5]=this.aux[6]=1;}
    if(l==6)
    {this.aux[2]=this.aux[3]=this.aux[6]=this.aux[7]=this.aux[9]=1;
this.aux[4]=this.aux[5]=this.aux[8]=this.aux[10]=0;}
    if(l==7)
    {this.aux[2]=this.aux[4]=this.aux[5]=this.aux[6]=this.aux[10]=1;
this.aux[3]=this.aux[7]=this.aux[8]=this.aux[9]=0;}
    if(l==8)

```

```

        {this.aux[3]=this.aux[4]=this.aux[5]=this.aux[7]=this.aux[8]=1;
this.aux[2]=this.aux[6]=this.aux[9]=this.aux[10]=0;}
        if(l==9)
        {this.aux[2]=this.aux[7]=this.aux[8]=this.aux[10]=1;
this.aux[3]=this.aux[4]=this.aux[5]=this.aux[6]=this.aux[9]=0;}
        if(l==10)
        {this.aux[3]=this.aux[5]=this.aux[9]=this.aux[10]=1;
this.aux[2]=this.aux[4]=this.aux[6]=this.aux[7]=this.aux[8]=0;}
        if(l==11)
        {this.aux[4]=this.aux[8]=this.aux[6]=this.aux[9]=1;
this.aux[2]=this.aux[3]=this.aux[5]=this.aux[7]=this.aux[10]=0;}

    }

    //Method to check if all output parameters are equal zero for Objective
Function
    public double Chromosome(double aux)
    {
        for(int i=0; i<Vrm.length; i++)
        {aux+=this.Vrm[i];}
        return aux;
    }

    //Applying Mutation in a chosen chromosome block
    public void mutation( int m, int a, int b)
    {
        int value;
        Random randomNumbers = new Random( );

        do
        {value = randomNumbers.nextInt(b+1);}
        while(value<a || value>b);

        this.Vrm[m] = value;
    }
}

```

R coding

```
rm(list = ls( )) # clear the workspace of all prior variables

G <- c(-1,1,-1,1,-1,1,-1,1,-1,1,0,0,0,0)
D <- c(-1,-1,1,1,-1,-1,1,1,0,0,-1,1,0,0)
T <- c(-1,-1,-1,-1,1,1,1,1,0,0,0,-1,1,0)

y1 <- c(4.1050, 5.9685, 5.1600, 4.2204, 3.3343, 3.9651, 6.8087, 5.5688, 4.5548, 7.0001, 5.5304,
4.3390, 5.7254, 4.9842, 5.5688)
y2 <- c(3.6675, 3.4588, 4.6401, 3.4648, 1.6065, 3.0887, 1.5279, 3.1989, 4.0277, 3.0595, 2.9203,
3.6711, 3.3722, 2.7130, 3.1991)
y3 <- c(483.9, 493.8, 501.9, 486.0, 365.1, 425.9, 409.0, 396.4, 425.9, 479.0, 380.1, 429.1, 469.6,
395.3, 423.4)

model.y1 <- lm(y1 ~ (G+D+T)^3 + I(G^2) + I(D^2) + I(T^2))
model.y2 <- lm(y2 ~ (G+D+T)^3 + I(G^2) + I(D^2) + I(T^2))
model.y3 <- lm(y3 ~ (G+D+T)^3 + I(G^2) + I(D^2) + I(T^2))

summary(model.y1)
summary(model.y2)
summary(model.y3)

layout(matrix(1:4,2,2))
plot(model.y1)

layout(matrix(1:4,2,2))
plot(model.y2)

layout(matrix(1:4,2,2))
plot(model.y3)
```

TestingRSM class

```

import java.util.Scanner;

public class TestingRSM
{
    public static void main(String args[ ])
    {
        //Defining RSM object
        RSM w1 = new RSM( );

        Scanner in = new Scanner (System.in);
        System.out.printf("Define the number of generations desired! \n");
        int rsm = in.nextInt( );

        System.out.println("Please insert the number of experiments for the
following generations.");
        int follow_gen = in.nextInt( );

        //Initialising RSM generation
        w1.initialRSM_G(follow_gen);

        //Creating desirability numbers
        w1.fDesirability(follow_gen);

        for(int i=0; i<rsm; i++)
        {
            //Evaluating desirability
            w1.avaliaFitness(follow_gen);

            //Applying crossover
            w1.crossOver(follow_gen);

            //Applying mutation
            w1.mutation( );

            //Visualising new population
            w1.visualizePopN(follow_gen);

            //Applying the regression model
            w1.regressionModel(follow_gen, i);

            //Creating desirability numbers
            w1.fDesirability(follow_gen);
        }
    }
}

```

RSM subclass

```

import java.util.Scanner;
import java.util.Random;

public class RSM extends TestingRSM
{
    protected SolutionRSM response[ ];           //Object to access
    subclass - response type
    protected SolutionRSM Levels[ ];           //Object to access
    subclass - CCD levels
    protected SolutionRSM units[ ];           //Object to access
    subclass - CCD units
}

```



```

    protected SolutionRSM ccd[ ]; //Object to access
    subclass - Central Composite Design
    protected SolutionRSM VgaI[ ]; //Object to access
    subclass - input parameters
    protected SolutionRSM VgaO[ ]; //Object to access
    subclass - output parameters
    protected SolutionRSM vga[ ]; //Object to store new
    population for exchange during crossover
    protected SolutionRSM Desired[ ]; //Object to define
    desired output parameters
    protected int inparameter; //Number of input
    parameters
    protected int outparameter; //Number of output
    parameters
    private double probability = 0.95; //Probability of
    Crossover
    private double mutation = 0.01; //Probability of
    Mutation
    protected double f[ ]; //Storage of the
    percentage of a Chromosome in the Roulette
    protected double number[ ]; //Probability of a
    Chromosome to be selected for the New Generation
    protected double Mtotal; //Storage of the sum of
    all values for the roulette
    protected int inout; //Sum of total
    parameters to be analysed
    protected double Df[ ]; //Storage of final
    desirability function values
    protected double aux[ ]; //Storage of
    desirability function values
    protected SolutionRSM Terms[ ]; //Object to store
    terms of regressions models
    private String vector[ ]; //Array to control
    titles of columns in the matrices created

    //Validating number of parameters
    public void setNparameter(int inparameter, int outparameter)
    {inout = inparameter+outparameter;}

    //Sum of all values from final desirability function to build the
    roulette
    public void setMtotal(double var)
    {Mtotal = var;}

    //Returning sum of all values from desirability function to build the
    roulette
    public double getMtotal( )
    {return Mtotal;}

    //Generating initial RSM population
    public void initialRSM_G(int follow_gen)
    {
        Scanner in = new Scanner (System.in);
        System.out.println("Please insert the number of input parameters: 2
or 3.");
        inparameter = in.nextInt( );

        int inp = 1;

        if (inparameter == 2 || inparameter == 3)
        {inp = 0;}

        if (inp == 1)
        {

```

```

        do
        {
            System.out.printf("Not a valid choice! \n Please try
again...\n\n");
            System.out.printf("Please insert the number of input
parameters: 2 or 3.\n");
            inparameter = in.nextInt( );

            if (inparameter == 2 || inparameter == 3)
            {inp = 0;}

            else
            {inp = 1;}
        } while (inp == 1);
    }

    System.out.println("Please insert the number of output parameters: 2
or 3.");
    outparameter = in.nextInt( );

    int outp = 1;

    if (outparameter == 2 || outparameter == 3)
    {outp = 0;}

    if (outp == 1)
    {
        do
        {
            System.out.printf("Not a valid choice! \n Please try
again...\n\n");
            System.out.println("Please insert the number of output
parameters: 2 or 3.\n");
            outparameter = in.nextInt( );

            if (outparameter == 2 || outparameter == 3)
            {outp = 0;}

            else
            {outp = 1;}
        } while (outp == 1);
    }

    setNparameter(inparameter,outparameter);

    VgaI = new SolutionRSM[follow_gen];
    VgaO = new SolutionRSM[follow_gen];
    vga = new SolutionRSM[follow_gen+1];
    Levels = new SolutionRSM[inparameter];
    Terms = new SolutionRSM[outparameter];
    Desired = new SolutionRSM[1];
    ccd = new SolutionRSM[follow_gen];
    units = new SolutionRSM[inparameter];
    response = new SolutionRSM[outparameter];

    //Allocating spaces to objects
    for (int i=0; i<follow_gen; i++)
    {
        VgaI[i] = new SolutionRSM(inparameter);
        VgaO[i] = new SolutionRSM(outparameter);
        vga[i] = new SolutionRSM(inparameter);
        ccd[i] = new SolutionRSM(inparameter);
    }

    //Allocating spaces to vectors

```

```

    for (int i=0; i<Levels.length; i++)
    {
        int aux = 3;
        Levels[i] = new SolutionRSM(aux);
        units[i] = new SolutionRSM(aux);
    }

    for (int i=0; i<response.length; i++)
    {
        int aux = 3;
        response[i] = new SolutionRSM(aux);
    }

    for (int i=0; i<Terms.length; i++)
    {
        Terms[i] = new SolutionRSM(inparameter);
    }

    //Defining the type of response and output parameters
    for (int i=0; i<response.length; i++)
    {
        response[i].defResponse(i);
        System.out.printf("\n");
    }

    //Defining input parameters
    for (int i=0; i<Levels.length; i++)
{Levels[i].rangeCCD(i);units[i].rangeUnits(i);System.out.printf("\n");}

    //Allocating values for terms of the regression models
    for(int m=0; m<Terms.length; m++)
    {Terms[m].terms(m, inparameter);}

    //Creating random values between -1 and 1 for the CCD matrix
    for(int m=0; m<ccd.length; m++)
    {
        for(int n=0; n<Levels.length; n++)
        {
            ccd[m].initialccd(n);
        }
        System.out.printf("\n");
    }

    //Converting CCD to actual values and filling input matrix
    for(int m=0; m<ccd.length; m++)
    {
        for(int n=0; n<units.length; n++)
        {
            VgaI[m].initialMatrix(ccd[m], units[n], Levels [n], n);
        }
    }

    //Creating responses based on the regression models
    for(int m=0; m<ccd.length; m++)
    {
        for (int n=0; n<Terms.length; n++)
        {
            {VgaO[m].responses(ccd[m], inparameter, Terms[n]);}
        }
    }

    //Printing the output matrix - results from the regression models
    System.out.printf("***** CENTRAL COMPOSITE DESIGN MATRIX -

```

```

RESPONSE *****\n");

    //Defining an array to control strings
    vector = new String [6];
    vector[0] = "Input 1"; vector[1] = "Input 2"; vector[2] = "Input 3";
    vector[3] = "Output 1"; vector[4] = "Output 2"; vector[5] = "Output
3";

    System.out.printf("\n");
    String format = "%15s";
    String format1 = "%12s";

    System.out.printf(format,vector[3]);

    for(int m = 4; m<outparameter+3; m++)
    {System.out.printf(format1,vector[m]);}

    System.out.printf("\n");

    for(int m=0; m<VgaO.length; m++)
    {
        System.out.printf("Row %d:",m+1);
        VgaO[m].printChromosome( );
        System.out.printf("\n");
    }

    System.out.printf("\n");
}

//Showing new population after the GA method
public void visualizePopN(int follow_gen)
{
    System.out.print("*****NEW POPULATION *****\n");

    System.out.printf("\n");
    String format = "%15s";
    String format1 = "%12s";

    System.out.printf(format,vector[0]);

    for(int m = 1; m<inparameter; m++)
    {System.out.printf(format1,vector[m]);}

    System.out.printf("\n");

    for(int m = 0; m<follow_gen; m++)
    {
        System.out.printf("Row %d:",m+1);
        VgaI[m].printChromosome( );
        System.out.printf("\n");
    }
}

//Applying desirability function
public void fDesirability(int follow_gen)
{
    double var = 0.0;

    f = new double[follow_gen+1];
    number = new double[follow_gen];

    for(int a=0; a<f.length; a++)
    {f[a]=0.0;}

    for(int k=0; k<number.length; k++)

```

```

{number[k]=0.0;}

//Defining desirability function values
Df = new double [follow_gen];
aux = new double [outparameter];

double Value = 0.0;
for(int x = 0; x<Df.length; x++)
{
    for(int y = 0; y<response.length; y++)
    {aux[y]=VgaO[x].desirValue(response[y], y);}

    double value = aux[0];
    for(int y = 1; y<response.length; y++)
    {value *= aux[y];}

    double extra = 1./outparameter;
    Df[x] = Math.pow(value, (extra));

    var += Df[x];setMtotal(var);
}

//Printing matrix with both input and output parameters
System.out.print("*****GLOBAL MATRIX *****\n");

System.out.printf("\n");
String format = "%15s";
String format1 = "%12s";

System.out.printf(format,vector[0]);

for(int m = 1; m<inparameter; m++)
{System.out.printf(format1,vector[m]);}

for(int m = 3; m<outparameter+3; m++)
{System.out.printf(format1,vector[m]);}

System.out.printf("\n");

for(int m = 0; m<follow_gen; m++)
{
    System.out.printf("Row %d:",m+1);
    VgaI[m].printChromosome( );
    VgaO[m].printChromosome( );
    System.out.printf("\n");
}
System.out.printf("\n");

number[0] = (Math.random( ) *100);
System.out.printf("Number[1] = %.1f\n\n", number[0]);

for(int d=1; d<number.length; d++)
{
    number[d] = (Math.random( ) *100);
    System.out.printf("Number[%d] = %.2f\n\n",d+1,number[d]);
}

f[0] = (Df[0]/getMtotal( )) *100;
System.out.printf("f[1] = %.1f\n\n", f[0]);

for(int d=1; d<f.length-1; d++)
{
    f[d] = (Df[d]/getMtotal( )) *100 + f[d-1];
    System.out.printf("f[%d] = %.2f\n\n",d+1,f[d]);
}

```

```

    }
}

//Chosen chromosomes for new generation based on the roulette
public void avaliaFitness(int follow_gen)
{
    //Selecting chromosomes
    for(int e=0; e<number.length; e++)
    {
        vga[e] = new SolutionRSM(inparameter);
        if(number[e]<=f[0])
        {
            vga[e].copy(VgaI[0]);
            System.out.printf("*** Applying desirability (%.2f < %.2f)
**\n", number[e], f[0]);
            System.out.printf("Chromosome 1 selected: ");
            vga[0].printChromosome( );

            System.out.printf("\n\n");
        }
        else
        {
            for(int a=0; a<f.length-1; a++)
            {
                if(number[e]>f[a] && number[e]<=f[a+1])
                {
                    vga[e].copy(VgaI[a+1]);
                    System.out.printf("*** Applying desirability (%.2f <
%.2f) **\n", number[e], f[a+1]);
                    System.out.printf("Chromosome %d selected: ", a+2);
                    vga[e].printChromosome( );

                    System.out.printf("\n\n");
                }
            }
        }
    }

    System.out.printf("\n");

    for (int i=0; i<follow_gen; i++)
    {VgaI[i] = new SolutionRSM(inparameter);}

    //Generating new population
    for(int i=0; i<VgaI.length; i++)
    {VgaI[i].copy(vga[i]);}

    System.out.printf("*****POPULATION AFTER DESIRABILITY
FUNCTION*****\n");

    System.out.printf("\n");
    String format = "%15s";
    String format1 = "%12s";

    System.out.printf(format, vector[0]);

    for(int m = 1; m<inparameter; m++)
    {System.out.printf(format1, vector[m]);}

    System.out.printf("\n");

    for(int g=0; g<VgaI.length; g++)
    {System.out.printf("Row
%d:", g+1); VgaI[g].printChromosome( ); System.out.printf("\n");}

```

```

        System.out.printf("\n\n");
    }

    //Applying Crossover
    public void crossOver(int follow_gen)
    {
        int father1=0, father2, first = 0;
        double x;

        Random randomNumbers = new Random( );

        for(int i=0; i<follow_gen; i++)
        {
            x = randomNumbers.nextDouble( );
            father2 = i;
            if(x < probability)
            {
                first++;
                if(first % 2 == 0)
                {
                    System.out.printf("** Applying Crossover (%.2f <
%.2f)**",x,probability);
                    System.out.println("\nFather1: "+(father1+1));
                    VgaI[father1].printChromosome( );
                    System.out.println(" ");
                    System.out.println("Father2: "+(father2+1));
                    VgaI[father2].printChromosome( );
                    System.out.println("");
                    System.out.printf("\n");
                    System.out.printf("**%.2f < %.2f**\n",x,probability);
                    VgaI[father1].chromosome(VgaI[father2], inparameter);
                }
                else father1 = i;
            }
        }
    }

    //Applying Mutation
    public void mutation( )
    {
        Random randomNumbers = new Random( );
        double x;

        for(int i=0; i<VgaI.length; i++)
        {
            for(int m=0; m<Levels.length; m++)
            {
                x = randomNumbers.nextDouble( );
                if(x < mutation)
                {
                    System.out.printf("\n** Mutation (%.2f < %.2f) -
Chromosome %d**",x,mutation,i+1);
                    System.out.printf("\nBefore Mutation: ");
                    VgaI[i].printChromosome( );

                    VgaI[i].mutation(m, Levels[m]);

                    System.out.printf("\nAfter Mutation: ");
                    VgaI[i].printChromosome( );
                    System.out.printf("\n");
                }
            }
        }
        System.out.printf("\n\n");
    }
}

```

```

//Applying regression models from the second generation on
public void regressionModel(int experiments, int var)
{
    ccd = new SolutionRSM[experiments];
    VgaO = new SolutionRSM [experiments];

    for (int i=0; i<ccd.length; i++)
    {ccd[i] = new SolutionRSM(inparameter); VgaO[i] = new
SolutionRSM(outparameter);}

    if (var == 0)
    {
        for(int m=0; m<ccd.length; m++)
        {
            for(int n=0; n<Levels.length; n++)
            {
                ccd[m].initialccd(n);
            }
            System.out.printf("\n\n");
        }
    }
    else
    {
        for(int m=0; m<ccd.length; m++)
        {
            for(int n=0; n<Levels.length; n++)
            {
                ccd[m].CCD(Levels[n], VgaI[m], units[n], n);
            }
            System.out.printf("\n\n");
        }
    }

    for(int m=0; m<ccd.length; m++)
    {
        for (int n=0; n<Terms.length; n++)
        {
            {VgaO[m].responses(ccd[m], inparameter, Terms[n]);}
        }
    }

    System.out.printf("***** CENTRAL COMPOSITE DESIGN MATRIX -
RESPONSE *****\n");

    System.out.printf("\n");
    String format = "%15s";
    String format1 = "%12s";

    System.out.printf(format,vector[3]);

    for(int m = 4; m<outparameter+3; m++)
    {System.out.printf(format1,vector[m]);}

    System.out.printf("\n");

    for(int m=0; m<ccd.length; m++)
    {System.out.printf("Row
%d:",m+1);VgaO[m].printChromosome( );System.out.printf("\n");}
    System.out.printf("\n");
}
}

```


SolutionRSM subclass

```

import java.util.Scanner;
import java.util.Random;

public class SolutionRSM extends RSM
{
    protected double Vrm[ ];           //Vector that allows access from GA
    Class                               //Vector that allows creation of
    protected double vrm[ ];           Orthogonal Array
    protected int aux [ ];             Array Matrix
    protected double terms [ ];       //Auxiliar vector for the Orthogonal
    and constant terms for regression models

    //Constructor with parameters
    public SolutionRSM(int inparameter)
    {
        Vrm = new double [inparameter+1];
        vrm = new double [inparameter];
        aux = new int [inparameter*4-1];
        terms = new double [20];

        for(int j=0; j<Vrm.length; j++)
        {this.Vrm[j]=0;}

        for(int j=0; j<vrm.length; j++)
        {this.vrm[j]=0;}
    }

    //Defining ranges for output parameters and type of response
    public void defResponse(int i)
    {
        Scanner in = new Scanner (System.in);

        System.out.printf("Please define the response type for output
parameter %d: 'Maximise', 'Minimise' or 'Target is best!' \n", i+1);
        String gen = in.nextLine( );

        int variable = 1;

        if (gen.toUpperCase( ).equals("MAXIMISE") ||
gen.toUpperCase( ).equals("MINIMISE") || gen.toUpperCase( ).equals("TARGET
IS BEST"))
        {variable = 0;}

        if (variable == 1)
        {
            do
            {
                System.out.println("Not a valid choice!\n Please try
again...\n");
                System.out.printf("Please define the response type for
output parameter %d: 'Maximise', 'Minimise' or 'Target is best!' \n", i+1);
                gen = in.nextLine( );

                if (gen.toUpperCase( ).equals("MAXIMISE") ||
gen.toUpperCase( ).equals("MINIMISE") || gen.toUpperCase( ).equals("TARGET
IS BEST"))
                {variable = 0;}
            }
        }
    }
}

```

```

        else
            {variable = 1;}
        } while (variable == 1);
    }

    if (variable == 0)
    {
        switch(gen.toUpperCase( ))
        {
            case "MAXIMISE":
                System.out.printf("Insert the lower value for output
parameter %d. \n", i+1);
                this.Vrm [0] = in.nextDouble( );
                this.Vrm [1] = 0;
                System.out.printf("Insert the target value for output
parameter %d. \n", i+1);
                this.Vrm [2] = in.nextDouble( );
                this.Vrm [3] = 1;

                int max = 1;

                if (this.Vrm[0]<this.Vrm[2])
                    {max = 0;}

                if (max == 1)
                {
                    do
                    {
                        System.out.printf("Not a valid choice! %.2f
equal or bigger than %.2f.\n Please try
again...\n\n",this.Vrm[0],this.Vrm[2]);
                        System.out.printf("Insert the lower value for
output parameter %d. \n", i+1);
                        this.Vrm [0] = in.nextDouble( );
                        System.out.printf("Insert the target value for
output parameter %d. \n", i+1);
                        this.Vrm [2] = in.nextDouble( );

                        if (this.Vrm[0]<this.Vrm[2])
                            {max = 0;}

                        else
                            {max = 1;}
                    } while (max == 1);
                }

                break;
            case "MINIMISE":
                this.Vrm [0] = 0;
                System.out.printf("Insert the upper value for output
parameter %d. \n", i+1);
                this.Vrm [1] = in.nextDouble( );
                System.out.printf("Insert the target value for output
parameter %d. \n", i+1);
                this.Vrm [2] = in.nextDouble( );
                this.Vrm [3] = -1;

                int min = 1;

                if (this.Vrm[2]<this.Vrm[1])
                    {min = 0;}

                if (min == 1)
                {

```

```

        do
        {
            System.out.printf("Not a valid choice! %.2f
equal or bigger than %.2f.\n Please try
again...\n\n",this.Vrm[2],this.Vrm[1]);
            System.out.printf("Insert the upper value for
output parameter %d. \n", i+1);
            this.Vrm [1] = in.nextDouble( );
            System.out.printf("Insert the target value for
output parameter %d. \n", i+1);
            this.Vrm [2] = in.nextDouble( );

            if (this.Vrm[2]<this.Vrm[1])
            {min = 0;}

            else
            {min = 1;}
        } while (min == 1);
    }

    break;
    case "TARGET IS BEST":
        System.out.printf("Insert the lower value for output
parameter %d. \n", i+1);
        this.Vrm [0] = in.nextDouble( );
        System.out.printf("Insert the target value for output
parameter %d. \n", i+1);
        this.Vrm [2] = in.nextDouble( );
        this.Vrm [3] = 0;

        int var = 1;

        if (this.Vrm[0]<this.Vrm[2])
        {var = 0;}

        if (var == 1)
        {
            do
            {
                System.out.printf("Not a valid choice! %.2f
equal or bigger than %.2f.\n Please try
again...\n\n",this.Vrm[0],this.Vrm[2]);
                System.out.printf("Insert the lower value for
output parameter %d. \n", i+1);
                this.Vrm [0] = in.nextDouble( );
                System.out.printf("Insert the target value for
output parameter %d. \n", i+1);
                this.Vrm [2] = in.nextDouble( );

                if (this.Vrm[0]<this.Vrm[2])
                {var = 0;}

                else
                {var = 1;}
            } while (var == 1);
        }

        if(var == 0)
        {
            System.out.printf("Insert the upper value for output
parameter %d. \n", i+1);
            this.Vrm [1] = in.nextDouble( );

            int target = 1;

```



```

    }

    if(var == 0)
    {
        System.out.printf(" 1 --> ");
        this.Vrm [2] = in.nextDouble( );

        int variable = 1;

        if (this.Vrm[0]<this.Vrm[2] && this.Vrm[1]<this.Vrm[2])
        {variable = 0;}

        if (variable == 1)
        {
            do
            {
                System.out.printf("Not a valid choice! %.2f and/or %.2f
equal or bigger than %.2f.\n Please try
again...\n\n",this.Vrm[0],this.Vrm[1],this.Vrm[2]);
                System.out.printf("Please insert the required CCD level
for input parameter %d.\n", i+1);
                System.out.printf(" 1 --> ");
                this.Vrm [2] = in.nextDouble( );

                if (this.Vrm[0]<this.Vrm[2] && this.Vrm[1]<this.Vrm[2])
                {variable = 0;}

                else
                {variable = 1;}
            } while (variable == 1);
        }
    }
}

//Defining ranges for Central Composite Design in units
public void rangeUnits(int i)
{
    this.Vrm [0] = -1; this.Vrm [1] = 0; this.Vrm [2] = 1;
}

//Initialising Central Composite Design coded units
public void initialccd(int n)
{
    this.vrm[n] = Math.random( )*(1-(-1))-1;
}

//Converting actual values to coded units
public void CCD(SolutionRSM Levels, SolutionRSM VgaI, SolutionRSM units,
int n)
{
    if(Levels.Vrm[0]<=VgaI.Vrm[n] && VgaI.Vrm[n]<=Levels.Vrm[1])
    {
        this.vrm[n] = units.Vrm[0] - ((units.Vrm[0]-
units.Vrm[1])*(Levels.Vrm[0]-VgaI.Vrm[n])/(Levels.Vrm[0]-Levels.Vrm[1]));
    }
    if(Levels.Vrm[1]<=VgaI.Vrm[n] && VgaI.Vrm[n]<=Levels.Vrm[2])
    {
        this.vrm[n] = units.Vrm[1] - ((units.Vrm[1]-
units.Vrm[2])*(Levels.Vrm[1]-VgaI.Vrm[n])/(Levels.Vrm[1]-Levels.Vrm[2]));
    }
}

//Creating initial matrix based on coded units from Central Composite
Design
public void initialMatrix(SolutionRSM ccd, SolutionRSM units,

```

```

SolutionRSM Levels, int n)
{
    if(units.Vrm[0]<=ccd.vrm[n] && ccd.vrm[n]<=units.Vrm[1])
    {
        this.Vrm[n] = Levels.Vrm[0] - ((Levels.Vrm[0]-
Levels.Vrm[1])*(units.Vrm[0]-ccd.vrm[n])/(units.Vrm[0]-units.Vrm[1]));
    }

    if(units.Vrm[1]<=ccd.vrm[n] && ccd.vrm[n]<=units.Vrm[2])
    {
        this.Vrm[n] = Levels.Vrm[1] - ((Levels.Vrm[1]-
Levels.Vrm[2])*(units.Vrm[1]-ccd.vrm[n])/(units.Vrm[1]-units.Vrm[2]));
    }
}

//Providing terms of the regression models to apply in the prediction
process
public void terms(int m, int inparameter)
{
    Scanner in = new Scanner (System.in);
    System.out.printf("Please insert the terms of the regression model -
output variable %d!\n\n", m+1);

    if(inparameter == 2 || inparameter == 3)
    {
        System.out.printf("Constant: ");this.terms[0] =
in.nextDouble( );
        System.out.printf("x1: ");this.terms[1] = in.nextDouble( );
        System.out.printf("x1^2: ");this.terms[4] = in.nextDouble( );
        System.out.printf("x2: ");this.terms[2] = in.nextDouble( );
        System.out.printf("x2^2: ");this.terms[5] = in.nextDouble( );
        System.out.printf("x1*x2: ");this.terms[7] = in.nextDouble( );
    }

    if(inparameter == 3)
    {
        System.out.printf("x3: ");this.terms[3] = in.nextDouble( );
        System.out.printf("x3^2: ");this.terms[6] = in.nextDouble( );
        System.out.printf("x1*x3: ");this.terms[8] = in.nextDouble( );
        System.out.printf("x2*x3: ");this.terms[9] = in.nextDouble( );
        System.out.printf("x1*x2*x3: ");this.terms[10] =
in.nextDouble( );
    }
    System.out.printf("\n");
}

//Creating responses based on regression models and coded units from
Central Composite Design
public void responses(SolutionRSM ccd, int inparameter, SolutionRSM
Terms)
{
    if(inparameter == 2)
    {
        for(int a=0; a<inparameter; a++)
        {
            this.Vrm[a] = Terms.terms[0] + Terms.terms[1]*ccd.vrm[0] +
Terms.terms[2]*ccd.vrm[1] + Terms.terms[4]*Math.pow(ccd.vrm[0],2)
+ Terms.terms[5]*Math.pow(ccd.vrm[1],2) +
Terms.terms[7]*ccd.vrm[0]*ccd.vrm[1];
        }
    }

    if(inparameter == 3)
    {
        for(int a=0; a<inparameter; a++)

```

```

        {
            this.Vrm[a] = Terms.terms[0] + Terms.terms[1]*ccd.vrm[0] +
Terms.terms[2]*ccd.vrm[1] + Terms.terms[3]*ccd.vrm[2] +
Terms.terms[4]*Math.pow(ccd.vrm[0],2)
                + Terms.terms[5]*Math.pow(ccd.vrm[1],2) +
Terms.terms[6]*Math.pow(ccd.vrm[2],2) + Terms.terms[7]*ccd.vrm[0]*ccd.vrm[1]
                + Terms.terms[8]*ccd.vrm[0]*ccd.vrm[2] +
Terms.terms[9]*ccd.vrm[1]*ccd.vrm[2] +
Terms.terms[10]*ccd.vrm[0]*ccd.vrm[1]*ccd.vrm[2];;
        }
    }

    /*
    this.Vrm[0] = 21.6304 - 0.056*ccd.vrm[0] + 0.001*ccd.vrm[1] -
0.096*ccd.vrm[2] - 0.0056*Math.pow(ccd.vrm[0],2)
                - 0.0006*Math.pow(ccd.vrm[1],2) -
0.0056*Math.pow(ccd.vrm[2],2) + 0.00125*ccd.vrm[0]*ccd.vrm[1]
                - 0.01125*ccd.vrm[0]*ccd.vrm[2] +
0.00125*ccd.vrm[1]*ccd.vrm[2] + 0.00125*ccd.vrm[0]*ccd.vrm[1]*ccd.vrm[2];

        this.Vrm[1] = 21.8087 - 0.031*ccd.vrm[0] - 0.001*ccd.vrm[1] -
0.051*ccd.vrm[2] + 0.0017*Math.pow(ccd.vrm[0],2)
                + 0.0017*Math.pow(ccd.vrm[1],2) -
0.0083*Math.pow(ccd.vrm[2],2) - 0.00125*ccd.vrm[0]*ccd.vrm[1]
                - 0.00625*ccd.vrm[0]*ccd.vrm[2] -
0.00125*ccd.vrm[1]*ccd.vrm[2] - 0.00125*ccd.vrm[0]*ccd.vrm[1]*ccd.vrm[2];

        this.Vrm[2] = 3.591 + 0.551*ccd.vrm[0] - 0.012*ccd.vrm[1] +
0.925*ccd.vrm[2] + 0.3389*Math.pow(ccd.vrm[0],2)
                - 0.00111*Math.pow(ccd.vrm[1],2) +
0.07389*Math.pow(ccd.vrm[2],2) - 0.0025*ccd.vrm[0]*ccd.vrm[1]
                + 0.115*ccd.vrm[0]*ccd.vrm[2] -
0.005*ccd.vrm[1]*ccd.vrm[2] - 0*ccd.vrm[0]*ccd.vrm[1]*ccd.vrm[2];*/
    }

    //Defining the desirability values based on the response type
    public double desirValue(SolutionRSM response, int y)
    {
        double df = 0.0;

        if(response.Vrm[3]==1)
        {
            if(this.Vrm[y]>response.Vrm[2])
            {df = 1;}

            if (response.Vrm[0]<=this.Vrm[y] &&
this.Vrm[y]<=response.Vrm[2])
            {df = (this.Vrm[y]-response.Vrm[0]) / (response.Vrm[2]-
response.Vrm[0]);}
        }

        if(response.Vrm[3]==-1)
        {
            if(this.Vrm[y]<response.Vrm[2])
            {df = 1;}

            if (response.Vrm[2]<=this.Vrm[y] &&
this.Vrm[y]<=response.Vrm[1])
            {df = (this.Vrm[y]-response.Vrm[1]) / (response.Vrm[2]-
response.Vrm[1]);}
        }

        if(response.Vrm[3]==0)
        {

```

```

        if (response.Vrm[0]<=this.Vrm[y] &&
this.Vrm[y]<=response.Vrm[2])
        {df = (this.Vrm[y]-response.Vrm[0])/(response.Vrm[2]-
response.Vrm[0]);}

        if (response.Vrm[2]<=this.Vrm[y] &&
this.Vrm[y]<=response.Vrm[1])
        {df = (this.Vrm[y]-response.Vrm[1])/(response.Vrm[2]-
response.Vrm[1]);}
        }

    return df;
}

//Crossover in SolutionGA
public void chromosome(SolutionRSM father2, int inparameter)
{
    int point;
    double son1[ ] = new double[inparameter+1];
    double son2[ ] = new double[inparameter+1];

    if(inparameter == 2)
        point = 1;
    else
        do
            {point = (int) (Math.random( )*inparameter);}
        while(point==0);

    System.out.printf("Point: %d",point);

    for(int i = 0; i<point; i++)
    {
        son1[i] = this.Vrm[i];
        son2[i] = father2.Vrm[i];
    }

    for(int i = point; i<Vrm.length; i++)
    {
        son1[i] = father2.Vrm[i];
        son2[i] = this.Vrm[i];
    }

    for(int i=0; i<Vrm.length; i++)
    {
        this.Vrm[i] = son1[i];
        father2.Vrm[i] = son2[i];
    }

    System.out.printf("\nSon1::::: ");
    this.printChromosome( );
    System.out.printf("\n");
    System.out.printf("Son2::::: ");
    father2.printChromosome( );
    System.out.printf("\n");
}

//Copy method for Crossover
public void copy(SolutionRSM Vga)
{
    for(int i=0; i<Vrm.length; i++)
        {this.Vrm[i]=Vga.Vrm[i];}
}

//Printing Chromosome
public void printChromosome( )

```



```
{
    for(int i=0; i<Vrm.length-1; i++)
        {System.out.format("\t%5.2f\t", this.Vrm[i]);}
    }

    //Applying Mutation in a chosen chromosome block
    public void mutation( int m, SolutionRSM Levels)
    {
        double value;
        Random randomNumbers = new Random( );

        do
            {value = Levels.Vrm[0] + (randomNumbers.nextDouble( ) *
            (Levels.Vrm[2] - Levels.Vrm[0]));}
        while(value<Levels.Vrm[0] || value>Levels.Vrm[2]);

        this.Vrm[m] = value;
    }
}
```

Appendix C

All-weld tensile test plots

Introduction

This appendix includes all plots regarding the all-weld tensile tests performed for a better understanding of the work carried out.

Chapter 4

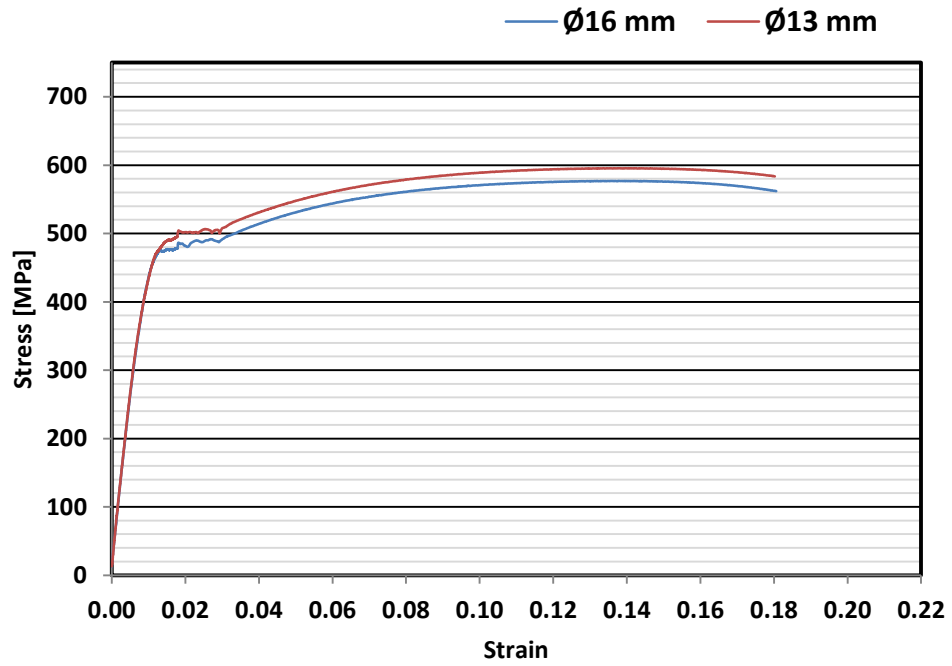


Fig. C 1 Stress-strain curves for 9 L/min SGFR.

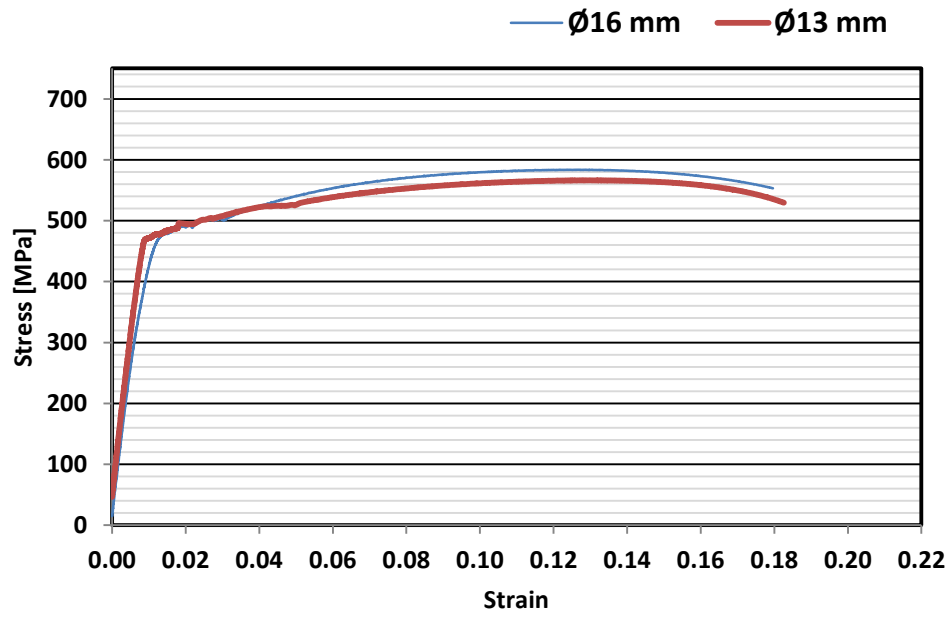


Fig. C 2 Stress-strain curves for 5 L/min SGFR.

Chapter 5

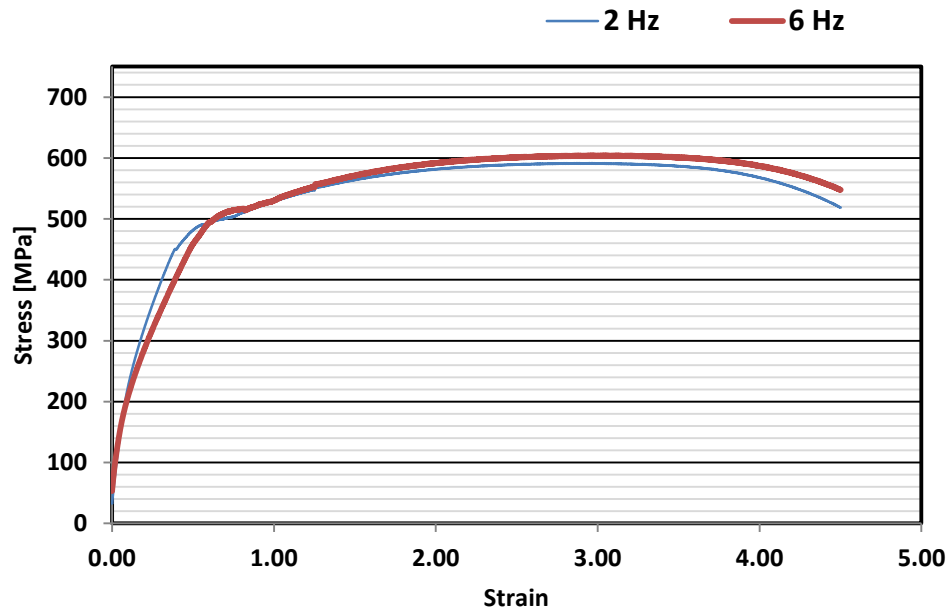


Fig. C 3 Stress-strain curves for 15Ar-15He cases.

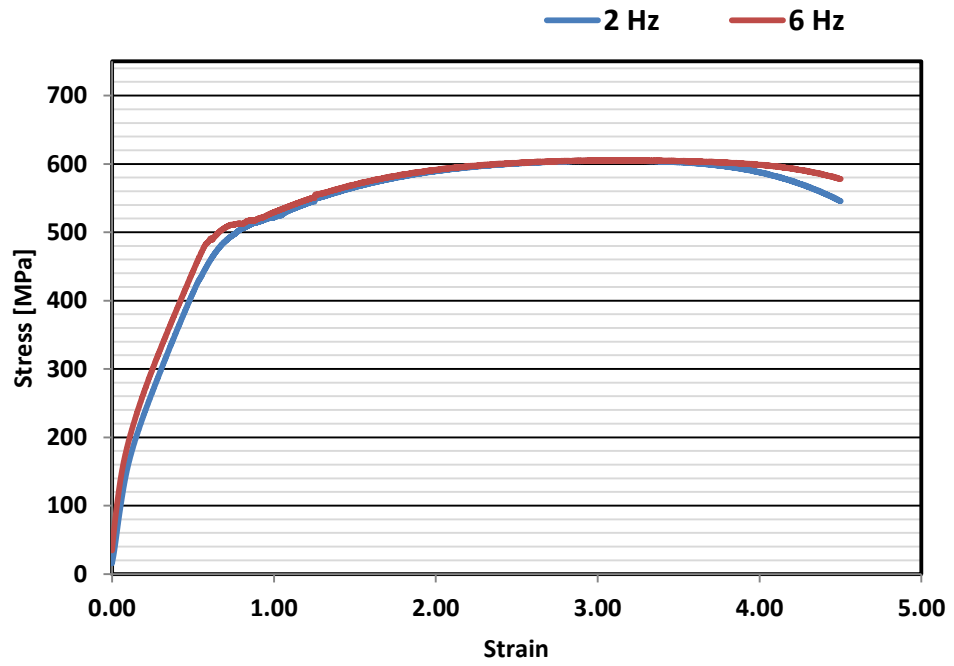


Fig. C 4 Stress-strain curves for 15Ar-6He cases.

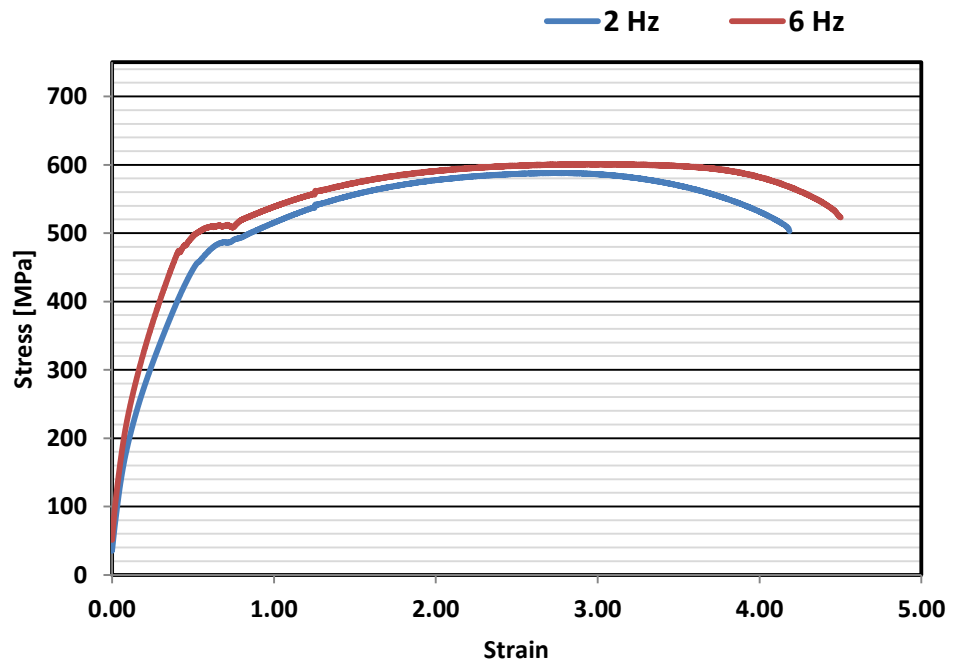


Fig. C 5 Stress-strain curves for 6Ar-15He cases.

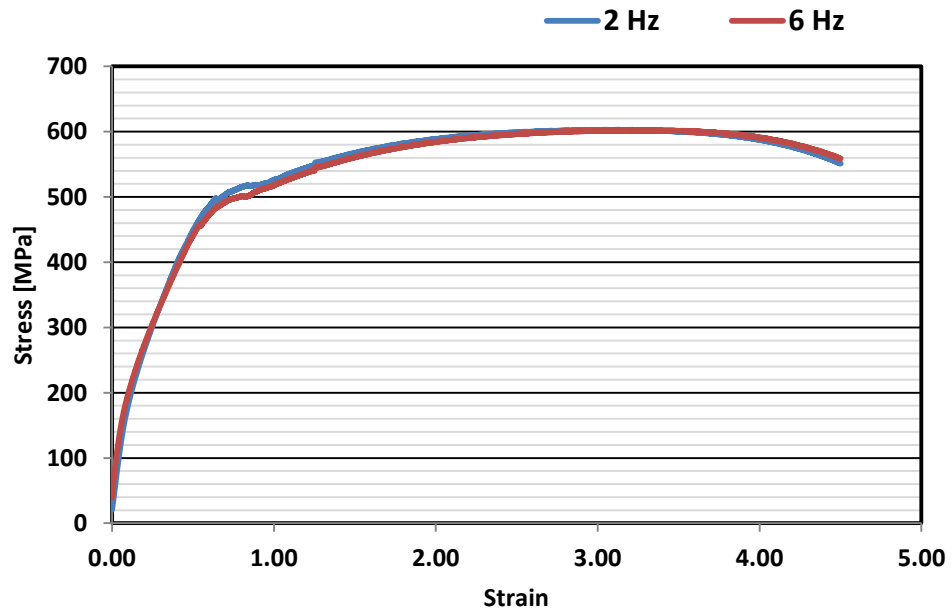


Fig. C 6 Stress-strain curves for 6Ar-6He cases.

Chapter 6

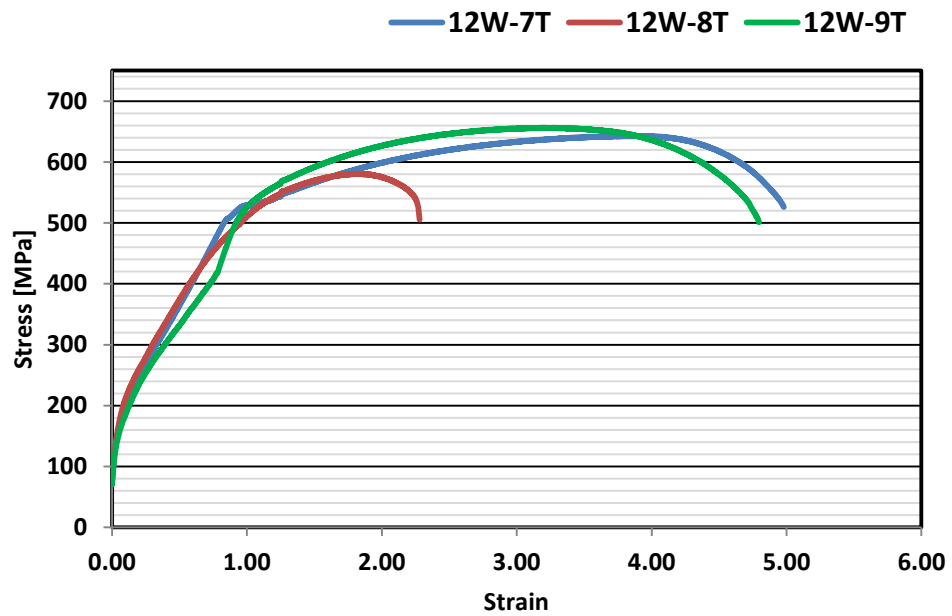


Fig. C 7 Stress-strain curves for 12 m/min wire-feed speed - Ar₅N₂ + He cases.

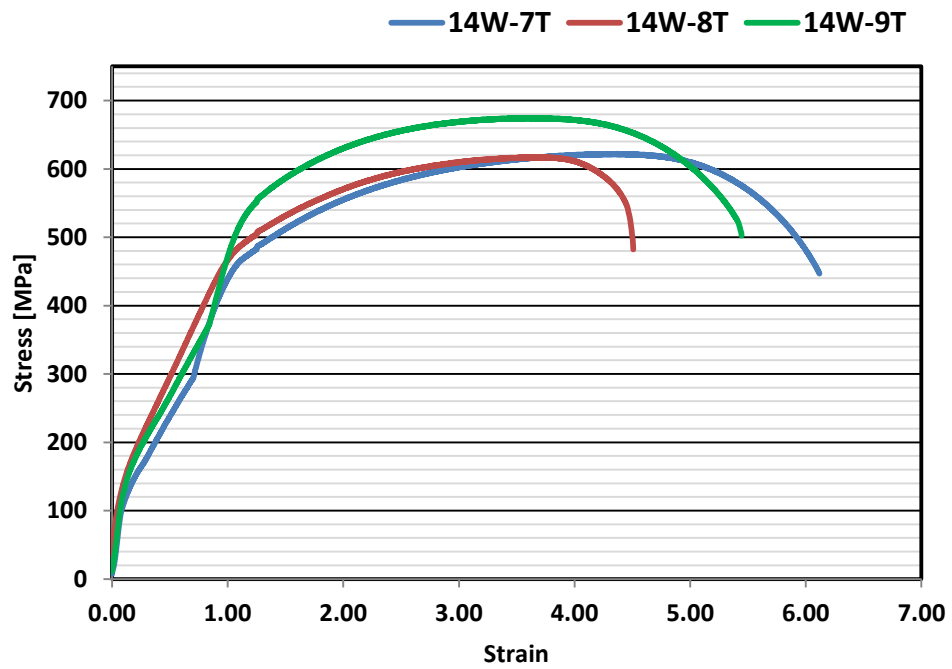


Fig. C 8 Stress-strain curves for 14 m/min wire-feed speed - Ar₅N₂ + He cases.

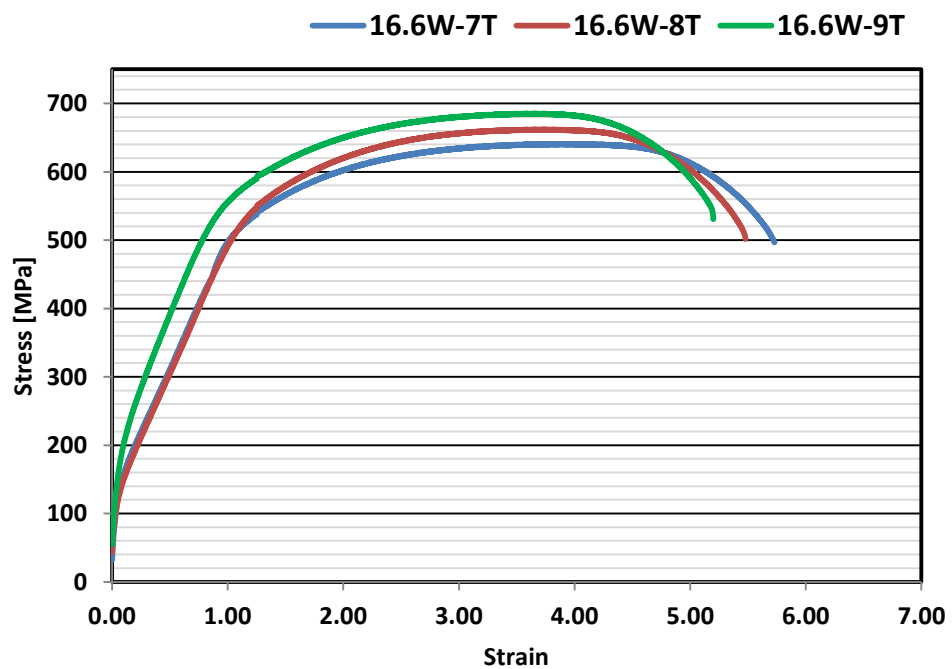


Fig. C 9 Stress-strain curves for 16.6 m/min wire-feed speed - Ar₅N₂ + He cases.

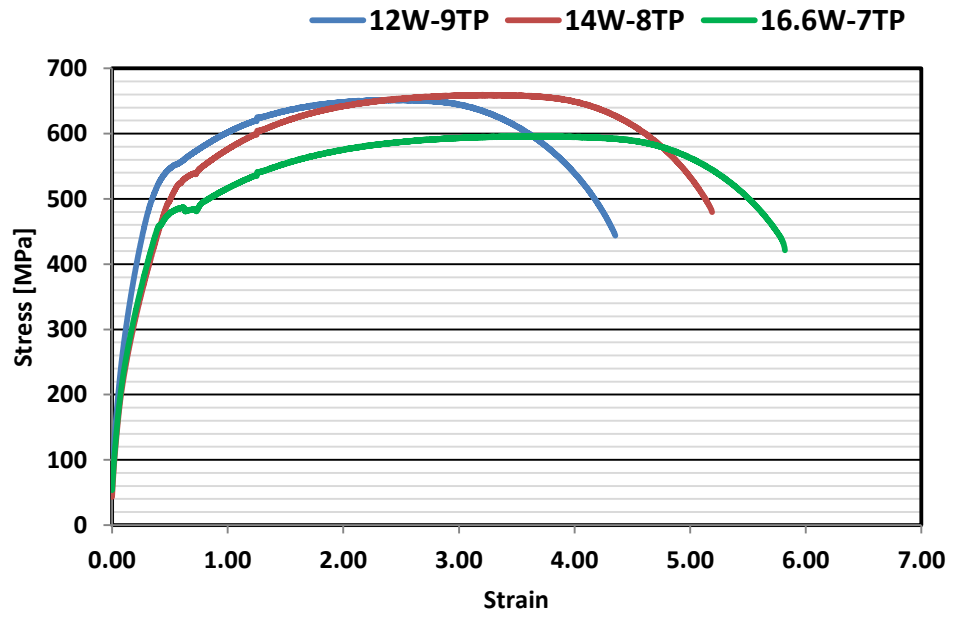


Fig. C 10 Stress-strain curves for the Ar5N₂ cases.

Chapter 7

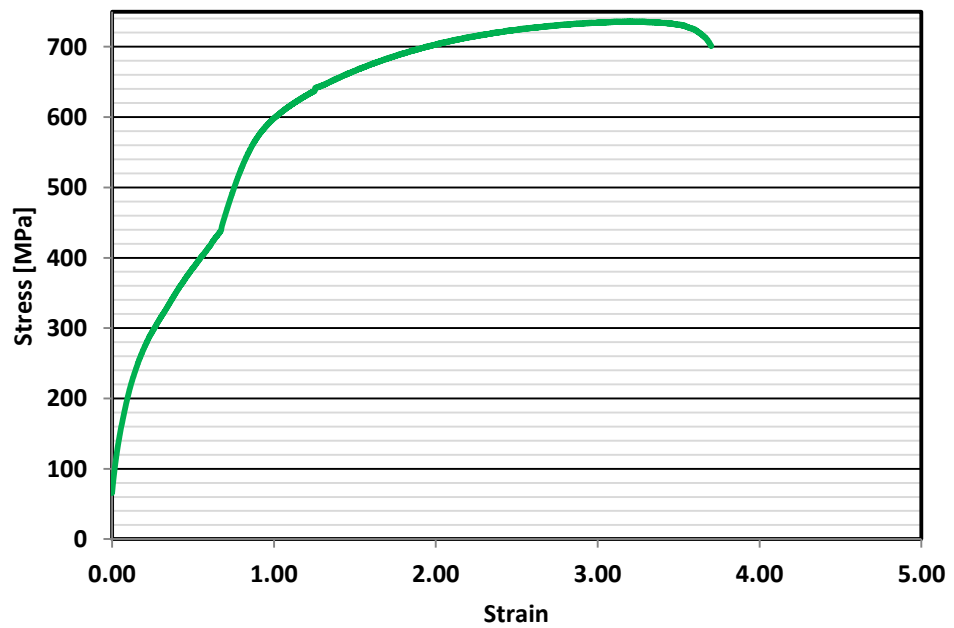


Fig. C 11 Stress-strain curve for the experimental validation.